CNS

Annual Report 2004

Center for Nuclear Study,
Graduate School of Science, the University of Tokyo

Editors
  T. Kawabata
  H. Ayabe

Center for Nuclear Study

Annual Report 2004

Center for Nuclear Study,
Graduate School of Science, the University of Tokyo

Preface

This is the annual report of the Center for Nuclear Study (CNS), Graduate School of Science, the University of Tokyo. This report includes activities during the fiscal year 2004 (April 2004 through March 2005).

During this period, the position-sensitive γ-ray detector array, CNS GRAPE, was successfully operated for in-beam γ-ray spectroscopy experiment for neutron-rich nuclei around ^{32}Mg using α induced reactions in inverse kinematics. In order to obtain better position determination, the R&D of pulse shape analysis based on an artificial neural network algorithm was also performed. A prototype BGO Compton suppressor for GRAPE was made. In addition, a development of CdTe detectors is in progress.

The mass range of RI beams at CRIB was expanded to the region of $A = 40$. An ^{39}Ar beam was successfully separated from the primary ^{40}Ar beam by the Wien filter. One of the key astrophysical reactions ^{8}Li$(\alpha,n)^{11}$B was successfully investigated using the high quality beam of ^{8}Li from the CRIB together with monolithic Si detectors. Some other reactions relevant to the rp process were also investigated.

The polarized proton solid target was improved after detailed studies on optical pumping by Ar-ion lasers and studies on microwave resonators. A high-statistics measurement of the analyzing power for the $p + {}^6$He elastic scattering is being planned with the polarized target. A polarimeter for GeV-energy polarized deuterons is being constructed at the internal target station of Nuclotron at Dubna, for a collaboration program of CNS and Joint Institute for Nuclear Physics.

The Hyper ECR ion source was improved to provide Li^{2+} ions by using a LiF-rod method. To improve beam injection efficiency, a metal alloy RF cavity was tested. A new project of charge breeding ECR ion source (CBECR) aiming at an intense and a high-charge state metal ion beams has started.

The PHENIX experiment at Relativistic Heavy Ion Collider (RHIC) at Brookhaven National Laboratory made a steady progress toward the understanding of hot and dense matter created by smashing energetic nuclei. The CNS group has been playing major roles in the various data analysis, subjects of which includes high-p_T charged and neutral hadron production, single photon production, single electron production, J/ψ yields in $p + p$, $d + $ Au and Au $+$ Au collisions. The development and study of basic characteristics of gas electron multiplier (GEM) was performed. GEM is a new type of gaseous detector and is to be used in the future PHENIX upgrade.

Theoretical studies have been carried out by large-scale nuclear structure calculations in collaboration with RIKEN. Shell-model calculations, in particular, those by the Monte Carlo Shell Model, have produced crucial results to clarify exotic structure of nuclei far from β stability line. Many of such theoretical studies have been made in collaboration with various groups over the world.

The 3rd CNS International Summer School (CISS04) has been organized in August 2004 with many invited lecturers including three foreign distinguished physicists. There were 107 participants from 6 countries mainly from Asia. The 4th summer school will be held this August.

The RIKEN RI beam facility (RIBF) which is under construction will deliver very exotic RI beams in 2007. Matching with the construction, we are currently promoting two future projects, the upgrade of the AVF cyclotron and the construction of the high resolution spectrometer SHARAQ.

The upgrade plan of RIKEN AVF cyclotron is to provide high-intensity and low-energy RI beams of about 10^8 pps. In 2004, power suppliers for the main and trim coils were upgraded, which have increased the K-value to 78. All other parts such as the RF system were also re-tuned to increase the Dee voltage.

The SHARAQ spectrometer is exclusively designed for high resolution spectroscopic studies with RI beams at 200–400 MeV/nucleon. We have determined the basic specification of the SHARAQ spectrograph and started to design the ion-optical configuration including the high resolution beam

line. Construction of the superconducting quadrupole doublet started in 2004.

In February 2005, our research activities since the establishment of CNS in 1997 were reviewed by the international review committee appointed by the dean of the Graduate School of Science, the University of Tokyo. The committee members are Prof. M. Inoue, Prof. H. Orihara, Prof. R. H. Siemssen (chair), Dr. T. J. Symons, Prof. B. M. Sherrill and Prof. H. Toki. We appreciate the committee for the precise and detailed review report. We are highly encouraged by the recommendation that our current research activities should be expanded, future projects should be pursued and eventually a center of excellence in heavy-ion physics should be created.

The previous director, Professor Hideyuki Sakai, has resigned as he was assigned to the deputy dean of science. We are very grateful to his invaluable contributions to the Center while his directorship.

Takaharu Otsuka
Director of CNS

Table of Contents

1a. Experimental Nuclear Physics: Low and Intermediate Energies

1b. Experimental Nuclear Physics: PHENIX Experiment at BNL-RHIC

2. Accelerator and Instrumentation

3. Theoretical Nuclear Physics

4. Other Activities

Appendices

Experimental Nuclear Physics: Low and Intermediate Energies

Study of Proton Resonant States in ^{22}Mg using a Radioactive Beam of ^{21}Na

J. J. He[a], S. Kubono[a], T. Teranishi[a,e], M. Notani[a,g], H. Baba[a], S. Nishimura[b], J. Y. Moon[c],
M. Nishimura[b], S. Michimasa[a,b], H. Iwasaki[d], Y. Yanagisawa[b], N. Hokoiwa[e], M. Kibe[e], J. H.
Lee[c], S. Kato[f], Y. Gono[e] and C. S. Lee[c]

[a]*Center for Nuclear Study, Graduate School of Science, University of Tokyo*
[b]*RIKEN (The Institute of Physical and Chemical Research)*
[c]*Department of Physics, Chung-Ang University, Korea*
[d]*Department of Physics, University of Tokyo*
[e]*Department of Physics, Kyushu University*
[f]*Department of Physics, Yamagata University*
[g]*Argonne National Laboratory, USA*

1. Introduction

The nuclear structure of ^{22}Mg nucleus has received great interests in recent years both by experimentalists and by theorists because of its role in determining the astrophysical reaction rates relevant to the production of ^{22}Na in explosive stellar scenarios [1, 2].

It is known that ^{22}Mg shows a two-particle feature and its levels are populated substantially in two-nucleon transfer reactions such as ^{24}Mg$(p, t)^{22}$Mg [3,4,5,6]. The nuclear levels above the proton threshold (Q = 5.508 MeV) had been studied using many reactions, such as the ^{20}Ne(^{3}He, $n\gamma$) [7, 8, 9], the ^{25}Mg(^{3}He, ^{6}He) [10], the ^{24}Mg(^{4}He, ^{6}He) [11], and the ^{12}C(^{16}O,^{6}He) [12]. In addition, the nuclear levels above the α threshold (Q = 8.14 MeV) had also been studied via the ^{18}Ne(α, p)^{21}Na reaction [13, 14] up to 11.13 MeV. Furthermore, the resonant properties of states just above the proton threshold have been investigated by the (p, γ) measurements using the DRAGON recoil separator at TRIUMF [15, 16]. Additionally, the resonant states in ^{22}Mg had also been investigated by the resonant elastic and inelastic scattering of ^{21}Na+p using a thick target method [17, 18]. In Ref. [18], four resonant states were observed in ^{22}Mg at excitation energies of 6.332, 6.590, 6.615 and 6.795 MeV. The 6.332-MeV state decays to the ground state of ^{21}Na and other three states decay to the first excited state as well as to the ground state in ^{21}Na. Based on these previous studies, the astrophysical implications were discussed. The conclusion is that the resonance at $E_x = 5.714$ MeV dominates at nova temperatures and the resonance at $E_x = 6.332$ MeV dominantes above $T = 1.1$ GK.

In a recent report [19], the authors claimed that no further measurements of the ^{21}Na(p, γ)^{22}Mg are needed to determine resonant reaction rates under nova conditions. Therefore, we would like to investigate the resonant properties of those high-energy proton resonant states (in ^{22}Mg) which contribute to the higher temperature astrophysical phenomena, such as X-ray burst or supernova. Especially, the resonant states above the α threshold are relevant to the stellar ^{18}Ne(α, p)^{21}Na reaction which is probably one of the key reactions for the break-out from the hot CNO cycle in X-ray burst [20]. In the present experiment the scan of the excited states in ^{22}Mg was extended up to about 9 MeV, and this will provide better information for estimating the reaction rate of the ^{18}Ne(α, p)^{21}Na reaction.

We have investigated proton resonant states in ^{22}Mg using the resonant elastic scattering of a ^{21}Na RI beam on a thick hydrogen target.

2. Experimental measurement

The experiment was performed using the CNS radioactive-ion-beam separator (CRIB) [21,22]. An 8.1-AMeV ^{20}Ne^{8+} beam bombarded a water-cooled ^{3}He gas target (0.36 mg/cm^2). A ^{21}Na beam was produced by the ^{3}He(^{20}Ne, ^{21}Na)X reaction. The secondary ^{21}Na beam was separated and used in the experiment as described elsewhere [23, 24] in detail.

A thick (CH$_2$)$_n$ foil of 7.9 mg/cm^2 was used in the experiment. A carbon target of 9.3 mg/cm^2 was also used in a separate run for evaluating the background contribution. At the secondary target position, the average intensity of ^{21}Na was 1.5×10^4 particles/s with a purity of 8.3%. The mean energy was 4.00 MeV/nucleon with a width (FWHM) of 0.16 MeV/nucleon. The ^{21}Na particles were stopped in the target, and only the recoiled products were measured using the ΔE-E Si telescopes. The identification of beam particles and recoiled protons was also described in Ref. [24].

The center-of-mass energies (E_{cm}) were deduced using the elastic scattering kinematics of ^{21}Na+p with correction of the energy loss of particles in the target. Any contribution from inelastic scattering ^{21}Na(p, p'γ(0.33 MeV))^{21}Na is not considered in the present report. At $\theta_{cm} \approx 172°$, the typical energy resolutions are approximately 20 keV at $E_{cm} = 0.5$ MeV and 45 keV at $E_{cm} = 3.5$ MeV in FWHM. The systematic uncertainties are approximately ± 12 keV at $E_{cm} = 1.0$ MeV and ± 20 keV at $E_{cm} = 3.5$ MeV.

3. Results and Discussion

Figure 1 shows an experimental proton spectrum for the ^{22}Mg+p scattering at an averaged scattering angle of $\theta_{lab} \approx 4°$ (*i. e.* at $\theta_{cm} \approx 172°$, covering $170° \sim 180°$). The data at the dead layer region (between ΔE and E) were removed from the figure. After correction for the number of ^{21}Na beam particles and the stopping power (dE/dx) of the beam particles in the target material, the differential cross sections (dσ/dΩ) of ^{21}Na+p elastic scattering were deduced [25].
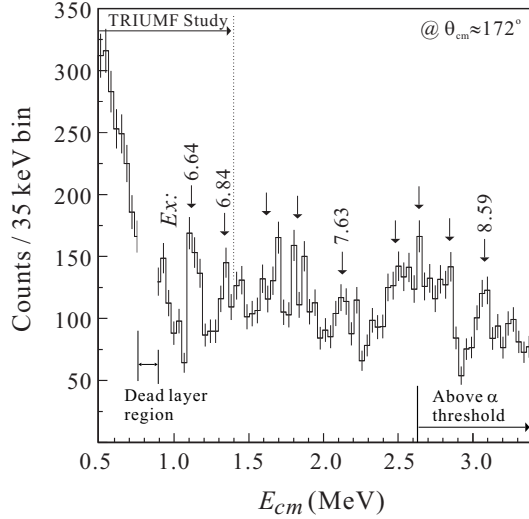
Figure 1. Experimental center-of-mass energy spectrum for ^{21}Na+p elastic scattering at θ_{cm}=172° (Dead-layer region is removed).

The excitation energies indicated on the figure are calculated from $E_x = E_r + 5.50$ MeV, where the resonant energies E_r are deduced roughly from Gaussian fits and their precise values should be derived from the R-matrix analysis. The arrows indicate possible proton resonances observed in the present experiment. The region investigated by the TRIUMF group is shown, and those two resonant states well observed at $E_x = 6.64$, 6.84 MeV are correreponding to the 6.615 and 6.795 MeV states within the energy uncertainties. In addition, some resonances were clearly seen above the α threshold, which could be very difficult (or even impossible) to be observed by the ^{18}Ne(α, p)^{21}Na reaction. The resonant properties of these states are of great interest for calculating the reaction rates.

The experimental differential cross sections are being analyzed by the R-matrix code SAMMY-M6-BETA [26], which enables multi-level R-Matrix fits to neutron and charged-particle cross-sectional data using Bayes' equations. The resonance properties such as E_r, Γ_p and J^π can be deduced from the analysis. The data analysis is still in progress.

References

[1] I. Iyudin *et al.*, Astron. Astrophys. **300** (1995) 422.
[2] M. Wiescher, K. Langanke, Z. Phys. A **325** (2002) 309.
[3] R. A. Paddock *et al.*, Phys. Rev. C **5** (1971) 485.
[4] N. Bateman *et al.*, Phys. Rev. C **63** (2001) 035803.
[5] S. Michimasa *et al.*, Eur. Phys. J. A **14** (2002) 275.
[6] B. Davids *et al.*, Phys. Rev. C **68** (2003) 055805.
[7] A. B. MacDonald and E. G. Adelberger, Nucl. Phys. A **144** (1970) 593.
[8] C. Rolfs *et al.*, Nucl. Phys. A **191** (1972) 209.
[9] W. P. Alford *et al.*, Nucl. Phys. A **457** (1986) 317.
[10] J. A. Caggiano *et al.*, Phys. Rev. C **66** (2002) 015804.
[11] G. P. A. Berg *et al.*, Nucl. Phys. A **718** (2003) 608(c).
[12] A. A. Chen *et al.*, Phys. Rev. C **63** (2001) 065807.
[13] W. Bradfield-Smith *et al.*, Phys. Rev. C **59** (1999) 3402.
[14] D. Groombridge *et al.*, Phys. Rev. C **66** (2002) 055802.
[15] S. Bishop *et al.*, Phys. Rev. Lett. **90** (2003) 162501.
[16] J. M. D'Auria *et al.*, Phys. Rev. C **69** (2004) 065803.
[17] C. Ruiz *et al.*, Phys. Rev. C **65** (2002) 042801(R).
[18] C. Ruiz *et al.*, Phys. Rev. C **71** (2005) 025802.
[19] D. Seweryniak *et al.*, Phys. Rev. Lett. **94** (2005) 032501.
[20] M. Wiescher *et al.*, J. of Phys. G **25** (1999) 133.
[21] S. Kubono *et al.*, Eur. Phys. J. A **13** (2002) 217.
[22] T. Teranishi *et al.*, Phys. Lett. B **556** (2003) 27.
[23] J. J. He *et al.*, CNS Annual Report 2002 (2003) 51.
[24] J. J. He *et al.*, CNS Annual Report 2003 (2004) 34.
[25] S. Kubono, Nucl. Phys. A **693** (2001) 221.
[26] N. M. Larson, *A Code System for Multilevel R-Matrix Fits to Neutron Data Using Bayes' Equations*, ORNL/TM-9179/R5 (Oct. 2000).

Study of Proton Resonant States in ^{23}Al using a Radioactive Beam of ^{22}Mg

J. J. He[a], S. Kubono[a], T. Teranishi[a,e], M. Notani[a,g], H. Baba[a], S. Nishimura[b], J. Y. Moon[c],
M. Nishimura[b], S. Michimasa[a,b], H. Iwasaki[d], Y. Yanagisawa[b], N. Hokoiwa[e], M. Kibe[e], J. H.
Lee[c], S. Kato[f], Y. Gono[e] and C. S. Lee[c]

[a]*Center for Nuclear Study, Graduate School of Science, University of Tokyo*
[b]*RIKEN (The Institute of Physical and Chemical Research)*
[c]*Department of Physics, Chung-Ang University, Korea*
[d]*Department of Physics, University of Tokyo*
[e]*Department of Physics, Kyushu University*
[f]*Department of Physics, Yamagata University*
[g]*Argonne National Laboratory, USA*

1. Introduction

The stellar ^{22}Mg(p, γ)^{23}Al reaction is an important reaction in the Hot NeNa-cycle, because it possibly influences the production of ^{22}Na in nova ejecta [1, 2]. The higher energy proton resonant states in ^{23}Al may also contribute to the X-ray burst and supernova events. In addition, in nuclear physics point of view the nuclear structure data in ^{23}Al are very scarce. Although several excited states have been observed, the properties are not known yet [2, 3, 4]. Due to a small proton separation energy in ^{23}Al ($S_p = 0.123$ MeV [2]), possibly ^{22}Mg ($S_p = 5.502$ MeV [5]) can be considered as a very good inert core, and it will help us to understand the nuclear structure in this loosely bound nucleus.

In the present study, we investigated proton resonant states in ^{23}Al directly by resonant elastic scattering of a ^{22}Mg RI beam on a thick hydrogen target. The experimental method, the setup and procedures had already been described previously [6,7,8,9]. This report will only show the recent results.

2. Results and Discussion

Figure 1 shows the experimental proton spectrum for the ^{22}Mg+p scattering at averaged scattering angle of $\theta_{lab} \approx 4°$ (*i. e.* at $\theta_{cm} \approx 172°$, covering $170° \sim 180°$). As shown in the figure, the C background contribution is almost flat in energy region of $1.0 \sim 3.5$ MeV. Data in the dead layer region (between ΔE and E detectors) were removed as indicated. The identification of excited states in ^{23}Al constructed by the elastic and inelastic scattering events were discussed in Ref. [9]. As a conclusion, the 3.00-MeV state decays to the ground state in ^{22}Mg, while all other states mainly decay to the first excited state in ^{22}Mg. A new level scheme of ^{23}Al is proposed in Fig. 2.

The differential cross sections ($d\sigma/d\Omega$) for ^{22}Mg+p scattering were deduced [10] from the proton spectrum by equation (1).

$$\frac{d\sigma}{d\Omega}(E_{cm}) = \frac{N}{I_0 N_s (\Delta\Omega)}, \qquad (1)$$

where N is the proton counts within a specific energy region of dE_{cm} (at E_{cm}). I_0 is the total number of ^{22}Mg beam particles bombarded the $(CH_2)_n$ target, and it is con-
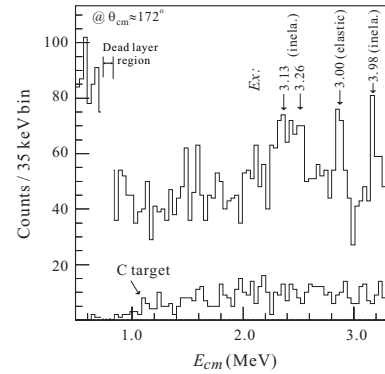
Figure 1. Experimental proton spectrum for ^{22}Mg $+ p$ scattering at $\theta_{lab} \approx 4°$ (*i.e.*, $\theta_{cm} \approx 172°$). The C background spectrum is also shown for comparison.
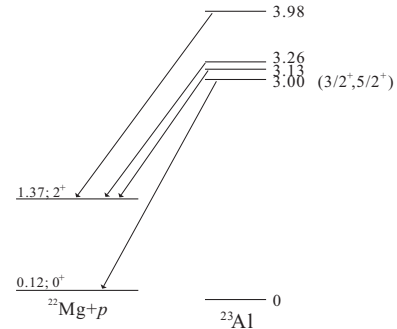
Figure 2. Level scheme of ^{23}Al proposed by the present experiment.

sidered as a constant in the whole energy region. The dead-time and detection-efficiency corrections were made for the quantities, N and I_0. $\Delta\Omega$ is the solid angle of Si telescope, N_s is the number of target nucleus per unit area, which is proportional to the energy-dependent target thickness per energy bin (dx/dE) [11]. Only statistical uncertainties are included in the following $d\sigma/d\Omega$ plot.

The differential cross sections were analyzed by an R-matrix [12] code SAMMY-M6-BETA [13], which enables multi-level R-Matrix fits to neutron and charged-particle cross-section data using Bayes' equations. The Reich-Moore approximation [14] is used in the code, *i. e.*, neglecting the level-level interference for the capture channels. Here, we assume that the gamma widths (Γ_λ^γ) are

negligible comparing to the particle widths ($\Gamma_{\lambda c}$), and the R-matrix takes the form of

$$R_{cc'} = \sum_{\lambda} \frac{\gamma_{\lambda c}\gamma_{\lambda c'}}{E_\lambda - E}. \qquad (2)$$

Here the subscripts c and c' represent only particle channels. The sum over λ includes an infinite number of levels (*i. e.*, resonances), and limiting this to a finite number is one approximation in R-matrix theory. E_λ is the resonance energy, and the particle channel width is defined as $\Gamma_{\lambda c} = 2\gamma_{\lambda c}^2 P_\ell$, and where $\gamma_{\lambda c}$ is referred to as reduced particle width amplitude. The Coulomb penetrability P_ℓ is given by

$$P_\ell = \frac{kR}{(F_\ell^2 + G_\ell^2)_{|R}}, \qquad (3)$$

where k is the wave number, F_ℓ and G_ℓ are the regular and irregular Coulomb functions, respectively. The channel (or interaction) radius is defined by $R = r_0(A_t^{1/3}+A_p^{1/3})$, and A_t, A_p are the mass numbers of the target and projectile, respectively. Although the penetrability depends sensitively upon r_0, the deduced proton partial width is only slightly dependent upon r_0 [15]. Here $r_0 = 1.25$ fm was used in calculating penetrabilities and level phase shifts, and $r_0 = 1.40$ fm was used in calculating potential scattering phase shifts.

Since the spin-parity of proton is $J^\pi = 1/2^+$ and that of the ground state in ^{22}Mg is 0^+, the channel spin is determined uniquely to be $s = 1/2$. As for the resonant state at $E_x = 3.00$ MeV, the SAMMY analysis was performed and only d-wave fits can reproduce the experimental data very well as shown in Fig. 3. An s-wave fit is also indicated in the figure for comparison. The p-wave fits are impossible due to their negative-peak (dip) shapes. In the calculations, the Bayes' χ^2/N (N is the number of data points in the fitted region) is useful for comparing results of different fits. As shown in Fig. 3, the calculated χ^2/N values are 1.09 and 1.25 for $J^\pi = 3/2^+$ and $J^\pi = 5/2^+$ fits, respectively, and this small difference indicates that both of the assignments are possible. On the contrary, the χ^2/N value (=2.93) of the s-wave fit is much larger than those of the d-wave fits. Therefore, a spin-parity of $(5/2^+, 3/2^+)$ is assigned to this state. In $J^\pi = 3/2^+$ case, the proton partial width is determined to be $\Gamma_p = 32 \pm 5$ keV, while $\Gamma_p = 17 \pm 3$ keV in $J^\pi = 5/2^+$ case. The excitation energy is determined to be 3.00 ± 0.02 MeV, whose uncertainty include both systematic and fitted uncertainties. The further SAMMY analysis for the states at 3.13, 3.26 and 3.98 MeV (via the inelastic decays) is still in progress.

As a conclusion, the states at 3.00 and 3.98 MeV are the newly observed excited states in ^{23}Al, and one of the excited states at 3.13 and 3.26 MeV could correspond to the previously observed state at 3.204 MeV [2] (possibly a doublet). The shell-model calculations are being performed to interpret the deduced nuclear structure of ^{23}Al nucleus, and the nuclear astrophysical implications are being evaluated.

References

[1] I. Iyudin *et al.*, Astron. Astrophys. **300** (1995) 422.
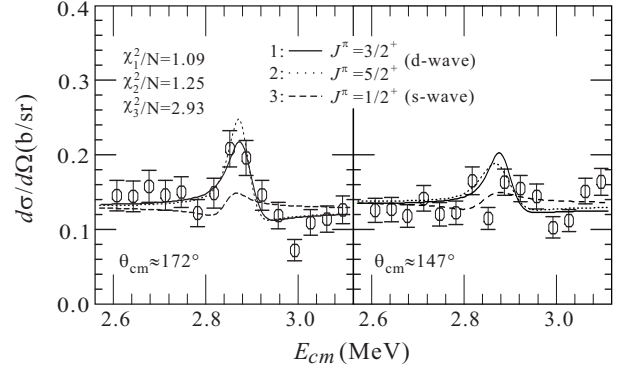
Figure 3. SAMMY analysis for resonant elastic scattering of ^{22}Mg+p at $E_x = 3.00$ MeV at two scattering angles. The d-wave fits with $J^\pi = 3/2^+$ (solid line) and $J^\pi = 5/2^+$ (dotted line) are shown, together a fit with an s-wave (dashed line).

[2] J. A. Caggiano *et al.*, Phys. Rev. C **64** (2001) 025802.
[3] B. Blank *et al.*, Z. Phys. A **357** (1997) 247.
[4] T. Gomi *et al.*, Nucl. Phys. A **718** (2003) 508c.
[5] G. Audi and A. H. Wapstra, Nucl. Phys. A **565** (1993) 1.
[6] S. Kubono *et al.*, Eur. Phys. J. A **13** (2002) 217.
[7] T. Teranishi *et al.*, Phys. Lett. B **556** (2003) 27.
[8] J. J. He *et al.*, CNS Annual Report 2002 (2003) 51.
[9] J. J. He *et al.*, CNS Annual Report 2003 (2004) 34.
[10] S. Kubono, Nucl. Phys. A **693** (2001) 221.
[11] J. F. Ziegler *et al.*, *The Stopping and Range of Ions in Solids* (Pergamon Press, New York, 1985).
[12] A. M. Lane and R. G. Thomas, Rev. Mod. Phys. **30** (1958) 257.
[13] N. M. Larson, *A Code System for Multilevel R-Matrix Fits to Neutron Data Using Bayes' Equations*, ORNL/TM-9179/R5 (Oct. 2000).
[14] W. C. Reich and M. S. Moore, Phys. Rev. **111** (1958) 929.
[15] R. O. Nelson *et al.*, Nucl. Instrum. Methods. A **236** (1985) 128.

Study of ^{13}N $+ p$ Resonance States

T. Teranishi[a], S. Kubono, H. Yamaguchi, J. J. He, A. Saito, Y. Wakabayashi[a], H. Fujikawa,

G. Amadio, S. Nishimura[b], M. Nishimura[b], J. Y. Moon[c], C. S. Lee[c], A. Odahara[d], D. Sohler[e],

M. Niikura, Z. H. Li[f], G. Lian[f] and L. H. Khiem[g]

Center for Nuclear Study, Graduate School of Science, University of Tokyo
[a]*Department of Physics, Kyushu University*
[b]*RIKEN (The Institute of Physical and Chemical Research)*
[c]*Chung-Ang University, Korea*
[d]*Nishinippon Institute of Technology*
[e]*ATOMKI (Institute of Nuclear Research of the Hungarian Academy of Sciences), Debrecen, Hungary*
[f]*China Institute of Atomic Energy, China*
[g]*Institute of Physics and Electronics, Vietnam*

1. Introduction

We have studied resonance levels in ^{14}O using a ^{13}N+p elastic resonance scattering. Figure 1 shows the energy level diagram of ^{14}O. The properties of low-lying resonances in ^{14}O above the ^{13}N+p threshold are important to study the stellar ^{13}N(p,γ)^{14}O reaction rates and the nuclear structure of ^{14}O. It is known that the 5.17-MeV level in ^{14}O dominates the ^{13}N(p,γ) rates in the hot CNO cycle [1]. However, information on some low-lying resonances is incomplete. For example, the spin and width of the 6.79-MeV level are not determined yet and widths of 5.92 and 6.59-MeV levels are given only as the upper limits [2]. Determination of these values help understand the nuclear structure and may modify the scenarios of hydrogen burning involving the ^{13}N(p,γ) reaction at high temperatures.

2. Experiment

The ^{13}N+p experiment was performed in inverse kinematics with a secondary ^{13}N beam and a proton target. The ^{13}N beam was produced by the ^{13}C(p,n)^{13}N reaction in inverse kinematics. The primary ^{13}C beam was accelerated using an upgraded AVF cyclotron at RIKEN up to 6.0 MeV/nucleon with an intensity of 400 pnA. The production target was a hydrogen gas with a thickness of 0.33 mg/cm^2. The gas was confined in a cell with a pressure of 1 atm by two Havar window foils of 2.2 μm. After the CRIB separator [3], the ^{13}N secondary beam had an energy of 3.7 MeV/nucleon and an intensity of 3.2×10^5 particles/sec.

A thick-target method [4, 5] was used to measure the excitation function of the ^{13}N+p scattering efficiently. A polyethylene sheet of 8.2 mg/cm^2 was set as a proton target. Due to the energy-loss process of the beam in the target, a wide center-of-mass energy (E_{CM}) range was scanned without changing the beam energy before the target. While the beam particles were completely stopped in the target, most of the recoil protons went out from the target with small energy losses. The recoil protons were detected by the three sets of silicon detectors at laboratory angles of θ_{LAB} = 0°, 16°, and 24°. Each set consisted of ΔE and E layers with thicknesses of 75 and 1500 μm, respectively. Protons were identified with the information of ΔE, E, and timing.
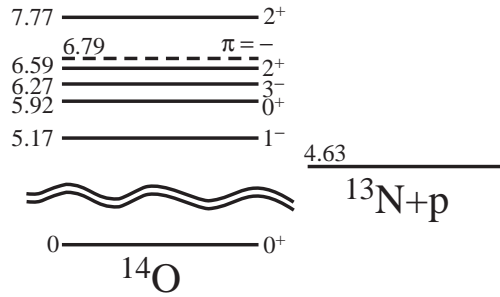
Figure 1. Energy levels of ^{14}O. Energy, spin and parity values are shown with the levels. The energy values are in MeV and relative to the ground state of ^{14}O.

The E_{CM} and center-of-mass angle (θ_{CM}) were determined by measuring the energy and angle of protons.

3. Results

The analysis is in progress to evaluate new information on E_x, Γ, and J^π of the ^{13}N+p resonances. In the preliminary spectra of ^{13}N+p, there were peaks corresponding to the levels at 5.17, 6.27, 6.79, and 7.77 MeV. The spin and width of the 6.79-MeV level were newly deduced from the spectra. The spectral shapes for the 5.17, 6.27, and 7.77-MeV levels were consistent with their known E_x, Γ, and J^π values. The signature of the 5.92 and 6.59-MeV levels were not clear in the spectra, indicating that their widths are much smaller than the present experimental resolution of about 30 keV (FWHM).

References

[1] P. Decrock *et al.*, Phys. Lett. B **304** (1993) 50, and references therein.
[2] F. Ajzenberg-Selove, Nucl. Phys. A **523** (1991) 1.
[3] Y. Yanagisawa *et al.*, Nucl. Instrum. Methods. A **539** (2005) 74.
[4] K.P. Artemov *et al.*, Sov. J. Nucl. Phys. **52** (1990) 408.
[5] S. Kubono, Nucl. Phys. A **693** (2001) 221, and references therein.

Study of the Proton Resonance States in ^{27}P by using a Radioactive Beam of ^{26}Si

J. Y. Moon, C. S. Lee, J. H. Lee, C. C. Yun, J. C. Kim[a], M. Youn[a],
S. Kubono[b], T. Teranishi[b], J. J. He[b], M. Notani[b], S. Nishimura[c], M. Nishimura[c],
V. Guimarães[d], R. F. Lihitenthaler[d] and S. Kato[e]

Department of Physics, Chung-Ang University, Korea
[a]Department of Physics, Seoul National University, Korea
[b]Center for Nuclear Study, Graduate School of Science, University of Tokyo
[c]RIKEN (The Institute of Physical and Chemical Research)
[d]Instituto de Física, Universidade de São Paulo, Brazil
[e]Department of Physics, Yamagata University

1. Introduction

Gamma-rays from the space which are measured by satelites provide important knowledge of nucleosynthesis occuring in the universe. Recently, the space telescope, COMPTEL, onboard CGRO has updated the 1.809-MeV γ-ray sky map. It shows that in the Galaxy, nucleosynthesis is going on very actively based on the fact that 1.809 MeV gamma-rays are still observed even in the much shorter life time of an emitter, ^{26}Al ($\tau = 1.04 \times 10^6$ y), compared to the age of the universe. To complete the evolution model of massive stars regarded as dominating sources, one should know the production rate of ^{26}Al inside the stellar sites. For the production rate, all nuclear reaction channels around ^{26}Al in the thermonuclear runaway should be taken into account. In this work, the proton resonance states in ^{27}P which play an important role in the resonant capture reaction of ^{26}Si(p, γ)^{27}P have been studied by using elastic scattering of ^{1}H(^{26}Si, p)^{26}Si and the thick target method [1, 2]. In the previous work [3], only two levels above the proton threshold were reported.

2. Experimental procedure

A radioactive beam ^{26}Si was obtained by the CNS radioactive ion beam separator (CRIB) [4, 5]. As a production target, a ^{3}He gas target of a thickness of 0.32 mg/cm^2 was used and irradiated by a primary beam of ^{24}Mg^{8+} at 7.434 A MeV with an intensity of 500 enA. The ^{26}Si beam selected by adjusting the magnetic fields of CRIB went through two PPACs and bombarded a secondary target of (CH$_2$)$_n$ of a thickness of 8.137 mg/cm^2 at 3.96 A MeV with an intensity of 1.6 kcps. The recoiled protons from inverse elastic scatterings between hydrogen targets contained in (CH$_2$)$_n$ and ^{26}Si beam particles were detected by two ΔE - E telescope systems, each of which consists of a thin PSD(Position-sensitive silicon detecter) of 75 μm thickness and a thick Si detector of 1500 μm thickness. They covered scattering angular range of -4.6° $\sim$ 4.6° with an angular resolution of 1.36° (FWHM) and 11.4° $\sim$ 23.2° with an angular resolution of 1.57° (FWHM). Trajectories of the beam particles and recoiled protons were obtained from two PPACs and PSD.They were used in conversion of the spectra in the laboratory system to those in the center-of-mass

(C.M.) system for the proton-incident excitation function. The energy resolution of the detector system in the C.M. frame was influenced by energy straggling of protons in the (CH$_2$)$_n$ material, the detector geometry, and the intrinsic detector resolution as well. To get a realistic energy resolution, a Monte Carlo method was used by including beam positions and directions on the target measured during the experiment in addition to those effects. It gave the overall energy resolution of 34 keV (FWHM) at 0° and 52 keV (FWHM) at 17°, respectively. Also, to estimate the contribution of carbon in the (CH$_2$)$_n$ target, the carbon-target runs were carried out and their proton spectra were used in background subtraction.

3. Results and discussion

The proton spectra after subtraction of the carbon background were converted into the cross section in the C.M. frame, where the solid angle of each detector system was calculated by using the Monte Carlo method and was 103 msr for 0° and 160 msr for 17° in the C.M. frame. These excitation functions have been analyzed by the R-matrix theory. We have determined the resonance parameters such as resonance energy, proton decay width, orbital angular momentum (L), and spin-parity of the resonance state, taking into account all combinations of different parameters in fitting. A fitting code, SAMMY M6-beta [6] was used. Figure 1 is a fitting result showing a good agreement with the experimental spectrum with a smallest reduced χ^2 value. Extracted values from the fitting are summarized in Table 1. In the code used in sorting data, we assumed every proton event to be elastic and thus for an inelastic peak, its position should be changed with different angles. With the comparison between two spectra, peak (a) could be regarded as an inelastic transition from the Peak (d) which corresponds to E$_x$ = 3.453 MeV seen in J. A. Caggiano *et al.* [3] to E$_x$ = 1.796 MeV in ^{26}Si because of its significant change, which was not involved in fitting. The peak (b) was fitted with an assumption that it consists of two peaks in view of its asymmetrical shape and the comparison with the mirror nucleus, ^{27}Mg. Also, this peak has been seen in other work [7] that used a Coulomb dissociation method that derived a spin-parity of 5/2$^+$ or 3/2$^+$, which is in agreement
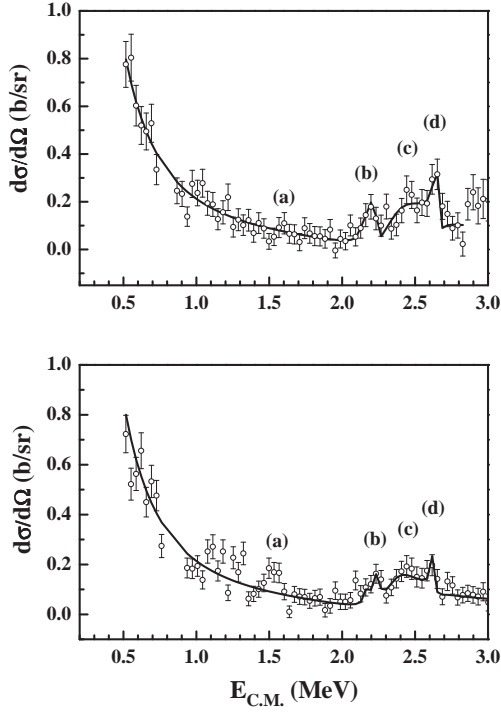
Figure 1. The proton-incident excitation functions compared with
R-matrix calculation (solid line): The upper one was obtained
from the $0°$ measurement and the lower one was obtained from
the $17°$ measurement.

with the present work. In near future, the contribution of
newly found levels to production rate of ^{26}Al will be calcu-
lated and presented.

	J^π	E_x[MeV]	Γ_p[keV]	L	Ref. [3]
(b)*	7/2+	3.040(35)	7.53±0.55	4	
	3/2+	3.084(35)	20.5±1.2	2	
(c)	3/2-	3.253(37)	309±19	1	
(d)	5/2-	3.499(35)	10.31±0.67	3	3.453(22)

*See text and figure for details.

Table 1. The resonance parameters extracted from the R-matrix
analysis by SAMMY M6-Beta code, where $E_x = 0.859$ MeV
$+ E_R$ [3].

References

[1] K. P. Artemov *et al.*, Sov. J. Nucl. Phys. **52** (1990) 408.
[2] S. Kubono, Nucl. Phys. A **693** (2001) 221, and refer-
    ences therein.
[3] J. A. Caggiano *et al.*, Phys. Rev. C **64** (2001) 025802.
[4] T. Teranishi *et al.*, Phys. Lett. B **556** (2003) 27.
[5] Y. Yanagisawa *et al.*, Nucl. Instrum. Methods. A **539**
    (2005) 74.
[6] N. M. Larson, A Code System for Multilevel R-
    matirx Fits to Neutron Data Using Bayes' Equations
    ORNL/TM-9179/R5 (Oct. 2000).
[7] Y. Togano *et al.*, in private communication. .

Production of ^{39}Ar at the CRIB Facility

Zs. Fülöp[a], H. Yamaguchi, Z. Elekes[a], S. Kubono, G. Amadio, H. Fujikawa, J.J. He, S. Michimasa[b],
J. Niikura, S. Nishimura,[b] A. Saito, T. Teranishi[c], Y. Wakabayashi[c] and Y. Yanagisawa[b]

Center for Nuclear Study, Graduate School of Science, University of Tokyo
[a]ATOMKI (Institute of Nuclear Research of the Hungarian Academy of Sciences), Debrecen, Hungary
[b]RIKEN (The Institute of Physical and Chemical Research)
[c]Department of Physics, Kyushu University

The half-life is one of the basic properties of nuclei; consequently, it is well known for the majority of isotopes. However, there are many questions not only for isotopes far from the valley of stability, but also for isotopes having half-lives of around a hundred years or more, in which the determination of the decay curve is getting difficult and the measurement should be very long. Alternative methods such as accelerator mass spectrometry (AMS) and half-life determinations based on geochemical considerations improve the situation, but also have limitations. Recently, we have developed a novel, fast and absolute implantation method, by which the isotope in question is produced as a radioactive beam, and implanted into a stopper, and its specific activity is measured after the irradiation. The advantage of the implantation method is that it allows absolute half-life determination with minimum systematic error and maximum versatility. It is also important that the measurement gives reasonable error without years of data gathering. The first measurement with this technique aimed at the half-life of ^{44}Ti and the results [1,2] confirmed the recent data.

half-life	error	method	reference
265 y	30 y	mass spectr. + activity	[5]
325 y	?	relative to ^{37}Ar	[7]
269 y	3 y	relative to ^{37}Ar	[6]
269 y	3 y	compilation	[8]
268 y	8 y	re-evaluation of [6]	[9]

Table 1. Half-life measurements and compilations for ^{39}Ar

^{39}Ar is a 100% beta-decaying isotope with a half-life of 269 years. It can be produced by the ^{39}K(n,p)^{39}Ar reaction underground [3] and by cosmic-ray-induced spallation reactions [4]. The determination of the ^{39}Ar concentration in rocks and groundwater gives valuable data for geochemical studies. By comparing the concentration of ^{37}Ar ($T_{1/2} = 35$ d) with that of ^{39}Ar in meteorites, the cosmic ray distribution in the solar system can be estimated [4]. As shown in Table 1, apart from an early study [5] with large errors, there is only one measurement on the half-life of ^{39}Ar. Stoenner et al. [6] determined the half-life by mass spectrometry and activity determination and gave a result of 269 ± 3 y, upgrading their preliminary value of 325 y [7]. This value is widely accepted and cited in compilations [8]. It should be noted, however, that according to Holden [9] the error in the original data is underestimated by a factor of three and having reanalyzed the errors, 268 ± 8 y was proposed. The half-life of ^{39}Ar is too

long to obtain its decay curve. For example, in the case of ^{32}Si ($T_{1/2} = 170$ y), a measurement of four years was necessary to give a result. Since argon is a noble gas, the AMS technique is also difficult to apply, because a negative ion source is needed [10, 11]. The implantation method, however, is suitable for the ^{39}Ar half-life measurement, because it is not necessary to determine the decay curve, but only to detect the activity of the implanted isotopes. As a first step towards the determination of ^{39}Ar half-life, the production of ^{39}Ar was tested at the CNS low-energy in-flight type RI beam separator, CRIB. The ^{39}Ar particles were produced by (^{3}He,^{4}He) reaction in inverse kinematics using a 4.5 MeV/nucleon ^{40}Ar with a ^{3}He gas target. The ^{39}Ar products were separated at charge states of 15^+ and 16^+ by the CRIB separator, and further separation was provided by a Wien filter. Two PPACs and a silicon detector served as detectors for particle identification and position determination. The ^{39}Ar particles were completely separated from ^{40}Ar at a beam rate of 10^4 cps, and the ^{39}Ar content was around 500 cps. In summary, the achieved intensity allows the preparation of ^{39}Ar samples by implantation to investigate its half-life.

References

[1] Zs. Fülöp et al., in *Proceedings Nuclei in the Cosmos V*, edited by N. Prantzos and S. Harissopulos (1998) 281.
[2] T. Hashimoto et al., Nucl. Phys. A **686** (2001) 591.
[3] T. Florkiwski, J. Phys. G **17** (1991) S513.
[4] R. C. Reedy et al. Science **219** (1983) 127.
[5] H. Zeldes et al., Phys. Rev. **86** (1952) 811.
[6] R. W. Stoenner et al., Science **148** (1965) 1328.
[7] R. W. Stoenner et al., J. Geophys. Res. **65** (1960) 3025.
[8] P. M. Endt, Nucl. Phys. A **521** (1990) 1.
[9] N. E. Holden, Pure Appl. Chem. **62** (1990) 941.
[10] W. Kutschera, Annu. Rev. Nucl. Part. Sci. **40** (1990) 411.
[11] I. Ahmad et al., ANL Annual Report 2001, ANL-02/15 (2002) 79.

Study of Low Energy Nuclear Reaction Measurements using Monolithic Silicon Telescope at CRIB

S. Nishimura, M. Kurata-Nishimura, H. Fujikawa[a], A. Guilherume[a], J. J. He[a], S. Kubono[a],
H. Yamaguchi[a], T. Teranishi[b], Y. Wakabayashi[b], S. Bishop, M. Kurokawa, T. Kishida and
T. Motobayashi

RIKEN (The Institute of Physical and Chemical Research)
[a]*Center for Nuclear Study, Graduate School of Science, University of Tokyo*
[b]*Department of Physics, Kyushu University*

1. Introduction

The ^{8}Li(α,n)^{11}B reaction has recently been identified as one of important reaction paths for passing through the valley of A=8 in the synthesis of ^{12}C and heavy elements in the early stages of Big Bang. Similarly, the inclusion of the pathway that involves the ^{8}Li(α,n)^{11}B reaction in r-process nucleosynthesis changes the final heavy nuclei abundances according to full network calculations [1].

Various experiments in the past decade have attempted to determine the reaction cross section of ^{8}Li(α,n)^{11}B [3,4,5,6]. However, previous measurements have produced inconsistent results and have been unable to study the lowest resonances of interest due to the difficulties of particle identification of low-energy ^{11}B ions from the background particles, which mainly consists of elastically scattered ^{8}Li ions, and α particles as well as the decay products of ^{8}Li.

A new approach for exploring the low-energy nuclear reactions using ultrathin silicon detector has been investigated in the simulation code GEANT4 [7, 8]. Our studies show that application of monolithic detector [9] consisting of five ultrathin silicon pads (ΔE) of 1 μm thickness supported by 508-μm-thick silicon detector (E) enables us to measure the low energy nuclear reactions in the gas target. The performance of the monolithic silicon detector itself has been studied using low-energy ^{11}B and ^{7}Li ions from an accelerator together with α particles from a source (^{241}Am) [10]. Our result shows that the monolithic silicon detector has an excellent capability for identifying the low-energy ^{11}B from the ^{7}Li ions and α particles down to the energy of 0.11 MeV/u, which corresponds to the lowest separation energy of this detector as determined by the stopping range of the incident ^{11}B ions within the first ΔE layer. Here, our first attempt of ^{8}Li(α,n)^{11}B reaction measurement using the monolithic silicon detector array will be reported.

2. Experiment

The ^{8}Li(α,n)^{11}B reaction was measured in the inverse kinematics at CRIB, where the primary beam of ^{7}Li ions were accelerated up to 24 MeV and were impinged on deutron gas target at the F0. ^{8}Li nuclides produced via the reaction d(^{7}Li,p)^{8}Li were then monmentum-filtered from the intense ^{7}Li primary beam by an aperture inserted at the dispersive focal plane at F1. In addition, a Wien filter in conjunction with the time-of-flight information among the RF and two PPACs enabled us to extract pure ^{8}Li ions at the detector section of F3. The energies of ^{8}Li ions passing
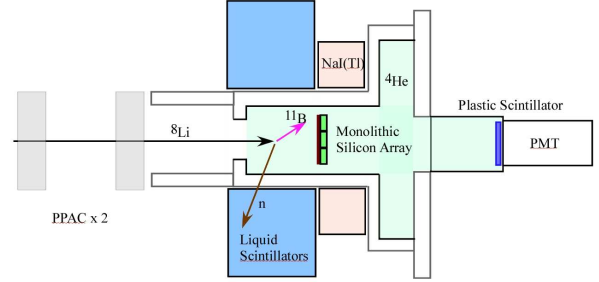
Figure 1. Schematic diagram of the experimental setup at CRIB.

through 7 μm Mylar foil, two tracking detectors (PPACs), and the entrance window of gas cell (2 μm thick Mylar foil) were decreased to 0.25 $\pm$ 0.05 MeV/u corresponding to the E$_{cm}$ of $\sim$ 0.5 MeV. The incident ^{8}Li beam and reaction products in the 6 cm He gas cell were detected by 18 sets of monolithic silicon detectors in the downstream. The intensity of the ^{8}Li beam was about $3\pm2 \times 10^3$ nuclides/s after the gas cell window. In addition, the He gas cell were surrounded by an array of neutron detectors and γ-ray detectors to measure any coincident neutrons as well as the γ-rays corresponding to the decay of excited states in ^{11}B. Figure 1 shows a schematic view of the experimental setup. Data is gathered using beam-triggering mode by PPAC without requiring extra detector biases as a primary experiment.

3. Results

Figure 2(a) and (b) show the preliminary results obtained using the monolithic silicon detectors, where the different spectra were obtained between the ^{4}He gas pressures of 0 and 100 Torr. Since the incident ^{8}Li are directly implanted to the monolithic silicon detectors, large amount of ^{8}Li ions is seen in the ΔE below 2000 ch. The data is collected with minimum bias data. The cluster in large ΔE region indicates the ^{11}B from the ^{8}Li(α,n)^{11}B reactions.

4. Summary

We have performed the first experiment for the ^{8}Li(α,n)^{11}B reaction using the ultrathin monolithic silicon detectors. The results show that the monolithic silicon detector array enables us to identify the ^{8}Li(α,n)^{11}B reactions even at the E$_{cm}$ around 0.5 MeV efficiently. The analysis of the neutron and the γ-ray measurements is in progress for the evaluation of possible reaction trigger for the future experiments with higher beam intensities above 10^6 cps.
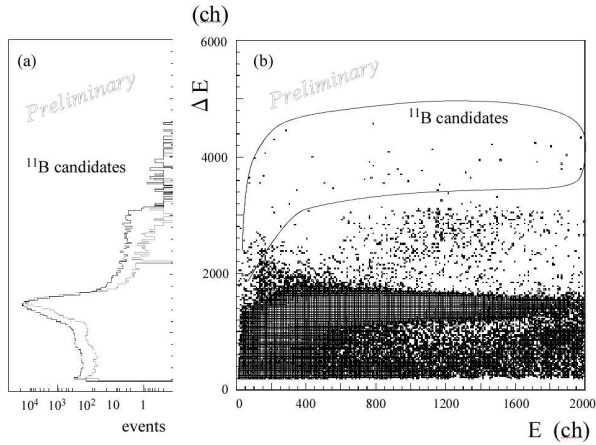
Figure 2. (a) Comparison of ΔE spectrum between the empty target runs and ^{4}He target runs. (b) Correlation between the energy deposited in ΔE and E layers. There are clusters at large ΔE area where the reaction products of the ^{11}B are expected from the ^{8}Li$(\alpha,\text{n})^{11}$B reactions.

References

[1] M. Terasawa *et al.*, Astro. J. **562** (2001) 470.

[2] T. Kajino *et al.*, Nucl. Phys. A **704** (2002) 165c.

[3] X. Gu *et al.*, Phys. Lett. B **343** (1995) 31.

[4] R. N. Boyd *et al.*, Phys. Rev. Lett. **68** (1992) 1283 .

[5] Y. Mizoi *et al.*, Phys. Rev. C **6206** (2000) 5801.

[6] S. Cherubini *et al.*, Eur. Phys. J. A **20** (2004) 355.

[7] M. K-Nishimura *et al*, RIKEN Accel. Prog. Rep. **37** (2004) 183.

[8] M. K-Nishimura *et al.*, Nucl. Phys. A **758** (2005) 162c.

[9] A. Musumarra *et al.*, Nucl. Instrum. Methods. A **409**, (1998) 414.

[10]S. Nishimura *et al.*, RIKEN Accel. Prog. Rep. **38** (2005) 142.

Simulations on the γ-ray Detection in the $^7\mathrm{Be} + p$ Scattering Experiment

G. Amadio, H. Yamaguchi and S. Kubono,

Center for Nuclear Study, Graduate School of Science, University of Tokyo

Despite much effort has been made [1]- [6] to improve the measurements of the $^7\mathrm{Be}(p,\gamma)^8\mathrm{B}$ reaction cross section, it still remains as one of the experimental challenges in the road to a better understanding of the nature of our Universe. Once it produces, mostly, the high energy neutrinos to which experiments on earth, like Super Kamiokande (Kamioka, Japan) and SNO (Sudbury, Canada), are sensitive, it plays an important role in testing the existing solar models, thus helping to solve the solar neutrino problem [7]. Not surprisingly, the structure of $^8\mathrm{B}$ itself is not yet well known to certain extent, and also deserves some attention from experimentalists. For instance, the parameters for a suggested broad state (possibly 2^-) at about 3.0~3.5 MeV in excitation energy, that could have some influence in the $S_{17}(0)$ factor are not precisely determined. Spin-parity assignment can also be thought as somewhat doubtful, once data from existing $^7\mathrm{Be}+p$ elastic scattering experiments are either poor [8] or do not cover this energy region [9], in which case the assignment depends on the effects of this state at lower energies. Taking these considerations as a motivation, we thought it would be interesting to study the $^7\mathrm{Be}+p$ elastic scattering with a broader energy range, to improve confidence of assignments for the parameters of this state. In addition, there are some interesting analog states that may be seen in the experiment, as they are also not well known in $^8\mathrm{Li}$.
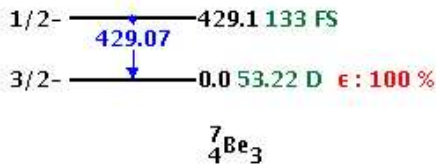
Figure 1. Diagram showing the decay of $^7\mathrm{Be}$

The thick target method has the advantage that excitation funtion can be measured at once, decreasing the total time needed for the experiment. It is not possible, however, to know the total energy, since $^7\mathrm{Be}$ stops inside the target. Therefore, one of the natural concerns that arise is the contribution of inelastic scattering to the cross section we want to measure. In the energy region of interest, only the first excited state has significant contribution, and detection of the γ-rays from the decay to the ground state ($E_\gamma = 429$ keV) in coincidence with proton should be enough to make elastic and inelastic scatterings distinguishable.

As NaI detectors cannot be used inside vacuum, we need some other way to bring them close to the target. In the current setup (shown in Figs. 2 and 3) this is done by using a cylindrical flange placed at the top of F3 chamber of CRIB. The surface that separates NaI detectors from vacuum should have minimum γ-ray absorption and hold 1atm pressure without a large bending. We chose a 2mm thick
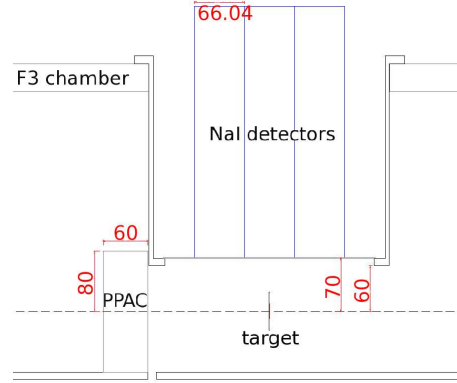
Figure 2. Side view of experimental setup
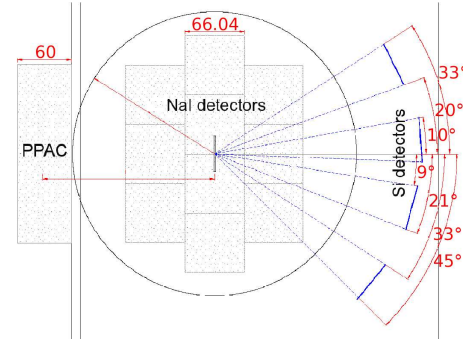
Figure 3. Top view of experimental setup

Al plate, which is attached to the bottom of the flange by a ring and screws. The calculated bending due to pressure is roughly 6mm.

To calculate the total detection efficiency for this setup, Monte Carlo techniques were used, and the results are presented. The simulations of crystal efficiency were made using the EGSnrc code [10] and the XCOM database [11]. EGSnrc consists basically of a FORTRAN-like programming language in which the user is requested to provide a function describing the geometry of the system. Total efficiency (solid angle $\times$ crystal efficiency) for a distance of 72mm is 16.3%. From this value we should subtract the loss due to absorption in the Al plate and detector cover materials, which varies with incident angle, and is roughly $0.8 \sim 1.2\%$ (absolute value). The solid angle alone is presented in Fig.4 as a function of distance for the cases where nine and ten detectors are used.

In this setup, we should also consider the background due to the β-decay of $^7\mathrm{Be}$ deposited in the polyethylene target to the first excited state of $^7\mathrm{Li}$ ($E_\gamma = 470\mathrm{keV}$). If we consider the decay law equation, adding the beam as a source for particles, we get the following differential equation

$$dN = I - \lambda N$$
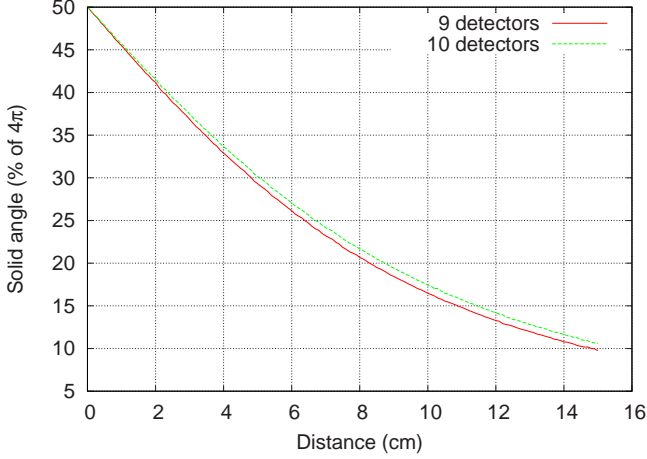
Figure 4. Solid angle as a function of the distance from the bottom of detectors to beam line

where I is the beam intensity and $\lambda = ln(2)/\tau_{1/2}$ the decay constant for ^{7}Be. The solution for this equation is

$$N(t) = (I/\lambda)(1 - e^{-\lambda t}).$$

If we take $I = 10^6$ particles per second, $\tau_{1/2}(^7\text{Be}) = 53$ days, $\Gamma = 10.52\%$ (branching ratio of these decays to the first excited state of ^{7}Li), and the ratio $\sigma_{in}/\sigma_{el} = 1/4$, we get a value of $\approx 0.5\%$ of inelastic counts as background. Figs. 5 and 6 show examples of simulations with 2% and 6% background contribution, with a gaussian fit to the ^{7}Be* γ-ray peak, to show the small contribution of the background. The expression for the background (for 1 day ^{7}Be accumulation) is

$$Bg(\%) = 8.64 I \lambda \Gamma \frac{\sigma_{el}}{\sigma_{inel}} \times \Gamma_{gate}(\mu s),$$

so that

$$8.64 \times 10^6 \times \frac{ln(2)}{53 \times 86400} \times \frac{4}{1} \times 1 \approx 0.55.$$

for a gate of $1\mu s$. This value means that when we take coincidence of Si detectors and NaI detectors, 0.5% of the counts are due to β-decay of ^{7}Be. The assumed beam intensity corresponds to the limit that can be used with PPAC.

The last thing is how to subtract this background from elastic scattering events and how to distinguish between background and inelastic events, since inelastic events are also useful for nuclear structure analysis. Also, these background events are actually unlucky elastic events that coincided with a β-decay γ-ray, they need to be added again to the elastic spectrum. One way of making this distinction, if we have good energy resolution and enough statistics, is to subtract the spectrum of events in coincidence with the lower energy portion of inelastic peak from the events in coincidence with the higher energy portion, which gives just the background event spectrum, then subtract this from the total coincidence spectrum to get inelastic-only events.
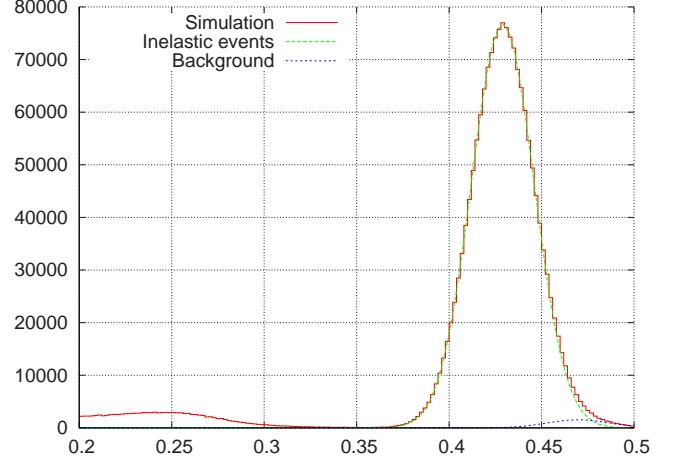
Figure 5. Simulation for 2% background contribution
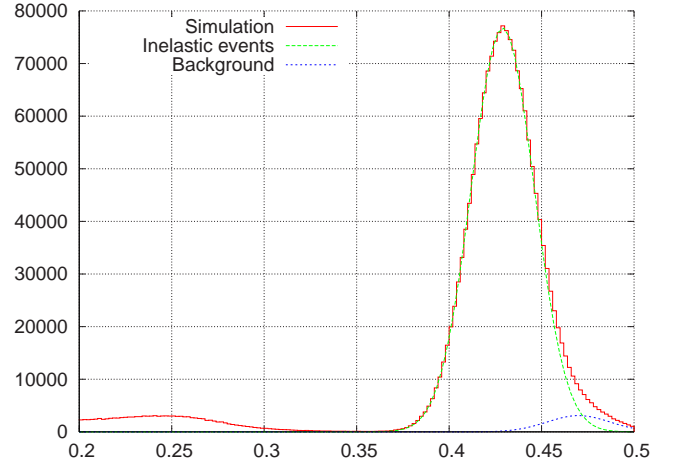
Figure 6. Simulation for 6% background contribution

References

[1] E. G. Aldberger *et al.*, Rev. Mod. Phys. **70** (1998) 1265.

[2] F. Hammache *et al.*, Phys. Rev. Lett. **86** (2001) 3985.

[3] T. Motobayashi *et al.*, Phys. Rev. Lett. **73** (1994) 2680.

[4] T. Kikuchi *et al.*, Phys. Lett. B **391** (1997) 261.

[5] N. Iwasa *et al.*, Phys. Rev. Lett. **83** (1999) 2910.

[6] B. Davids *et al.*, Phys. Rev. Lett. **86** (2001) 2750.

[7] J. N. Bahcall, *Neutrino Astrophysics* (Cambridge University Press, Cambridge, 1989).

[8] V. Z. Gol'dberg, G. V. Rogachev, M. S. Golovkov, V. I. Dukhanov, I. N. Serikov and V. A. Timofeev, JETP Lett. **67** (1998) 1013.

[9] G. V. Rogachev, J. J. Kolata, F. D. Becchetti, P. A. DeYoung, M. Hencheck, K. Helland, J. D. Hinnefeld, B. Hughey, P. L. Jolivette, L. M. Kiessel, H. Y. Lee, M. Y. Lee, T. W. O'Donnell, G. F. Peaslee, D. Peterson, D. A. Roberts, P. Santi and S. A. Shaheen, Phys. Rev. C **64** (2001) 0616101.

[10] W. R. Nelson, H. Hirayama and D.W.O. Rogers, The EGS4 code system, Stanford Linear Accelerator Center (1985).

EGSnrc http://www.slac.stanford.edu/egs/

[11] XCOM Photon Cross Section Database, http://physics.nist.gov/PhysRefData/Xcom/Text/XCOM.html

Development of a High-Precision Method for Alpha Resonant Scattering Measurements for Nuclear Astrophyics

H. Fujikawa[a], S. Kubono[a], A. Saito[a], H. Yamaguchi[a], G. Amadio[a], J. J. He[a], L. H. Khiem[b], S. Nishimura[c], H. Ohta[d], A. Ozawa[d], Y. Tagishi[c], Y. Wakabayashi[a,e], M. Yamaguchi[d] and T. Yasuno[d]

[a]Center for Nuclear Study, Graduate School of Science, University of Tokyo
[b]Institute of Physics and Electronics, Vietnam
[c]RIKEN (The Institute of Physical and Chemical Research)
[d]Institute of Physics, University of Tsukuba
[e]Department of Physics, Kyushu University

1. Introduction

The α-induced reactions such as (α,p), (α,n) are important in astrophysical nucleosynthesis. For instance, in novae and X-ray bursts, the rapid proton-capture (rp-) process is considered to start with nuclear reactions of the breakout process from the hot-CNO cycle. One of the breakout reactions for X-ray bursts is the $^{14}O(\alpha,p)^{17}F$ reaction [1], partly because the hydrogen burning of ^{14}O is inhibited since ^{15}F is proton unbound. Another example is the $^8Li(\alpha,n)^{11}B$ reaction [2], recognized as an important reaction to pass through the valley of $A=8$ in the primordial nucleosynthesis. Thus, properties of α resonances especially in unstable nuclei are important for nuclear astrophysics.

We have been working to establish an experimental method to measure such α resonances with high precision. This method should be useful for studies of astrophysical (α,p) reaction and α-clustering aspects in nuclear structures. A gaseous helium target cooled down to 30 K confined in Havar windows was used in our previous experiment [1]. In the present study, a helium gas target at room temperature was used for the α resonant scattering with the thick target method [3]. The silicon detectors for recoil particles are set in the gas to minimize the energy loss and the multiple scattering of the incident and recoil particles in confining foils. We aimed at measuring the energy and the scattering angle of recoil α particles.

2. Experimental Method

In order to obtain information on the scattering angle of α particles, the position where the corresponding elastic scattering occurred has to be determined precisely by taking into account the energy loss of the α particles in the gas and the kinematics in addition to the hit position at the telescope. Figure 1 shows a schematic view of the experimental setup. It was assumed that an incident particle goes into helium gas with a pressure of 500 Torr at $z=0$ mm and goes along the z axis with decreasing its kinetic energy. Then, an elastic scattering could occur at a z-position with a corresponding center-of-mass energy, and an α particle could be recoiled with some scattering angle toward an position sensitive detector which is located at $z=360$ mm. Then, the position where the elastic scattering occurred can be de-duced from the energy of the recoil particle, the position of detector and the energy loss in the gas. Figure 2 shows the acceptance (the ranges of E_α and $\theta_\alpha^{c.m.}$ covered by the detector) of a 50×50 mm^2 detector located at $x_{center}=0$ and $x_{center}=50$ mm. Each dotted line corresponds to different strips at $x_{strip}=3, 6, 9, 12, 15, 18, 20, 25, 40, 50, 70, 75, 80$ and 100 mm. Dashed lines show the relation between the kinetic energy and the angle of recoil α particles from $z=150$ mm ($E_1^{c.m.}$) and $z=230$ mm ($E_2^{c.m.}$). The dash-dotted line shows the detection limit, since recoil particles with lower energies would stop in the helium gas, before reaching the detector. The spectrum of each strip along these dashed lines shows the angular distribution of the scattered particles at certain center-of-mass energy.
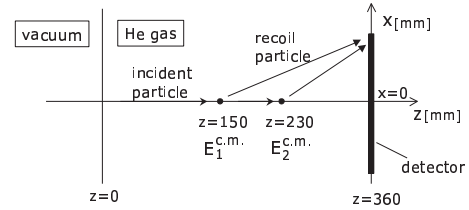
Figure 1. The schematic view of the experimental setup
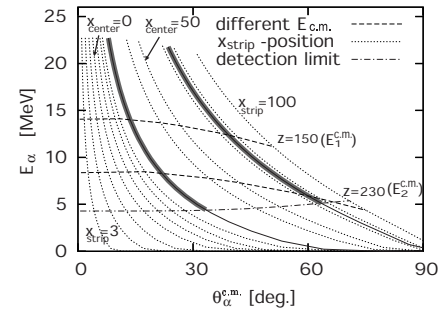
Figure 2. The acceptances of a 50×50 mm^2 detector are shown. Heavy lines show the edges of the detector when located at $x_{center}=0$ and $x_{center}=50$ mm.

3. Experiment

The experiment was performed for a development on the method to measure α resonant scattering. The elastic scattering of $\alpha+^{16}O$ was chosen since the properties of the α resonances in ^{20}Ne are well known. Figure 3 shows the

schematic view of the experimental setup. An ^{16}O beam at 40 MeV was supplied by the 12UD Pelletron tandem accelerator at the University of Tsukuba Tandem Accelerator Center (UTTAC). In the beam-monitoring section, the beam was collimated by a double-collimator system. A carbon foil with a thickness of 100 μg/cm^2 was set after the collimator. A silicon detector was set at 12 deg. relative to the beam direction in order to monitor the beam current using the ^{16}O+^{12}C elastic scattering.
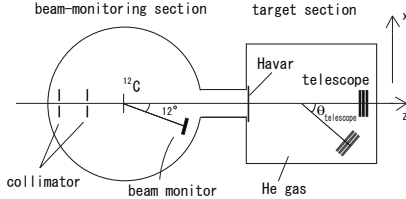
Figure 3. The schematic view of the experimental setup

The setup for measuring the α resonant scattering is shown in the target section in Fig. 3. A helium gas at room temperature was used as a target. The gas was confined by a Havar foil whose thickness and areal size were 2.2 μm and 20 mm$^\phi$, respectively. In order to use the thick target method, the pressure of helium gas was adjusted so as to stop the beam particles fully before the telescope in the gas. The energy of the ^{16}O beam decreased down to 32.5 MeV after the carbon foil in the beam-monitoring section and the Havar foil. The thickness of the helium gas to fully stop the beam particles at 32.5 MeV was calculated to be 3.22 mg/cm^2. A telescope which consisted of two position sensitive silicon detectors (PSD1, PSD2) and a pad silicon detector (SSD) was set on the rotatable table to cover a certain range of scattering angle inside the gas. The telescope can be set at an arbitrary angle from the beam direction ($0° < \theta_{\text{telescope}} < 45°$). The recoil α particles were identified by jthe ΔE-E method. The thickness of PSD1, PSD2 and SSD were 0.02, 0.074 and 1.5 mm, respectively. The active areas of them were all 50×50 mm^2. PSD1 and PSD2 were segmented to 16 strips. PSD1 has strips in horizontal direction, and PSD2 has in vertical. The distance between the Havar foil and the telescope at 0 deg. was 310 mm.

The measurements were performed at several settings of the gas pressure and the angle of the telescope summarized in Table 1. Figure 4 shows a energy spectrum of α particles measured by the strip at 0 deg. in the 470 Torr helium gas. Several peaks were observed which correspond to known levels in ^{20}Ne [4].

pressure [Torr]	$\theta_{\text{telescope}}$ [deg.]
600	0, 7, 15, 22, 30, 37.5, 45
500	0, 20, 40
470	0
450	0, 20, 40

Table 1. The gas pressure and the angle of the telescope for each measurement.
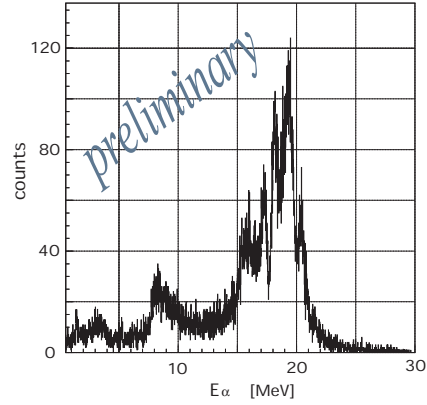
Figure 4. Energy spectrum of recoil α particles measured at 0 deg.

4. Summary

An experiment was performed for a development on an experimental method that enables to measure heavy ion + α resonant scattering. The excitation function of α+^{16}O resonant scattering was measured with the thick target method that used a helium gas at room temperature and the silicon detector set in the gas. Further analysis to improve resolutions of the energy and the angle is in progress.

References

[1] M. Notani, *et al.*, Nucl. Phys. A **738** (2004) 411.
[2] M. K-Nishimura, *et al.*, CNS Annual Report 2003 (2004) 42.
[3] S. Kubono, *et al.*, Nucl. Phys. A **693** (2001) 221.
[4] D. R. Tilley, *et al.*, Nucl. Phys. A **636** (1998) 249.

Search for High-Spin Isomers in $N = 51$ Isotones using a Secondary ^{17}N Beam

Y. Wakabayashi[a,c], A. Odahara[b], Y. Gono[d], T. Fukuchi[e], T. Teranishi[a], S. Kubono[c],
H. Yamaguchi[c], A. Saito[c], E. Ideguchi[c], S. Nishimura[d], J. J. He[c], H. Fujikawa[c], G. Amadio[c],
S. Ota[f], J. Y. Moon[g], M. Notani[h], Y. Yanagisawa[d], S. Michimasa[d], S. Shimoura[c], H. Watanabe[i],
T. Kishida[d], H. Baba[d], M. Nishimura[d] and T. Ishii[j]

[a] *Department of Physics, Kyushu University*
[b] *Nishinippon Institute of Technology*
[c] *Center for Nuclear Study, Graduate School of Science, University of Tokyo*
[d] *RIKEN (The Institute of Physical and Chemical Research)*
[e] *Department of Physics, Rikkyo University*
[f] *Department of Physics, Kyoto University*
[g] *Chung-Ang University, Korea*
[h] *Physics Division, Argonne National Laboratory, USA*
[i] *Department of Nuclear Physics, The Australian National University, Australia*
[j] *Japan Atomic Energy Research Institute*

1. Introduction

High-spin isomers are known in N=83 isotones systematically [1]. These isomers are of stretch coupled configurations of valence nucleons excited across the neutron 82 shell gap as well as the proton 64 shell gap. They are considered to be shape isomers caused by sudden shape changes from near spherical to oblate shapes. In order to search for high-spin shape isomers in other mass regions, we selected N=51 isotones which have one neutron outside the magic 50 core and proton numbers close to the semi-magic 40 core.

Configurations of the isomers in $N = 51$ isotones are expected to be $[\nu(d_{5/2}g_{7/2}h_{11/2})\pi g_{9/2}^2]_{39/2^-}$ for odd nuclei and $[\nu(d_{5/2}g_{7/2}h_{11/2})\pi(p_{1/2}g_{9/2}^2)]_{20^+}$ for odd-odd nuclei.

2. Experimental procedure

We developed a ^{17}N secondary beam using the low-energy radioisotope beam separator (CRIB) [2] of the Center for Nuclear Study (CNS), Graduate School of Science, University of Tokyo, in order to search for high-spin isomers in $N = 51$ isotones. Since the nuclei with $Z < 40$ of $N = 51$ isotones are close to the line of stability, it is difficult to produce high-spin states in these nuclei using fusion reactions by combinations of stable beams and targets. Therefore, it is very effective to use radioisotope beams. By means of the γ spectroscopy method, high-spin isomers can be searched for the nuclei ^{90}Y, ^{89}Sr, ^{88}Rb produced by the α5n, αp5n, 2α3n channels of the ^{82}Se+^{17}N reaction, respectively.

A ^{17}N secondary beam was produced by using CRIB which consists of two dipole (D1, D2), three quadrupole (Q1, Q2, Q3), small correction magnets (M1, M2) and a Wien Filter.

An experiment for isomer search was performed in Dec. 2004. A self-support ^{9}Be target of 2.3 mg/cm^2 was bombarded by an ^{18}O^{8+} primary beam at 126 MeV to obtain a ^{17}N beam. The beam current of the ^{18}O^{8+} was 0.55 pμA at the primary target position.

A parallel plate avalanche counter (PPAC) was set at a dispersive focal plane (F1) for the tuning of secondary beam before the Wien Filter. In order to identify ^{9}Be+^{18}O reaction products, a PPAC (F2-PPAC) and a Si detector of 1.5 mm thick (F2-SSD) were installed at an achromatic focal plane (F2). A ^{82}Se secondary target of 4.9 mg/cm^2 was placed at an final focal plane (F3). A PPAC (F3-PPAC) and a 72 μm thick Si detector (F3-SSD) were also placed just upstream and downstream of the secondary target, respectively, to separate the secondary fusion reaction products from the secondary beam. Two clover Ge detectors were set to measure γ rays emitted from nuclei produced by the secondary fusion reaction. These Ge detectors were surrounded by paraffin, cadmium and lead to reduce background γ rays from thermal neutron capture reaction products. Another PPAC was placed downstream of the secondary target position in order to monitor the non-interacted secondary beam.

Particle identification of the secondary beam was made by using energies of reaction products and time differences between RF and F2-PPAC signals. Energy of ^{17}N^{7+} was determined to be 104±2 MeV. As F2-SSD was moved out during the γ-ray measurement, ^{17}O^{7+} was not separated from the ^{17}N^{7+}. The intensity of the secondary beam of ^{17}N^{7+}+^{17}O^{7+} was 2.1 × 10^5 particles/s. And the purity of that beam was 28% of total secondary beams at F2.

Data acquisition was triggered when F3-PPAC and one Ge detector were hit. A signal of F3-SSD was used to veto the accidental events during the secondary beams reached without making a secondary reaction.

3. Experimental results

In this experiment, some γ rays from nuclei, such as ^{93}Nb, produced by the ^{82}Se+^{17}N reaction were observed in the energy spectra of Ge detectors, as shown in Fig.1. The spectrum (a) shows the γ-γ prompt projection spectrum which was made by setting a gate only on a prompt peak of

the time spectrum of γ-γ coincidence. The gate width of the prompt timing of the γ-γ coincidence was set to 200 nsec. The spectrum (b) shows a delayed γ-γ projection spectrum. The delayed time condition was set in a range of 100 to 300 nsec apart from γ-γ prompt timing peak. The spectrum (c) shows another delayed γ-γ projection spectrum whose delayed time was set in a range of 1 to 2 μsec from prompt timing.

nagisawa *et al.*, Nucl. Instrum. Methods. A **539** (2005) 74.
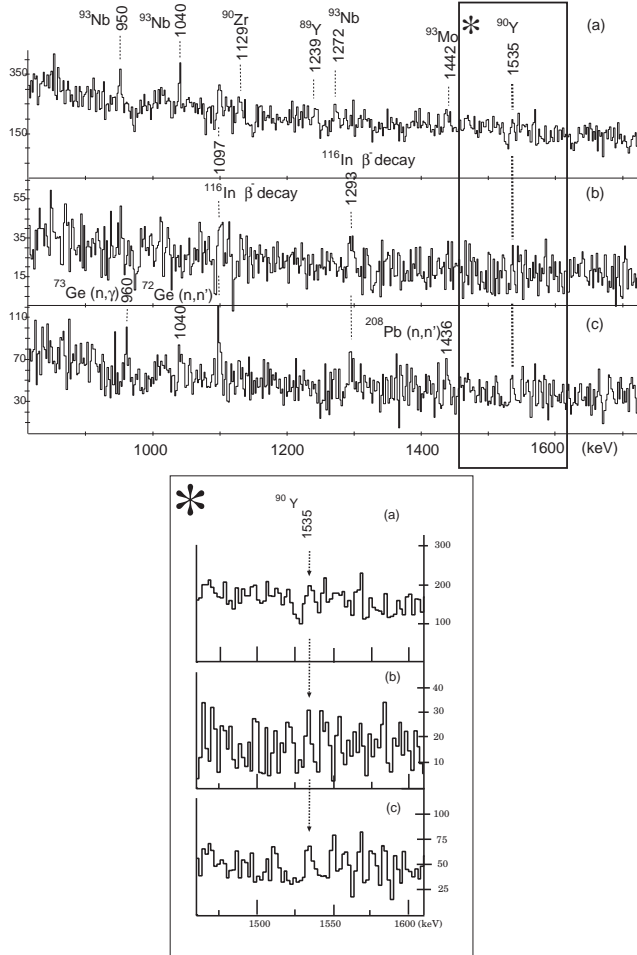
Figure 1. Projection spectra of γ-γ coincidence in various time conditions. Time conditions of spectra (a), (b) and (c) are given in the text.

A candidate of a γ ray deexciting through a new high-spin isomer was found in ^{90}Y, as a known 1535-keV transition in ^{90}Y was observed in the spectra (a), (b) and (c) of Fig. 1. This nucleus is one of the relevant nuclei in N=51 isotones. The further data analysis will be performed optimizing various gate conditions to prove the existence of a relatively long lived isomer in ^{90}Y.

References

[1] Y. Gono *et al.*, Eur. Phys. J. A **13** (2002) 5, and references therein.

[2] S. Kubono *et al.*, Eur. Phys. J. A **13** (2002) 217; Y. Ya-

Study of High-Spin States in ^{91}Zr

T. Fukuchi, N. Hokoiwa[a], Y. Wakabayashi[a,b], Y. Gono[c], A. Odahara[d], T. Shinozuka[e], M. Fujita[e], A. Yamazaki[e], T. Sonoda[e] and T. Suzuki[e]

Department of Physics, Rikkyo University
[a]*Department of Physics, Kyushu University*
[b]*Center for Nucler Study, University of Tokyo*
[c]*RIKEN (The Institue of Physical and Cehmical Research)*
[d]*Nishi-Nippon Institute and Technology*
[e]*Cyclotron and Radioisotoe Center, Tohoku University*

High-spin isomers were reported in N=83 isotones systematically [1], namely ^{143}Nd, ^{144}Pm, ^{145}Sm, ^{146}Eu, ^{147}Gd, ^{148}Tb, ^{149}Dy, ^{150}Ho and ^{151}Er. Their lifetimes range from 10 ns to a few μ sec. The excitation energies are close to each other ranging between 8.5 and 9.0 MeV, and their spin-parity is the same with J^π=49/2$^+$ and 27$^+$ for odd-A and odd-odd nuclei, respectively, except for those in ^{150}Ho and ^{151}Er.

The decay scheme and the characteristics of the high-spin isomer in ^{147}Gd were studied in detail experimentally and theoretically [2]. This high-spin isomer has been known to be the 49/2$^+$ state at 8.6 MeV and has a 510 ns half life. The deformation parameter β of this state was determined to be –0.19 based on the measurements of the static quadrupole moment. The configuration of this isomer was found to be $[\nu(f_{7/2}h_{9/2}i_{13/2})\otimes\pi(h^2_{11/2})]_{49/2^+}$ based on the g-factor obtained experimentally. These results indicate that high-spin isomer may be caused by a sudden shape change from near spherical to oblate shape. Therefore, these isomers could be described as high-spin shape isomers. Recently the same type of isomer observed in N=83 isotones was reported in ^{93}Mo which is a member of N=51 isotones [3]. In order to study the existence of the isomers of this type in other member of N=51 isotones, the high-spin states in ^{91}Zr were studied.

Experiments were performed at Cyclotron and Radioisotope Center (CYRIC) in Tohoku University. Excited states in ^{91}Zr were populated using the reaction ^{82}Se(^{16}O,α3n)^{91}Zr. The ^{82}Se target of 5.2 mg/cm^2 was enriched to 90% and a target foil was backed by 500 μg/cm^2 Au for a mechanical support. For the γ-ray detection, four clover type Ge detectors with anti-Compton shields were used. The clover detectors were operated in the add-back mode for γ-γ-t coincidence measurement. The distances between the target and the surfaces of the Ge detectors were about 13 cm. The total detection efficiency of γ-ray was 0.73% at 1.3 MeV in the singles mode. A total of 1.0×10^9 coincidence events was recorded in event by event mode.

The level scheme of ^{91}Zr is known up to the 21/2$^+$ isomer at 3167 keV [4]. The lifetime of this isomer is 4.3 μsec. In our investigation, high-spin states above 21/2$^+$ isomer were identified using delayed γ-γ coincidence technique. Figure 1 shows representative γ-ray spectrum obtained by gating on the transitions below the 21/2$^+$ isomer. Four transitions which belong ^{91}Zr were clearly identified. These de-
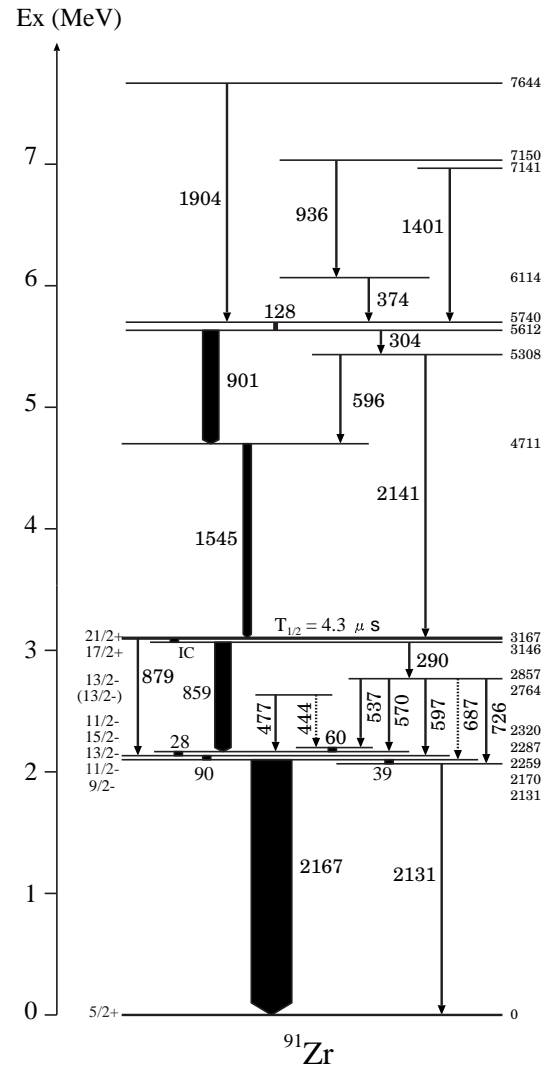
Figure 2. The proposed level scheme for ^{91}Mo. The width of the arrows indicate γ-ray intensities, while the numbers are the energies given in keV units. The transitions above 21/2$^+$ isomer are new ones.

17
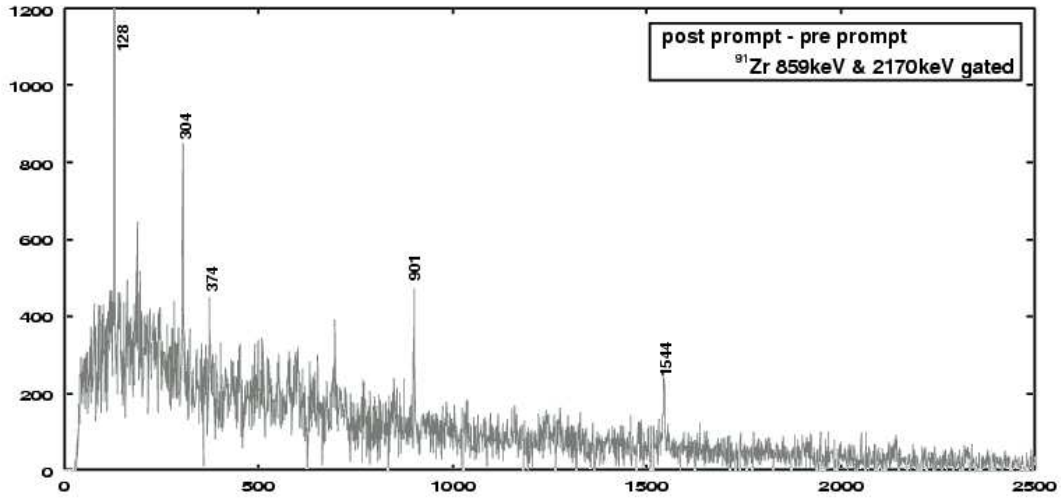
Figure 1. Gamma-ray energy spectrum obtained by gating on delayed transitions below $21/2^+$ isomer.

E_γ(keV)	I_γ	$E_i \rightarrow E_f$
1544	100	$4711 \rightarrow 3167$
901	99	$5612 \rightarrow 4711$
2141	50	$5308 \rightarrow 3167$
304	88	$5612 \rightarrow 5308$
128	84	$5740 \rightarrow 5612$
596	6	$5308 \rightarrow 3167$
1904	17	$7644 \rightarrow 5740$
1401	8	$7141 \rightarrow 5740$
374	11	$6114 \rightarrow 5740$
936	11	$7150 \rightarrow 6114$

Table 1. Measured γ-ray energies and intensities above $21/2^+$ isomer in ^{91}Zr. Relative intensities are normalized to the 1544 keV γ-ray intensity.

layed transitions are identified by requiring $t \geq 1$ μsec. in the time spectrum. The level scheme above the $21/2^+$ isomer was constructed from the spectra gated by each γ-ray peak which is seen in Fig. 1 and sum of those spectra. Ten γ rays and 8 levels were newly found above $21/2^+$ isomer. Intensities and placements in the level scheme of all γ-rays observed in this work are given in Table 1. Figure 2 shows proposed level scheme of ^{91}Zr.

The high-spin states were studied here up to 7.6 MeV excitation energy. Based on these high-spin data, we will continue to perform an experiment to search for the high-spin isomer.

References

[1] Y. Gono *et al.*, Eur. Phys. J. A **13** (2002) 5 and references therein.
[2] T. Døssing *et al.*, Phys. Scr. J. **24** (1981) 258.
[3] T. Fukuchi *et al.*, Eur. Phys. A **24** (2005) 249.
[4] B. A. Brown, P.M.S. Lesser and D.B. Fossan, Phys. Rev. C **13** (1976) 1900.

A Rotational Band in ^{107}In

E. Ideguchi, B. Cederwall[a], E. Ganioğlu[a,f], B. Hadinia[a], K. Lagergren[a], T. Bäck[a], S. Eeckhaudt[b],
T. Grahn[b], P. Greenlees[b], A. Johnson[a], D. T. Joss[c], R. Julin[b], S. Juutinen[b], H. Kettunen[b],
M. Leino[b], A.-P. Leppanen[b], P. Nieminen[b], M. Nyman[b], J. Pakarinen[b], E. S. Paul[d], P. Rahkila[b],
C. Scholey[b], J. Uusitalo[b], R. Wadsworth[e], D. R. Wiseman[d] and R. Wyss[a]

Center for Nuclear Study, Graduate School of Science, the University of Tokyo
[a]*Department of Physics, Royal Institute of Technology*
[b]*Department of Physics, University of Jyväskylä*
[c]*CCLRC, Daresbury Laboratory*
Department of Physics, Osaka University
[d]*Oliver Lodge Laboratory, Department of Physics, University of Liverpool*
[e]*Department of Physics, University of York*
[f]*Department of Physics, Faculty of Science, Istanbul University*

The structures of nuclei close to ^{100}Sn have received increasing attention in recent years. Excited states of neutron deficient nuclei with Z$\sim$50 are expected to be predominantly of single-particle nature due to the presence of a spherical shell gap for protons. However, recent experimental and theoretical investigations have elucidated additional important excitation mechanisms, such as magnetic rotation [1] and deformed rotational bands exhibiting smooth band termination [2, 3]. The wealth of excitation modes in these nuclei make them particularly interesting systems to study. In this report a study of high-spin states in ^{107}In is presented.

The experiment was performed at the JYFL accelerator facility at the University of Jyväskylä, Finland. The ^{52}Cr ions, accelerated by the JYFL K130 cyclotron to an energy of 187 MeV, were used to bombard a target consisting of two stacked self-supporting foils of isotopically enriched (99.8%) ^{58}Ni. The targets were of thickness 580 μg/cm^2 and 640 μg/cm^2, respectively. The average beam intensity was 4.4 pnA during 5 days of irradiation time. High-spin states in ^{107}In were populated by the fusion-evaporation reaction ^{58}Ni(^{52}Cr, 3p)^{107}In. Prompt γ-rays were detected at the target position by the JUROGAM γ-ray spectrometer consisting of 43 EUROGAM [4] type escape-suppressed high-purity germanium detectors. The germanium detectors were distributed over six angles relative to the beam direction with five detectors at 158°, ten at 134°, ten at 108°, five at 94°, five at 86°, and eight at 72°. In this configuration, JUROGAM had a total photopeak efficiency of about 4.2% at 1.3 MeV.

The fusion-evaporation products were separated in flight from the beam particles using the gas-filled recoil separator RITU [5, 6] and implanted into the two double-sided silicon strip detectors (DSSSD) of the GREAT [7] focal plane spectrometer.

The signals from all detectors were recorded independently and provided with an absolute "time stamp" with an accuracy of 10 ns using the total data readout (TDR) [8] acquisition system. The multifold event data was sorted offline into a E_γ-E_γ correlation matrix and a E_γ-E_γ-E_γ cube. Angular distribution and directional correlation (DCO) analyses [9] were also performed for the observed gamma rays in order to determine the multipolarities of the transitions in ^{107}In.

High-spin states in ^{107}In were previously studied up to the ($I = 33/2$) state at 6.989 MeV excitation energy [10]. The spin-parity of the ground state is $9/2^+$, arising from its $\pi g_{9/2}$ hole character. Above the isomeric $19/2^+$ level, two sequences of magnetic dipole transitions have previously been observed to connect negative parity states up to $33/2^{(-)}$ [10]. In our data, the gamma transitions previously reported were confirmed and, in addition, a rotational gamma-ray cascade consisting of the 514, 659, 822, 933, 1054, 1218, 1386, 1571, and 1786 keV transitions was observed as shown in Fig. 1. A 1972 keV transition was tentatively placed on top of the band. Another gamma-ray transition at 2334 keV, which is in coincidence with the in-band transitions, was also observed.
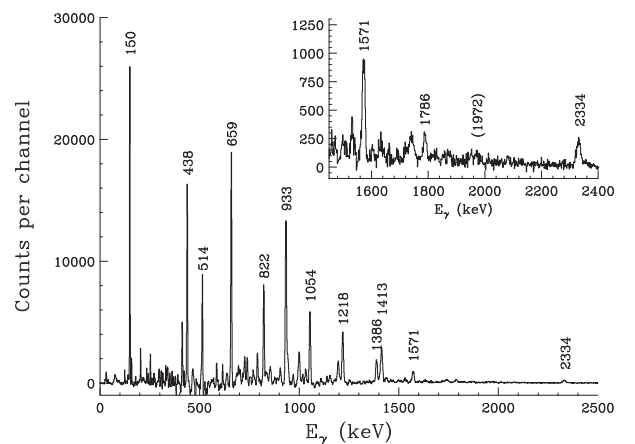
Figure 1. Sum of gamma-ray energy spectra gated by the 514, 822, 1054, 1386, 1572, and 1786 keV transitions.

The 933 keV transition has a larger intensity than the other neighbouring in-band transitions, 822 and 1054 keV since it is a self-coincident doublet. The 2334 keV γ ray is in coincidence with the assigned in-band transitions as well as the low-lying transitions, 150, 438, 413, and 1413 keV

(see Fig. 2). Since this γ ray is strongly in coincidence with the lowest-lying member of the band, it is assigned as a linking transition which connects the lowest level of the band with the $19/2^+$ state. However, we can not rule out that other, unobserved, transitions take part in depopulating the band.
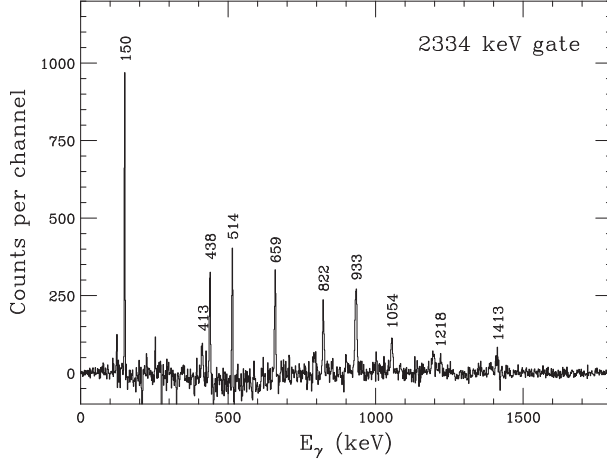
Figure 2. Gamma-ray spectrum gated by the 2334 keV transition.

The results of the angular distribution and DCO analyses are in consistent with the multipolarities of the in-band transitions being of stretched E2 character. However, due to lack of statistics, the multipolarity of 2334 keV transition was not deduced.

In order to investigate the presence of deformed configurations at high spin in ^{107}In, total Routhian surface (TRS) calculations were performed. Deformed minima in the total energy surfaces were found at $(\beta_2, \gamma) \sim (0.20, 6°)$ for both signatures at positive parity $(+,\pm1/2)$ and at $(\beta_2, \gamma) \sim (0.26, 8°)$ for the negative parity, negative signature configuration $(-,-1/2)$ as shown in Fig. 3.
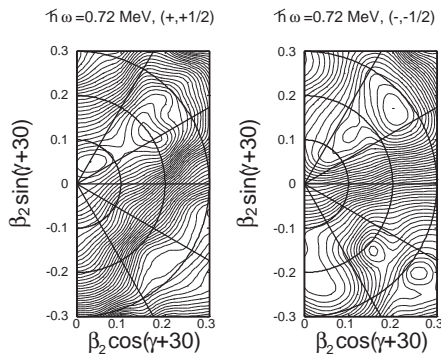
Figure 3. Calculated total Routhian surfaces at a rotational frequency of 0.72 MeV. The lowest positive parity configuration with signature +1/2 is shown in the left panel while the lowest negative parity, signature -1/2 configuration is plotted on the right hand side.

Fig. 4 shows a comparison between the experimental and calculated energies, angular momenta and dynamical moments of inertia ($J^{(2)}$). The excitation energies are given relative to a rigid rotor reference. The relative behaviour
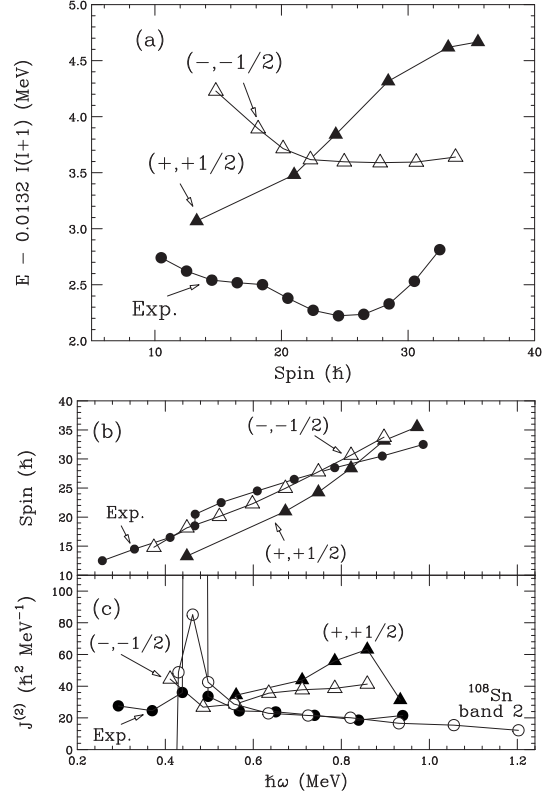
Figure 4. Comparison of experimental and calculated energy values (panel a) as a function of rotational frequency. A rigid-rotor reference energy has been subtracted from each energy value. In panels b) and c) experimental and calculated spin and $J^{(2)}$ values are plotted as a function of rotational frequency. In the $J^{(2)}$ plot, the values for band 2 in the isotone ^{108}Sn have been included for comparison.

rather than the absolute energies are of interest here since the uncertainty in the calculated absolute excitation energies is significant. Since the multipolarity of the 2334 keV linking transition was not measured, the spin-parity of the band could not be determined. We have assumed the spin of the lowest level of the band to be 21/2. As can be seen in Fig. 4, the TRS calculation for the configuration with $(\pi, \alpha)=(-,-1/2)$ is in better agreement with the experimental properties of the rotational E2 cascade than the other predicted deformed configurations (e.g. $(\pi, \alpha)=(+,+1/2)$).

The experimental data exhibit a band crossing at $\hbar\omega \approx 0.45$ MeV. It might correspond to a two-particle excitation of $g_{9/2}$ protons across the $Z = 50$ spherical shell gap into the $g_{7/2}d_{5/2}$ subshell. For the $(\pi, \alpha)=(-,-1/2)$ configuration, the lower spin states correspond to a $\pi g_{9/2}^{-1}h_{11/2} \otimes \nu(g_{7/2}, d_{5/2})^6 h_{11/2}^2$ quasiparticle structure, where the angular momentum vectors of the $h_{11/2}$ neutrons are aligned with the rotational axis. This configuration, with the possible addition of the above mentioned $\pi g_{9/2}^{-2}(g_{7/2}, d_{5/2})^2$ two-particle two-hole excitation, is predicted to be yrast in the high-spin region where the band structure is populated. Interestingly, the observed rotational band has strong similarities with two of the deformed intruder bands (bands 2 and 3) observed in ^{108}Sn [11]. A band crossing occurring

at a similar rotational frequency to what is found in ^{107}In was also observed in ^{108}Sn, band 2 where it was tentatively suggested to be due to an accidental level interaction. Since a similar alignment effect is observed also in ^{107}In a more likely scenario would be a band crossing, possibly due to a $\pi g_{9/2}^{-2}(g_{7/2}, d_{5/2})^2$ two-particle two-hole excitation or a similar $\pi(g_{7/2})^2$ quasiparticle alignment. This point will be addressed by more detailed calculations.

References

[1] A. Gadea *et al.*, Phys. Rev. C **55** (1997) R1.

[2] I. Ragnarsson *et al.*, Phys. Rev. Lett. **74** (1995) 3935.

[3] R. Wadsworth *et al.*, Phys. Rev. C **53** (1996) 2763.

[4] C.W. Beausang *et al.*, Nucl. Instrum. Methods. A **313** (1992) 37.

[5] M. Leino *et al.*, Nucl. Instrum. Methods. B **99** (1995) 653.

[6] M. Leino *et al.*, Nucl. Instrum. Methods. B **126** (1997) 320.

[7] R.D. Page *et al.*, Nucl. Instrum. Methods. B **204** (2003) 634.

[8] I.H. Lazarus *et al.*, IEEE Trans. Nucl. Sci. **48** (2001) 567.

[9] K.S. Krane *et al.*, Nucl. Data Tables A **11** (1973) 351.

[10] S.K. Tandel *et al.*, Phys. Rev. C **58** (1998) 3738.

[11] R. Wadsworth *et al.*, Nucl. Phys. A **559** (1993) 461.

Study of High-Spin States in $^{49-51}$Ti

M. Niikura, E. Ideguchi, T. Fukuchi[a], H. Baba[b], N. Hokoiwa[c], C. Ishida[d], H. Iwasaki[e], T. Koike[f], T. Komatsubara[g], T. Kubo[b], M. Kurokawa[b], S. Michimasa[b], K. Miyakawa[g], K. Morimoto[b], T. Ohnishi[b], S. Ota[h], A. Ozawa[g], S. Shimoura, T. Suda[b], M. Tamaki, I. Tanihata[i], Y. Wakabayashi[c] and K. Yoshida[b]

Center for Nuclear Study, Graduate School of Science, University of Tokyo
[a]Department of Physics, Rikkyo University
[b]RIKEN (The Institute of Physical and Chemical Research)
[c]Department of Physics, Kyushu University
[d]Department of Physics, Royal Institute of Technology
[e]Department of Physics, Graduate School of Science, University of Tokyo
[f]Department of Physics, Tohoku University
[g]Institute of Physics, University of Tsukuba
[h]Department of Physics, Faculty of Science, Kyoto University
[i]Physics Division, Argonne National Laboratory, USA

1. Introduction

In-beam gamma-ray spectroscopy by using fusion-evaporation reactions is one of the most efficient methods for the study of the nuclear structure at high-spin since large angular momentum can be brought into the system. However, nuclei produced by the fusion reaction using stable isotope beams are limited in many cases to the proton-rich side relative to the line of β-stability. In order to investigate high-spin states of neutron-rich nuclei by the fusion reaction, it is necessary to use neutron-rich secondary beams. In the nuclei ^{50}Ti and its neighbors, onsets of deformed collective states due to the presence of deformed shell gaps in $Z = 22$ and $N = 28$ are expected at high-spin states likewise the recently observed superdeformed band in ^{40}Ca [1]. In this report, study of the high-spin states in neutron-rich Ti isotopes by the secondary fusion reaction, $^{9}\text{Be}\left(^{46}\text{Ar}, xn\right)^{55-x}\text{Ti}$, is described.

2. Experiment

The experiment was performed at RIKEN Accelerator Research Facility. An ^{46}Ar secondary beam was produced by a projectile fragmentation reaction of a 63 MeV/nucleon ^{48}Ca beam incident upon a 1.0-mm thick ^{9}Be target. The fragments were separated by the RIKEN Projectile-fragment Separator (RIPS) [2]. An aluminum wedge degrader with a mean thickness of 221 mg/cm^2 placed at the momentum dispersive focal plane (F1) was used to achieve a clear isotope separation and to lower the energy of the secondary beam to $\sim$30 MeV/nucleon. The particle identification of the fragments was performed by measuring time-of-flight (TOF) and energy loss (ΔE). The TOF and ΔE information were obtained from the timing of a plastic scintillator relative to the RF signal of the cyclotron and from the energy loss in a 0.5-mm thick silicon detector placed at the achromatic focal plane (F2), respectively. The purity of the ^{46}Ar beam was measured to be 90%.

The ^{46}Ar beam was further lowered in energy using an aluminum rotatable degrader of 0.5-mm thickness placed at F2 and transported to the final focal plane (F3), where a thin 10-μm thick ^{9}Be secondary target was placed for the fusion reaction. The energy of the secondary beam was measured event-by-event by the TOF deduced from the timing between the plastic scintillator at F2 and a PPAC (Parallel Plate Avalanche Counter) [3] at F3. The mean energy and an intensity of the beam were 4.0 MeV/nucleon and 1.0×10^5 pps at the secondary target, respectively.

Gamma rays emitted from the high-spin states of fusion products were detected by the CNS-GRAPE (Gamma-Ray detector Array with Position and Energy sensitivity) [4]. In this experiment the CNS-GRAPE was composed of 17 Ge detectors and each detector has two cylindrical-shaped planar crystals that share a common anode. Cathode sides are divided into nine segments. The segmentations make it possible to determine interaction points of the detected gamma rays using pulse shape analysis [5,6]. These detectors were placed around the secondary target to cover the angular range between 60° and 120° relative to the beam direction. With a trigger condition of two or more Ge detectors firing in coincidence with the plastic and the PPACs, a total of 1×10^7 events was collected in one day measurement.

3. Analysis and Results

A Doppler-shift correction was performed based on the beam position at the target, velocity of the outgoing particle and hit positions of gamma rays on the CNS-GRAPE. These information was deduced from the position and the timing of two PPAC counters installed at up-stream and another PPAC placed down-stream of the target. After the Doppler-correction, previously known cascade gamma transitions of $^{49-51}$Ti [7,8,9] were clearly observed [10].

In ^{49}Ti four gamma transitions from the high-spin states were previously reported at the energies of 1543, 963, 785 and 1093 keV [7]. To search for higher spin states, γ-γ coincidence analysis was carried out. Figure 1 shows a sum of spectra gated on the known gamma rays of ^{49}Ti.

In the figure gamma peaks from ^{49}Ti and ^{50}Ti are marked by closed and open circles, respectively. Coinsidence relation between known gamma rays are comfirmed and a new gamma peak at 2370 keV was observed. Since the 2370 keV gamma ray is not coinsidence with gamma rays of ^{50}Ti, this new peak is identified a gamma ray from ^{49}Ti.
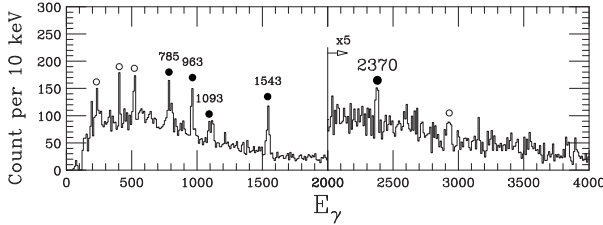
Figure 1. A sum of gated spectra with known transitions of ^{49}Ti. Gamma rays from ^{49}Ti and ^{50}Ti are marked by closed and open circles, respectively.

For ^{51}Ti we observed known gamma peaks at the energies of 1437, 907, 410 and 890 keV [9]. In fig. 2 gamma-ray spectra gated by 890, 907 and 1437 keV are shown. Coincidence relations between known gamma rays were confirmed. In addition a new gamma peak at 761 keV was observed, which is in coincidence with all gamma transitions below 3644 keV state (see fig. 3).
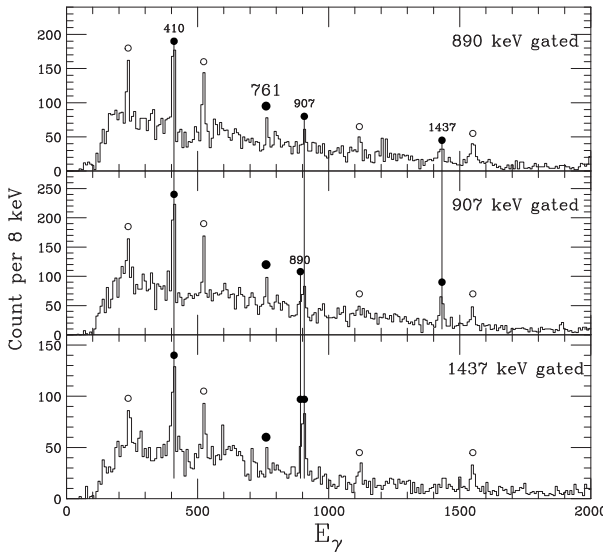
Figure 2. Gamma-ray spectra gated by 890, 907 and 1437 keV of ^{51}Ti. Gamma rays from ^{51}Ti and ^{50}Ti are marked by closed and open circles, respectively.

In this experiment the energy of the ^{46}Ar beam was broadened between 2 and 7 MeV/nucleon at the center of the secondary target due to the energy straggling after passing through the degraders and the beam-line detectors. Since cross sections of the reaction depend on the incident beam energy, the behavior of the excitation function can help identifying the evaporation channel. By gating different region of the beam energy, relative gamma-ray intensity mormalized by the beam intensity as a function of the beam energy was obtained [10]. The behavior of the relative intensity of newly observed 761 keV transition is consistent with that it is emitted from ^{51}Ti.

In fig. 3, normalized gamma-ray yields of ^{51}Ti relative to that of the lowest gamma transition at 1437 keV were plotted as a function of the beam energy. As incident beam energy increases, larger angular momentum can brought to the system and consequently a relative population of higher spin states will increases. The behavior of relative gamma-ray yields of the known transitions support the previously reported order of the cascade decay. Since the newly observed 761 keV gamma transition is largely populated in higher incident beam-energy region than the other transitions, it is assigned as the transition above the known (13/2,17/2) state at 3644 keV.
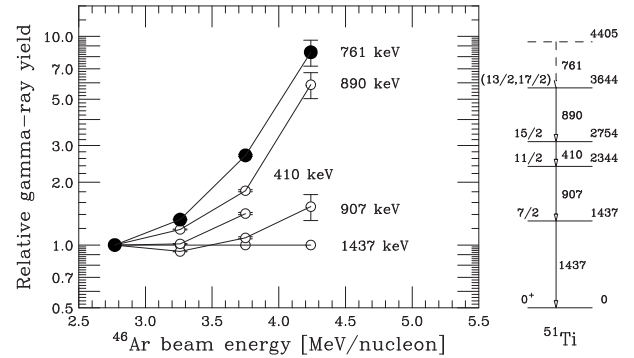
Figure 3. Relative gamma-ray yields of ^{51}Ti as a function of the incident beam energy.

4. Summary

We have studied the high-spin states in neutron-rich Ti isotopes, $^{49-51}$Ti by the secondary fusion reaction. The excitation function measurement and the γ-γ coincidence analysis were performed. The new gamma transitions from high-spin states in ^{49}Ti and ^{51}Ti were observed. Further analysis is in progress.

References

[1] E. Ideguchi et al., Phys. Rev. Lett. **87** (2001) 222501.

[2] T. Kubo et al., Nucl. Instrum. Methods B **461** (1992) 309.

[3] H. Kumagai et al., Nucl. Instrum. Methods A **470** (2001) 562.

[4] S. Shimoura, Nucl. Instrum. Methods A **525** (2004) 188.

[5] M. Kurokawa et al., IEEE Trans. Nucl. Sci. **50** (2003) 1309.

[6] C. Ishida et al., CNS Annual Report 2003 (2004) 9.

[7] M. Behar et al., Nucl. Phys. A **366** (1981) 61.

[8] B. Gass et al., Phys. Rev. Lett. **40** (1978) 1313.

[9] S. E. Arnell et al., Phys. Scr. **6** (1972) 222.

[10] E. Ideguchi et al., AIP Conf. Proc. **764** (2004) 136.

Measurement of ^{4}He(^{32}Mg,^{33}Alγ) Reaction

S. Ota, S. Shimoura[a], N. Aoi[b], E. Takeshita[c], S. Takeuchi[b], H. Suzuki[d], H. Baba[b], T. Fukuchi[a],
T. Fukui Y. Hashimoto[e], E. Ideguchi[a], K. Ieki[c], N. Iwasa[f], H. Iwasaki[d], S. Kanno[c], Y. Kondo[e],
T. Kubo[b], K. Kurita[c] T. Minemura[b], S. Mitimasa[b], T. Motobayashi[b], T. Murakami
T. Nakabayashi[e], T. Nakamura[e], M. Niikura[a], T. Okumura[c], T. K. Onishi[d], H. Sakurai[d],
M. Shinohara[e], D. Suzuki[d], M. K. Suzuki[d], M. Tamaki[a], K. Tanaka[b], Y. Togano[c], Y. Wakabayashi[g]
and K. Yamada[b]

Department of Physics, Kyoto University
[a]*Center for Nuclear Study, Graduate School of Science, University of Tokyo*
[b]*RIKEN (The Institute of Physical and Chemical Research)*
[c]*Department of Physics, Rikkyo University*
[d]*Department of Physics, University of Tokyo*
[e]*Department of Physics, Tokyo Institute Technology*
[f]*Department of Physics, Tohoku University*
[g]*Department of Physics, Kyushu University*

A picture of the evolution of the shell structure is being obtained based on the experimental result [1, 2] about the magicity loss in the $N = 8$, 20 neutron rich nuclei. The shell structure formed by the mean-field depends on the nuclear deformation, the isospin of the nuclei, and/or the occupation number of the single particle orbits. To clarify the change of the shell structure, the systematic studies on the single particle states as functions of the numbers of protons and neutrons is important.

Near the ^{33}Al, the $N = 20$ nucleus ^{32}Mg is known to have large quadrupole collectivity and to be of large deformation [2] while other $N = 20$ nucleus ^{34}Si is believed to be spherical in its ground state. The property of the ground state in ^{33}Al have been studied by Morton *et. al* via beta decay measurement [3] and the decay of ^{33}Al is described well by an *sd* shell model calculation. The candidate of a 2p-2h state of the spin and parity same as the ground state $5/2^+$ is found and its energy was 730 ± 50 keV [4], which is consistent with the shell model prediction, 672 keV (Ref. in [4]). These two different experiments suggest that those two states in ^{33}Al may be normally spherical. But the shell structure of other excited states is not clear since the single particle orbits may be affected by the deformed mean field by the ^{32}Mg core. In the present study we aim at finding new excited states and assigning their spins, parities and spectroscopic factors in ^{33}Al identified by the energies of de-excited gamma-rays and measuring the angular distributions of the differential cross sections of the proton transfer reaction ^{4}He(^{32}Mg,^{33}Alγ).

The experiment was performed with RIKEN Projectile-fragment Separator (RIPS) [5] at RIKEN Accelerator Facility. Table 1 lists apparatuses placed along the beam line. A ^{32}Mg beam was produced by projectile fragmentation of the primary beam of ^{40}Ar at 63 MeV/nucleon bombarding the primary target of 1 mm-thick carbon and separated by RIPS. The ^{32}Mg beam was contaminated with other neutron-rich isotopes such as ^{33,34}Al and ^{35,36}Si. These isotopes were identified event-by-event using time-of-flight

(TOF)-ΔE method. The TOF was obtained from the timing information of two plastic scintillator of 1 mm thickness placed at two foci of F2 and F3 and ΔE was measured by Si detector of 100 μm thickness. The position of the fragments at F2 was measured by a PPAC in order to check that RIPS was tuned to be optimal for ^{32}Mg. The energy of ^{32}Mg beam at F3 was 40 ± 2 MeV/nucleon.

The ^{32}Mg beam bombarded a liquid helium target [6] at F3. The thickness of the liquid helium target was estimated to be about 150 mm/cm^2 from the velocity difference of outgoing particles in the measurements with and without the liquid helium. The target was kept below 4 K and around 1 atm and monitored the temperature and pressure during the experiment.

Three PPAC's were placed upstream of the target for monitoring incident particles and two PPAC's were placed downstream for outgoing particles. The position information of the reaction point and the scattering angle of outgoing particles are obtained from the vertical and horizontal position measured by these five PPAC's. To improve the position resolution at reaction point for the sake of better correction to Doppler-shift of gamma-ray energy, these PPAC's were located nearby the target and apart from each other as far as possible.

We had a new focus (F4) after the liquid helium target by using Super-conducting Triplet Quadrupole magnets (STQ) [7] in order to unspread the outgoing particles, which made the size of ΔE- and E-detectors smaller and the flight length longer. For the ΔE and E-detector, 4 silicon detectors with 10 cm $\times$ 10 cm $\times$ 4 active area located after STQ and 36 NaI(Tl) detectors with 3 cm $\times$ 3 cm $\times$ 36 active areas located after Si detectors, respectively.

Outgoing particles were identified event-by-event using TOF-ΔE-E method. The TOF was obtained from the timing information of two plastic scintillators of 300 μm thickness placed at downstream of the target with 3.8m flight length and ΔE and E were measured by Si and NaI(Tl) detectors, respectively.

	Apparatus	Thickness	Note
F0	Carbon	1 mm	(c)
F1	Al	221 mg/cm^2	Degrader
F2	PPAC	(a)	100 mm x 100 mm
	SSD	100 μm	50 mm x 50 mm
	Plastic	100 μm	50 mm x 50 mm
F3	PPACa	(a)	100 mm x 100 mm
	PPACb	(a)	100 mm x 100 mm
	Plastic	100 μm	50 mm x 50 mm
	PPACc	(a)	100 mm x 100 mm
	Liq. He	150 mg/cm^2 (b)	(d)
	GRAPE		(e)
	PPACd	(a)	100 mm x 100 mm
	Plastic	100 μm	150 mm x 150 mm
	PPACe	(a)	150 mm x 150 mm
	STQ		
F4	PPACa	(a)	150 mm x 150 mm
	Plastic	100 μm	150 mm x 150 mm
	PPACb	(a)	100 mm x 100 mm
	SSD	100 μm	50 mm x 50 mm
			x 4 pieces
	NaI(Tl)	50 mm	31 mm x 31 mm
			x 36 pieces

Table 1. The list of apparatuses placed along the beam line. (a) PPAC's were operated with C_3F_8 gas at 10 Torr pressure. (b) An estimated value as described in the body. (c) A rotational primary target of carbon. (d) A reaction target with 6 μm-thick Havar windows of ϕ30 mm diameter. (e) Array of Germanium detectors with 306 outputs.

For detection of gamma-rays from the excited states in the in-flight ^{33}Al, Gamma-Ray detector Array with Position and Energy sensitivity (GRAPE) [10] surrounded the target. It consists of 17 pairs of segmented planar Germanium detectors. The gamma-ray detection point is obtained from the pulse shape analysis of outputs from GRAPE.

The transfer reaction to the ground state in the ^{33}Al was also measured with other trigger condition, which was prepared based on the velocity shift after the stripping reaction. The velocity shift was about TOF $\times$ 1/$A \sim$ 1.5 ns ($A = 30$) and larger than the time resolution of plastic scintillators so that the transfer rection products could be distinguished from the non-interact beam particles.

Data analysis is in progress.

References

[1] H. Iwasaki *et al.*, Phys. Lett. B **481** (2000) 7.

[2] T. Motobayashi *et al.*, Phys. Lett. B **346** (1995) 9.

[3] A. C. Morton *et al.* Phys. Lett. B **544** (2002) 274.

[4] W. Mittig *et al.* Eur. Phys. J. A **15**,(2002) 157160.

[5] T. Kubo *et al.*, Nucl. Instrum. Methods. B **70** (1992) 309.

[6] H. Akiyoshi *et al.*, CNS Annual Report 2000, p73; H. Akiyoshi *et al.*, RIKEN Accel. Prog. Rep. **34** (2001) 193.

[7] N. Aoi *et al.*, RIKEN Accel. Prog. Rep. **38** (2005) 176.

[8] M. Niikura *et al.* RIKEN Accel. Prog. Rep. **37** (2004) 155.

[9] H. Kumagai *et al.*, Nucl. Instrum. Methods. A **470** (2001) 562.

[10] S. Shimoura *et al.*, CNS Annual Report 2001 (2002) 5; CNS Annual Report 2003 (2004) 87.

Proton Single Particle States in ^{23}F

S. Michimasa, S. Shimoura[a], H. Iwasaki[b], M. Tamaki[a], S. Ota[c], N. Aoi, H. Baba[a], N. Iwasa[e],
S. Kanno[d], S. Kubono[a], K. Kurita[d], M. Kurokawa, T. Minemura, T. Motobayashi, M. Notani[a],
H. J. Ong[b], A. Saito[a], H. Sakurai[b] E. Takeshita[d], S. Takeuchi, Y. Yanagisawa and A. Yoshida

RIKEN (The Institute of Physical and Chemical Research)
[a]*Center for Nuclear Study, Graduate School of Science, University of Tokyo*
[b]*Department of Physics, University of Tokyo*
[c]*Department of Physics, Kyoto University*
[d]*Department of Physics, Rikkyo University*
[e]*Department of Physics, Tohoku University*

1. Introduction

The nuclear shell structure is mainly interpreted by single-particle motion in a mean-field including a spin-orbit potential. Recent findings of the disappearance of conventional magic numbers and/or the appearance of new magic numbers in the neutron-rich nuclei may indicate that the mean-field changes as a function of neutron/proton numbers. In this respect, neutron-rich fluorine isotopes locate in a stimulating region connecting the exotic nuclear phenomena: the new magic number of $N = 16$ [1] and an island of inversion [2]. In the present work, we have studied excited states in ^{23}F by γ-ray spectroscopy with one-proton transfer reaction. A one-proton transfer reaction is a good probe for investigation on proton shell structure, because this reaction selectively populates single-particle states. Furthermore, we have measured an α inelastic scattering and a neutron knockout reaction to reach excited state in ^{23}F. Comparison of population strengths in the different reactions demonstrates single-particle nature of observed states. We are mainly interested in a difference between energies of the proton single-particle states in ^{23}F and in ^{17}F, since these nuclei are full and empty of the $d_{5/2}$ orbitals with neutrons, respectively. If there is a difference, it is considered to reflect a change of mean-field, especially spin-orbit splitting of proton $d_{5/2}$-$d_{3/2}$ due to the occupation number of neutrons in the $d_{5/2}$ orbitals.

2. Experiment

The experiment was performed at the secondary beam line RIPS [3] in RIKEN Accelerator Research Facility. The secondary beam was a cocktail of unstable ^{22}O, ^{23}F and ^{24}F nuclei, which were produced by a projectile-fragmentation reaction of ^{40}Ar with a ^{9}Be target. The secondary beams bombarded a liquid helium target [4]. The reaction products of a secondary reactions were detected by a telescope consisting of 9 SSDs and 36 NaI(Tl) detectors [5] and de-excited γ rays from the reaction product were detected by an array of 150 NaI(Tl) scintillators DALI2 [6] surrounding the secondary target. In order to measure scattering angles of the reaction products, three PPACs were located on the beam line. The two PPACs were placed before the secondary target and the other PPAC was placed after the target. Further details about the present experiment were

written in ref. [7].

3. Results and Discussions

We have obtained γ-ray spectra in ^{23}F from the proton transfer reaction ^{4}He(^{22}O,^{23}Fγ), the inelastic scattering ^{4}He(^{23}F,^{23}Fγ) and the neutron knockout reaction ^{4}He(^{24}F,^{23}Fγ). In order to determine the energies of excited states in ^{23}F, we reconstructed the cascade γ-decay scheme based on γ-γ coincidence data. Figure 1 shows a proposed level and γ-decay scheme and relative cross sections to populate excited states. The two measurements have performed so far for searching excited states in ^{23}F [8,9]. The level scheme obtained in the present experiment is consistent with that of the previous works. Additionally eight new excited states were found at 3385(10), 3887(19), 3985(40), 4630(17), 4756(3), 5545(23), 5564(27) and 6872(36) keV. Errors shown with the energies are statistical ones estimated by an accuracy of maximum likelihood fitting. Systematic errors for the γ and level energies were estimated to be ± 0.76 % from known γ-decays in oxygen and fluorine isotopes.

Population strengths of excited states are sensitive to compatibility between the nature of the states and the reaction mechanism. The proton transfer reaction mainly populates proton particle states. The α inelastic scattering induces core excitations and non-spin flip proton single-particle excitation, while the neutron knockout reaction populates neutron hole states. The 4.061-MeV state, which was strongly populated by the transfer reaction but hardly identified in the inelastic scattering, is therefore a candidate for a proton particle state on the d orbital.

In order to deduce the angular momentum of the 4.061-MeV state, we used an angular distribution of outgoing ^{23}F for the state by the transfer reaction. Figure 2 shows the angular distribution together with predictions by a distorted-wave Born approximation (DWBA) calculation to transfer a proton into the s, d and f orbitals. The DWBA curves shown in the figure are obtained using optical potentials described in refs. [10,11]. The adopted optical potentials for the initial and final channels were listed in table 1. The measured angular distribution is found to agree with the $\ell = 2$ transition, and we assigned the 4.061-MeV state to have $J^{\pi} = 3/2^+$ or $5/2^+$. The previous works [8,12,13] re-
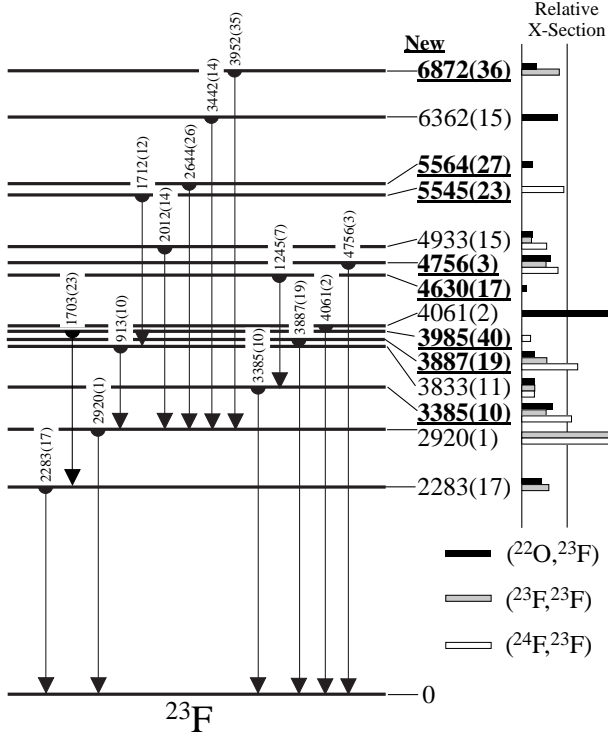
Figure 1. Level and γ-decay scheme in ^{23}F observed in the $(^{22}$O,^{23}F$\gamma)$, $(^{23}$F,^{23}F$\gamma)$ and $(^{24}$F,^{23}F$\gamma)$ reactions. The level energies with underlined bold style show newly observed excited levels in the present experiment. Shown errors with γ ray and excited energies are statistical errors obtained by fittings of γ-ray spectra with simulated response functions of DALI2. The bars in the right side of the excitation energies show relative cross sections to these state.

Figure 2. Angular distribution for the 4.061-MeV state from the proton transfer reaction. Dotted, solid and dashed curves in the figure show the DWBA predictions corresponding to transferred angular momenta of $\ell = 0$, 2 and 3, respectively. The optical potential parameters are listed in table 1.

Set	V [MeV]	r_V [fm]	a_V [fm]	W [MeV]	r_W [fm]	a_W [fm]
A1	70.690	1.277	0.728	13.179	1.885	0.426
A2	63.343	1.389	0.702	14.564	1.844	0.485
T1	69.652	1.253	0.760	17.220	1.714	0.674

Table 1. Optical potentials for DWBA calculations. Sets A1 and A2 were used for ^{22}O$+\alpha$ channel, and set T1 was used for ^{23}F$+t$ channel, respectively.

ported that the ground state in ^{23}F to have $5/2^+$. Therefore, the state at 4.061 MeV is considered reasonably to have $3/2^+$ as a proton single-particle state in $d_{3/2}$. The analysis is now in progress to extract the spectroscopic factor of the single-particle state.

We discuss here the energies of the single particle state in ^{17}F and ^{23}F. The single particle state in ^{17}F to have $3/2^+$ was reported to locate at 5.00 MeV in ref. [14]. The present result naively suggests that the six neutrons in the $d_{5/2}$ orbitals attract a proton in the $d_{3/2}$ orbital. However, the state was observed to be more excited than the prediction by the USD shell-model calculation [15], which was that a single-particle state to have $3/2^+$ located at 3.497 MeV. Therefore, the 4.061-MeV state may indicate the monopole interaction between the isospin-spin partners in the sd orbitals is slightly weaker than the prediction.

References

[1] A. Ozawa *et al.*, Phys. Rev. Lett. **84** (2000) 5493.
[2] E.K. Warburton *et al.*, Phys. Rev. C **41** (1990) 1147.
[3] T. Kubo *et al.*, Nucl. Instrum. Methods. B **70** (1992) 322.
[4] H. Akiyoshi *et al.*, RIKEN Accel. Prog. Rep. **34** (2001) 193.
[5] M. Tamaki *et al.*, CNS Annual Report 2002 (2003) 76.
[6] S. Takeuchi *et al.*, RIKEN Accel. Prog. Rep. **36** (2003) 148.
[7] S. Michimasa *et al.*, CNS Annual Report 2003 (2004) 3.
[8] N.A. Orr *et al.*, Nucl Phys. A **491** (1989) 457.
[9] D. Guillemaud-Mueller, Eur. Phys. J. A **13** (2002) 63.
[10] A.Ingemarson *et al.*, Nucl. Phys. A **676** (2000) 3.
[11] A.Ingemarson *et al.*, Nucl. Phys. A **696** (2001) 3.
[12] D.R. Goosman *et al.*, Phys. Rev. C **10** (1974) 756.
[13] E. Sauvan *et al.*, Phys. Rev. C **69** (2004) 044603.
[14] M. Yasue *et al.*, Phys. Rev. C **46** (1992) 1242.
[15] B.H. Wildenthal, Prog. Part. Nucl. Phys. **11** (1984) 5.

Isoscalar $E0$ and $E1$ Responses in ^{14}O

H. Baba, S. Shimoura, T. Minemura[a], Y. U. Matsuyama[b], A. Saito, H. Akiyoshi[a], N. Aoi[a],
T. Gomi[a], Y. Higurashi[a], K. Ieki[b], N. Imai[c], N. Iwasa[d], H. Iwasaki, S. Kanno[b], S. Kubono,
M. Kunibu[b], S. Michimasa[a], T. Motobayashi[a], T. Nakamura[e], H. Sakurai[f], M. Serata[b],
E. Takeshita[b], S. Takeuchi[a], T. Teranishi[g], K. Ue[f], K. Yamada[a] and Y. Yanagisawa[a]

Center for Nuclear Study, University of Tokyo
[a]*RIKEN (The Institute of Physical and Chemical Research)*
[b]*Department of Physics, Rikkyo University*
[c]*Institute of Particle and Nuclear Studies, High Energy Accelerator Research Organization (KEK)*
[d]*Department of Physics, Tohoku University*
[e]*Department of Applied Physics, Tokyo Institute of Technology*
[f]*Department of Physics, University of Tokyo*
[g]*Department of Physics, Kyushu University*

1. Introduction

Intermediate energy RI beams enable us to investigate the excited unstable nuclei using secondary reactions in inverse kinematics. As a probe for excitation, inelastic α scattering is useful for exciting isoscalar states, and the best tool to investigate the isoscalar monopole ($E0$) and dipole ($E1$) excitation. They are compressional excitation called the "breathing mode" and the "squeezing mode" and are relevant to the incompressibility of the nuclear matter. For light stable nuclei, isoscalar electric multipole strength has been systematically studied [1, 2] by using inelastic scattering of 60 A MeV α and discussed about compressional responses. In order to open the studies of isoscalar compressional responses in unstable nuclei, we performed an experiment of inelastic scattering of 60 A MeV α on light unstable nucleus ^{14}O in inverse kinematics. The energy spectrum of ^{14}O shows a semi-double-closed-shell nature since the first excited state is not 2^+ but 1^- with a rather high excitation energy. This characteristic is the same as that of its mirror nucleus ^{14}C and indicates that both the nuclei are to be spherical and to have essentially the same nuclear structure. Difference between the ^{14}O and the ^{14}C nuclei arises from a break of the isospin symmetry mainly due to the Coulomb interaction, which leads that the ^{14}O has no bound states whereas the ^{14}C has 6 bound states. This fact may affects isoscalar responses, since not only the discrete resonant states but also the continuum states which start from the threshold energies may be excited by the α inelastic scattering. The present experiment aimed at measuring the isoscalar $E0$ and $E1$ strengths in wide energy range.

2. Experimental Procedure

The experiment was carried out at RIKEN Accelerator Research Facility. A 135 A MeV primary beam of ^{16}O was used to bombard on a ^{9}Be production target of 1.3 g/cm^2 thickness. The reaction products were selected by the RIKEN projectile-fragment separator (RIPS). A 60 A MeV secondary beam of ^{14}O was transmitted to a liquid ^{4}He target [3] of 120 mg/cm^2 thickness. An ^{14}O secondary beam

was identified event-by-event by the time-of-flight (TOF) measured by two 0.5 mm thick plastic scintillators placed 5.3 m apart. The incoming angle and position of secondary beam on the target were measured using two sets of Parallel Plate Avalanche Counters (PPACs) installed upstream of the target. The outgoing particles were detected in coincidence by a plastic scintillator hodoscope with a 1×1 m^2 active area, which was located at 3.9 m downstream from the secondary target. The hodoscope was installed in a vacuum chamber and consisted of a 5 mm thick ΔE plane and two 60 mm thick E planes ($E1$, $E2$). The ΔE plane was divided horizontally into 13 slats, and the $E1$ and $E2$ planes consisted of 16 and 13 scintillator bars set perpendicular to the ΔE slats, respectively. The momentum vectors of the decay particles were determined by combining their velocities and hit positions on the hodoscope.

3. Analysis and Results

In this work, following decay channels were measured: ^{14}O$^* \rightarrow ^{13}$N$ + p$, ^{12}C$ + p + p$, ^{12}C$_1^* + p + p$, ^{10}C$ + \alpha$, and ^{10}C$_1^* + \alpha$. The excitation energy was deduced from the momentum vectors of decay products with the invariant-mass method. Angular distribution of differential cross-section was also deduced from the momentum vectors of decay products.

In order to obtain the multipole strength distributions, we carried out the multipole decomposition (MD) analysis [4] with the distorted wave Born approximation (DWBA). In this work the DWBA calculation was carried out using the single-folding model with a density-dependent nucleon-α interaction. The details of this calculation were described in Ref. [5].

In the MD analysis, the cross-sections $\left(\frac{d^2\sigma}{d\Omega dE}\right)^{EXP}$ are expressed as a sum of the contributions from the various multipole components:

$$\left(\frac{d^2\sigma}{d\Omega dE}\right)^{EXP} = \sum_L a_L(E) \left(\frac{d^2\sigma}{d\Omega dE}\right)^{DWBA}, \quad (1)$$

where E, $a_L(E)$, and $\left(\frac{d^2\sigma}{d\Omega dE}\right)^{DWBA}$ are the excitation en-
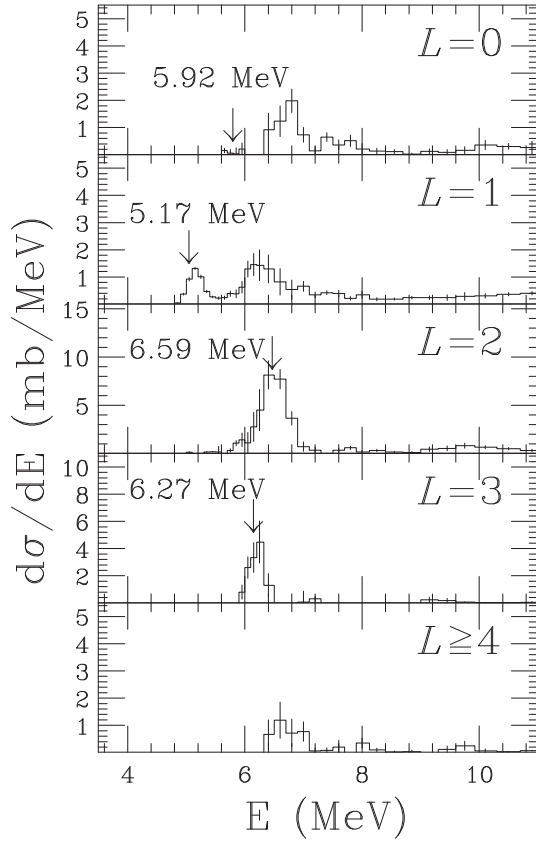
Figure 1. Decomposed cross-sections for low excitation energy range. Four known discrete states and unknown continua strength for $L = 0, 1$ were seen.

Figure 2. Decomposed EWSR fractions of $E0$ and $E1$ responses. The strengths were fragmented in wide excitation energy range without massive peaks.

ergy, fraction of the energy-weighted sum rule (EWSR), and the DWBA cross-sections exhausting the full EWSR for the transfered angular momentum L folded with the detector resolution, respectively. The fractions of the EWSR for various multipole components were determined by minimizing χ^2. In this work multipole components were taken into account up to $L = 4$ in the fitting of the MD analysis. Figure 1 shows the decomposed cross-section distributions for low excitation energy range. Using the MD analysis these low-lying known states of 5.17 MeV 1^-, 5.92 MeV 0^+, 6.27 MeV 3^- and 6.59 MeV 2^+ were clearly decomposed with some continuum components. This suggests that the MD analysis is capable to decompose any overlapping peaks or continua to each L component even in inverse kinematics.

For measured decay channels the integrated EWSR values up to 25.0 MeV deduced from the MD analysis with DWBA calculations were identified as 45 ± 11 and $61 \pm 14\%$ of the isoscalar $E0$ and $E1$ EWSR, respectively. The obtained EWSR fractions which are shown in Fig. 2 were fragmented in the wide excitation energy range and massive resonance peaks above EWSR $\geq 50\%$ were not found. The experimental results can not strictly compare with other experiments higher than 13.8 MeV excitation energy, because of the decay channel of $\alpha + \alpha + \alpha + p + p$ which have 13.8 MeV threshold energy was not measured in this exper-

iment. Nevertheless, the $E0$ and $E1$ strength in ^{14}O and light stable nuclei of ^{12}C and ^{16}O are in some agreement for their strength distributions. Therefore, this fragmented distribution without massive peak may be common in light nuclei, regardless stable or unstable.

In Fig. 2, additional $E0$ and $E1$ strengths to the known 0^+ and 1^- states were identified at $E = 6$–9 MeV. This energy region corresponds to the bound states in the mirror nucleus ^{14}C where neither 0^+ nor 1^- state was found, these strengths may come from the continuum. This strengths should arise from effect of lower proton threshold energy, because of these appreciable strengths of $E0$ and $E1$ transition were observed just above the threshold energy. Similar low energy isoscalar $E0$ and $E1$ responses have been predicted in neutron drip line nucleus ^{28}O [6, 7]. In addition to soft-dipole mode, this low-lying isoscalar compressional response is the new characteristic transition in unstable nucleus.

References

[1] B. John et al., Phys. Rev. C **68** (2003) 014305.
[2] Y.-W. Lui et al., Phys. Rev. C **64** (2001) 064308.
[3] H. Akiyoshi et al., RIKEN Accel. Prog. Rep. **34** (2001) 193.
[4] M. Itoh et al., Phys. Lett. B **549** (2002) 58.
[5] H. Baba et al., CNS Annual Report 2003 (2004) 5.
[6] I. Hamamoto and H. Sagawa, Phys. Rev. C **53** (1996) R1492.
[7] I. Hamamoto et al., Phys. Rev. C **57** (1998) R1064.

^{6}He+^{6}He Cluster States in ^{12}Be via α-Inelastic Scattering

A. Saito, S. Shimoura, T. Minemura[a], Y. U. Matsuyama[b], H. Baba[a], H. Akiyoshi[a], N. Aoi[a],
T. Gomi[a], Y. Higurashi[a], K. Ieki[b], N. Imai[c], N. Iwasa[d], H. Iwasaki[e], S. Kanno[b], S. Kubono,
M. Kunibu[b], S. Michimasa[a], T. Motobayashi[a], T. Nakamura[f], H. Sakurai[a], M. Serata[b],
E. Takeshita[b], S. Takeuchi[a], T. Teranishi[g], K. Ue, K. Yamada[a] and Y. Yanagisawa[a]

Center for Nuclear Study, Graduate School of Science, University of Tokyo
[a]*RIKEN (The Institute of Physical and Chemical Research)*
[b]*Department of Physics, Rikkyo University*
[c]*Institute of Particle and Nuclear Studies, KEK*
[d]*Department of Physics, Tohoku University*
[e]*Department of Physics, University of Tokyo*
[f]*Department of Physics, Tokyo Institute of Technology*
[g]*Department of Physics, Kyushu University*

Cluster structure in neutron-rich beryllium isotopes is one of the most interesting phenomena in unstable nuclei. For ^{12}Be, recently observed highly excited states with $J^\pi=4^+$ to 8^+ above ^{6}He+^{6}He threshold are considered to form a rotational band with a developed ^{6}He+^{6}He cluster structure [1]. These excited states have been reasonably reproduced by several theorietical calculations. The microscopic coupled-channels calculation predicted that several rotational bands with different couplings, such as $0^+\otimes2^+$, appear at high-excitation energy region [2]. Strong mixing between ^{6}He+^{6}He and α+^{8}He was predicted by the microscopic cluster model calculation [3]. The Antisymmetrized Molecular Dynamics reproduced the experimentally observed rotational band [4]. The deduced density distribution showed a developed cluster structure in highly excited states. Therefore several excited states with developed cluster structure are expected to overlap each other above the ^{6}He+^{6}He or α+^{8}He thresholds.

We aimed at searching for excited states with low spins such as 0^+ and 2^+, which may lie just above the ^{6}He+^{6}He decay threshold. The α-inelastic scattering at $60A$ MeV with the inverse kinematics using a liquid helium target [5] was used to populate these excited states. Since the (α,α') reaction has the advantage of well-known reaction mechanism, and here it is possible to determine spins by angular distributions of the inelastic scattering compared with Destorted Wave Born Approximation (DWBA) calculations. In the present work, the angular correlations between decay particles are also compared with DWBA predictions. Since the density of levels is rather high, the multipole decomposition analysis (MDA) with the DWBA was used.

The experiment was carried out at RIKEN Accelerator Research Facility. A primary beam of ^{18}O at 100 MeV/nucleon was supplied by RIKEN Ring Cyclotron accelerator. The intensity of the primary beam was 150 pnA. A radioactive ^{12}Be beam was produced using a projectile-fragmentation reaction of the ^{18}O beam on a ^{9}Be target. The ^{12}Be beam was separated from the other fragments using RIKEN Projectile-fragment Separator (RIPS)

[6]. Remaining contaminants were rejected in the analysis using the time-of-flight (TOF) and energy losses measured by two plastic scintillators separated by 5.3 m each other. A typical intensity of the secondary beam was 3×10^4 particles per second. The ^{12}Be beam bombarded a liquid helium target, which was confined in a cell with a 6-μm-thick Havar window of 24-mm diameter. The direction and the hit position of each beam particle at the secondary target were measured by two sets of Parallel Plate Avalanche Counters (PPAC's) installed upstream of the secondary target. The energy of the ^{12}Be secondary beam was $60A$ MeV in the middle of the secondary target.

The reaction products of two helium isotopes were measured and identified using a hodoscope of a plastic scintillator array with an active area of 1×1 m^2 located 3.9 m downstream of the target. the thicknesses of the ΔE, $E1$, and $E2$ layers were 5 mm, 60 mm, and 60 mm, respectively. The resolutions (in sigma) of the TOF, horizontal, and vertical positions were 0.15 ns, 0.9 cm, and 1.3 cm, respectively. The decay energy for ^{12}Be$\rightarrow$^{6}He+^{6}He was extracted by the invariant-mass method. The resolution of the decay energy was estimated using Monte Carlo simulations taking resolutions of the detectors and the multiple scattering effects of the beam and the reaction products into account. The energy resolution was proportional to a square root of the decay energy ($\sqrt{E_d}$) as $\Delta E_{\mathrm{FWHM}} = 0.34 \times \sqrt{E_d}$ MeV.

The MDA based on DWBA calculations has been used by including angular correlations of decay particles as well as the angular distribution of the inelastic scattering. In this analysis, the DWBA calculations for α-inelastic scattering were performed using the computer code TWOFNR [7]. A single-folding model with density-dependent effective nucleon-α interactions was used in the DWBA calculations [8]. The details of the transition densities are described in Ref. [9]. Figure 1 shows the excitation energy spectra for multipoles of ΔL=0, 2, and 4 deduced by the MDA. Figure 2 shows angular distributions of (a) the differential cross section of the inelastic scattering, (b) the angular correlation between breakup products respect to the beam axis, and (c) the one respect to the transfered momen-

tum, corresponding to the excitation energy E_x=12.4 MeV. The black dashed, dotted, and dash-dotted curves correspond to ΔL=0, 2, and 4, respectively. The gray dashed, dotted, and dash-dotted curves are interferences of 0⊗2, 0⊗4, and 2⊗4, respectively. The calculated angular correlations show good agreements with the data by including the contributions of the interference between different multipoles. In Figs. 1 (a) and (b), the peaks indicated by arrows are newly observed ones for ΔL=0 and 2, respectively. For ΔL=4 spectrum, no distinctive peaks are observed because of large statistical errors.
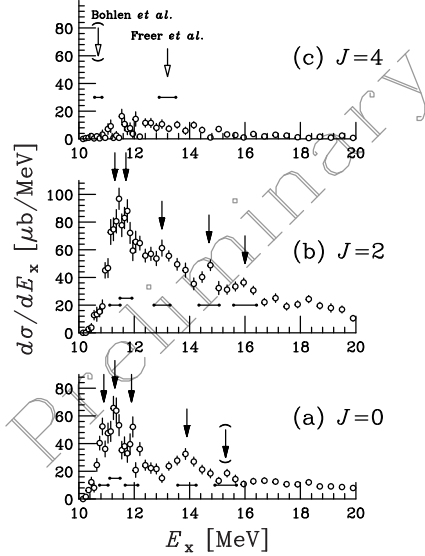
Figure 1. Decay-energy spectra for (a) ΔL=0, (b) ΔL=2, and (c) ΔL=4, for the ^{4}He(^{12}Be,^{6}He^{6}He) reaction.
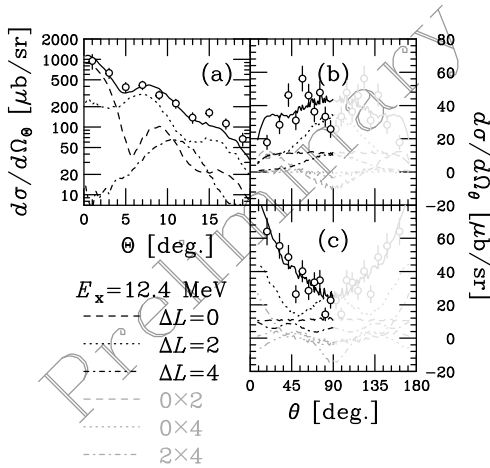
Figure 2. Angular distributions of (a) the differential cross section of the inelastic scattering, (b) the correlation between breakup products respect to the beam axis, and (c) the one respect to the transfered momentum, corresponding to the excitation energy E_x=12.4 MeV.

The energy-spin systematics is shown in Fig. 3. Closed circles are new levels observed in the present work. Open circles and open triangles are data taken from Refs. [1] and [10], respectively. The moment of inertia of the solid lines correspond to $\hbar^2/2\mathcal{I}$=139 keV, which is close to that of ^{6}He

touching each other with radii given by $r = 1.5 \times A^{1/3}$. The first and the second lowest 0^+ and 2^+ levels may be members of the rotational band with a developed ^{6}He+^{6}He cluster structure in ^{12}Be [1]. By assuming each rotational band has moment of inertia closed to each other, the third lowest 0^+ and 2^+ states may be connected to previously observed 6^+ state at 18.6 MeV [1].
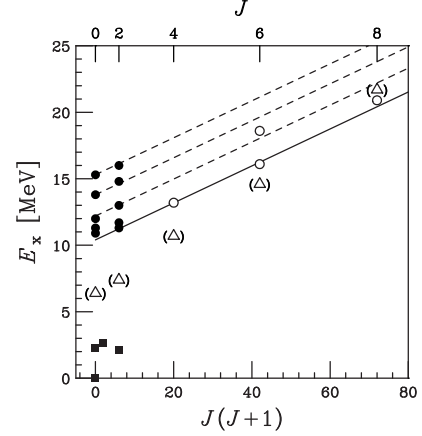
Figure 3. Energy-spin systematics for ^{12}Be. Closed circles are levels observed in the present work. Open circles and open triangles are data of Refs. [1] and [10], respectively.

In summary, the α-inelastic scattering of ^{12}Be with the inverse kinematics was measured using the liquid helium target. The multipole decomposition analysis was performed using the angular distributions of the inelastic scattering and the angular correlations of decay particles. Newly observed excited states with 0^+ and 2^+ may be members of rotational bands with large moments of inertia corresponding to the developed ^{6}He+^{6}He cluster structure in ^{12}Be.

References

[1] M. Freer *et al.*, Phys. Rev. Lett. **82** (1999) 1383.
[2] M. Ito and Y. Sakuragi, Phys. Rev. C **62** (2000) 064310.
[3] P. Descouvemont and D. Baye, Phys. Lett. B **505** (2001) 71.
[4] Y. Kanada-En'yo and H. Horiuchi, Phys. Rev. C **68** (2003) 014319.
[5] H. Akiyoshi *et al.*, CNS Annual Report 2001 (2002) 73; *ibid.* RIKEN Accel. Prog. Rep. **34** (2001) 193.
[6] T. Kubo *et al.*, Nucl. Instr. Meth. Phys. Res. B **70** (1992) 309.
[7] M. Igarashi, DWBA code TWOFNR, unpublished.
[8] A. Kolomiets *et al.*, Phys. Rev. C **61** (2000) 34312.
[9] G. R. Satchler *et al.*, Nucl. Phys. A **472** (1987) 215.
[10] H. G. Bohlen *et al.*, Nucl. Phys. A **722** (2003) 3c.

Bell's Inequality Test via the ^{1}H(d,^{2}He)n Reaction

T. Saito[a], H. Sakai[a,b], T. Ikeda[c], K. Itoh[c], T. Kawabata[b], H. Kuboki[a], Y. Maeda[b], N. Matsui[d],
M. Sasano[a], Y. Satou[d], K. Sekiguchi[e], K. Suda[b], A. Tamii[f], T. Uesaka[b] and K. Yako[a]

[a] *Department of Physics, Graduate School of Science, University of Tokyo*
[b] *Center for Nuclear Study, Graduate School of Science, University of Tokyo*
[c] *Department of Physics, Saitama University*
[d] *Department of Physics, Tokyo Institute of Technology*
[e] *RIKEN (The Institute of Physical and Chemical Research)*
[f] *Research Center for Nuclear Physics, Osaka University*

It is well-known that Einstein, Podolsky and Rosen (EPR) [1] asserted quantum mechanics is incomplete in terms of local realism, which has been a basic view on nature of classical theories. According to the local realistic theories, objects should have definite properties whether they are measured or not (reality), and there is no action-at-a-distance in nature (locality). Some attempts were made to explain quantum mechanical phenomena from a view of the local realistic theories. Bell, however, showed quantum mechanical correlations between entangled systems can be stronger than those by the local realistic theories [2]. Since Bell's proof was given by an inequality which can be tested experimentally, many experiments have been devoted to test the inequality by measuring polarization correlations between entangled two photons and have yielded results which are consistent with quantum mechanics. A brief history of these experiments is summarized in Refs. [3] and [4].

It should be noted, however, that most of such experiments used entangled systems produced by electromagnetic interaction except for one by Lamehi-Rachti and Mittig (LRM) [5]. LRM used strong interaction to test the Bell's inequality. Since the strong interaction is a short range interaction, entangled particles are produced with extremely short coherence length. It is of considerable interest to investigate whether an entanglement between two particles are robustly maintained even if the two particles are spatially separated from each other by a distance extremely beyond their coherence length.

LRM measured spin-correlations between two protons in the spin-singlet ($^1S_0$) state which was produced by the proton-proton S-wave elastic scattering. They prepared a pair of polarimeters which measured signs of spins of two protons after the scattering. Each polarimeter had a special direction along which the spins of incident protons were measured. Although they obtained results which showed violation of Bell's inequality, we consider there is a crucial weak point in this experiment. In their setup, one of the spin-measuring axes of the polarimeters was fixed along the normal of the scattering plane of the pp-scattering. In this case, even if the two protons after the scattering were not in the $^1S_0$ state described by $|^1S_0\rangle = (|\uparrow\rangle|\downarrow\rangle - |\downarrow\rangle|\uparrow\rangle)/\sqrt{2}$ but in a different state given by a factorized expression of $|\uparrow\rangle|\downarrow\rangle$ or $|\downarrow\rangle|\uparrow\rangle$ with respect to the scattering normal, they would have obtained the same results.
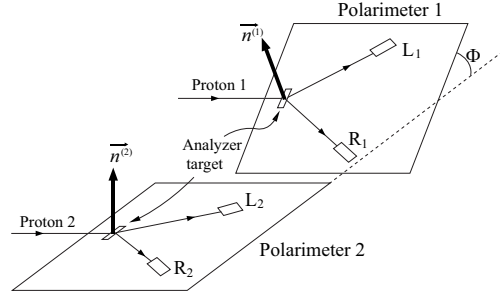
Figure 1. Illustrative experimental setup to measure spin-correlations between two protons.

Thus one cannot conclude that the two protons were in the entangled state even though Bell's inequality was violated.

In this article, we report a spin-correlation measurement of two protons produced by the ^{1}H(d,^{2}He)n reaction. Here ^{2}He denotes a pair of protons coupled to the $^1S_0$ state. Making use of this reaction, our experiment has a distinguished feature that the directions of the spin-measuring axes are not pre-fixed by the experimental setup, which enabled us to solve the problem in LRM's experiment.

To explain the principle of the spin-correlation measurement, let us utilize an illustrative setup shown in Fig. 1. This setup consists of a pair of polarimeters, each of which has an analyzer target and a pair of detectors L and R. A pair of protons are injected into the analyzer targets. In each polarimeter the scattered protons are detected by detectors L or R. If the beam of proton 1 has a polarization $p^{(1)}$ with respect to the direction of the scattering normal of polarimeter $\vec{n}^{(1)}$, there appears an asymmetry in the counts by detector L_1 and R_1 as $(N_{L1} - N_{R1})/(N_{L1} + N_{R1}) = p^{(1)}A^{(1)}$ where $A^{(1)}$ is the effective analyzing power of polarimeter 1. Thus each polarimeter is sensitive to the spin component of the incident protons along the direction of $\vec{n}^{(i)}$ ($i = 1, 2$). Here, we define a spin-correlation function $C(\vec{n}^{(1)}, \vec{n}^{(2)})$ as the expectation value of the product of the signs of two proton spins with respect to the spin-measuring axes $\vec{n}^{(1)}$ and $\vec{n}^{(2)}$. In this setup, polarimeter 1 is rotated by an angle of Φ from polarimeter 2. If the incident protons are in the $^1S_0$ state, the quantum mechanical prediction of $C(\vec{n}^{(1)}, \vec{n}^{(2)})$ is given by $C_{\mathrm{QM}}(\vec{n}^{(1)}, \vec{n}^{(2)}) \equiv \langle \vec{\sigma}^{(1)} \cdot \vec{n}^{(1)} \ \sigma^{(2)} \cdot \vec{n}^{(2)} \rangle = -\cos\Phi$. Experimentally, $C(\vec{n}^{(1)}, \vec{n}^{(2)}) (\equiv C(\Phi))$ is given
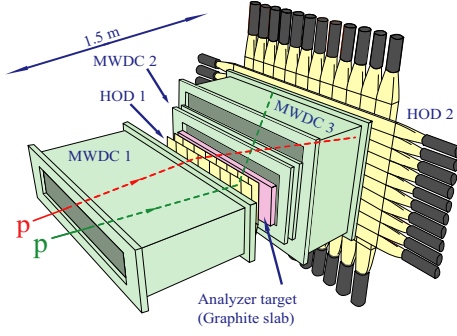
Figure 2. Schematic view of the polarimeter EPOL to measure the spin-correlations of two protons from the $^1\text{H}(d,^2\text{He})n$ reaction.

by [5]

$$C_{\exp}(\Phi) =$$
$$\frac{1}{A^{(1)}A^{(2)}} \frac{N_{LL} + N_{RR} - N_{LR} - N_{RL}}{N_{LL} + N_{RR} + N_{LR} + N_{RL}}, \quad (1)$$

where N_{LR} is the number of coincidences between the detector L_1 and R_2.

Bell's inequality of CHSH type [6] states that any local realistic theories must satisfy the following inequality for arbitrary directions $\vec{a}$, $\vec{b}$, $\vec{a}'$ and $\vec{b}'$:

$$|C(\vec{a},\vec{b}) - C(\vec{a},\vec{b}')| + |C(\vec{a}',\vec{b}) + C(\vec{a}',\vec{b}')| \leq 2. \quad (2)$$

Our experiment was carried out using a magnetic spectrometer SMART [7] at RIKEN Accelerator Research Facility. A deuteron beam of $E_d = 270$ MeV from the ring cyclotron was injected into a liquid hydrogen target. Two protons emitted at $\theta_{\text{lab}} = 0°$ by the $^1\text{H}(d,^2\text{He})n$ reaction were simultaneously momentum-analyzed by the spectrometer and were injected into a focal-plane polarimeter EPOL. A schematic view of EPOL is presented in Fig. 2. EPOL consisted of a spin-analyzer target (graphite slab), plastic scintillation counter hodoscopes and multi-wire drift chambers (MWDCs). For each event, the incident two protons were simultaneously scattered by the graphite slab. Their trajectories before and after the graphite slab were measured with the MWDCs. By selecting proton pairs whose relative energies were less than 1 MeV, a pure ensemble of the spin-singlet proton pairs were obtained. The purity of the ensemble is better than 98%.

$C_{\exp}(\Phi)$ can be derived by analyzing the correlations of the scattering angles of two protons at the graphite slab. EPOL did not have a pair of polarimeters as those shown in Fig. 1, but it was equipped with MWDCs instead which recorded trajectories of two protons event by event. The spin measuring axes $\vec{n}^{(1)}$ and $\vec{n}^{(2)}$ can be freely determined by software after the experiment.

The effective analyzing power $A^{(i)}$ were calibrated by injecting a polarized proton beam into EPOL and measuring the left-right asymmetry of the scattering at the graphite slab. The value of $A^{(i)}$ varied in a range of 0.17 - 0.23, depending on the kinetic energy of the incident proton.

We derived $C_{\exp}(\Phi)$ at different angles of Φ in a range of $-\pi \leq \Phi \leq \pi$ from the same data set by changing the rela-
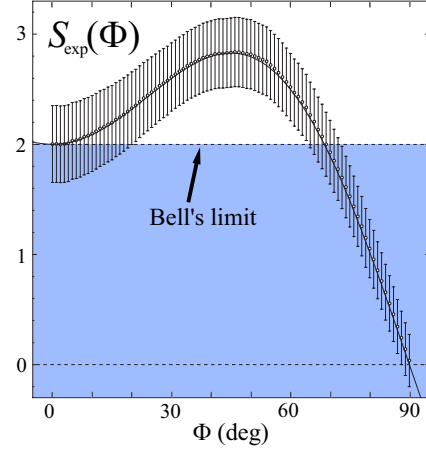
Figure 3. Obtained spin-correlation function $S_{\exp}(\Phi)$. The error-bars show the sum of the statistical and systematic errors. Since all the data points were derived from the same data set, each point is not statistically independent to each other.

tive angle between $\vec{n}^{(1)}$ and $\vec{n}^{(2)}$. To compare the results with Bell's inequality, we calculated a correlation function of CHSH type: $S_{\exp}(\Phi) \equiv 2C_{\exp}(\Phi) + C_{\exp}(-\Phi) - C_{\exp}(3\Phi)$. Bell's inequality of Eq. (2) is equivalent to $|S(\Phi)| \leq 2$. The results of $S_{\exp}(\Phi)$ are presented in Fig. 3. The data are in excellent agreement with the quantum mechanical prediction $S_{\text{QM}}(\Phi) = 3\cos\Phi - \cos 3\Phi$. We obtained a value of $S_{\exp}(\pi/4) = 2.83 \pm 0.24_{\text{stat}} \pm 0.07_{\text{sys}}$. This shows the violation of the inequality by a confidence level of 99.3%. The systematic error was mainly caused by uncertainty in the determination of the effective analyzing powers of EPOL.

We have thus demonstrated the violation of Bell's inequality with entangled protons produced by strong interaction. Although the accuracy of verification is comparable with that of LRM's experiment, our results are more significant than LRM's since we analyzed the spin-correlations with spin-measuring axes which were freely defined by software and randomly rotated. The further detail of this experiment will be published elsewhere.

References

[1] A. Einstein, B. Podolsky and N. Rosen, Phys. Rev. **47** (1935) 777.
[2] J. S. Bell, Physics **1** (1964) 195.
[3] J. F. Clauser and A. Shimony, Rep. Prog. Phys. **41** (1978) 1881.
[4] A. Aspect, Nature **398** (1999) 189.
[5] M. Lamehi-Rachti and W. Mittig, Phys. Rev. D **14** (1976) 2543.
[6] John F. Clauser, Michael A. Horne, Abner Shimony and Richard A. Holt, Phys. Rev. Lett. **23** (1969) 880.
[7] T. Ichihara *et al.*, Nucl. Phys. A **569** (1994) 287c.

Determination of Vector and Tensor Analyzing Powers in Deuteron-Proton Elastic Scattering via the ^{12}C($\vec{d}, \alpha$)^{10}B*[2$^+$] Reaction

K. Suda, H. Mardanpour[a], H. R. Amir Ahmadi[a], N. Kalantar-Nayestanaki[a], T. Kawabata,
H. Kuboki[b], Y. Maeda, J. G. Messchendorp[a], S. Sakaguchi, H. Sakai[b], N. Sakamoto[c], Y. Sasamoto,
K. Sekiguchi[c], Y. Takahashi[b], T. Uesaka and K. Yako[b]

Center for Nuclear Study, Graduate School of Science, University of Tokyo
[a]*Kernfysisch Versneller Instituut (KVI)*
[b]*Department of Physics, University of Tokyo*
[c]*RIKEN (The Institute of Physical and Chemical Research)*

An experimental program has started at KVI aiming at the study of three-nucleon forces. Analyzing powers and spin-transfer coefficients in the $\vec{d}$–p elastic and breakup reactions will be measured at $E_d = 100$–180 MeV. To obtain accurate data is crucial for a better insight of the three-nucleon forces. The incident beam polarization must be known with high accuracy in order to determine these observables. At KVI and RIKEN, polarization of deuteron beams at intermediate energies is determined by using beam line polarimeters which applies the $\vec{d}$-p elastic scattering as a polarimetry [1, 2]. The vector and tensor polarization of the deuteron beam are deduced from the measured asymmetries of the $\vec{d}$–p scattering and the known analyzing powers. At intermediate energies, the vector and tensor analyzing powers for the $\vec{d}$–p elastic scattering have been experimentally measured with a sufficient precision only for a few incident energies. In order to use the $\vec{d}$–p elastic scattering for the measurement of beam polarization extensively at intermediate energies, more data on vector and tensor analyzing powers are needed. Particularly for the experimental program at KVI, reliable calibration data at $E_d = 100$–180 MeV are essential to investigate the dependence on the beam energy. Such data can be provided by a calibration measurement performed at RIKEN.

The ^{12}C($\vec{d}, \alpha$)^{10}B reaction at $\theta = 0°$ has been proposed as a calibration standard at intermediate energies and its usefulness is demonstrated by the measurement at RIKEN [3]. It can be shown that the tensor analyzing power T_{20} is $1/\sqrt{2}$ due to the parity conservation if the final state of ^{10}B has natural parity except for 0^+. Therefore, by using this reaction the tensor polarization of the deuteron beam is unambiguously determined. Among the levels of ^{10}B, the 2^+ state at 3.59 MeV is advantageous because energy differences between adjacent levels are more than 1 MeV. Moreover, even if the tensor polarized beam has a component of vector polarization, it does not influence on the measurement of the tensor polarization because $A_y = 0$ at $0°$. In case the spin axis is normal to the scattering plane, the cross section σ for the ($\vec{d}, \alpha$) reaction at $\theta = 0°$ is written as

$$\sigma = \sigma_0 \left[1 - \frac{1}{\sqrt{8}} T_{20} P_{ZZ} \right],$$

where σ_0 is the cross section for unpolarized beam and P_{ZZ} is the tensor polarization of the deuteron beam. The polarization axis Z is defined by the rotation symmetry axis at the ion source. The tensor polarization is obtained from this equation.

The calibration experiment was performed at RIKEN Accelerator Research Facility using polarized deuteron beam at 180 and 130 MeV. Three polarization modes of deuteron beam $(P_Z, P_{ZZ}) = (0, 0), (1/3, -1), (1/3, +1)$ were used. These modes were switched every few seconds to reduce systematic uncertainties. The ^{12}C($\vec{d}, \alpha$)^{10}B reaction was measured at $\theta = 0°$ by using SMART spectrograph in order to deduce beam polarization. A thin polyethylene film with a thickness of 6 mg/cm^2 was used as a carbon target. Scattered particles were momentum analyzed by the analyzing magnets of the SMART and detected at the second focal plane. Figure 1 shows an excitation energy spectrum for the ^{12}C($\vec{d}, \alpha$)^{10}B reaction at $E_d = 180$ MeV. The 2^+ state of interest at 3.59 MeV is well separated from adjacent levels. The deduced angular distribution of the asymmetry $(\sigma - \sigma_0)/\sigma_0$ for the 2^+ state is shown in Fig. 2. The beam polarization is extracted by extrapolating asymmetries at finite angles to $\theta = 0°$. The extrapolation is performed by fitting a second order polynomial function to data. The magnitude of the vector polarization p_Z can be deduced multiplying tensor polarization by one third. This relation is fairly robust since it is not affected by the efficiency of the RF transition of the polarized ion source. Simultaneously using the same beam with the ($\vec{d}, \alpha$) measurement, the $\vec{d}$-p elastic scattering was measured by using the D-room polarimeter to determine the vector and tensor analyzing powers. A thin polyethylene film with a thickness of 3 mg/cm^2 was used as a hydrogen target. Scattered deuterons and recoil protons were detected in kinematical coincidence. The detector configuration was the same as that in Ref. [3] except for the measured angles (Table 1). The detectors were

$\theta_{c.m.}$ (deg)	θ_{lab}^d (deg)	θ_{lab}^p (deg)
83.2	24.8	47.3 (47.6)
89.1	26.2	44.3 (44.6)
95.2	27.3	41.3 (41.6)
101.2	28.4	38.3 (38.6)
111.2	29.6	33.3 (33.6)
118.7 (119.2)	30.0	29.7

Table 1. Measured angles for the $\vec{d}$–p elastic scattering at $E_d = 180(130)$ MeV.

Figure 1. Excitation energy spectrum for the ^{12}C$(\vec{d}, \alpha)^{10}$B reaction at $E_d = 180$ MeV. The 2^+ state of interest at 3.59 MeV is well separeted from adjacent levels.

Figure 2. Asymmetry for the ^{12}C$(\vec{d}, \alpha)^{10}$B[2^+] reaction at $E_d = 180$ MeV. The data for the second and third polarization modes are shown by open circles and filled triangles, respectively. The solid lines represent the results of the fitting by using second order polynomial function.

designed to measure asymmetries of the scattering at six angles at the same time. It is because the cross section of the $(\vec{d}, \alpha)$ reaction is hundreds of times smaller than that for the d–p elastic scattering and it takes several hours to obtain sufficient statistics of the beam polarization, even with a beam intensity of 100 nA. Asymmetries were measured by using four sets of plastic scintialtion detectors placed around the beam axis in the directions of Left, Right, Up, and Down. One set of detectors consisted of one deuteron detector and six proton detectors. The deuteron detector was 5 mm in thickness and covered $\theta_{lab} = 23°$–$29°$. Each of proton detectors was 10 mm in thickness. The angular spread was set to be $\Delta\theta_{lab} = 1.0°$, which determines the solid angles of the measurement. The proton detector set at $\theta_{lab} = 29.7°$ detected both deuterons and protons scattered to $\theta_{c.m.} \simeq 120°$, and deuterons to $\theta_{c.m.} = 111.2°$. A wedge-shaped iron degrader was placed in front of proton

detectors (except for the one at $\theta_{lab} = 29.7°$) to maximize energy loss of proton in scintillator and to increase signal-to-noise ratio.

The spin axis of the deuteron beam was also measured after the $(\vec{d}, \alpha)$ measurement at each energy. As reported in Ref. [3], spin axis can be inclined by several degrees after acceleration. Since it may determine the accuracy of the calibration data, it is necessary to measure spin axis (β, ϕ). The measurement was performed by using the same method used in Ref. [3]. The swinger dipole magnet of the SMART spectrograph was rotated to $90°$, and the precession of the spin axis was measured by using two polarimeters, the D-room and swinger polarimeters. The swinger polarimeter was placed just after the swinger magnet, and it had the same configuration with the D-room polarimeter, but only one angle can be measured. The advantage of this method is that the spin axis can be determined even without any information on the analyzing powers.

The vector and tensor analyzing powers for the $\vec{d}$-p elastic scattering are determined from the magnitude of beam polarization obtained from the $(\vec{d}, \alpha)$ measurement and the spin axis, and the asymmetry of the $\vec{d}$–p elastic scattering. Further analysis is in progress.

References

[1] R. Bieber *et al.*, Nucl. Intrum. Methods Phys. Res. A **457**, (2001) 12.
[2] N. Sakamoto *et al.* Phys. Lett. B **367** (1996) 60.
[3] K. Suda *et al.*, RIKEN Accel. Prog. Rep. **35** (2002) 174.

Polarization Measurement of Polarized Proton Solid Target
via the $\vec{p}+^4$He Elastic Scattering

S. Sakaguchi[a], T. Wakui[a], T. Uesaka[a], K. Itoh[b], T. Kawabata[a], H. Kuboki[c], Y. Maeda[a],
H. Sakai[a,c], Y. Sasamoto[a], M. Sasano[c], K. Sekiguchi[d], K. Suda[a], Y. Takahashi[c] and K. Yako[c]

[a]*Center for Nuclear Study, Graduate School of Science, University of Tokyo*
[b]*Department of Physics, Saitama University*
[c]*Department of Physics, University of Tokyo*
[d]*RIKEN (The Institute of Physical and Chemical Research)*

1. Introduction

We have recently succeeded in constructing a polarized solid proton target which has a unique capability of operating in a low magnetic field of 80 mT at a high temperature of 100 K [1]. The target was used, for the first time, in an experiment to measure the spin-dependent asymmetry of $\vec{p}+^6$He elastic scattering in 2003 [2]. During the scattering experiment, proton polarization was monitored with nuclear magnetic resonance (NMR) measurement. The NMR signal is usually calibrated by measuring a polarization under thermal equilibrium (TE), which is a function of temperature and magnetic field. For our target, however, there is difficulty in measuring the TE signal, primarily because of the small TE proton polarization in a low magnetic field of 80 mT at a high temperature of 100 K, and secondarily because of the limited NMR sensitivity due to the target design specialized to scattering experiment. It is thus impractical to relate the NMR signal to the absolute polarization using TE measurement technique. As an alternative method, a nuclear reaction was used for determination of the absolute value of proton polarization. Accordingly, spin-dependent asymmetry of the $\vec{p}+^4$He elastic scattering at the energy of 80 MeV/nucleon was measured. Polarization P_y is obtained as

$$P_y = \frac{1}{A_y}\frac{N_L - N_R}{N_L + N_R},\qquad(1)$$

where A_y is the analyzing power, and N_L/N_R are left/right yields. The analyzing power A_y of this reaction at the same energy has already been measured by Togawa *et al.* [3]. Details of the experiment are reported in this article.

2. Experiment

The experiment was performed in the E3 experimental area of RIKEN Accelerator Research Facility. The energy and the typical intensity of ^{4}He beam were 80 MeV/nucleon and 200 kcps, respectively. The beam size on the target was 3 mmϕ (FWHM).

The target material was a single crystal of naphthalene doped with 0.01 mol% pentacene. The cross section and thickness of the target were 14 mmϕ and 1 mm, respectively. Protons in the target were polarized at 88 mT and 100 K making use of a spontaneous electron alignment in the photo-excited triplet state of aromatic molecules and of the cross-polarization method [4]. Figure 1 shows the time development of the NMR signal amplitude, which is

proportional to proton polarization. Polarization measurements for spin "up/down" were carried out for compensation of spurious asymmetry. The target was polarized in the "up" direction from t =0 to 29.2 h. The polarization was once broken, and then built up in the "down" direction from t =33.1 to 52.6 h. Polarization measurements using ^{4}He beam were carried out during periods shown as shaded regions in Fig. 1. Decrease in polarization was observed with the beam irradiation. This effect is considered to depend on beam intensity per unit area of the target [5]. The decrease in polarization will be much smaller in RI beam experiments, since typical spot size of RI beam is almost one order of magnitude larger than that of ^{4}He beam used in this experiment.
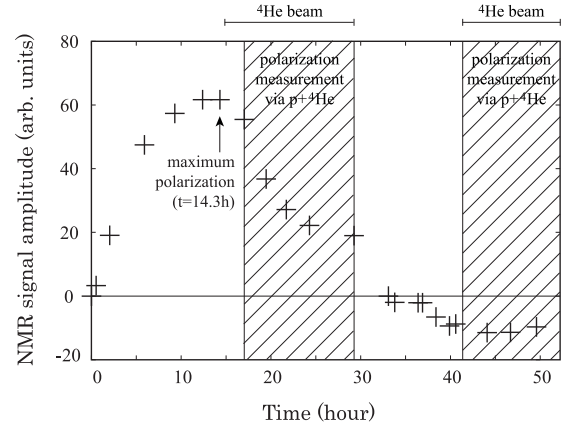
Figure 1. Time development of proton polarization measured by pulsed NMR. The vertical axis denotes the NMR signal amplitude, which is proportional to the proton polarization. The origin of the horizontal axis denotes the time when proton polariation was started in the "up" direction.

Figure 2 shows a schematic view of the experimental setup. Scattered ^{4}He particles were detected with a multiwire drift chamber (MWDC) and three layers of plastic scintillation detectors placed downstream of the MWDC. The MWDC provides the scattering angle of ^{4}He. The ΔE and E information is given by three-layers of plastic scintillation detectors, whose thicknesses are 5 mm in the first layer and 30 mm in the other.

Recoiled protons were detected with a pair of counter telescopes placed left and right sides of the beam axis. Each telescope consists of two layers of position sensitive silicon detectors (X-PSD, Y-PSD) and plastic scintillation detectors. The PSD has a 50×50 mm^2 active area divided into

10 strips on the front face. Two PSDs with an orthogonal strip direction located at 120 mm and 140 mm from the target, respectively, provided scattering angles and ΔE information of recoiled protons. The E information of protons was given by the plastic scintillation detectors.
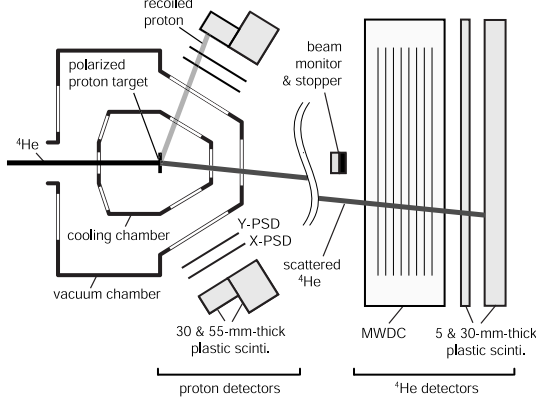
Figure 2. Schematic view of experimental setup. The distances from the target to plastic scintillators for ^{4}He and protons are approximately 1 m and 180 mm, respectively.

3. Results

The p+^{4}He elastic scattering events are identified by requiring kinematical consistency to identified protons and ^{4}He particles. Proton identification is mainly carried out with the ΔE data from the PSDs and E data from the plastic scintillation detectors. About half of the protons recoiled to backward angle of 68–70° do not fire plastic scintillator, since they have low energy of 10–20MeV. Part of these protons can be identified by the energy loss correlation between X-PSD and Y-PSD. The overall efficiency of proton detection and identification in the most backward strip (strip #10) was about 70% while those in other strips were almost 100%. Scattered ^{4}He particles were identified using the ΔE and E data from three-layers of plastic scintillation detectors.
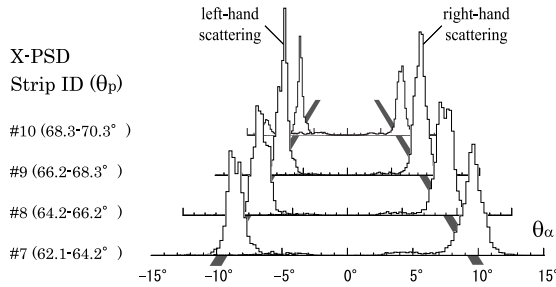
Figure 3. The correlation between the proton recoiling angle and the ^{4}He scattering angle. Proton recoiling angle is represented by X-PSD strip ID. The broad lines in the left and right show the kinematically calculated angular correlation.

Figure 3 shows correlation between the scattering angle of ^{4}He measured by the MWDC and the recoiling angle of proton, represented by X-PSD strip ID. Clear peaks are observed corresponding to p+^{4}He elastic scattering events. Yields $N_L^\uparrow$, $N_R^\uparrow$, $N_L^\downarrow$, and $N_R^\downarrow$ are obtained by integrating the peaks of left and right detectors in both cases where the po-

larizations are "up" and "down". Here, indices L/R represent the direction of scattering left/right and $\uparrow/\downarrow$ represent the direction of the polarization up/down. Averaged polarization $\overline{P}_y$ is obtained as

$$\overline{P}_y = \frac{1}{A_y} \frac{\sqrt{N_L^\uparrow N_R^\downarrow} - \sqrt{N_R^\uparrow N_L^\downarrow}}{\sqrt{N_L^\uparrow N_R^\downarrow} + \sqrt{N_R^\uparrow N_L^\downarrow}}, \qquad (2)$$

canceling spurious asymmetry due to imbalance of detection efficiency and instrumental geometry.

Results obtained in X-PSD strips #7–10 (θ_p = 62.1–70.3°) are shown in Table 1. The averaged proton polarization is observed to be 4.8±1.9 %. NMR signal amplitude is calibrated using this value. The maximum polarization during the experiment was then determined to be 15.5 ± 6.3 % corresponding to the point t =14.3 h in Fig. 1. The offline maximum polarization, achieved 20 hours before the beam irradiation, was 23 ± 9.1 %.

X-PSD strip ID	$\overline{P}_y$	$\Delta\overline{P}_y$
#10 (θ_p =68.3–70.3°)	2.9%	3.2%
#9 (θ_p =66.2–68.3°)	4.0%	3.5%
#8 (θ_p =64.2–66.2°)	7.5%	4.9%
#7 (θ_p =62.1–64.2°)	6.1%	9.6%
#7–10 (θ_p =62.1–70.3°)	4.8%	1.9%

Table 1. Averaged proton polarization obtained in X-PSD strips #7–10.

4. Summary

We have constructed a polarized solid target which can be operated under a low magnetic field of 80 mT at a high temperature of 100 K. The absolute value of the proton polarization was measured via the $\vec{p}$+^{4}He elastic scattering. The averaged and the maximum value of the proton polarization were 4.8 ± 1.9% and 15.5 ± 6.3 %, respectively. This target will be used in the $\vec{p}$+^{6}He elastic scattering experiment where analyzing power is to be measured with improved resolution and accuracy from the previous measurement [2].

References

[1] T. Uesaka *et al.*, Nucl. Instrum. Methods. A **526** (2004) 186.

[2] M. Hatano *et al.*, Proc. of 4th International Conference on Exotic Nuclei and Atomic Masses (ENAM 04), to be published.

[3] H. Togawa *et al.*, RCNP Annual Report (1987) 1.

[4] T. Wakui *et al.*, Nucl. Instrum. Methods. A (in press).

[5] T. Wakui *et al.*, CNS Annual Report 2004 (2005) 77.

Measurements of the nd Elastic Scattering at 250MeV and Three Nucleon Force Effects

Y. Maeda, K. Fujita[b], M. B. Greenfield[g], Y. Hagiwara[d], K. Hatanaka[b], M. Hatano[a], K. Itoh[f],
H. Kamada[h], J. Kamiya[b], T. Kawabata, H. Kuboki[a], T. Kudoh[d], Y. Nagasue[d], H. Okamura[c],
T. Saito[a], H. Sakai[a], Y. Sakemi[b], M. Sasano[a], K. Sekiguchi[e], Y. Shimizu[b], K. Suda, A. Tamii[b],
T. Wakasa[d] and K. Yako[a]

Center for Nuclear Study, Graduate School of Science, University of Tokyo
[a]Department of Physics, University of Tokyo
[b]Research Center for Nuclear Physics, Osaka University
[c]CYRIC, Tohoku University
[d]Department of Physics, Kyushu University
[e]RIKEN (The Institute of Physical and Chemical Research)
[f]Department of Physics, Saitama University
[g]International Christian University
[h]Department of Physics, Kyushu Institute of Technology

One of the interesting problems for the few-nucleon system is the three-nucleon force (3NF) properties.

Recently, highly precise measurements of the dp elastic scattering for the deuteron energies of $E_d^{\mathrm{lab}} = 140$, 200 and 270 MeV have been performed [1]. The calculations with NN forces only fail to reproduce the data of cross sections and vector analyzing powers, but these discrepancies are filled by adding the 2π exchange 3NFs. These results support the prediction that the Nd elastic scattering at intermediate energy is a good probe to study the 3NF effects. However, it should be noted that all discussions are made by the comparison between the precise pd data and the rigorous nd Faddeev calculations because performing the three-body calculation with the long-range Coulomb repulsion is extremely difficult.

To study the 3NF effects in a Coulomb-free system, we have carried out the $\vec{n}d$ elastic scattering at 250 MeV at the Research Center for Nuclear Physics (RCNP). We measured the differential cross sections and vector analyzing powers for $\theta_{cm} = 10° - 180°$. To cover such a wide angular region, we applied two kinds of technique to perform the forward and the backward measurements, respectively.

The Measurements for the backward angular region ($\theta_{cm} \geq 60°$) were carried out at the (n, p) facility [2] at RCNP. The nearly mono-energetic polarized neutron beam was produced by the $^7\mathrm{Li}(\vec{p}, \vec{n})^7\mathrm{Be}$(g.s.+0.4 MeV) reaction at 250MeV. We used the self-supporting deuterated polyethylene (CD$_2$) sheets [3] with a thickness of $100 - 220$ mg/cm^2 as the deuteron targets. The deuteron targets are mounted in the multi-wire drift chamber (MWDC). In this work, we have also measured the np scattering for the normalization. Then we used the polyethylene (CH$_2$) sheets with a thickness of $90 - 190$ mg/cm^2 as proton targets. The recoil deuterons or protons were momentum analyzed by Large Acceptance Spectrometer (LAS).

The measurements for the forward angular region ($\theta_{cm} \leq 60°$) were carried out at the neutron time-of flight (NTOF) facility [4] at RCNP. The polarized neutron beam was also produced by the $^7\mathrm{Li}(\vec{p}, \vec{n})$ reaction. The produced neutrons bombarded the deuteron target which was located 2 m downstream from $^7\mathrm{Li}$ target. The deuterated liquid scintillator BC537 was used as the deuteron target and the coincidence measurements were performed. To remove the background events originating from the gamma rays, we introduced the $n\gamma$ discrimination method. The scattered neutrons run through 70 m distance and detected by NPOL II. The energy of the detected neutron was determined by the TOF technique.

The results of the differential cross sections and vector analyzing powers are shown in Fig. 1 by solid circles and squares with statistical errors only. Dark (light) shaded bands represent the results of Faddeev calculations with (without) the Tucson-Melbourne 3NF [5]. Solid and dotted lines represent the calculations with AV18+UrbanaIX-3NF and CD-BONN+TM′-3NF respectively. Concerning about the differential cross sections, it can be seen that the calculations including 3NF better reproduce the data but still underestimate largely at backward region. These discrepancies may be an indication of the relativistic effects [6] which are not taken into account in these calculations. The data of the vector analyzing powers contain large statistical errors but these are consistent with the $\vec{p}d$ data within the systematic error of the $\vec{n}d$ data. We can see that the calculations fail to reproduce the angular distribution of the data at $\theta_{cm} = 110° \sim 140°$.

As predicted in Ref. [7], the effects of the 3NF are expected to be relatively large at higher energy. On the other hand, a precise measurement of the nd total cross section [8, 9] revealed that the corrections resulting from relativistic kinematics are comparable in size with the 3NF effects at higher energy. Very recently, the relativistic Faddeev calculations have been performed for the nd elastic scattering at 250 MeV [10]. In Fig. 2, we show the non-relativistic (solid
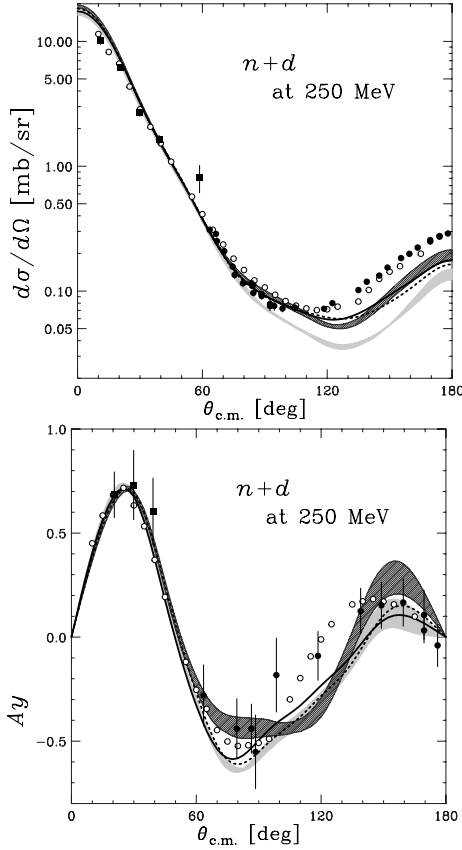
Figure 1. Differential cross sections and vector analyzing powers for the $\vec{n}d$ elastic scattering at $E_n = 250$ MeV. The solid circles and squares (open circles) are the results of $\vec{n}d$ ($\vec{p}d$) measurements. The statistical errors are shown in the figures. The Faddeev calculations including various NN potentials with (dark shaded band) and without (light shaded band) TM-3NF, AV18+UrbanaIX (solid line) and CD-BONN+TM′-3NF (dotted line) are also shown.

Figure 2. The differential cross sections for the nd elastic scattering at 250 MeV (solid circles and squares). The solid line is the prediction with CDBonn only and the two kinds of relativistic predictions with different approximations (dashed and dotted lines) are also shown.
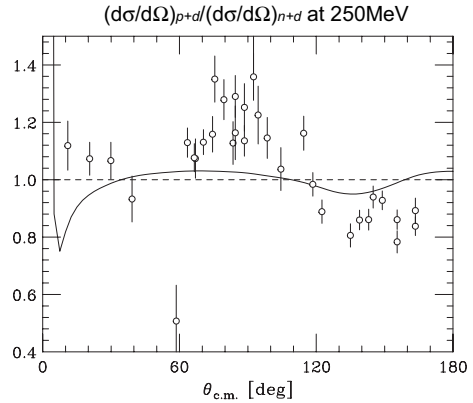
Figure 3. The ratio of the cross section of pd to that of nd. The circles shows the results deduced from the data of this work and the pd data. The solid line shows the theoretical predictions deduced by including the Coulomb interaction approximately.

line) and relativistic (dashed and dotted lines) predictions. It should be noted that all relativistic calculations include no 3NF. We can see that the fully relativistic calculations improve the fit to the data at $\theta_{cm} \geq 160°$ but improvements are not enough.

We have also carried out the $\vec{p}d$ measurements at 250 MeV [11] and these results are shown by open circles. This allows us to compare the nd and pd data directly. In Fig. 3, the ratio of the cross sections are plotted with open circles. The solid line represents the theoretical prediction at 250 MeV [12] which is based on the CDBonn. In the calculation of the pd elastic scattering, the Coulomb force is included in an approximate way [13]. The magnitudes of the discrepancies from unity are much larger for the data than for the prediction. However the angles where the data cross unity around $\theta_{cm}= 110°$ are well reproduced by the theoretical prediction.

[3] Y. Maeda *et al.*, Nucl. Instrum. Methods. A **490** (2002) 518.

[4] H. Sakai *et al.*, Nucl. Instrum. Methods. A **369** (1996) 120.

[5] S.A. Coon *et al.*, Nucl. Phys. A **317** (1979) 242.

[6] H. Witała *et al.*, Phys. Rev. C **57** 2111 (1998)

[7] H. Witała, W. Glöckle, J. Golak, A. Nogga, H. Kamada, R. Skibiński and J. Kuroś-Żołnierczuk, Phys. Rev. C **63** (2001) 024007.

[8] W.P. Abfalterer, *et al.*, Phys. Rev. Lett. **81** (1998) 57.

[9] H. Witała, H. Kamada, A. Nogga, W. Glöckle, Ch. Elster and D. Hüber, Phys. Rev. C **59** (1999) 3035.

[10]H. Witała, *et al.*, Phys. Rev. C **71** (2002) 054001.

[11]K. Hatanaka *et al.*, Phys. Rev. C **66** (2002) 044002.

[12]H. Kamada, private communication.

[13]P. Doleschall *et al.*, Nucl. Phys. A **380** (1982) 72.

References

[1] K. Sekiguchi *et al.*, Phys. Rev C **65** (2002) 034003.

[2] K. Yako *et al.*, Nucl. Phys. A **684** (2001) 563c.

Quadrupole Excitation Strengths and Cluster Structures in ^{11}B

T. Kawabata, H. Akimune[a], H. Fujita[b], Y. Fujita[c], M. Fujiwara[b], K. Hara[b], K. Hatanaka[b],
M. Itoh[b], Y. Kanada-En'yo[d], S. Kishi[e], K. Nakanishi[b], H. Sakaguchi[e], Y. Shimbara[b], A. Tamii[b],
S. Terashima[e], M. Uchida[b], T. Wakasa[f], Y. Yasuda[e], H. P. Yoshida[b] and M. Yosoi[b]

Center for Nuclear Study, Graduate School of Science, University of Tokyo
[a]*Department of Physics, Konan University*
[b]*Research Center for Nuclear Physics, Osaka University*
[c]*Department of Physics, Osaka University*
[d]*Yukawa Institute for Theoretical Physics, Kyoto University*
[e]*Department of Physics, Kyoto University*
[f]*Department of Physics, Kyushu University*

It is well known that many light nuclei possess a prominent cluster structure and the α particle plays an important role as a constituent of the cluster state. Such cluster structures are generally observed near the α-decay threshold energy as expected in the Ikeda diagram [1]. For example, it has been suggested that the 7.65-MeV 0_2^+ state in ^{12}C has an 3α-cluster configuration [2]. This state located at 0.39 MeV above the 3α-decay threshold energy has a structure where 3α clusters interact predominantly in relative S waves [3].

Recently, the Gamow-Teller (GT) and spin-flip $M1$ strengths in ^{11}B were successfully measured and it was found that the $3/2_3^-$ state in ^{11}B is not described by the shell model calculations [4]. This state is located at $E_x = 8.56$ MeV where it is just 100 keV below the α-decay threshold. This $3/2_3^-$ state is, therefore, inferred to be a cluster state. For further clarification, it is necessary to measure quadrupole excitation strengths. The quadrupole excitations are one of the most fundamental excitation modes in nuclei, and the excitation strengths are closely related to the nuclear structure.

The quadrupole excitation strengths were extensively examined by means of γ-decay measurements. However, the electromagnetic probes are sensitive only to protons but not to neutrons. Most of the cluster states in nuclei are excited by the isoscalar transitions in which both protons and neutrons carry the transition strengths. Therefore, the isoscalar quadrupole transition strengths should be measured.

The electric quadrupole ($E2$) strength $[B(E2)]$ and isoscalar quadrupole strength $[B(E2; IS)]$ are described by

$$B(E2) = \frac{1}{2J_i + 1} |M(p)|^2 e^2,$$

$$B(E2; IS) = \frac{1}{2J_i + 1} |M(p) + M(n)|^2.$$

where J_i is the spin of the initial state. $M(p)$ and $M(n)$ are the proton and neutron quadrupole transition matrix elements. $M(p)$ and $M(n)$ are given by

$$M(p) = \frac{1}{2} \langle f \| (1 - \tau_z) r^2 Y_2 \| i \rangle,$$

$$M(n) = \frac{1}{2} \langle f \| (1 + \tau_z) r^2 Y_2 \| i \rangle,$$

where τ_z is the isospin Pauli matrix defined by $\tau_z |p\rangle = -|p\rangle$ and $\tau_z |n\rangle = |n\rangle$.

For light self-conjugate ($N = Z$) nuclei, it is expected that the neutron transition strengths are similar to the proton transition strengths under the assumption of the charge symmetry. Thus, the isoscalar quadrupole strengths are obtained only from the proton transition strengths. For the other nuclei, however, the neutron transition strengths could be different from the proton transition strengths, and the isoscalar strengths must be determined by different measurements.

One possible method to obtain the isoscalar transition strengths is to measure the $E2$ strengths for mirror nuclei. However, since mirror nuclei of stable nuclei are generally unstable, it is difficult to measure decay properties of such unstable nuclei. Especially, for nuclei with non-zero ground-state spin, the extraction of the $E2$ strengths becomes difficult because not only the quadrupole transition but also the other multipole transitions are allowed. In case of the $A = 11$ system, the $E2$-decay strengths were measured for several low-lying states in stable ^{11}B nucleus, but no $E2$ strengths were known for the excited states in unstable ^{11}C nucleus.

Another possible method to obtain the isoscalar transition strengths is to measure the hadron scattering. Hadron scattering provides a good probe for excitation strengths because there is a good proportional relation between the cross sections and the relevant excitation strengths. Since both the isoscalar and isovector strengths coherently contribute to the excitation strengths in $N \neq Z$ nuclei with non-zero ground-state isospin, isoscalar probes like deuteron or ^{4}He should be used to extract the isoscalar excitation strengths.

In the present work, the elastic and inelastic deuteron scatterings from ^{11}B were measured to obtain the isoscalar quadrupole excitation strengths in ^{11}B.

The experiment was performed at the Research Center for Nuclear Physics, Osaka University, using a 200-MeV polarized deuteron beam. The detailed explanations for the experimental procedures have been given in Ref. [4] and references therein. The ^{11}B(d, d') cross section is given by an incoherent sum over the cross sections for the different multipole transitions. Since the angular distribution of the cross section for each multipole transition changes depend-

J^π	E_x (MeV)	Experiment		Shell model		AMD-VAP	
		$B(E2;IS)$ (fm^4)	$B(E2)$ (e^{2}fm^4)	$B(E2;IS)$ (fm^4)	$B(E2)$ (e^{2}fm^4)	$B(E2;IS)$ (fm^4)	$B(E2)$ (e^{2}fm^4)
$1/2_1^-$	2.12	11 ± 2	2.6 ± 0.4	12.0	1.8	11.9	2.0
$5/2_1^-$	4.44	56 ± 6	21 ± 6	49.5	16.5	67.5	19.4
$3/2_2^-$	5.02	4.7 ± 1.5	< 1.3	14.2	1.7	2.9	0.05
$7/2_1^-$	6.74	38 ± 4	3.7 ± 0.9	42.9	4.4	35.8	3.9
$3/2_3^-$	8.56	< 3.5				4.0	0.5
$5/2_2^-$	8.92	0.4 ± 0.3	1.6 ± 1.2	0.012	0.014	1.1	0.3

Table 1. Measured isoscalar quadrupole strengths $B(E2; IS)$ for several transitions in ^{11}B compared with the electric quadrupole strengths $B(E2)$ taken from Ref. [5]. Theoretical predictions by the shell model [6] and AMD-VAP calculations are also listed.

ing on its transfered angular momentum, it is possible to decompose the cross section into each multipole component by measuring the angular distribution. The isoscalar quadrupole strength is obtained from the cross section for the $\Delta J^\pi = 2^+$ transition.

The obtained isoscalar quadrupole strengths $B(E2; IS)$ are tabulated together with the $B(E2)$ values taken from Ref. [5] in Table 1. Although the $3/2_3^-$ state at $E_x = 8.92$ MeV can be excited by the $\Delta J^\pi = 0^+, 1^+, 2^+$ and 3^+ transitions, the main part of the transition is due to $\Delta J^\pi = 0^+$. Since the observed $\Delta J^\pi = 0^+$ transition strength is much stronger than the expected $\Delta J^\pi = 2^+$ strength, the $\Delta J^\pi = 2^+$ component of the transition strength can not be reliably extracted for the $3/2_3^-$ state.

The experimental values are compared with the recent shell model calculation by Suzuki, Fujimoto, and Otsuka (SFO) [6] and the variational calculation after spin-parity projection (VAP) under the framework of the antisymmetrized molecular dynamics (AMD) [7]. Since the shell model prediction with the bare electric charges of $e_p = 1$ and $e_n = 0$ underestimates the experiment by a factor of 2–3, the effective charges are introduced to improve the theoretical prediction. The shell-model values in Table 1 are calculated using the effective charges of $e_p^{eff} = 1.24$ and $e_n^{eff} = 0.22$. On the other hand, no effective charges are used in the AMD-VAP calculation.

The AMD-VAP calculation successfully describes the $3/2_3^-$ state, while the shell model calculation fails to predict this state. According to the AMD-VAP calculation, the $3/2_3^-$ state has a well-developed cluster structure with the $2\alpha + t$ configuration and the quadrupole strengths for this state is relatively weak. This result strongly supports our previous expectation that the $3/2_3^-$ state in ^{11}B has a cluster structure.

For the $5/2_2^-$ state, the shell model calculation with the SFO interaction predicts much smaller values of the quadrupole strengths although this calculation gives a reasonable estimation of the spin-flip $M1$ strengths [4]. On the other hand, the AMD-VAP calculation well explains both the quadrupole and spin-flip $M1$ strengths for this state, simultaneously. In the AMD-VAP calculation, the $5/2_2^-$ state is described as a mixed state of the cluster and shell-model-like components. The cluster component is considered to be a rotational state of the $3/2_2^-$ state. The quadrupole and spin-flip $M1$ strengths for the $5/2_2^-$ state are mainly

carried by the cluster and shell-model-like components, respectively. In the other words, the cluster component carries almost no spin-flip $M1$ strengths while the shell-model-like component carries almost no quadrupole strengths . This AMD-VAP prediction is consistent with the fact that the shell model calculation reasonably well estimates the spin-flip $M1$ strength but not the quadrupole strength for the $5/2_2^-$ state. Both the shell-model-like and cluster structures are, therefore, necessary to explain the experimental result on the $5/2_2^-$ state. As a conclusion, the present result suggests coexistence of the two different structures in the $5/2_2^-$ state.

In summary, we measured the cross section for the ^{11}B(d, d') reaction to study the isoscalar quadrupole excitation strengths. The obtained isoscalar quadrupole strengths were compared with the shell model calculation with the SFO interaction and the AMD-VAP calculations. It was found that the $3/2_3^-$ state has a well-developed $2a + t$ cluster structure while the $5/2_2^-$ state has both the cluster and shell-model-like structures.

References

[1] K. Ikeda, N. Takigawa and H. Horiuchi, Prog. Theor. Phys. Suppl. Extra Number, (1968) 464.

[2] H. Morinaga, Phys. Rev. **101** (1956) 254; Phys. Lett. **21** (1966) 78.

[3] Y. Fujiwara, H. Horiuchi, K. Ikeda, M. Kamimura, K. Kato, Y. Suzuki, and E. Uegaki, Prog. Theor. Phys. Suppl. **68** (1980) 60.

[4] T. Kawabata *et al.*, Phys. Rev. C **70** (2004) 034318.

[5] F. Ajzenberg-Selove, Nucl. Phys. A **506** (1990) 1.

[6] Toshio Suzuki, Rintaro Fujimoto, and Takaharu Otsuka, Phys. Rev. C **67** (2003) 044302.

[7] Y. Kanada-En'yo Phys. Rev. Lett. **81** (1998) 5291.

SHARAQ Project

T. Uesaka, S. Shimoura, S. Kubono, T. Kawabata, E. Ideguchi, H. Yamaguchi and H. Sakai[a]

Center for Nuclear Study, Graduate School of Science, University of Tokyo
[a]Department of Physics, University of Tokyo

1. Introduction

RI beams have a variety of isospin (T), internal energy (mass excess) , and spin (S), while light stable beams such as proton, deuteron, and ^{3,4}He have $T, S < 1$ and the minimum internal energies among isobars. Due to the properties, RI-beam induced reactions can have a unique potential to be used to *probe* nuclear many body systems.

RI beams produced in RI beam factory (RIBF) at RIKEN will have an energy ranging 100–300 MeV/A which is most appropriate for spectroscopic purposes. It is well known that, at these energies, nucleon-nucleon interaction is weakest and thus a nucleus is most transparent. As a natural consequence of this, absorption or distortion effects should be smaller than at lower or higher energies. Particular emphasis should be also placed on additional advantage of 100–300 MeV/A beams that the spin-isospin modes are most strongly excited relative to the spin-isospin independent ones. The spin-isospin excited states are most clearly observed in this energy region.

Full use of these unique properties of RI beams from RIBF will open a new research field in nuclear physics, which we call "**S**pectroscopy of **HA**dronic systems by **R**adio-**A**ctive **Q**uantum beams", **SHARAQ**. CNS has decided to concentrate its major resources on the SHARAQ project and to construct a high resolution magnetic spectrograph, SHARAQ spectrograph. Physics investigation in the SHARAQ project are described in the next section. In section 3, overview of SHARAQ spectrograph is presented.

2. Physics with SHARAQ

2.1. Charge exchange reactions

Charge exchange reaction is a tool to probe larger (sometimes smaller) isospin states. It is also useful to deduce spin-isospin responses of nuclei. The reactions induced by light stable nuclear beams have been proven to be effective to investigate excited states at low excitation energies.

However, when extended to higher excitation energies, they are sometimes less effective than at lower excitation energies. This is mainly due to large momentum transfer which necessarily accompanies the reaction. Since states of interest here can be most clearly observed at small momentum transfer, $q \sim 0$, a new method to approach the highly excited states should realize $q \sim 0$ and large ω simultaneously. This can be uniquely achieved by exothermal charge exchange reactions induced by RI beams. By use of the reactions, we will be able to produce states which have been hardly obvserved so far, for example, multi-neutron systems, isovector spin monopole resonance, and double Gamow-Teller resonance.

Multi-neutron systems attract much attention in connection to understanding of few-nucleon systems and many-nucleon forces which are to be tested by precise *ab initio* calculations with modern nucleon-nucleon interactions. The systems are also interesting from the viewpoint of the limits in the nuclear system beyond the neutron dripline where correlations in multi-body scattering states play an essential role.

There are several theoretical works on the existence of the three- and four-neutron states, where neither bound states nor resonant states are predicted by using modern nucleon-nucleon interactions [1,2]. Experimentally, no evidence has been found in the direct reactions between heavy ions and (π^-,π^+) reactions until a few years ago [3]. However, possible candidates of neutron clusters have been reported recently in breakup reactions of neutron-rich ^{14}Be beams [4], where correlating neutron cluster(s) in neutron-rich nuclei is considered.

In the SHARAQ project, we plan to approach four neutron final states via the double charge exchange (DCX) reaction (^{8}He,^{8}Be) on ^{4}He , where the momentum transfer is much less than that of the DCX reactions of stable beams or the (π^-,π^+) reaction. This is because of a large internal energy of the ^{8}He nucleus. Information on the final states is deduced from the missing mass spectra of the DCX reaction. This DCX method is also applied for the heavy hydrogen isotopes such as ^{6,7}H by using ^{6,7}Li targets.

Giant resonances which have been hardly within the reach of conventional probes can be effectively populated by RI-beam induced single and double charge exchange reactions. They are isovector spin monopole resonance (IVSMR) and double Gamow-Teller resonance (DGTR).

IVSMR is a compressional mode with an operator of $\sigma\tau r^2$ and its excitation energy and width are related to the spin compressibility of the nuclear matter. Only one experimental evidence was reported in the (p,n) reactions at 800 MeV [5] indicating its excitation energy of 20–50 MeV for the β^- direction. In order to establish the IVSMR, exothermal heavy-ion charge exchange reactions probing the spin-isospin strength at nuclear surface around 250 MeV/nucleon are the best tool. Since the transition density of IVSMR changes its sign inside a nucleus, the surface sensitivity is indispensable property of the probe to avoid undesirable cancellation of the strength. The (^{12}N, ^{12}C) and (^{12}B, ^{12}C) reactions for the β^- and β^+ directions, respectively, are the best tools due to their large positive Q-values.

DGTR, which is of particular importance in relevance to double beta decay, is still unobserved experimentally, while other multi-phonon giant resonances, such as double isobaric analogue and double giant dipole resonances, have

been observed via the (π^+, π^-) reactions. Attempts to find double Gamow-Teller strengths via the heavy ion double charge exchange reactions have been made at GANIL and at RCNP by using the $(^{18}\text{O}, ^{18}\text{Ne})$ and the $(^{11}\text{B}, ^{11}\text{Li})$ reactions, respectively. No clear evidence has been found so far. The $(^{20}\text{Mg}, ^{20}\text{Ne})$ reaction is a suitable tool to probe the double Gamow-Teller states in several respects. In the reaction, an energy used to excite the target nucleus, typically $E_x \sim 20$–30 MeV for the double Gamow-Teller resonance states, is provided from the internal energy of the ^{20}Mg neuclus. As a result of this, momentum-transfer measurement can be kept as small as ~ 5 MeV/c at $0°$ and at $E/A = 300$ MeV. This exhibits a striking contrast to the the $(^{18}\text{O}, ^{18}\text{Ne})$ and the $(^{11}\text{B}, ^{11}\text{Li})$ reactions where larger momentum transfers is necessarily accompanied. It should be also emphasized continuum background is expected to be considerably suppressed in the $(^{24}\text{Mg}, ^{20}\text{Ne})$ reaction due to the recoilless condition of $q \sim 0$.

2.2. Multi-nucleon transfer reactions

Another application of SHARAQ is a measurement of nuclear mass in the vicinity of the r-process. Interesting reactions for the present purpose include massive neutron transfer reactions like $(^{18}\text{C}, ^{10}\text{C})$ $(+8n)$, massive proton pick-up reactions like $(^{18}\text{C}, ^{26}\text{Si})$ $(-8p)$. Although these reactions involve many-nucleon transfers, the reaction Q-values are very favorable, because the reaction Q-values are nearly zero or positive. The latter reaction, however, is less feasible because of the energy matching conditions due to the large charge change. If there is some coherent transfer process of paired protons, the cross sections might be not so small. It is an interesting subject to be investigated, and could be a unique probe for investigation of the r-process nuclei. It may be difficult to discuss the reaction mechanism for these reactions, but they are useful to identify the nuclear levels and also to determine the nuclear masses. This study enables us to study the levels not only of bound states but also of neutron resonant states. The particle identifications would not be so serious, but the cross sections need to be investigated carefully.

One of the crucial mass regions that we try to investigate is the waiting point regions of the possible r-process at N = 82 and 126. The r-process pathways predicted differ strongly depending on the mass formulae used. The waiting points there are roughly $7 - 12$ protons away from the line of stability. Thus, some crucial nuclei near the waiting points can be reached by the multi-proton pickup reactions. These studies are very useful for learning the shell closure in the region of very neutron-rich, unstable heavy mass region even if the transfer reaction really does not reach the waiting point nuclei.

3. Design of Spectrometer

SHARAQ spectrograph is designed to achieve a momentum resolution of $\delta p/p = 1/15000$ for particle with magnetic rigidity of $B\rho = 6.8$ Tm at maximum. Normal-conducting dipole magnets with an orbital radius of 4.8 m are needed to meet the design criterion. Since the availale space of the experimental area in RIBF building is limited,

the new spectrometer is designed to change the bending direction between two dipole magnets (back-beding configuration) as shown in Fig. 1.

The new spectrometer consists of three quadrupole magnets and two dipole magnets. Horizontal trajectories are schematically shown in Fig. 1. Particle trajectories are drawn for $\Delta x = \pm 2$ mm, $\Delta\theta = \pm 30$ and 0 mr, $\Delta p/p = \pm 3\%$, as a result of a third-order ion optical calculation. According to the third-order calculation, the angular acceptance is 60 mr $\times$ 200 mr $= 12$ mSr and the momentum bite is 6%, which satisfy our design goal.
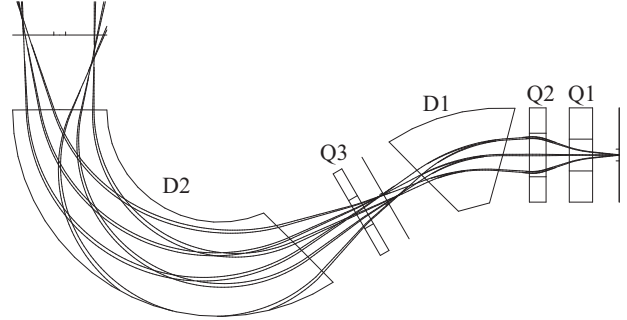
Figure 1. Schematic view of the magnet layout. Particle trajectories are drawn for $\Delta x = \pm 2$ mm, $\Delta\theta = \pm 30$ and 0 mr, and $\Delta p/p = \pm 3\%$ as a result of a third-order ion optical calculation.

A resolving power of $\Delta p/p = 1/15000$ can be expected if a beam position is detemined with a accuracy of $\Delta x = 1$ mm. The horizontal and vertical scattering angles can be determined from the horizontal angle and vertical position at the focal plane.

In the measurement using a high resolution spectrometer, a momentum spread of the beam usually limits the resulting energy resolution. This is much more serious when we use secondary radio-active beams. A dispersion matching technique or an event-by-event monitoring of the beam momentum will be introduced for the purpose to compensate the momentum spread of the RI beam. Effectivenesses of the two methods depends on the beam intensity. The beamline needs to have a large dispersion at the SHARAQ target, and detailed investigation is in progress.

References

[1] A. Hemmdan, W. Glöcle, and H. Kamada, Phys. Rev. C **66** (2002) 054001.
[2] N.K. Timofeyuk, J. Phys. G **29** (2003) L9.
[3] D.R. Tilley, H.R. Weller and G.M. Hale, Nucl. Phys. A **541** (1992) 1.
[4] Marqués *et al.*, Phys. Rev. C **65** (2002) 044006.
[5] D.L. Prout *et al.*, Phys. Rev. C **63** (2000) 014603.
[6] R.G.T. Zegers *et al.*, Phys. Rev. Lett. **90** (2003) 202501.

Experimental Nuclear Physics: PHENIX Experiment at BNL-RHIC

Progress of the PHENIX Experiment in the Year 2004

H. Hamagaki, K. Ozawa, T. Sakaguchi, M. Inuzuka, S. Kametani, F. Kajihara, T. Gunji, T. Isobe,
N. Kurihara, S. X. Oda, Y. Morino, S. Saito, J. Kikuchi[a], Y. Yamaguchi[a] and Y. Tanaka[b],
for the PHENIX Collaboration

Center for Nuclear Study, Graduate School of Science, University of Tokyo
[a] *Advanced Research Institute for Science and Engineering, Waseda University*
[b] *Nagasaki Institute of Advanced Science*

1. Introduction

Experimental studies at the Relativistic Heavy Ion Collider (RHIC) of Brookhaven National Laboratory, USA, has been producing many interesting results since the first successful collisions between Au ions in June 2000. The goal of the studies at RHIC is to find evidence of the QCD phase transition from normal nuclear matter to deconfined quark matter, called quark-gluon plasma (QGP), and to study the properties of the hot QCD matter.

The CNS group has been participating in the PHENIX experiment, which is one of the major experiments at RHIC. A schematic view of the the PHENIX experimental setup is shown in Fig. 1. It consists of two central arms (East and West), two muon arms (North and South) and inner detectors for event trigger and event characterization. The PHENIX experiment aims to address as many signatures as possible for QGP formation, by having a very unique capability to measure photons, electrons and muons as well as hadrons.

In this article, progress of the PHENIX experiment and the activities of the CNS group in the Japanese fiscal year (JFY) 2004 are briefly summarized.
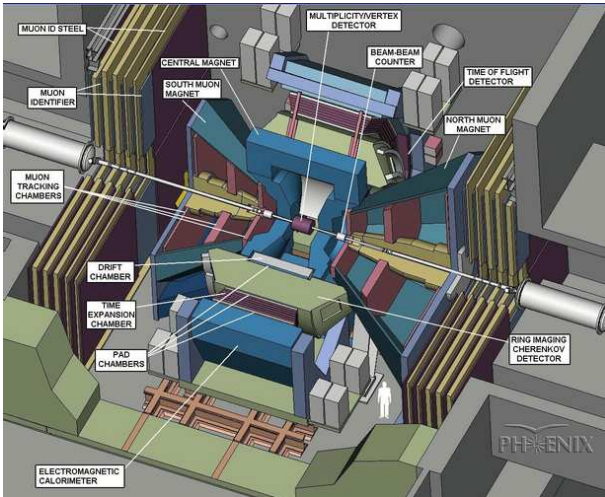
Figure 1. Layout of the PHENIX experiment.

2. Year-5 RUN at RHIC

In the JFY 2004, the latter half of the fourth physics run, RHIC RUN-4, and the first half of the fifth physics run, RHIC RUN-5, were successfully executed. In RUN-4, PHENIX collected a significant amount of Au + Au col-

lision data both at $\sqrt{s_{NN}} = 200$ GeV and $\sqrt{s_{NN}} = 62.4$ GeV. In RUN-5, Cu + Cu collisions instead of Au + Au collisions were employed, in order to have controlled data for collisions between light-mass nuclei. 8.6 G events were accumulated at $\sqrt{s_{NN}} = 200$ GeV, and 1.1 G events at lower energy, $\sqrt{s_{NN}} = 63$ GeV. After the heavy ion runs, a polarized proton run at $\sqrt{s_{NN}} = 200$ GeV is continued to the next fiscal year.

3. Activities of the CNS group

The CNS group had several distinct activities in the JFY 2004. Only brief introductions are provided in this article, and detailed descriptions will be found in the separate articles.

3.1. RICH and AEROGEL operation

The RICH (Ring Imaging CHerenkov) subsystem, which is a Cherenkov counter using CO_2 as a radiation gas, is a main device for electron identification of the PHENIX experiment. The CNS group has been responsible for its maintenance, operation during the run, and calibration for data analysis. The RICH subsystem worked without serious problems throughout the RUN-4 and RUN-5.

PHENIX has unique capability of identifying charged hadrons in a wide momentum region, with the high-resolution TOF and RICH. With increase of interest to the hadron production in the medium to high momentum region, extension of particle identification (PID) was made by adding an AEROGEL Cherenkov counter with refractive index $n \sim 1.01$. The AEROGEL project, carried out by the collaboration of Tsukuba, BNL, Russia and CNS, was completed in this year, and was successfully used in the RUN-5. Performance of the AEROGEL counter and preliminary results are described in Ref. [1].

3.2. Data analysis and results

Four physics papers were published from the PHENIX collaboration in JFY 2004, as listed in the publication list of this annual report. Several others have been submitted and are in different stages before final publication.

Major efforts of the CNS group has been on the physics with photons and leptons, and various achievements were made as described below.

Single photon is considered to be a sensitive probe of various stages of collision processes, with its property of penetration through dense matter. Detecting single photons is challenging because of very low production rate and competing backgrounds. The PHENIX succeeded in measuring direct photons from pQCD hard process in Au + Au col-

lisions. The result clearly demonstrates that N_{coll} scaling holds well for pQCD hard photon production, as described in Ref. [2]. The result also provides strong support to the interpretation that the jet quenching is a final state effect.

Systematic studies of jet quenching effect is needed to understand better the energy loss mechanism and properties of dense matter. For that purpose, π^0 production in Au + Au collisions was investigated at a lower energy of $\sqrt{s_{NN}} = 62.4$ GeV taken in the RUN-4, and preliminary results are presented in Ref. [3].

Single electron production in p + p, d + Au, and Au + Au collisions has been investigated. Sources of single electrons are categorized into two; 'photonic' and 'non-photonic'. Main 'non-photonic' sources at the RHIC energies are leptonic decay of charm and bottom mesons, which are considered to be good probes of hard processes. 'Photonic' sources, majority of which comes from Dalitz decay of neutral mesons and external conversion of photons, are severe background sources for measuring 'non-photonic' sources. Converter method was employed to estimate and subtract the photonic background sources, which is considered to have smaller ambiguity compared to a Cocktail method which depends heavily upon the simulation. Current status of analysis efforts are described in Ref. [4].

Suppression of J/ψ yield has been considered to be a direct evidence of deconfinement. Recently, possible enhancement of the yield has been proposed by theorists which is due to coalescence production of J/ψ from charm and anti-charm quarks in QGP phase or in the hadronization stage. The CNS group has been taking leading roles in the analysis of J/ψ productions through electron-positron decay channel. The J/ψ production in d + Au collisions from RUN-3 is in its final stage [5], whose result should serve as a reference to that in heavy ion collisions. The J/ψ yield as well as p_T distribution for a few centrality bins in Au + Au collisions has been preliminary obtained from the RUN-4 [6].

Important research subjects still left over at RHIC are low-mass vector mesons and low-mass lepton-pair continuum. Measuring vector mesons via lepton-pair decay channel is crucial in order to extract information relevant to chiral symmetry restoration. Importance of low-mass lepton-pair continuum originated from thermal sources cannot be over-emphasized. Huge combinatorial background makes it impossible to deduce clear signals of light-mass vector mesons. Current status of analysis of low-mass electron-pairs are presented in ref. [7]. HBD (hadron blind detector), which is the gaseous Cherenkov counter with a UV-photon detector, is the most promising yet ambitious detector for reducing background sources, and the current status of its development for the PHENIX experiment is also mentioned in the report.

3.3. R & D efforts

GEM (gas electron multiplier) has been a central subject of detector development and application of our group in the last few years. GEM (gas electron multiplier), which has a very simple structure having regularly arrayed holes pierced through a Kapton sheet coated at both sides with copper foils, was originally developed at CERN. The CERN-GEM has an intrinsic problem of gain variation due to charge-up, and a new method of piercing the holes was recently established to reduce significantly the variation. Current status is presented in Ref. [8].

A micro-TPC (Time Projection Chamber) prototype with GEM's for electron multiplication were developed and tested using the unseparated beams from KEK-PS. Performance of this prototype is presented in Ref. [9].

3.4. R & D of ALICE TRD

The CNS group has being involved in the R & D effort for the development of TRD (transition radiation detector) in the ALICE experiment at CERN-LHC, which is planned to start operation in 2007. The TRD, when installed, will provide unique capability of electron identification to the ALICE experiment.

The CNS group participated in the test of TRD large-scale prototypes using secondary beams from CERN-PS in the fall of 2004. The prototypes have the same size with the production ones, with prototype electronics installed. Performance of TRD performance are currently under investigations [10].

4. Summary and Outlook

In the year 2004, the PHENIX experiment had two successful runs, RUN-4 and RUN-5, and had archived large amount of data for Au + Au and Cu + Cu collisions at $\sqrt{s_{NN}} = 200$ GeV and $\sqrt{s_{NN}} = 63$ GeV, as well as polarized p + p collisions.

The major activities of the CNS groups are presented, which includes data analysis efforts, R & D efforts related to GEM, and ALICE TRD.

References

[1] N. Kurihara *et al.*, CNS Annual Report 2004 (2005) 57.
[2] T. Isobe *et al.*, CNS Annual Report 2004 (2005) 55.
[3] T. Sakaguchi *et al.*, CNS Annual Report 2004 (2005) 47.
[4] F. Kajihara *et al.*, CNS Annual Report 2004 (2005) 49.
[5] S. Kametani *et al.*, CNS Annual Report 2004 (2005) 51.
[6] T. Gunji *et al.*, CNS Annual Report 2004 (2005) 53.
[7] K. Ozawa *et al.*, CNS Annual Report 2004 (2005) 59.
[8] Y. L. Yamaguchi *et al.*, CNS Annual Report 2004 (2005) 93.
[9] S. X. Oda *et al.*, CNS Annual Report 2004 (2005) 89.
[10] Y. Morino *et al.*, CNS Annual Report 2004 (2005) 91.

Direct Photon Measurement at RHIC-PHENIX

T. Sakaguchi, H. Hamagaki[a], T. Isobe[a], G. David, S. Mioduszewski, D. d'Enterria[b], J. Frantz[c],
C. Klein-boesing[d], K. Reygers[d] and T. Awes[e], for the PHENIX Collaboration

Brookhaven National Laboratory, Physics Department, New York, U.S.A.
[a]Center for Nuclear Study, Graduate School of Science, University of Tokyo
[b]Columbia University, Department of Physics, New York, U.S.A.
[c]SUNY Stony Brook, Department of Physics & Astronomy, New York, U.S.A.
[d]Institute für Kernphysik, University of Münster, Münster, Germany.
[e]Oak Ridge National Laboratory, Oak Ridge, Tennessee, U.S.A.

1. Introduction

The suppression of high transverse momentum (p_T) hadrons in central Au+Au collisions called as "jet quenching" has been of great interest since its first discovery by the PHENIX experiment at RHIC [1]. The question has been asked, however, whether or not the phenomenon is attributed to energy loss of hard-scattered partons in a hot and dense medium (final state effect).

Photons are excellent probes for extracting the direct information of where they are produced because they do not interact strongly with medium once produced. Thus, they are expected to provide hints to answer questions of whether the jet quenching is due to initial or final state effect. The leading process of photon production is dominated by compton scattering of quarks and gluons ($q(\bar{q})g \rightarrow q(\bar{q})\gamma$) and the annihilation of quarks and antiquarks ($q\bar{q} \rightarrow g\gamma$), and the next leading process is dominated by bremsstrahlung and fragmentation.

In this report, the latest results on direct photon measurement from the PHENIX experiment are shown, and the source of photons is discussed.

2. Detector and Analysis

The description of PHENIX detector can be found in the literature [2]. In this analysis, electromagnetic calorimeter (EMCal) was used for measuring the energy of photons. The EMCal consists of six lead-scintillator sandwich type calorimeters and two lead-glass homogeneous type calorimeters. The drift chambers and pad chambers were used to track charged particles to estimate charged hadron contamination in EMCal clusters.

The analysis of direct photons requires determining background photons decaying from known hadronic sources such as π^0 and η. PHENIX has measured the p_T spectra of π^0 up to 13 GeV/c in Au+Au collisions at $\sqrt{s_{NN}}$=200 GeV [3, 4]. The momentum spectra of η and other hadronic sources were estimated by using a fit to π^0 p_T spectrum and applying m_T scaling: $p_T \rightarrow (p_T{}^2 - M_\pi{}^2 + M_h{}^2)^{1/2}$. The normalization factor of h/π^0 at $p_T = \infty$ is obtained either from simulation or measurement. In case of η, η/π^0 was measured to be 0.45±0.05. The number of photons decaying from known hadronic sources are then obtained from these spectra.

The inclusive photon spectra were reconstructed by applying several photon ID cuts on the measured cluster energy distributions, and correcting for hadron contamination and PID efficiency. The photon PID is realized by consisting likelihood functions from several quantities measured by EMCal such as shower shape or ratio of energies among towers, and by applying thresholds to them. It resulted in a significant reduction of hadronic clusters in the sample. Since the ratio of γ to π^0 cancels their common systematic errors, the excess of the measured photon over the estimated background photon is evaluated in terms of $R_\gamma \equiv (\gamma/\pi^0)_{measured}/(\gamma/\pi^0)_{estimated}$ (double ratio). The direct photon spectra are extracted as $\gamma_{direct} = (1 - R_\gamma{}^{-1}) \cdot \gamma_{measured}$. The final systematic errors on the spectra are at the level of ~15-20 % [6].

3. Results

Fig. 1 shows the γ/π^0 double ratios over various centralities in Au+Au collisions together with next-to-leading order (NLO) pQCD calculation scaled by the number of binary collisions shown in solid lines [7]. The shaded bands
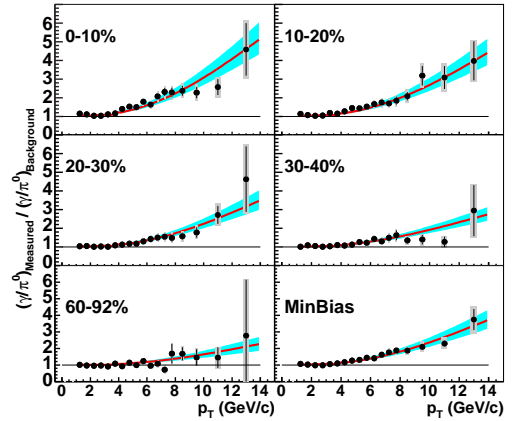
Figure 1. γ/π^0 double ratios in Au+Au collisions.

on the data points show the systematic errors, and the bars are the statistical errors. The shaded bands around the lines show the uncertainty of the pQCD calculation. The magnitude of the excess at and above p_T ~4 GeV/c increases with increasing centrality of collisions, and is consistent with the calculation. Fig. 2 shows the direct photon spectra extracted as described in the previous section. The lines show the same NLO pQCD calculation scaled by the number of binary collisions. It is clearly seen that all nine centralities including minimum bias are well described by the calculation. Fig. 3 shows nuclear modification factor R_{AA} as a
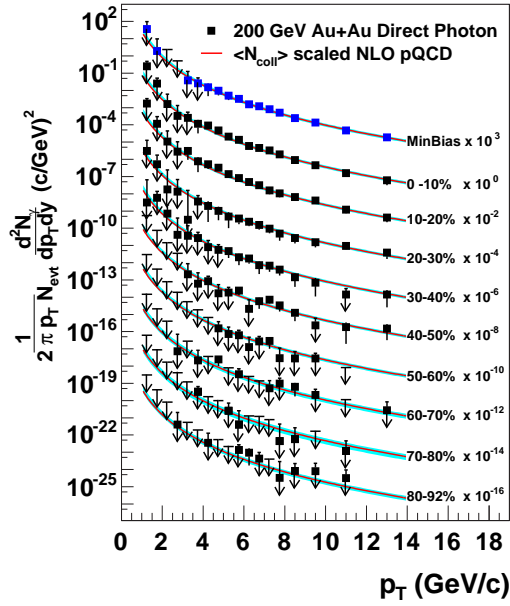
Figure 2. Direct photon spectra over centralities.

function of centrality, represented by N_{part}. The R_{AA} is defined as:

$$R_{AA} = \frac{(1/N_{AA}{}^{evt})d^2 N_{AA}/dp_T dy}{<N_{coll}>/\sigma_{pp}^{inel} \cdot d^s \sigma_{pp}/dp_T dy}.$$

The dotted lines show the uncertainty on the number of
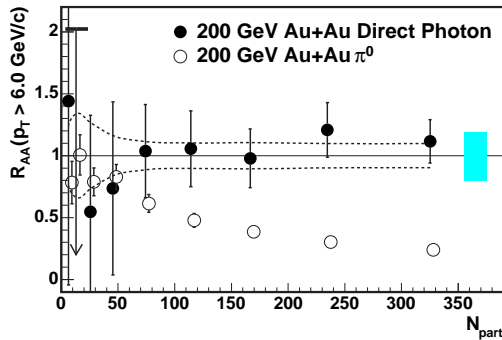
Figure 3. Nuclear Modification Factor (R_{AA}) for integrated yield of $p_T > 6$ GeV/c for π^0 (open) and direct photons (solid).

binary collisions, and the boxes show the uncertainty of the NLO pQCD calculation. The open circles are for π^0 [3], which clearly show a suppression with increasing centrality. In case of the direct photons shown in solid circles, the yield follows the number of binary collisions scaling.

¿From these results, we conclude that the hard scattering process at the initial stage follows the number of binary collisions scaling, and a large suppression of high p_T π^0 is attributed to the final state interaction with a dense medium.

4. Beyond hard process photons

There have been several theoretical predictions on photon contributions on top of hard process. Fig. 4 shows a comparison of 0-10 % central PHENIX data with a model including jet-photon conversion process. The jet-photon conversion is expected to occur, in the existence of QGP, by a

secondary interaction of a hard scattered parton with thermal partons in the medium [8]. In this plot, hard process is
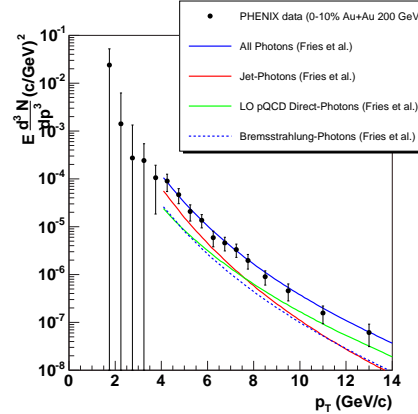
Figure 4. Comparison of the same data with a model including jet-photon conversion process.

calculated in leading-order pQCD with primordial k_T, and the next-leading-order contribution is partly compensated by bremsstrahlung process indicated in dotted lines. Although the pQCD calculation does not take full NLO processes into account, and therefore there is a possibility of underestimating the hard process contributions, the result suggests that the amount of the signal seen in p_T region of 4-6 GeV/c is related with the existence of QGP.

5. Conclusion

Direct photon measurements in Au+Au collisions at $\sqrt{s_{NN}}$=200 GeV from the PHENIX experiment at RHIC are presented. The yields for p_T>6 GeV/c are found to be consistent with NLO pQCD calculation scaled by the number of binary collisions. The result confirmed that the photons observed are produced through a hard scattering process in the initial stage, and the suppression of high p_T hadrons is attributed to a final state effect.

References

[1] K. Adcox *et al.*, Phys. Rev. Lett. **88** (2002) 022301.
[2] K. Adcox *et al.*, Nucl. Instrum. Methods. A **499** (2003) 469.
[3] S.S. Adler *et al.*, Phys. Rev. Lett. **91** (2003) 072301.
[4] J. Frantz, J. Phys. G **30** (2003) S1003.
[5] S.S. Adler *et al.*, Phys. Rev. Lett. **91** (2003) 241803.
[6] S.S. Adler *et al.*, nucl-ex/0503003.
[7] L.E. Gordon and W. Vogelsang, Phys. Rev. D **48** (1993) 3136.
[8] R.J. Fries, B. Müller and D.K. Srivastava, Phys. Rev. Lett. **90** (2003) 132301.

Single Electron Measurement in the d+Au Collisions at $\sqrt{s_{NN}} = 200$ GeV

F. Kajihara, Y. Akiba[a], R. Averback[b], S. Butsyk[b], H. Hamagaki, K. Ozawa, T. Tabaru[c],
M. Togawa[d] and X. Wei[c], for the *PHENIX* Collaboration

Center for Nuclear Study, Graduate School of Science, University of Tokyo
[a]*RIKEN (The Institute of Physical and Chemical Research)*
[b]*Department of Physics and Astronomy, Stony Brook University, New York, USA*
[c]*RIKEN BNL Research Center, Brookhaven National Laboratory, New York, USA*
[d]*Department of Physics, Kyoto University*

1. Introduction

Heavy-quark (charm and beauty) measurements provide valuable information for testing perturbative QCD (pQCD) predictions [1]. The measurements should impose stringent limitations on uncertainties in the Leading Order (LO) and the Next-to-Leading Order (NLO) pQCD calculations of heavy-quark productions which considerably depend on the gluon distribution function because heavy quarks are mainly produced *via* gluon fusions [2]. In heavy-ion collisions, non-pQCD effects, such as cold nuclear effects can also modify the gluon distribution. Since such nuclear effects are unknown in high-energy region, it is important to investigate these influences on the heavy-quark yield.

Heavy-quark production also has an important role in the investigation of the hot and dense matter created in heavy-ion collisions. The heavy-quark momentum spectrum may be affected by final state interactions such as its energy loss in the dense medium. On the other hand, energy loss of heavy quarks with a certain momentum is predicted to be smaller than that of light quarks with the same momentum due to the larger quark mass [3, 4]. The measurement of heavy quarks with momentum will verify the flavor dependence of energy loss. For precise measurements, it is essential to estimate properly the contributions from the above-mentioned nuclear effects. Data from the RHIC-PHENIX experiment of d+Au collisions at $\sqrt{s_{NN}} = 200$ GeV in 2003 (called Run-3) is suited to study the cold nuclear effects, since no high-energy-density matter is formed.

The measurement of single electrons (e^+ or e^-) from semi-leptonic decays of heavy quarks is a useful way to study heavy-quark production. Inclusive electrons can be categorized into two groups. The first group consists of "*photonic*" electrons mainly from (1) Dalitz decays of mesons (π^0, η, etc) and (2) the photon conversion. The second is termed "*non-photonic*" electrons. The decays of charm and bottom are the dominant sources of the second group. This report presents the status of the *non-photonic* electron measurements in the Run-3 d+Au experiment.

2. Electron Measurement in the PHENIX

In the PHENIX experiment, electron measurements were performed using two central arm spectrometers. Each arm is composed of a Drift Chamber (DC), Pad Chambers (PC), a Ring-Imaging Čerenkov counter (RICH) and Electro-Magnetic Calorimeters (EMCal), covering pseudo-rapidity $|\eta| < 0.35$ and $\pi/2$ in azimuth (ϕ) [5]. The PHENIX Minimum Bias (MB) trigger information is generated using two Beam-Beam Counters (BBC) which are placed at ± 145 [cm] from the center of the PHENIX along beam axis (z). The BBC provides measurement of centrality and vertex position, too. The DC measures charged particles trajectories in $r - \phi$ directions to determine p_T of the particles. The PC provides 3-D spatial point measurement for tracking of charged particles and longitudinal momentum reconstruction in combination with the DC hit information. The RICH and EMCal are main detectors to identify electrons in the PHENIX. The RICH detects the Čerenkov light which only electrons produce in its CO_2 radiator (1 atm) below 4.9 GeV/c (Čerenkov threshold momentum of charged pions). The EMCal can measure deposited energy and spacial positions of the electromagnetic showers by electrons. The RICH and EMCal form an electron trigger system, called the EMCal-RICH Trigger (ERT) [6]. To evaluate the ERT efficiency for electrons, a trigger simulator was developed in the PHENIX simulation framework.

3. "Converter Subtraction" Method

To extract *non-photonic* electron yield $N(p_T)$ by subtraction of *photonic* electron yield $P(p_T)$ from the total, the "converter subtraction" method is applied [7]. In the Run-3, special runs were performed with a photon converter, made of a brass sheet (1.68 % radiation length) around MVD (see the reference [5]). The photon-converter can enhance $P(p_T)$ by a certain factor R_γ since the internal (virtual) and external (real) photon conversion from (1) and (2) above have a similar form factor with a dependence of radiation length. Here, R_γ means the ratio of *photonic* electron yields with and without the converter. The measured inclusive electron yield $I(p_T)$ can be expressed as $I(p_T) = P(p_T) + N(p_T)$ without the converter and $I'(p_T) = R_\gamma P(p_T) + N(p_T)$ with the converter. $N(p_T)$ is given by these two equations.

4. Photonic Electron Simulation

In the converter subtraction method, the evaluation of R_γ is the most important issue. A GEANT based Monte Carlo simulation is used to estimate how much the *photonic* electron yield is increased by the photon converter and determine R_γ. The simulation was performed using the PHENIX-CCJ (Computing Center in Japan) and RIKEN Super Combined Cluster (RSCC).

The source of *photonic* electron in real data is a mix-

ture of mesons ($\pi^0, \eta, \eta', \omega$ and ϕ) decaying into real or virtual photons with their different p_T slopes. However, contributions from π^0 and η account almost all of them (Table 1). Therefore, *photonic* electrons from only π^0 and η were studied in the simulation.

Decay Mode	Branching Ratio of Each Meson
$\pi^0 \to 2\gamma$	98.798 ± 0.032 %
$\pi^0 \to \gamma e^+ e^-$	1.198 ± 0.032 %
$\eta \to 2\gamma$	39.43 ± 0.26 %
$\eta \to \gamma e^+ e^-$	0.60 ± 0.08 %
$\omega(782) \to \pi^0 e^+ e^-$	$(5.9 \pm 1.9) \times 10^{-4}$
$\eta'(958) \to \gamma e^+ e^-$	$< 9 \times 10^{-4}$
$\phi \to \eta e^+ e^-$	$(1.15 \pm 0.10) \times 10^{-4}$

Table 1. Main electron decay channels of light mesons. [8]

The R_γ of π^0 ($R_\gamma^{\pi^0}$) and the R_γ of η (R_γ^η) were determined separately. Then, the R_γ can be determined by combination of the $R_\gamma^{\pi^0}$ and R_γ^η, which are discussed below. For the original π^0 and η spectrum, we used the MB p_T distributions measured in Run-3 d+Au collisions (the π^0 spectrum was published in [10]). Figure 1 shows com-
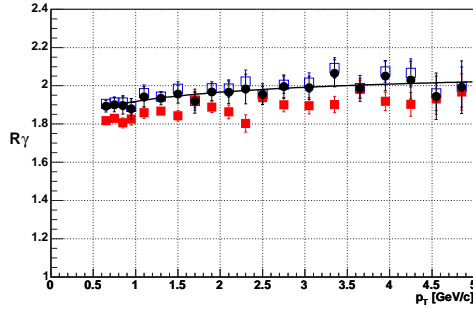
Figure 1. Combined R_γ (closed circle) of $R_\gamma^{\pi^0}$ (open square) and R_γ^η (closed square). The solid line is a fitting curve of the combined R_γ.

bined R_γ (closed circle) from $R_\gamma^{\pi^0}$ (open square) and R_γ^η (closed square). Since the η mass is larger than π^0 mass, the phase space of η Dalitz decay is slightly larger than that of π^0 Dalitz decay. The relative branching ratio: (Dalitz decay)/(two-γ decay) is 1.2 % for π^0 and 1.5 % for η. This difference makes R_γ^η smaller than $R_\gamma^{\pi^0}$. The combined R_γ can be determined by following expression:

$$R_\gamma = \frac{R_\gamma^{\pi^0} \cdot N_e^{\pi^0} + R_\gamma^\eta \cdot N_e^\eta}{N_e^{\pi^0} + N_e^\eta}$$
$$= \frac{R_\gamma^{\pi^0} + R_\gamma^\eta \cdot \epsilon^{\eta/\pi^0}}{1 + \epsilon^{\eta/\pi^0}}. \quad (1)$$
$$\epsilon^{\eta/\pi^0} = N_e^\eta / N_e^{\pi^0}. \quad (2)$$

In the above expressions, $N_e^{\pi^0}$ is a number of electrons from π^0 decays. N_e^η is a number of electrons from η decays. ϵ^{η/π^0} is a ratio of η and π^0 particle compositions. Since the uncertainty of η/π^0 ratio (0.45 ± 0.1) is not small, three kinds of spectra were calculated for the cases of $\eta/\pi^0 = 0.35, 0.45$ and 0.55. The η/π^0 dependence of the combined

R_γ was checked within 0.5 % flactuations. The value was assigned as a systematic error.

5. Non-photonic Electron Yield

Figure 2 shows Run-3 d+Au $N(p_T)$ (close square) which is calculated based on the result of *photonic* electron simulation. Each error bar indicates only statistic error and each square in background shows systematic error as described in Fig. 2. The yield is fully corrected for the trigger efficiency, the geometrical acceptance, the reconstruction and eID efficiency (see [9]). The spectrum is normalized with the binary collision cross section by scaling with $\sigma_{pp}/(Ncoll = 8.5)$ for MB triggered event to compare with the *non-photonic* electron spectrum in the Run2 p+p. The spectra in Fig. 2 show no strong nuclear modification. The d+Au spectrum is slightly enhanced around $p_T = 1.0$ GeV/c, which might indicate *Cronin* effect in charm production.
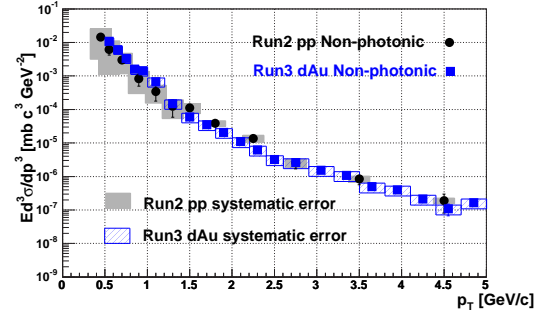
Figure 2. The *non-photonic* invariant cross sections as a function of p_T per binary N-N collision cross section by scaling with $\sigma_{pp}/(Ncoll = 8.5)$ for MB triggered event in d+Au collisions (closed square: Run-3 d+Au, closed circle: Run2 p+p).

6. Summary and Outlook

Photonic electron simulations were performed with high statistics to determine R_γ and the uncertainty. The analysis of *non-photonic* electrons in the high-p_T region (≥ 5 GeV/c) is in progress, which is important for the study of b quarks. We started to analyze data in the Run4 Au+Au at $\sqrt{s_{NN}} = 200$ GeV. The statistics is more than 20 times as that used in Run2 Au+Au analysis [7]. Significant reduction of statistical error is expected with these data.

References

[1] S. Frixione *et al.*, hep-ph/9702287.
[2] R. Vogt *et al.*, Z. Phys. C **71** (1996) 475.
[3] S. S. Adler *et al.*, Phys. Rev. Lett. **91** (2003) 072301.
[4] Y. L. Dokshitzer *et al.* , Phys. Lett. B **519** (2001) 199.
[5] K. Adcox *et al.*, Nucl. Instrum. Methods. A **499** (2003) 469,.
[6] F. Kajihara *et al.*, CNS Annual Report 2003 (2004) 49.
[7] S. S. Adler *et al.*, Phys. Rev. Lett. **94** (2005) 082301.
[8] K. Hagiwara *et al.*, Phys. Rev D **66** (2002) 010001.
[9] F. Kajihara *et al.*, CNS Annual Report 2003 (2004) 51.
[10] S. S. Adler *et al.*, Phys. Rev. Lett. **91** (2003) 072303.

Invariant Yield of $J/\psi \to e^+e^-$ in $d + \mathrm{Au}$ and $p + p$ Collisions

S. Kametani, H. Hamagaki, F. Kajihara, K. Ozawa, Y. Akiba[a], A. Lebedev[b] and X. Wei[c], for the PHENIX collaboration

Center for Nuclear Study, Graduate School of Science, the University of Tokyo
[a]RIKEN (The Institute of Physical and Chemical Research)
[b]Department of Physics and Astronomy, Iowa State University
[c]RIKEN BNL Research Center, Brookhaven National Laboratory, New York, USA

1. Introduction

The measurement of bulk properties of the relativistic heavy ion collisions attracts a lot of interests for the studies on QCD properties. For the side of the nuclear structure, one can suggest the issue on the modification of parton distribution in the nuclei. When a nucleon is a component of a nuclei, the parton distribution of the nucleon is different from that when a nucleon is isolated [1,2,3]. However, there is no universal explanation for that modification. The studies on heavy flavor production in heavy ion collision can give insights for models suggested [4]. The production of J/ψ in the hadronic reaction is dominated by the hard process [5] at initial collision. Therefore, the J/ψ yield is a useful probe to compare heavy ion collision with the superposition of the nucleon-nucleon collisions.

Meanwhile, the Cronin enhancement of heavy flavor by the multiple gluon scattering in the nucleus [6] is suggested as an issue on the dynamics of soft process in the gluon rich field. This effect has been observed as a broadening of p_T distribution in the past experiments [7,8].

Also, the produced J/ψ can interact with nucleons of projectile and can break into $D\bar{D}$. This absorption is small but not negligible to reduce the cross section off from linear A dependence [6,9]. This effect is well understood but continuous study for higher energy region is expected.

The study on these modification not only contribute to the study of bulk QCD properties. That can also be dedicated as a baseline study to understand the J/ψ production in nucleus-nucleus collisions, where a suppression [10] or an enhancement [11] has been predicted due to the formation of the Quark Gluon Plasma.

The PHENIX experiment had a very successful electron-pair measurement for d+Au collisions and p+p collisions at $\sqrt{s}_{NN} = 200$ GeV in the RHIC Year-3 run. The analysis overview and some results of J/ψ measurements at PHENIX achieved for the RHIC Year-3 run are described on this report.

2. Experiment and analysis

The experimental setup and method of electron identification are described on the previous report [12]. The reconstruction of $J/\psi \to e^+e^-$ was performed on electron trigger events. The number of used in the analysis was 3.5×10^6 for d+Au collision and 5.4×10^6 for p+p collision. Systematic error concerned with run-by-run fluctuation were reduced to 8.7 %.

Revised study on track selection for electron identification (eID) was performed for Year-3 data. The cut parameters were well tuned so as to minimize S/N ratio. The total eID efficiency of more than 90 % was achieved.

Figure 1(a) shows invariant mass spectrum for the opposite sign electron pair (e^+e^-) and the same-sign electron pair (e^+e^+ or e^-e^-). The combinatorial background in the opposite-sign pair spectrum was estimated from the same-sign pair spectrum. As a result of combinatorial background subtraction, the J/ψ peak was obtained as shown in Figure 1(b). For d+Au run, total count of J/ψ was 400 and the peak width in sigma was 100 MeV/c^2. However, the result of momentum resolution analysis using π, K, p requires the $J/\psi \to e^+e^-$ width to be 45 MeV/c^2. This is still a unsolved underlying problem.
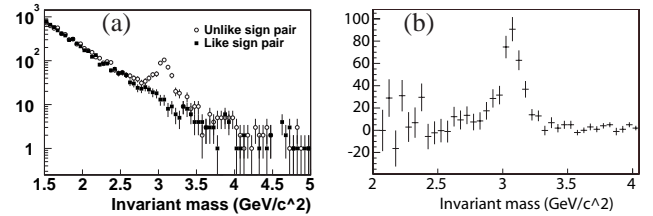
Figure 1. (a)Invariant mass spectrum of the opposite-sign electron pair (open circle) and the same-sign pair (square). (b) Opposite-sign pair spectrum subtracted by the same-sign pair spectrum. Statistical errors are also shown.

Acceptance calculation was performed using GEANT simulation. The detector response was well tuned to reproduce the experimental data. Systematic error which derives from p_T smearing, z-vertex resolution, etc, were well estimated. Fine studies on trigger to estimate total cross section and triggering efficiency of J/ψ is also performed. J/ψ yield is determined by applying these corrections.

3. Results

To understand the yield modification between the superposition of each nucleon-nucleon collision and nuclear-nuclear collision, an "invariant yield ratio" value R_{dAu} is introduced in the form of

$$R_{dAu} = \frac{Y_{dAu}}{Y_{pp} \times N_{coll}} = \frac{Y_{dAu}/N_{coll}}{Y_{pp}}, \qquad (1)$$
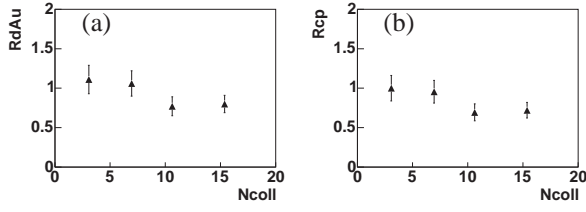
Figure 2. (a) R_{dAu} (Ratio of yield per binary collision of each centrality divided by yield in p+p collision) and (b) R_{cp} (Ratio of yield per binary collision of each centrality divided by that of most peripheral collision) as a function of N_{coll}. Only statistical error is shown.

where Y_{dAu} is J/ψ yield in d+Au collision and Y_{pp} is the J/ψ yield in p+p collision. Here, the Glauber model [13] is adopted for counting the number of nucleon-nucleon collision at d+Au collision, N_{coll}.

As nuclear effects appear strongly in central (small impact parameter) events, the impact parameter dependence of modification factor reveals the nuclear effects more clearly. However the impact parameter cannot be observed directly, the estimation of the impact parameter from the forward multiplicity is possible [14].

All the events analyzed was categorized into four bins called centrality by forward multiplicity:0-20 %, 20-40 %, 40-60 % and 60-88 %. $Y_{J/\psi}$ is calculated for each centrality. The mean N_{coll} for each centrality is also estimated with a Monte Carlo simulation based on the Glauber model. Figure 2(a) shows for R_{dAu} at each centrality.

As the multiplicity in p+p collision is much smaller than that in d+Au collision, the trigger condition is different between d+Au run and p+p run. To remove systematic errors for this difference, R_{cp} value for each centrality is introduced as standalone valuable for d+Au run analysis. R_{cp} is defined as

$$R_{cp\_i} = \frac{R_{dAu\_i}}{R_{dAu\_perif}} = \frac{Y_{dAu\_i}/N_{coll\_i}}{Y_{dAu\_perif}/N_{coll\_perif}}, \quad (2)$$

where R_{dAu_i} is R_{dAu} of each centrality bin and R_{dAu_perif} is R_{dAu} of the least central bin, called most peripheral, where the minimum nuclear effect is expected. Figure 2(b) shows for R_{cp} at each centrality. Assuming J/ψ yield is not modified in most peripheral events, absorption cross section which corresponds to R_{cp} at most central was calculated as $\sim$4.5 mb.

Figure 3 shows p_T distribution of J/ψ for d+Au run and p+p run. Small suppression at low p_T can be seen.

4. Summary and outlook

To understand nuclear effects on the J/ψ production in high energy heavy ion collisions, a J/ψ measurement was performed for the d+Au collisions.

The measurement of the J/ψ yield from di-electron detection in the d+Au and p+p collisions is described. The normalized J/ψ yield as a function of the number of nucleon-nucleon collisions is shown for d+Au collision.
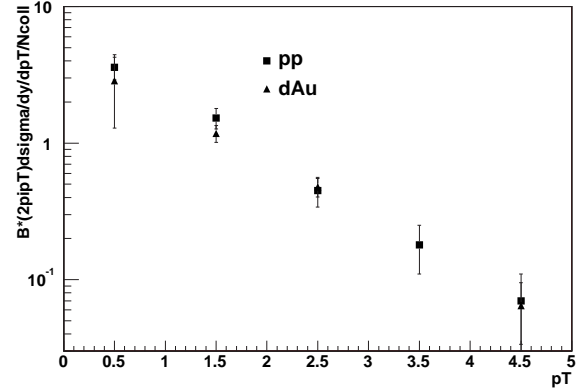
Figure 3. p_T distribution of $J/\psi \rightarrow e^+e^-$ for d+Au collision and p+p collision. Only statistical error is shown.

Also, p_T distribution of J/ψ in d+Au collision and in p+p collision is shown.

Results shown in this report is still work in progress. More elaborate studies are to be made. The final result is to be published in conjunction with large rapidity observation with PHENIX muon arm in near future.

References

[1] J. J. Aubert *et al.*, Phys. Lett. B **123** (1983) 275.

[2] P. Amaudruz *et al.*, Nucl. Phys. B **441** (1995) 3.

[3] M. R. Adams *et al.*, Phys. Rev. Lett. **68** (1992) 3266.

[4] S. R. Klein and R. Vogt, Phys. Rev. Lett. **91** (2003) 142301.

[5] P. Nason *et al.*, Nucl. Phys. B **327** (1989) 49.

[6] J. Hüfner *et al.*, Phys. Lett. B **215** (1988) 218.

[7] J. Badier *et al.*, Z. Phys. C **20** (1983) 101.

[8] M. J. Leitch *et al.*, Phys. Rev. Lett. **84** (2000) 3256.

[9] R. L. Anderson et. al., Phys. Rev. Lett. **38** (1977) 252.

[10]T. Matsui and H. Sats, Phys. Lett. B **178** (1986) 416.

[11]M. Gazdzichki and M. I. Gorenstein, Phys. Rev. Lett. **83** (1999) 4009.

[12]S. Kametani *et al.*, CNS Annual Report 2003 (2004) 55.

[13]R. J. Glauber, in Lectures in Theoretical Physics, edited by W. E. Brittin and L. G. Dunham (Interscience, N.Y., 1959), Vol. 1, p. 315.

[14]S. Kametani *et al.*, CNS Annual Report 2002 (2003) 47.

$J/\psi \to e^+e^-$ Measurements in $\sqrt{s_{NN}} = 200$ GeV Au+Au collisions at RHIC-PHENIX

T. Gunji, H. Hamagaki, K. Ozawa, S. Kametani, F. Kajihara, Y. Akiba[a], A. Lebedev[b] and C. L. Silva[c], for the PHENIX collaboration

Center for Nuclear Study, Graduate School of Science, University of Tokyo
[a]RIKEN (The Institute of Physics and Chemical Research)
[b]Iowa State University, USA
[c]Universidade de São Paulo, Instituto de Física, Brazil

1. Introduction

Lattice QCD calculations predict that there might be a phase transition from ordinary hadronic matter to deconfined quarks and gluons, called quark-gluon-plasma at extremely high temperature, $T_c \geq 160$ MeV. High energy heavy ion collisions are the only tool in the world to realize such a high temperature and to provide the characteristics of the quark-gluon-plasma. Relativistic Heavy Ion Collider (RHIC) at Brookhaven National Laboratory is a dedicated facility for the study of heavy ion collisions at relativistic high energies.

Measurements of heavy quarkonia has been long considered as one of the most promising probes to study the formation of quark-gluon-plasma and its proprieties. Suppression of heavy quarkonia yield was suggested as a signature of the deconfinement long ago, where the quark and anti-quark pair are screened by the color Debye potential [1]. Nuclear absorption and comover scattering also would lead to suppression of the heavy quarkonia yield at RHIC energies as observed in the several earlier experiments with lower collision energies [2].

A new idea has been proposed where J/ψ yield could be enhanced due to the incoherent recombination mechanisms involving uncorrelated c and $\bar{c}$ quarks since abundant c and $\bar{c}$ quarks are produced in the early stage of collisions [3, 4].

It is important, threfore, to study J/ψ yield for various collision systems to understand the J/ψ production mechanisms. RHIC has carried out p+p (2002), d+Au (2003), Au+Au (2002, 2004) and Cu+Cu (2005) collisions for recent five years. The collision system dependence of J/ψ yield has been investigated to clarify these competing scenario of J/ψ formation mechanisms [5].

2. Au+Au collisions at 2004

Au+Au collisions at $\sqrt{s_{NN}} = 200$ GeV were performed at RHIC in 2004. During the period, PHENIX recorded 1.6 billion events, which corresponds to the integrated luminosity of $\sim 240 \ \mu b^{-1}$. This is ~ 30 times larger than the number of events which were used in the J/ψ analysis in 2002. The data reconstruction has been done for 0.650 billion events and 0.350 billion events were used in this analysis after the good runs were selected by looking at the detector acceptance for electrons. J/ψ invariant mass spectra and invariant yield for 3 centrality classes will be shown in this article.

3. Data analysis

3.1. Electron identification at PHENIX

Electrons and positrons are measured with PHENIX central detectors, which are composed from two arms with the pseudo-rapidity coverage of $|\eta| = 0.35$ and azimuthal coverage of $\Delta\phi = 90°$ in each arm [6].

Electrons are identified by requiring the following cuts. The charged tracks were associated with a RICH ring ($\geq$ 3 hit PMT's in a ring) and with a EMCal ($\pm 2\sigma$ position association, energy-momentum matching within 2σ).

3.2. Invariant mass spectra for 3 centrality classes

After e^- and e^+ were identified as described above, invariant mass was calculated for each e^-e^+ pair. The results are shown in Fig. 1. The solid line is the invariant mass spectrum for e^+e^- pairs coming from the same collision event. The dotted line is the invariant mass spectrum obtained from mixed events, where there is no correlation between e^+ and e^-. Centrality corresponds to the impact parameter between two nuclei.
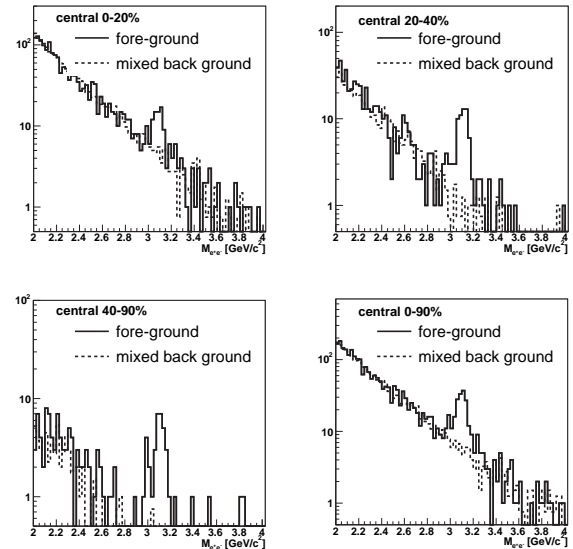
Figure 1. e^+e^- Invariant mass distribution for centrality of 0-20%(upper left),20-40% (upper right), 40-90% (lower left) and 0-90% (lower right). The solid line is the invariant mass of pairs and dotted line is the background from event mixing.

3.3. J/ψ efficiency calculation

The formula of J/ψ invariant yield is written as follows:

$$B\frac{dN}{dy} = \frac{N_{J/\psi}}{N_{evt}} \frac{1}{\Delta y \epsilon_{acc}\epsilon_{embed}}, \qquad (1)$$

where B is the branching ratio of e^+e^- decay mode (5.93% from PDG [7]), $N_{J/\psi}$ and N_{evt} stand for the number of J/ψ counts and number of analyzed event, respectively. Δy in Eq.(1) is the rapidity coverage. The correction factor, ϵ_{acc}, is the acceptance for e^- and e^+ pair from J/ψ, where detection efficiency of e^+ and e^- pairs and run-by-run fluctuation of the detector acceptance are taken into account. The correction factor, ϵ_{embed}, is the efficiency, which has a centrality dependence. In more central collisions, rate of track mis-reconstruction becomes higher due to higher hit occupancy.

To calculate the acceptance of e^+e^- pairs from J/ψ, ϵ_{acc}, single $J/\psi \to e^+e^-$ simulation was performed by using the Phenix Integrated Simulation Application (PISA), which is a GEANT-3 based simulation code. Single J/ψ events with a flat transverse momentum of $0 \leq p_T \leq 5.5$ GeV/c, a flat rapidity of $|y| \leq 0.5$, a flat azimuthal angle of $0 \leq \phi \leq 2\pi$ and a flat vertex $|z| \leq 40$ cm are generated and e^+ and e^- from J/ψ are thrown into the PHENIX detector acceptance. Then the same analysis codes and the calibration parameters as used in real data were used in the reconstruction chain. The acceptance, ϵ_{acc} is defined to be the ratio of number J/ψ's whose e^+ and e^- are satisfied with the same eID cuts as used in real data analysis to the number of generated J/ψ's. Figure 2 shows the acceptance of J/ψ as a function of p_T of J/ψ.
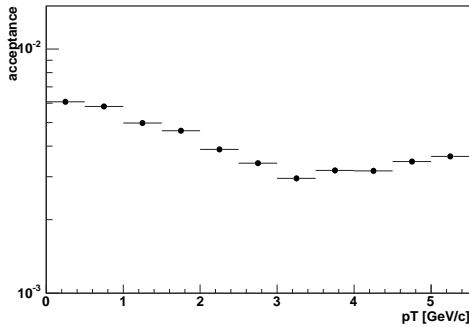
Figure 2. Acceptance of J/$\psi \to e^+e^-$ calculated from simulation.

The centrality dependent efficiency, ϵ_{embed}, was evaluated by embedding simulated single J/ψ events into real events. ϵ_{embed} is defined to be the ratio of the number of J/ψ's reconstructed after embedding to that before embedding. Table 3.3 is the results of ϵ_{embed} for 3 centrality classes.

4. J/ψ yield calculation

For the comparison of the J/ψ yield between Au+Au collisions and $p+p$ collisions, J/ψ yield calculated from Eq.(1) is scaled by number of binary collisions. The results are shown in Fig. 3. J/ψ yield from $p + p$ collisions is also

centrality	ϵ_{embed} (stat. err.)
0-20%	0.675 ± 0.022
20-40%	0.805 ± 0.024
40-90%	0.938 ± 0.017

Table 1. embedding efficiency for 3 centrality classes with its statistic uncertainty

shown with its 1 σ error. Since the systematic error has
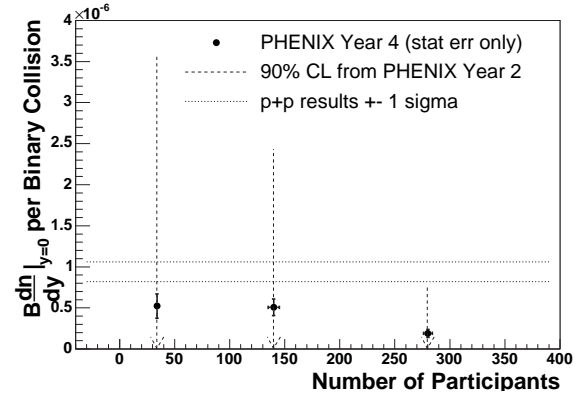
Figure 3. J/ψ invariant yield as a function of number of participants. Error is statistic error only. 90% CL evaluated from Year-2 data are shown as dotted arrow. J/ψ yield with 1σ from $p + p$ collisions are shown as dotted line.

not been taken into account, J/ψ production mechanisms in Au+Au collisions can not be discussed at this stage. The evaluation of the systematic error is on going.

5. Summary and Outlook

J/ψ analysis has been done for $\sim 40\%$ of all the data and J/ψ invariant yield as a function of centrality was shown.

Reconstruction of rest of the data set is in progress and the analysis will be done for upcoming reconstructed data. As the next step, J/ψ invariant yield and J/ψ p_T distributions will be evaluated for finer centrality binning.

References

[1] T. Matsui and H. Satz, Phys. Lett. B **178** (1986) 416.
[2] B. Alessandro, *et al.*, Phys. Lett. B **553** (2003) 167.
[3] Robert. L. Thews, *et al.*, Phys. Rev. C **63** (2001) 054905.
[4] A. Andronic, *et al.*, Phys. Lett. B **571** (2003) 36.
[5] S. Kametani, *et al.*, CNS Annual Report 2004 (2005) 51.
[6] K. Adcox, *et al.*, Nncl. Instrum. Methods. A **499** (2003) 489.
[7] K. Hagiwara *et al.*, Phys. Rev. D **66** (2002) 010001.

Measurement of Neutral Pion in Au+Au Collisions at RHIC-PHENIX

T. Isobe, H. Hamagaki, T. Sakaguchi[a], G. David[a] and S. Mioduszewski[a], for the PHENIX Collaboration

Center for Nuclear Study, Graduate School of Science, University of Tokyo
[a]Brookhaven National Laboratory, USA

1. Introduction

The PHENIX experiment [1] has been carried out at the Relativistic Heavy Ion Collider (RHIC) at Brookhaven National Laboratory (BNL) in order to find evidence of phase transition from normal nuclear matter to Quark Gluon Plasma (QGP). QGP is a new phase of matter consisting of de-confined quarks and gluons.

One of the most intriguing observations at RHIC is that the yield of π^0 at high transverse momentum (p_T) in central $\sqrt{s_{NN}}$=200 GeV Au+Au collisions compared to the yield in p+p collision scaled by the number of underlying nucleon-nucleon collisions in Au+Au is suppressed [2]. The observed suppression is interpreted as a consequence of jet-quenching effect, that is, hard-scattered partons produced in the initial stage suffer large energy loss while traversing the hot and dense matter.

There are models that provide quantitative predictions of the amount of suppression. Each model involves various effects: initial state effects, Cronin effect [4] and nuclear shadowing, or strong hadronic final state effects, and energy loss in a dense matter.

The amount of suppression can be quantitated with nuclear modification factor (R_{AA}). Nuclear modification factor is defined as following:

$$R_{AA}(p_T) = \frac{d^2 N^{AA}/dp_T d\eta}{T_{AA}(b) d^2 \sigma^{NN}/dp_T d\eta}, \qquad (1)$$

where the numerator is invariant π^0 yield in unit rapidity and denominator is expected yield in p+p collision binary scaled by the number of underlying nucleon-nucleon collisions ($T_{AA}(b)$) in Au+Au. $T_{AA}(b)$ is defined as following:

$$T_{AA}(b) = \frac{N_{collision}(b)}{\sigma_{NN}} \qquad (2)$$

where $N_{collision}(b)$ is the average number of binary nucleon-nucleon collisions with an inelastic cross section σ_{NN}. The number of collision ($N_{collision}(b)$) is calculated via a Glauber Monte Carlo calculation as a function of impact parameter b. Figure 1 shows nuclear modification factor for π^0s in central $\sqrt{s_{NN}}$=200 GeV Au+Au events compared to different theoretical calculations. It is seen that the calculation consists only the known cold nuclear effect, Cronin effect and nuclear shadowing. Large suppression is seen when comparing to cold nuclear matter.

The order of magnitude of the suppression and the p_T dependence above 3 GeV/c is well reproduced by the calculations as shown in Fig. 1. The GLV model calculation considers parton energy loss in a dense matter, and the cold nuclear effect [3, 5]. Other employs the parton energy loss
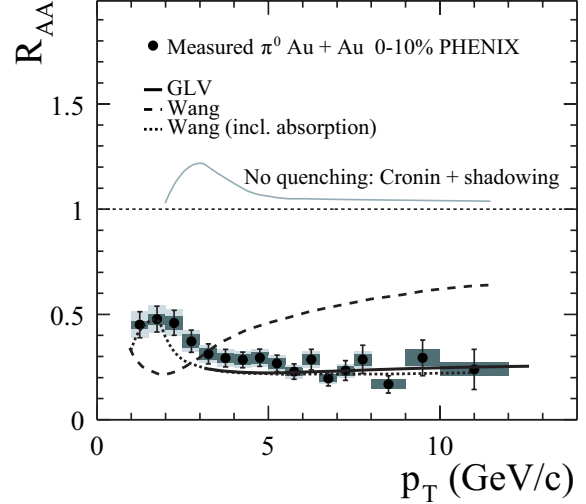
Figure 1. Comparison of R_{AA} predictions from suppression models [5, 6] against the PHENIX result in central $\sqrt{s_{NN}}$=200 GeV Au+Au collisions. It is compared to a model without jet-quenching effect, a parton energy loss calculation based on the GLV approach, the calculation without gluon absorption and from including gluon absorption.

of 7.3 GeV/fm in dense nuclear matter. However, the calculation fails to describe the p_T dependence of the data. This might be the indication that the thermally produced gluons and the stimulated emission of gluons in the QGP phase in addition to the induced gluon radiation in the QGP need to be considered [6]. With the employment of gluon absorption, the suppression can be reproduced well.

In order to reveal the parton energy loss mechanism in the dense matter, it is important to measure π^0 quantitatively in different system and p_T region.

2. π^0 measurement at PHENIX Year-4 Run

In RHIC Year-4 run PHENIX recorded the integrated luminosity of 0.24 nb^{-1} in $\sqrt{s_{NN}}$=200 GeV Au+Au collisions and 9.1μb^{-1} in $\sqrt{s_{NN}}$=62.4 GeV Au+Au collisions, which allows us to extend the measurement of π^0 to high transverse momentum as well as to measure π^0 at a low CMS energy.

π^0 is measured with the PHENIX electromagnetic calorimeter (EMCal) [7] via two-photon decay mode. EMCal is used to measure position and energy of photons. There are two types of calorimeters at PHENIX. One is a lead-scintillator sampling-type calorimeter, and another is a lead-glass Cherenkov calorimeter. The lead-scintillator calorimeter is used in this analysis.

Reconstruction efficiency to correct the raw π^0 yield is calculated using computer clusters at RIKEN-CCJ. The ge-
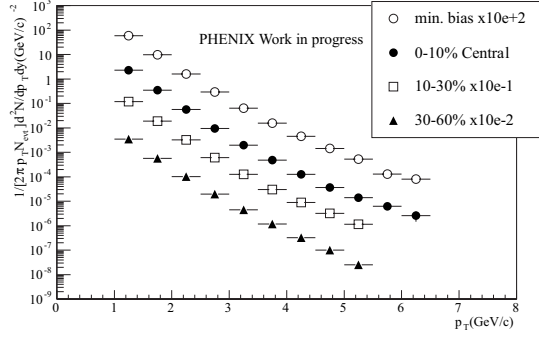
Figure 2. π^0 p_T spectra at $\sqrt{s_{NN}} = 62.4$ GeV
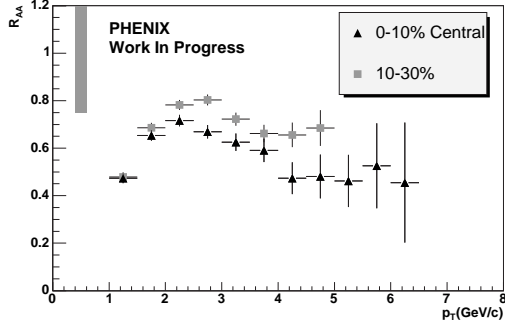
Figure 3. π^0 nuclear modification factor as a function of p_T in ($\sqrt{s_{NN}} = 62.4$ GeV.

Figure 4. Comparison of π^0 R$_{AA}$ PHENIX results, and prediction of R$_{AA}$ using the GLV model in $\sqrt{s_{NN}} = 62.4$ GeV and 200 GeV Au+Au collisions. Triangles and circles are PHENIX result in $\sqrt{s_{NN}} = 62.4$ GeV and 200 GeV, respectively. The gray band represents the perturbative QCD expectation for the suppression of π^0. Enhancement from cold nuclear effect without energy loss is given for comparison.

Year-2 200 GeV result. π^0 will be measured in $\sqrt{s_{NN}} = 200$ GeV Au+Au collisions from Year-4 data. It is expected that the p_T region is extended up to 18 GeV/c in minimum bias events.

References

[1] K. Adcox *el al.*, Nucl. Instrum. Methods. A **499** (2003) 469.
[2] S.S. Adler *el al.*, Phys. Rev. Lett. **91** (2003) 072301.
[3] M. Gyulassy *el al.*, Nucl. Phys. B **594** (2001) 371.
[4] J.W. Cronin *el al.*, Phys. Rev. D **11** (1975) 3105.
[5] I. Vitev, AIP Conf. Proc. **698** (2004) 721.
[6] X.-N. Wang, Phys. Lett. B **579** (2004) 299.
[7] L. Aphecetche *el al.*, Nucl. Instrum. Methods. A **499** (2003) 521.
[8] F.W. Busser *el al.*, Phys. Lett. B **46** (1973) 471.
[9] A.L.S. Angelis *el al.*, Nucl. Phys. B **327** (1989) 541.
[10]I. Vitev, nucl-th/0404052.

ometrical acceptance correction, particle identification efficiency, and over-lapping effect in high multiplicity is estimated.

3. Result on $\sqrt{s_{NN}}$ = 62.4 GeV Au+Au collisions

Centrality is obtained from the Beam-Beam counters and the Pad Chamber in $\sqrt{s_{NN}} = 62.4$ GeV Au+Au collisions.

Figure 2 shows the fully corrected π^0 invariant yield as a function of transverse momentum for each centrality of collision. From fully corrected p_T spectra, the nuclear modification factor (R$_{AA}$) as a function of p_T is obtained as shown in Fig. 3. For comparing with binary scaled p+p results, the CERN-SPS experimental results of π^0 cross section in p+p collision are used [8, 9]. There is discrepancy among the each CERN-SPS results and systematic error is assigned as 25 %. While Cronin enhancement seems to be much more prominent than 200 GeV result, π^0 measurement in $\sqrt{s_{NN}}$ = 62.4 GeV p+p and d+Au collisions is needed for detailed study.

π^0 nuclear modification factor is compared with prediction which employes the GLV model as shown in Fig. 4 [10]. The gray band represents the perturbative QCD expectation for the suppression of π^0. This prediction has reasonable agreement with PHENIX result at $p_T > 4$ GeV/c. But there is larger Cronin contribution at $p_T < 3$ GeV/c according to the data.

4. Summary and Outlook

The π^0 measurement is allowing to study the medium modifications of hard scattered particles. π^0 is measured in $\sqrt{s_{NN}} = 62.4$ GeV in RHIC Year-4, and it is compared with

Measurement of Charged Hadron Spectra in Au+Au Collision at $\sqrt{s_{NN}} = 62.4$ GeV at RHIC-PHENIX

N. Kurihara, H. Hamagaki, K. Ozawa, T. Sakaguchi[a], T. Chujo[b] and S. Esumi[c],
for the PHENIX Collaboration

Center for Nuclear Study, Graduate School of Science, University of Tokyo
[a]Brookhaven National Laboratory, New York,U.S.A
[b]Vanderbilt University, Tennessee, U.S.A
[c]High Energy Nuclear Physics Group,University of Tsukuba

1. Introduction

In high energy heavy ion collisions at RHIC, a large excess in the yield of protons (anti-protons) over poin yield was found in the medium to high transverse momentum (p_T) region [1]. p/π ratios increase gradually up to 2.5 GeV/c and stay almost flat. Top values of p/π^+ is about 1 and $\bar{p}/\pi^-$ is about 0.8 in most central collisions. This phenomenon was not expected from a general picture of hadron production through the jet fragmentation process [2]. High p_T particles are generated from a hard process at an early time of collisions. Thus, it is believed that particles over 2 GeV/c of transverse momentum follow the fragmentation model. However a barion excess has occurred around p_T $2 \sim 4$ GeV/c range.

To explain this phenomenon, a new idea of particle generation has been proposed, which is called a quark recombination model [3,4]. In this model, a high-momentum parton picks up some other partons from the abundant source of hot and dense deconfined matter, and they form mesons and baryons. The numerical calculations show that the process favors the baryon production in the momentum range between $2 \sim 4$ GeV/c.

It should be interesting to see the results at different collision energies, in order to investigate more deeply the hadron formation process. There is a low energy collision run at the PHENIX experiment $\sqrt{s_{NN}} = 62.4$ GeV in Run4.

2. Measurement of charged hadrons at PHENIX

The PHENIX detector has a pair of central-arm spectrometers, called as East-arm and West-arm, each of which covers mid-rapidity region from -0.35 to +0.35.

Measuring incoming particles to the beam axis is required to determine a centrality and vertex points. Beam-Beam Counter (BBC) and Zero Degree Counter (ZDC) are located at near the beam line and these devises measure the centrality and the vertex point in each collision. Drift Chamber (DC) serves as a device for particle tracking and momentum determination. Also Pad Chambers (PC) are located in each arms to rise a precision of tracking. Ring Imaging Cherenkov counter (RICH) and Electro Magnetic Calorimeter (EMC) are fully installed in each arms.

A main difference between West-arm and East-arm is that the West-arm has Aerogel Cherenkov Counter (ACC) and the East-arm has a Scintillation counter of Time of Flight (TOF). One of the scheme of particle identification (PID) is measuring particle momentum and time of flight, thus TOF is used as PID device. Another technique for PID is measuring a correlation between a Cherenkov light yields and momentum. High p_T particles can be identified by the ACC with measuring Cherenkov light emissions.

In this analysis, the ACC is used as a PID device for pions, while the TOF is used for protons. Preliminary results of charged hadrons analysis by TOF can be seen in [5].

ACC is a new detector subsystem which was installed before Run-4. The performance is reported in [6].

3. Analysis
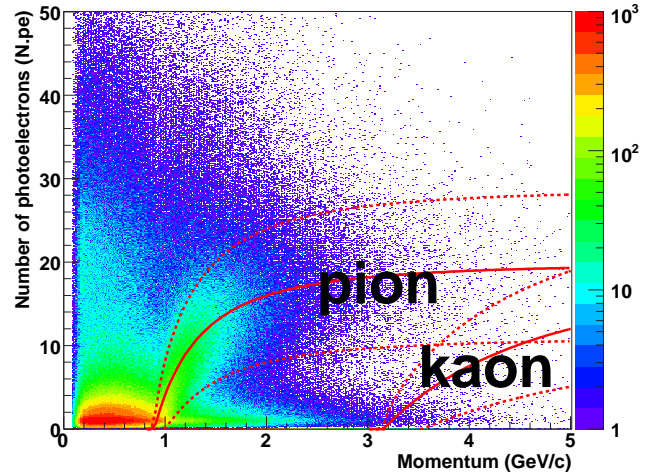
Figure 1. Particle identification range of pion and kaon for Aerogel Cherenkov counter.

38 M of minimum biased events were collected in the RUN4 Au+Au collisions at $\sqrt{s_{NN}}$ =62.4 GeV.

The centrality is distinguished in 4 centrality bins (0-10%, 10-30%, 30-60% and 60-83.7%) at this RUN period. Charge sum of BBC with corrections of multiplicity and vertex points are used to determine the centrality. However A basic technique to obtain a centrality which used at $\sqrt{s_{NN}} = 200$ GeV can't be applied for 62.4 GeV analysis, because energy deposit at the ZDC is too small to get a correlation between BBC and ZDC. Currently the most peripheral (60-83.7%) has some background events, therefore results of this centrality are not be shown. This centrality determination is commonly used among the PHENIX collaborations.

Tracking selections and the the PID method are explained in following. At First, all of charged tracks are measured by DC, and good qualified tracks are selected. Furthermore PC responses at projection points of tracks are checked and good tracks are selected. The particle identification has been done by ACC and EMC time-of-flight. Figure 1 shows a correlation between momentum and number of counted photo-electrons (p.e) at the ACC. Solid lines in Fig.1 are expected mean value of p.e for charged pion and kaon. Also dot-lines shows 2 σ range from mean value for each particles. The range between 2 σ lines are used for the PID selection. However an overlap region of pion and kaon above 3.5 GeV/c are exclude from charged pion analysis.

In order to determine the overall detector efficiency, single particle simulation data are generated. Total number of generated data are 4 M events. Collection factors for a detector inefficiency are calculated from the simulation data using a particle selection conditions same as the real data analysis.

4. Results
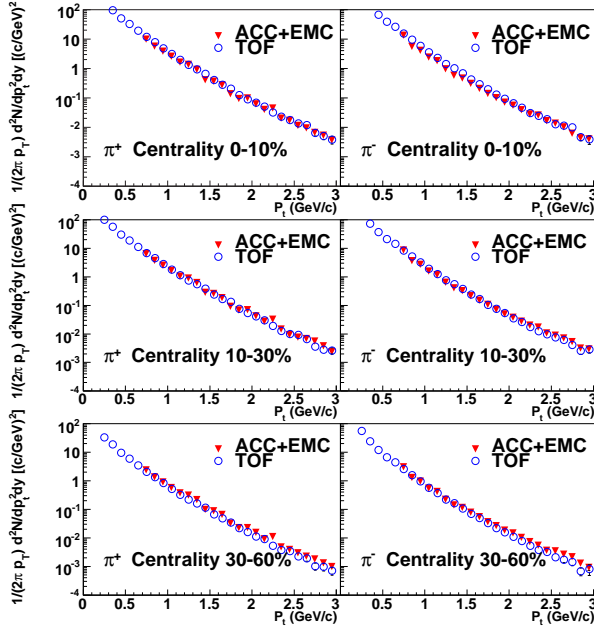
Figure 2. Charged pion spectra for each centrality.

Figure 2 shows charged pion invariant yield spectra for each centrality in Au+Au collisions at $\sqrt{s_{NN}} = 62.4\,GeV$. Inverse triangles mean pion spectra measured by ACC and EMC. Also open circles mean pion spectra measured by TOF. ACC and TOF results are consistent up to 3.0 GeV/c with in each centrality. ACC can identify charged pions up to 4.5 GeV/c, however more detail study is needed to show more high p_T region.

p/π^+ and $\bar{p}/\pi^-$ ratios in three different centrality bins are shown in Fig. 3. In this case proton and anti-proton spectra are refer from a TOF analysis [5]. It is clearly seen from the figure that an excess of proton (anti-proton) yield over pion yield become prominent with increase of centrality.

The proton excess is consistent to $\sqrt{s_{NN}} = 200$ GeV data
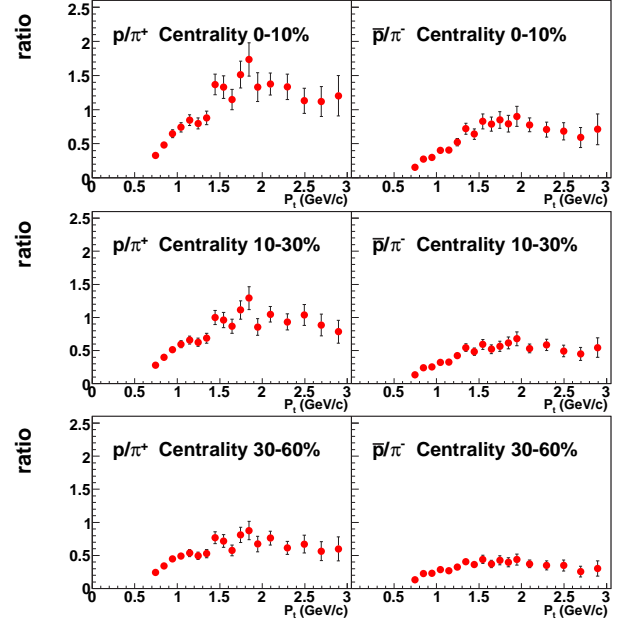
Figure 3. p/π ratios for each centrality.

at the region above 2.5 GeV/c. One difference between 62.4 GeV and 200 GeV data is that 62.4 GeV data tend to start increasing from more lower p_T than 200 GeV/c. One of the main process around 1.5 GeV/c is a soft process for the hadron productions. Therefor to explain the difference of the proton excess in low p_T region, other effects such as a shadowing effect should be considered.

5. Summary

Charged pion invariant yield spectra were measured using Aerogel Counter in RUN4 PHENIX Au+Au collisions at $\sqrt{s_{NN}} = 62.4\,GeV$. Combined with charged pion spectra and proton spectra which measured by TOF, p/π ratio were obtained. Proton excess was also clearly seen in $\sqrt{s_{NN}} = 62.4\,GeV$ Au+Au collision. More study for Aerogel analysis is needed to obtain more than 3.0 GeV p/π ratio.

References

[1] PHENIX Collaboration, Phys. Rev Lett. **91** (2003) 172301.
[2] Xin-Nian Wang, Phys. Rev Lett. **81** (1998) 2655.
[3] K. Adox *et.al.*, Phys. Rev. Lett. **88** (2002) 022301.
[4] K. Adox *et.al.*, Phys. Lett. B **561** (2003) 82.
[5] T. Chujo, PHENIX analysis note No.390 (2004).
[6] N. Kurihara, CNS Annual report 2003 (2004) 61.

Present and Future Measurements of Low-Mass Vector Mesons at RHIC Energies

K. Ozawa, H. Hamagaki, F. Kajihara, T. Gunji, T. Isobe, N. Kurihara, S.X. Oda, S. Saito and Y. Morino, for the PHENIX collaboration

Center for Nuclear Study, Graduate School of Science, University of Tokyo

1. Introduction

Since the first Au+Au collisions were observed at the Relativistic Heavy Ion Collider (RHIC) at Brookhaven National Laboratory (BNL), many new phenomena related to hot and dense nuclear matter have been discovered. In particular, the PHENIX experiment produced many new results on a wide range of physics subjects, including charged and neutral hadron production, single electron production, event isotropy, and many other topics [1].

In spite of these fruitful results, in the first three years of RHIC operation, there are still remaining questions to be answered to further characterize the state of matter formed at RHIC. In particular, chiral properties of the dense matter produced has not been obtained, and should be provided. In particular, measurements using electromagnetic probes are needed, since they carry direct information about conditions and properties of the medium at all stages of the reaction.

Of many vector mesons, $\phi(1020)$ is an interesting meson because the restoration of approximate chiral symmetry at high temperature may modify its mass and width [2]. These modifications can be shown in the line shape of the $\phi \longrightarrow e^+e^-$ peak. Also, the branching fraction of $\phi \longrightarrow K^+K^-$ and $\phi \longrightarrow e^+e^-$ could changed when the ϕ decays in medium [3]. Note that the ϕ lifetime $\tau \approx 44$ fm/c is longer than the expected lifetime of the coupled collision system, and thus only a fraction of produced ϕs may decay in the hot fireball. It has also been hypothesized that final state interactions of kaons from ϕ decay may lower the measured branching fraction in the kaon channel [4]. When the final state interaction is taken into account, only hadrons generated in the last stage can be observed.

In this paper, the current results on $\phi \longrightarrow e^+e^-$ in Au-Au collisions in Run4 are reported. Results on $\phi \longrightarrow K^+K^-$ in Au-Au collisions are quoted from [5]. Also, an upgrade plan for the PHENIX detector is briefly discussed.

2. ϕ meson measurements at PHENIX

The PHENIX experiment is specifically designed to measure low-mass lepton pairs. The current PHENIX detector consists of two central spectrometer arms for measuring electrons. Each central arm covers pseudo-rapidity of $|\eta| < 0.35$, transverse momentum of $p_T > 0.2$ GeV/c, and azimuthal angle of $\delta\phi = \pi/2$. Further details of the detector design and performance are given in [6].

During the fourth running period (Run4), RHIC delivered a luminosity of approximately 1400 μb^{-1} to the PHENIX intersection region within a vertex z range ($|z| < 45$ cm). PHENIX successfully recorded Au-Au events on order of 1.5 billion at $\sqrt{s_{NN}} = 200$ GeV after a vertex selection of
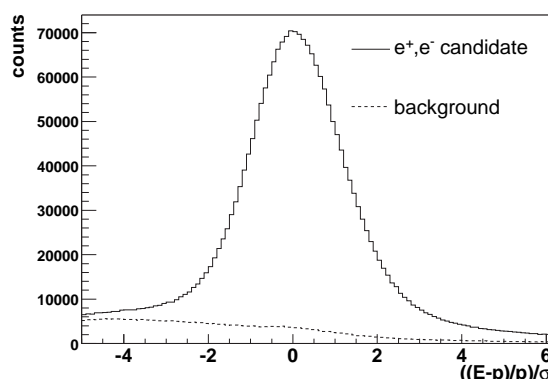
Figure 1. $(E - p)/p/\sigma$ distribution. A background of less than 10 %, caused by accidental association of tracks with RICH hits, still remains.

$|z| < 30$ cm.

PHENIX has an excellent electron identification capability that is necessary to separate electrons from the much more abundant charged pions. The RICH provides a threshold selection for electrons and the EMC confirms the matching of the tracked momentum and electromagnetic energy (E/p). Since electrons deposit all of their energy in the EMC, E/p for electrons should be approximately unity. Fig. 1 shows $(E - p)/p/\sigma$ distribution. Here the σ stands for the standard deviation of $(E - p)/p$. A background of less than 10 %, caused by accidental association of tracks with RICH hits, still remains in electron identification. In the analysis, the background is evaluated and subtracted as a combinatorial background.

Analisis of Run4 data is underway and the first results is appeared using a part of data. Figure 2 shows the e^+e^- invariant mass distribution after combinatorial background subtraction. There is an excess of counts around the ϕ mass with a signal strength of 340 ± 120(stat) and a signal to background ratio of 1/40. Within relatively large errors, the mass peak and width values agree with the values from the Particle Data Group and experimental mass resolution. The analysis of low mass di-electron pairs is underway. We can measure the yield of ϕ meson in electron decay mode and compare results in the Kaon decay mode. Thus, hot nuclear matter effects on ϕ meson production can be extracted.

3. Hadron Blind Detector

There are several measurements which are beyond the scope of the present PHENIX detector. To extend the capability of the measurement of lepton pairs, several upgrade projects of the detector are currently underway.
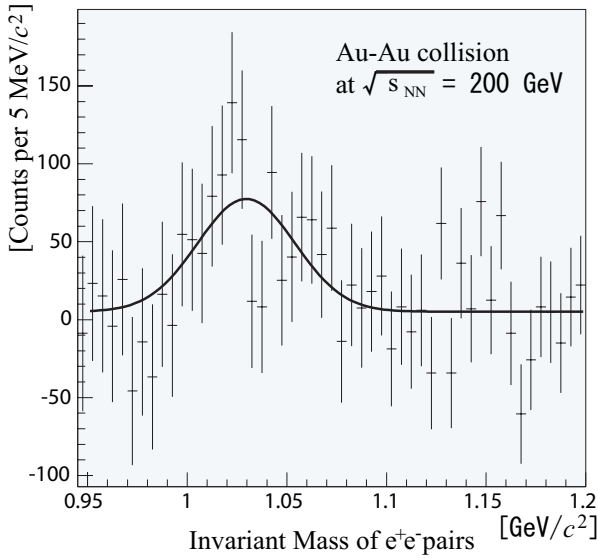
Figure 2. e^+e^- invariant mass distribution after mixed event subtraction for minimum bias (0-90% central) Au-Au collisions at $\sqrt{s_{NN}} = 200$ GeV in Run4.

Figure 3. Conceptual design of hadron blind detector. Large gas vessel as a gas radiator is shown in the figure. The center tube is placed around the beam pipe. Eight stacked GEM plates are placed on the inside of the gas vessel wall. The CSI coated first GEM is shown in the figure .

The difficulty of the measurement of low mass dileptons comes from the large combinatorial background, which is mainly contributed to by π^0 Dalitz decays and external conversion of photons. Thus, for this measurement, a Dalitz rejector with a large rejection power covering a large solid angle is needed.

The proposed Dalitz rejector is composed of two essential elements; zero magnetic field, and improved electron identification. Electron positron pairs from Dalitz decays and gamma conversions have a very small angle. Thus, these pairs produce very close hits in the electron identification detector under zero field conditions. The zero magnetic field is realized by canceling the magnetic field produced by the outer coils of the PHENIX central magnet with the reverse magnetic field produced by a set of inner coils.

To realize electron identification near the vertex region, a hadron blind detector (HBD), which is a threshold-type Čerenkov counter using CF_4 as a radiator gas [7], is proposed. The conceptual design of HBD is shown in Fig. 3. The detector consists of a 50 cm long radiator, directly coupled in a windowless configuration to a triple GEM detector which has CsI photocathode evaporated on the top face of the first GEM foil, and pad readout at the bottom of the GEM stack [8]. Eight modules of GEM stacks are shown in Fig. 3.

The R&D phase to demonstrate the validity of the HBD concept is nearly complete. A test of a prototype detector was performed at KEK using electron and charged π meson beams. The preliminary result of the test showed that charged π mesons produce only very small numberof photoelectrons ($\sim 3 - 5$). A subsequent test will be done at BNL to evaluate the total performance of the prototype. Construction of the final detector will start soon and the detector is expected to be installed in PHENIX in 2006.

4. Summary

Invariant mass spectra of $\phi \rightarrow e^+e^-$ are measured for the first time in Au-Au collisions at $\sqrt{s_{NN}} = 200$ GeV in Run4. Within relatively large errors, a mass peak is found at around ϕ meson mass region. The mass peak and width values agree with the values from the Particle Data Group and experimental resolution.

In the future, a Hadron Blind Detector will be installed in PHENIX that will enhance our capabilities of rejecting external photon conversion and Dalitz pairs, and will result in a significant reduction of the large combinatorial background. This will open up the possibility of studying chiral symmetry restoration as well as thermal di-electrons.

References

[1] K. Adcox *et al.*, nucl-ex/0410003, PHENIX whitepaper
[2] V. Koch, Int. J. Mod. Phys. E **6** (1997) 203. R. Rapp, Nucl. Phys. A **661** (1999) 238c
[3] D. Lissauer and E. V. Shuryak, Phys. Lett. B **253** (1991) 15.
[4] S. Johnson *et al.*, Eur. Phys. J. C **18** (2001) 645.
[5] S.S. Adler *et al.*, nucl-ex/0410012.
[6] K. Adcox *et al.*, Nucl. Instrum. Methods. A **499** (2003) 469.
[7] Z. Fraenkel *et al.*, Proposal for a Hadron Blind detector for PHENIX, PHENIX Technical Note **391** (2001).
[8] A. Kozlov *et al.*, Nucl. Instrum. Methods. A **523** (2004) 345.

Accelerator and Instrumentation

Extraction of Ar Ion Beam from a Small-Sized Kaufman-Type Ion Source

S. Watanabe, M. Nishiura[a] and Y. Ohshiro

Center for Nuclear Study, Graduate School of Science, University of Tokyo
[a]National Institute for Fusion Science

1. Introduction

A Kaufman-type ion source is well known as a large current ion source. A large volume of plasma chamber, a filament for electron emission, medium gas pressure and a magnetic electron confinement are the structural features of the Kaufman-type ion source. These features can include the performance that was excellent in the existing ion source, and can be progressed in the ion source that had the completely different feature by adding the new functions. To produce Ar^{1+} ion beam with an intense beam current, a proto type of the ion source [1] for producing the various kinds of the ion beams has been modified. The produced Ar^{1+} ion beam was injected into a high-temperature super-conducting material for the purpose of studying an ion beam etching. The second purpose of the one is application into a primary ion source of a charge-breeding ECR ion source (CBECR). Using the Ar^{1+} ion beam, the injection efficiency, the charge state multiplication rate and the optimization of the CBECR will be studied. A production rate of a negative hydrogen ion beam was confirmed by using the assembly of the proto type. In the present study, the extraction energy, the beam emitance and the beam current are measured.

2. Kaufman-type ion source

Plasmas are generated in the modified Kaufman-type ion source, as shown in Fig. 1. The size of the cylindrical ion source is 105 mm in diameter and 110 mm in length. Twelve rows of Nd-Fe-B magnets are attached on the sidewall of a plasma chamber and produce the multicusp magnetic fields for plasma confinement (indicated by dotted line in Fig. 1). The mean field strength of each magnet is 1 T at the surface. The extraction system consists of a plasma electrode and a Pierce-type extraction electrode. The figure shows cross-sectional view of the one with the 4-mm-diam holes. A plasma electrode with concave structure is set in front of the Pierce-type extraction electrode. To optimize the beam emittance, structure of the both electrodes has been determined with the aid of the computer simulation code.

The source body is connected to a potential of the acceleration power supply, V_{acc}, varies over 0–15 kV. Using a Teflon ring the source body and downstream the beam line are insulated. A surface distance of the Teflon ring in atmosphere is 13 mm in length. A filament power supply is 750 W with the regulation system of the output electric power to make the I-V constant. A filament for electron emission is made of tungsten wire of 0.8 mm in diameter and 100 mm in length with the shape of hairpin. Maximum arc discharge power is estimated to be 375W. An arc discharge circuit is composed of the filament and the sidewall. The
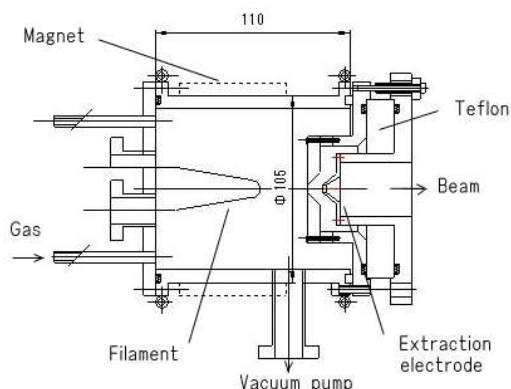
Figure 1. Cross-sectional view of a small-sized Kaufman-type ion source.

arc discharge current is depending on a gas pressure and an electron emission rate from the filament at the constant arc discharge voltage. A loss of arc discharge on the inner surface of the source body is absorbed by a water-cooling system. A water-cooling pipe is welded on the outer surface of the source body. An external gas inlet pipe is made of a 1/4-inch stainless pipe. Using a needle valve, which is located near the gas supplier, the gas pressure in the plasma chamber is controlled. Whole system including the power supplies is mounted on a high voltage terminal. An isolation transformer performs separation of the grounding potential of the ion source from the earth potential. A vacuum pump port for an evacuation of the plasma chamber is attached with an isolation valve.

3. Extraction of Ar ion beam

The extracted Ar ion beam current is shown in Fig. 2 as a function of extraction voltage together with calculated space charge limit, I_b, of the ion beam current. It is expected that the measured ion beam current is smaller than the calculated one due to a restriction of the beam aperture determined by the inner diameter of beam transport line. The extracted ion beam without the restriction of the aperture is to be estimated at 1 mA for an extraction voltage of 10 kV because of the relationship, $I \propto V^{3/2}$, from the Child-Langmuir law. The Ar ion beam current depends on the gas pressure under the same conditions of the filament current and extraction voltage. Gas pressure was changed between 3 to 6×10^{-3} Torr. We found small current deviation due to change of gas pressure. The extraction current is affected by the change of filament current. The optimized filament current should be searched to obtain maximized ion beam current. In our case, the filament voltage of 6.97 V and filament current of 39.9 A were the best conditions at the
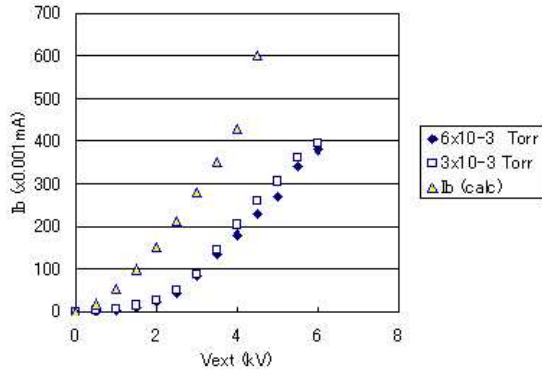
Figure 2. Ion beam extraction from a small-sized Kaufman-type ion source.

discharge voltage of 100 V and current of 0.2 A, respectively. The filament surface temperature was about 2773 K. The plasma electrode potential of 36.2 V and the current of 0.23 A were set so as to extract the maximum ion beam current.

4. Extraction of negative hydrogen ion beam

The production rate of the negative hydrogen ion beam was confirmed by using the present Kaufman-type ion source. In case of the negative hydrogen beam, an additional magnetic filter is attached on the 2nd chamber between the plasma and the extraction electrodes. The extraction electrode is changed from the Pierce-type to the parallel-plate type. First, production of the negative hydrogen ions has to be demonstrated in a volume production mode before to discuss Cesium or Xenon injection or other improvement [2]. The volume production mode requires a volume source consists of two chambers, which are connected by the magnetic filter. In the high temperature chamber, the plasma chamber as shown in Fig. 2, energetic electrons hit H_2 molecule, which become vibrantly excited. Excited molecules are also produced at the chamber walls out of H_2 and H^+. Electrons from the high temperature chamber move by diffusion through a perpendicular magnetic field into a second chamber. Whereas high-energy electrons are effectively blocked, slow electrons collect in the second chamber. In this low energy chamber, those electrons with a low temperature of 1 eV attach to the H_2^* producing H^- ions. As mentioned before, multi cusp magnets are used to confine the plasma in the high temperature chamber. In other words, extracted negative ions and electrons have to be separated by means of a magnetic dipole. To do that preliminary magnetic calculations have been performed to design the magnetic filter in the second chamber. In Fig. 1, the magnetic filter provided by the two Nd-Fe-B magnets is exclusively not indicated because of Ar ion beam extraction. Otherwise, the axial magnetic field to reach the plasma extraction area close to plasma electrode has also been calculated as well as the iron shielding. The preliminary study showed that 50 eμA of H^- could be extracted from this ion source.

5. Summary

To extract the intense ion beams from a small-sized Kaufman-type ion source, configuration of the beam extraction electrode was studied. On the basis of numerical study, determined structure of the extraction electrode was adopted to the ion source. The Pierce-type electrode was compared from the viewpoint of beam properties. The Ar beam current of 300 eμA was extracted from the slit of 4 mm in diameter at the extraction voltage of 5 kV. This result fulfills the requirements for a primary ion source of the charge breeding ECR. The parallel extraction electrode was studied for the negative hydrogen ion source. The details of negative hydrogen ion source will be discussed elsewhere.

References

[1] M. Nishiura *et al.*, Rev. Sci. Instrum. **71** (2000) 1171.
[2] M. Bacal *et al.*, Phys. Rev. Lett. **42** 1538 (1979); J. Phys. (Paris) **38** (1977) 1399.

Measurement of Longitudinal Bunching in an MA Cavity Driven HiECR Beam Line

S. Watanabe, T. Koseki[a] and Y. Ohshiro

Center for Nuclear Study, Graduate School of Science, University of Tokyo
[a] RIKEN (The Institute of Physical and Chemical Research)

1. Introduction

Purpose of the HiECR beam line [1] is to provide a beam monitor's test bench. Bunched beams are needed for calibrations of non-destructive beam monitors such as DC Current Transformer (DCCT) [2]. These monitors will be very sensitive current sensors having a dynamic range large enough to measure the full circulating current with a resolution and long-term stability of better than 10 nA. Calibration of the prototype DCCT, which is adapting high temperature superconductivity SQUID technology, was performed on this test bench [3]. The DCCT should measure both of DC beam current and bunched beam current correctly. Although the off-line calibration of the beam DCCT is made with a wire current, on-line calibration should be made by using a Faraday cup. The feature of the wide band sensitivity is also indispensable for evaluating the longitudinal bunching with an RF buncher. As for this Faraday cup, absolute measurement of the time structure of the ion beams from Hydrogen to Argon becomes research subjects.

2. RF buncher

A survey of the RF buncher was made for a composition, electric specification, bunching factor, and a voltage generating system. It takes up about existing RIKEN-AVF, AGOR cyclotron and CNS-SF cyclotron. The RIKEN-AVF provides a saw tooth buncher, which is driven by a hybrid sine wave combiner. The saw tooth buncher of AGOR [4] is driven by a saw tooth oscillator. The sine wave buncher was used in the CNS-SF cyclotron. A new RF buncher was studied [5], and R&D for HiECR beam line was performed [6]. As a magnetic alloy (MA) material installed into the cavity for the RF buncher (Fig. 1), Finemet of Hitachi Metals (FT-3M) was adopted. The Finemet is an amorphous tape-like metal wound many layers into the shape of a doughnut. It has a big permeability from DC to the higher frequency. The cut core with a 0.5 mm gap width is put in the cavity.

The MA cavity is designed so that $\lambda/4$ of standing wave length may stand with reentrant type. Therefore, as compared with core volume, low resonance frequency is realizable with large permeability. Two-mesh type metal plates are attached to an accelerating gap of the MA cavity. Each mesh has a nest type section of a bee in 2 mm pitch, and beam transmission efficiency through the mesh plates is designed to be 87%. Distance of the accelerating gap is determined from a viewpoint of both an electrostatic capacitance and a passing time of the beam.

3. Faraday cup

The Faraday cup was designed as shown in Fig. 2. The central part of the Faraday cup is a beam absorber. The
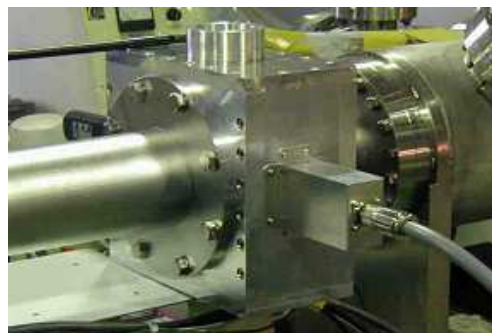
Figure 1. Photo of RF buncher in the HiECR beam line.

beam absorber is cylindrical block similar to an inner conductor of a coaxial transmission line. The beam absorber is made of copper with the diameter of 20 mm and the length of 70 mm, and measured the beam current with 50 Ω termination. A repelling grid is placed in front of the beam absorber. The space for installing a magnetic core is available in this structure. The emission rate of secondary electron needs to be evaluated, which is determined by the ion species, the number of charge states and the incident energy. An electric charge Q_c from the repelling grid (polarity is negative), and Q_t from the beam absorber give the total electron yield, $\gamma = z[-Q_c/(Q_t + Q_c)]$ [7]. It should be noted that the grid-absorber assembly is used as the Faraday cup. The electric charge of ion beam is given by $Q_{ion} = Q_t + Q_c$. A coefficient z is a given charge state of ion. The electric insulator supporting the beam absorber conducts the heating energy to the ground material. The structure for preventing invasion of noise was examined. To prevent scattered particles from the upstream, the aperture of window frame of the beam absorber is smaller than the area of beam absorber. The area of beam absorber is wider than focused ion beam. These structure is result in prevent the noise in the measured current.

The numerical specification of the Faraday cup is as follows; observation frequency = DC–100 MHz, $Z_L = 50\ \Omega$, VSWR ~ 1.2, and a beam diameter $\phi_b = 20$ mm. The repelling grid is made of a #50 tungsten mesh and $V_{\sup} = -10 \sim -500$ V where $V_{\sup}$ is bias voltage applied to the repelling grid. The beam power recommended into the Faraday cup is 10 W. The VSWR is a coefficient deduced from a ratio of a forward power to a reflection power, in which the Faraday cup is used in the measurement of bunched beam. This Faraday cup was installed in the end of beam line.

4. Beam bunching experiments

10 keV hydrogen beam (DC 20 μA) was extracted from the HiECR. An example of bunched beam signal measured
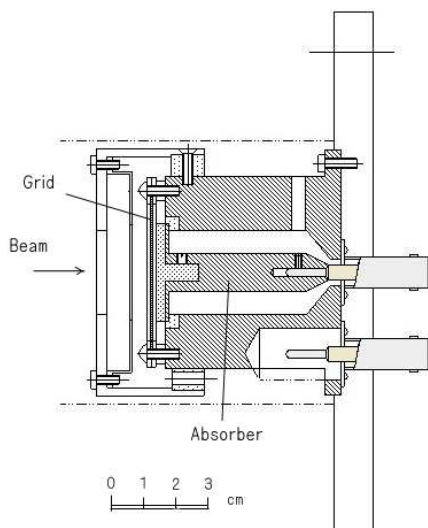
Figure 2. Cross-sectional view of the Faraday cup.
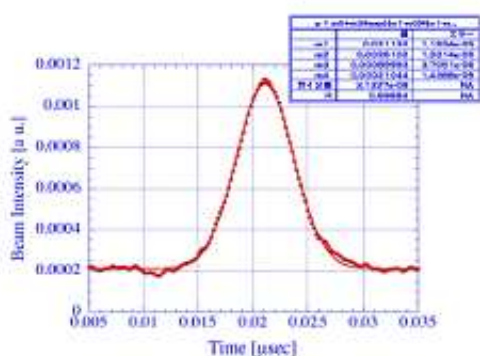
Figure 3. Typical bunched beam measured by the Faraday cup.

by the Faraday cup is shown in Fig. 3. The RF cavity was operated at the 30 MHz sine wave with a peak voltage of 150 V.

The ion species used in the bunching experiment were H^+, Ar^{2+}, Ar^{4+}, Ar^{6+}, Ar^{8+}, O^{4+}, O^{5+} and O^{6+}. The extraction energies were 11 keV (for Ar and O) or 10 keV (for H^+). The beam conditions for whole experiments were as follows; beam current was 10–30 eμA (DC), bunching frequency was 18–45 MHz, bunching voltage waveform is sine-wave, bunching voltage is 30–240 V (it depends on ion species and the number of charge state), and the bunching factor (BF), which is a ratio of DC current to a bunched current, was ~3 in general. Although the bunching voltage is adjusted so as to establish the optimum BF, it was looked out that influence of the space charge effect could not be eliminated and resultant BF brought was deteriorated.

5. Summary

The MA cavity has been installed in the HiECR beam line so as to evaluate the beam instrumentations. The frequency band of the MA cavity is a non-tuning type in 18–45 MHz. Velocity modulation was applied to H, O and Ar beams using the MA cavity, and the bunching characteristics of the beams were measured. The bunched beam signals were measured using the Faraday cup within the fre-

quency rage from DC to 100 MHz.

References

[1] S. Watanabe *et al.*, CNS Annual Report 2002 (2003) 58.
[2] T. Watanabe *et al.*, Proc. of the 14th Symp. on Accel. Sci. and Technology (2003) 99.
[3] T. Watanabe *et al.*, CNS Annual Report 2002 (2003) 71.
[4] S. Brandenburg *et al.*, Presented at cyclotron conference (ICCA16), 2001, East Lansing, Michigan, USA.
[5] M. Watanabe *et al.*, Proc. of the 14th Symposium on Accelarator Science and Technology, (2003) pp. 377.
[6] M. Watanabe *et al.*, Presented at cyclotron conference (ICCA17), Tokyo, Japan (2004), to be published.
[7] D. Hasselkamp *et al.*, in *Particle Induced Electron Emission II* (Springer-Verlag, Berlin and Heidelberg, 1992).

Upgrade of the RIKEN K70 AVF Cyclotron

M. Fukuda[ac], S. Watanabe[a], Y. Ohshiro[a], A. Goto[b], M. Nagase[b] and S. Kubono[a],

[a] Center for Nuclear Study, Graduate School of Science, University of Tokyo
[b] RIKEN (The Institute of Physical and Chemical Research)
[c] Takasaki Radiation Chemistry Research Estalishment, JAERI

1. Introduction

Researches on nuclear structures of unstable nuclei as well as nuclear astrophysics, using low energy radio-isotope(RI) beams, will be extended by increasing primary beam intensities, expanding the acceleration energy range and improving the beam quality. In order to enhance the capability of the RIKEN AVF cyclotron facility [1], some improvements of the cyclotron itself [2,3], the ECR ion source [4] and the beam lines for CRIB [5] and PA, have been phased over the last five years. The flat-top acceleration system of the AVF cyclotron [6] and the Hyper-ECR ion source [7] are utilized to provide the low energy RI beams with high intensity and high quality for the nuclear astrophysics experiments.

The present program for the RIKEN AVF cyclotron upgrade is focussed on an expansion of the energy range of accelerated ions. In order to increase the maximum acceleration energy, the K-number, expressing the nominal energy factor called a bending limit of a cyclotron, will be increased from 70 to around 80 by modifying power supplies of the main and trim coils [8]. A $^{15}N^{5+}$ ion beam will be accelerated up to 9 MeV/u, required for RI beam production in the nuclear astrophysics experiments.

The RIKEN AVF cyclotron was originally designed to accelerate light and light-heavy ions in the acceleration harmonic mode of H = 2. In order to derive heavy ions at very low energies as well as higher energies, other harmonic modes of H = 1 and 3 are required by changing the shape and the geometrical arrangement of electrodes in the center region of the AVF cyclotron. In principle, the beam orbits in the center region are different among the three acceleration harmonic modes, and both electrodes of an inflector and a puller are necessary to be exchanged every time the acceleration harmonic mode is changed. Feasibility of designing new electrodes common to the three acceleration harmonic modes will be explored, which enables one to avoid the time-consuming electrode exchange.

2. Increase of the Maximum Acceleration Energy

The maximum energy of accelerated ions is given by

$$E_{max}/A = K \times (Q/A)^2,$$

where A is a mass number and Q a charge state of the accelerated ions. The K-number is expressed as

$$K = \frac{(0.3BR_{ext})^2}{2m_0c^2},$$

where B is the magnetic field averaged at an extraction radius of R_{ext}, m_0 the mass unit and c the speed of light. The RIKEN AVF cyclotron has the maximum magnetic field of 17 kG and the extraction radius of 71.4 cm, which gives the K-number of 70.

A ^{15}N ion beam at energies more than 9 MeV/u and intensity over 10 particle-μA, is required for production of RI beams used in the astrophysics research. In the present AVF cyclotron, the energies of $^{15}N^{5+}$ and $^{15}N^{6+}$ ions are limited to 7.6 and 9.1 MeV/u, respectively. The beam intensity of the 9.1 MeV/u $^{15}N^{6+}$ ion beam is estimated to be 1 particle-μA after extracting from the cyclotron. The intensity of the 7.6 MeV/u $^{15}N^{5+}$ ion beam is expected to reach more than 10 particle-μA. The practical beam intensity is limited mainly by the performance of an ECR ion source and a beam transmission efficiency from the ion source through the cyclotron. An extensive improvement of the ion source is required to produce a high intensity ion beam with a higher charge state. In contrast, the maximum acceleration energy can be increased by enhancing a maximum main-coil current of the AVF cyclotron magnet. The K-number is required to be around 80 to accelerate the $^{15}N^{5+}$ ions up to 9 MeV/u.

The power supply of the main coil has been modified to increase the maximum output current and voltage from the rated values of 1100 A and 170 V to 1200 A and 190 V. Capacities of a main transformer and a chalk coil for a ripple filter circuit were replaced by new ones of higher current type, and an additional transistor bank was installed. The receiving capacity of the power supply has been increased by 35 KVA to 310 KVA.

In order to generate an isochronous field for acceleration of the 9 MeV/u $^{15}N^{5+}$ ions, the rated current and voltage of the trim coils, C5 and C6, have been increased from 70 A and 8 V to 200 A and 29 V for C5, and from 150 A and 13 V to 250 A and 22 V for C6, respectively.

3. Expansion of the Energy Range

The kinetic energy of the accelerated ions is expressed as

$$E/A = m_0c^2 \left(\frac{1}{\sqrt{1 - (2\pi f_{RF}R_{ext}/cH)^2}} - 1 \right),$$

where f_{RF} is a radio-frequency for an acceleration voltage. The available f_{RF} range is 12 to 24 MHz. The AVF cyclotron accelerates light and light-heavy ions, ideally, in the energy range from 3.8 through 15.4 MeV/u using the acceleration harmonic mode of H = 2. The energy range can be expanded to 1.7 through 66.6 MeV/u by using the acceleration harmonic mode of 1 or 3. A diagram of operation parameters, estimated for the expansion of the energy range by enhancing the maximum magnetic field and using the acceleration harmonic modes of 1 and 3, is shown in Fig. 1.

Optimum beam orbits in the center region of the AVF cyclotron, to achieve a high beam-transmission efficiency and a precise beam-phase control, are different in each acceleration harmonic mode. The beam orbits are determined by configuration of electrodes, such as an inflector, a puller, beam phase defining slits, the tip of a Dee electrode and an RF shield, generating the electric field in the first acceleration region. In a conventional cyclotron, the design of the electrodes in the center region was optimized individually for each acceleration harmonic mode. Usually, a costly electrode changing system without vacuum breaking needs to be developed to reduce a time for switching the acceleration harmonic mode.

The design of a new center region, hopefully common to all acceleration harmonic modes, is in progress to avoid substantial modification of the cyclotron.
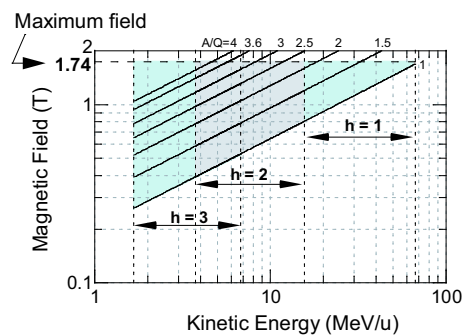
Figure 1. A diagram of cyclotron operation parameters estimated by increasing the maximum magnetic field and using the acceleration harmonic modes of H = 1, 2 and 3.

References

[1] A. Goto *et al.*, Proceedings of the 12th Int. Conf. on Cyclotrons and their Applications (1989) 51.

[2] T. Katayama *et al.*, CNS Annual Report 2001 (2002) 45.

[3] S. Watanabe *et al.*, CNS Annual Report 2001 (2002) 47.

[4] Y. Ohshiro *et al.*, CNS Annual Report 2000 (2001) 5.

[5] S. Watanabe *et al.*, CNS Annual Report 2000 (2001) 9.

[6] S. Kohara *et al.*, Nucl. Instrum. Methods. A **526** (2004) 230.

[7] Y. Ohshiro *et al.*, RIKEN Accel. Prog. Rep. **36** (2003) 279.

[8] M. Fukuda *et al.*, CNS Annual Report 2002 (2003) 74.

Development of Long Lifetime and High Intensity Boron Nano-cluster Ion Source

M. Imanaka, H. Arai[a], T. Nakagawa[a], S. Watanabe, Y. Ohshiro and T. Katayama

Center for Nuclear Study, Graduate School of Science, University of Tokyo
[a]RIKEN (The Institute of Physical and Chemical Research)

Although boron ion implantation is one of the most important processes in p^+ junction formation on semiconductor, there are some problems with boron monomer ion implantation for shallow junction in fabricating deep submicron devices. Because boron is light atom, shallow atom implantation is very difficult. It is attributed to the significant beam current drop due to the limitation imposed by the space charge effect at low implantation energy. Another problem in boron monomer implantation is transient enhanced diffusion (TED) during annealing process.

Recently the boron nano-cluster ion implantation [1, 2] has become more acceptable as an innovative alternative to the monomer ion implantation, because very low energy per atom can be realized. By using boron nano-cluster ion beam, it is possible to obtain high current beams with low energies per ion. Additionally, it is reported that TED of boron atoms is suppressed in the case of boron nano-cluster implantation [1].

For such application, we need the ion source, which can produce intense beam of boron nano-cluster ions. Plasma-gas-aggregation is a very effective method to produce large nano-clusters. Recently we have developed a magnetron type nano-cluster ion source using this method [3], and successfully produced boron nano-cluster ion beam. Although the magnetron type nano-cluster ion source is a very useful tool for studying the basic characteristics of nano-cluster, there are a few drawbacks. The lifetime of the source, which is the continuous running time to supply nano-cluster ion beam, is very short, e.g., about a half day. And the beam intensity is low, e.g., below ten microamperes. These problems are caused that just a tiny fraction of the sample can be sputtered in magnetron plasma source, and that the magnetron plasma is thrown into confusion in short time due to change of the target shape by sputtering.

To obtain longer lifetime and more intensive beam, we are developing a new type of nano-cluster ion source using another plasma source for sputtering. We adopted a waveguide-surfatron type plasma source based on surface-wave plasma [5], for producing ions and neutral particles.

Figure 1 shows a schematic drawing of the waveguide-surfatron type plasma source. This source consists of pyrex tube inside a rectangle waveguide. The injected microwave frequency is 2.45GHz. At the waveguide-surfatron, a plasma is ignited by applying very intense electric voltage on the gap [4]. And the plasma can be ignited in low vacuum of 0.1-2 Torr. Such pressure is required to obtain a sufficient high collision rate for nano-cluster growing.

The solid sample is sputtered by the gas ions, which are ionized in plasma and accelerated in electric field between plasma and its sample. This source can produce dense and
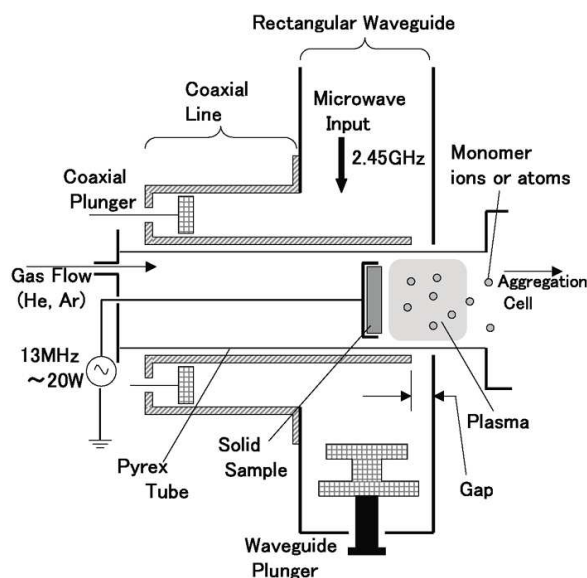
Figure 1. Schematic of waveguide-surfatron type nano-cluster ion source.

stable plasma independent of a shape or properties of the solid sample, and additionally it can produce a large size of plasma. Consequently whole area of the sample is sputtered. Therefore, we can expect very intense, stable and long life plasma source. It is expected to produce very intense beam of more than 10mA per atoms, and long lifetime, of more than 2 weeks.

We have developed a new time-of-flight (TOF) mass spectrometer for measurement of the masses of produced boron nano-cluster ions. Figure 2 shows a schematic drawing of our developed TOF system. Since the first report by Stephens [6], TOF mass spectrometry has become popular in the nano-cluster science because of its coverage of large mass range and compactness. For mass identification, we used a reflectron technique, which originally proposed by Mamyrin [7]. The reflectron was originally devised to focus the ions onto a micro channel plate (MCP) detector, and consequently the mass resolution was improved.

High voltages applied to several electrodes of ion optics are controlled with two MOSFET-switches synchronized with the start pulse. The total flight length is about 80cm. The output signal from the MCP detector is used as the stop input of multi-stop TDC. The estimated mass resolution ($\Delta m/m$) is 1600.
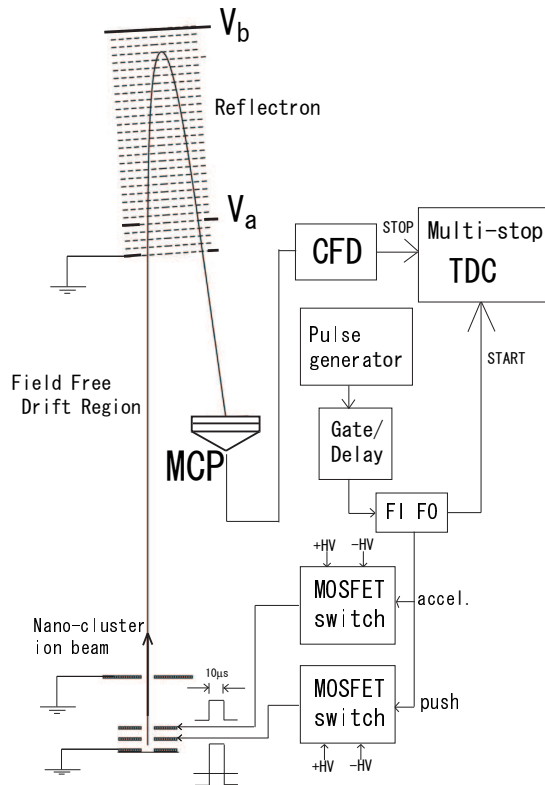
Figure 2. Schematic of the reflectron TOF system for measurements of masses of boron nano-clusters

References

[1] I. Yamada, J. Matsuo, N. Toyoda and A. Kirkpatrick, Mater. Sci. Eng. R **34** (2001) 231.

[2] X.-Y. Jin, J. Liu, P. A. W. van der Heide and W.-K. Chu, Phys. Lett. **76** (2000) 574.

[3] M. Imanaka, H. Arai, T. Nakagawa, C.-K. Chung, S.-M. Lee, Y. Ohshiro, S. Watanabe and T. Katayama, CNS Annual Report 2003 (2004) 74.

[4] J. Margot-Chaker, M. Moisan, M. Chaker, V. M. M. Glaude, P. Lauque, J. Paraszczak and G. Sauve, J. Appl. Phys. **66** (1989) 4131.

[5] M. Mosisan and Z. Zakrzewski, J. Phys. D **24** (1991) 1025.

[6] W. E. Stephens, Phys. Rev. **416** (1946) 691.

[7] B. A. Mamyrin, V. I. Karataev, D. V. Shnmikk and V. A. Zagulin, Sov. Phys. JETP **37** (1973) 45.

Beam Focusing and Separation Test of the Wien Filter for CRIB

H. Yamaguchi, A. Saito, J. J. He, Y. Wakabayashi, G. Amadio, H. Fujikawa, S. Kubono,
N. Yamazaki, T. Teranishi[a], Zs. Fülöp, Z. Elekes, Y. Yanagisawa[b], S. Michimasa[b], S. Nishimura[b]
and M. Niikura

Center for Nuclear Study, Graduate School of Science, University of Tokyo
[a]Department of Physics, Kyushu University
[b]RIKEN (The Institute of Physical and Chemical Research)
[c]ATOMKI (Institute of Nuclear Research of the Hungarian Academy of Sciences)

1. Introduction

CRIB (CNS Radioactive Ion Beam separator) [1, 2] is a facility at which low-energy and pure radioactive ion (RI) beams can be produced by in-flight separation method. Many fruitful results of nuclear and astrophysical interests have been obtained at CRIB [3, 4]. In the recent few years, we have developed a Wien filter system for CRIB, in order to have a better separation power for the RI beams.
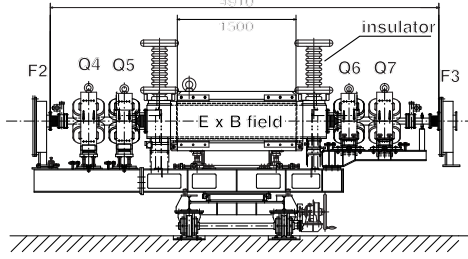
Figure 1. Side view of the Wien filter. Lengths are in mm. F2 and F3 are focal planes, and Q4–Q7 are quadrupole magnets.

The Wien filter system consists of a pair of high voltage electrodes, a dipole magnet, and four quadrupole magnets (see Figure 1). Two electrodes producing a static electric field were installed in the central vacuum chamber (the part indicated as "E x B field"). Positive and negative DC high voltages are applied for each of the electrodes, using power supply modules (Glassman Inc., PS/PG200) with maximum voltages of ± 200 kV. The two electrodes are 1.5 m-long and 160 mm-wide plates, made of an aluminum alloy (A5052). They are placed 80 mm distant from each other, perpendicular to the ground. Therefore, the applicable electric field is 50 kV/cm at maximum. To avoid discharges, the vacuum inside the central chamber is kept at a relatively high vacuum of few 10^{-5} Pa. The insulators for separating the high voltages from the ground were made by alumina (purity 99%), and they were proved to be durable for high voltages near 200 kV.

A dipole magnet is installed around the central chamber, to make a vertical magnetic field. The magnet is water-cooled, using hollow conductor coils, and having a pole gap of 400 mm. When the maximum current of 450 A is applied, it produces a magnetic field of 0.29 T at the center of the beam orbit.

The quadrupole magnet pairs were installed at both ends of the velocity separation part, and each magnet can produce magnetic field gradients of 10–20 T/m, in the center of the 3-inch beam duct. With these quadrupoles, the beam can be transported to the F3 focal plane without changing its emittance.

In case the beam width is much larger than a few millimeters order, the edge of the beam touches the inner wall of the beam duct mainly around Q6, and gets lost. In the real measurements, the transmission between F2 and F3 was measured as 30–70%, due to this effect.

2. Focusing Test

Although the optics of the Wien filter was designed as the one-to-one focusing between the focal planes F2 and F3 [5], the focal point can be moved to downstream by weakening the magnetic fields of Q6 and Q7. This feature is useful when we want to place the target and detectors distant from the original focal position. A test measurement of this focusing function was performed with an ^{40}Ar beam.
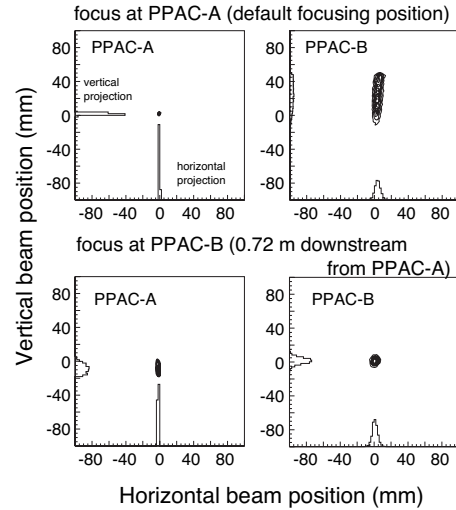
Figure 2. Beam profiles and their horizontal and vertical projections measured by two Parallel Plate Avalanche Counters (PPACs), for two focusing conditions. PPAC-A was located at the original focal plane, and PPAC-B was 0.72 m downstream along the beamline.

Figure 2 shows the measured beam profiles at two detector positions with two focusing conditions. The electric and dipole magnetic fields were not applied during this test. The strengths of the quadrupole magnets for the focusing were estimated by a transfer matrix calculation.

When the beam was focused onto PPAC-A (shown in the top two panels), the width (full width at half maximum) of the beam profile was 1.8 mm, which is consistent with the observation at F2. At PPAC-B, located at 0.72 mm downstream from PPAC-A, a diffused beam profile is observed. On the other hand, when focused to the PPAC-B position (bottom two panels), the beam width was observed as 7 mm, by PPAC-B. This was far narrower than the case focusing at PPAC-A, and narrow enough for typical measurements. The slender beam profile observed at PPAC-A in this case is due to the optics (horizontally-parallel beam inside the chamber) and the large vertical angle dispersion of the incoming beam.

3. Separation Test

^{39}Ar, mainly produced by cosmic-ray spallation processes [6] in nature, has a half-life of 269 years. The lifetime is important for geophysics with respect that it enables us to make chronological studies on rocks and waters, but it is not known very precisely. We performed a feasibility study on implanting the ^{39}Ar beam into an aluminum foil. If that implantation process is possible with an accurate knowledge of the number of implanted particles, we will be able to determine the lifetime of ^{39}Ar by an activation measurement of the alminum foil.

We performed a beam seperation test of the ^{39}Ar beam from the ^{40}Ar primary beam. The ^{3}He(^{40}Ar, ^{39}Ar)^{4}He reaction with the primary beam energy at 4.5 MeV/nucleon was used for the secondary beam production. Here, we selected ^{3}He gas (about 0.25 mg/cm^{2} thick) for the production target in order not to produce ^{39}Cl, which cannot be separated from ^{39}Ar even by the Wien filter[1]. It was extremely difficult to obtain a pure secondary beam. Even after the $B\rho$ was severely constrained ($\Delta p/p < 0.5\%$) to maximize the number of ^{39}Ar^{15+}, the primary ^{40}Ar^{15+} beam is still dominant, while the ^{39}Ar^{15+} beam is only about 2% of the total beam.
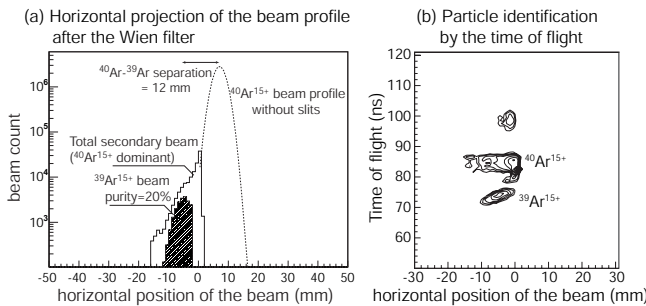
Figure 3. (a) Horizontal projection of of the beam profile. The shaded area was identified as a ^{39}Ar^{15+} beam by the time-of-flight method (see text). (b) The time of flight between the production target and F3 (with an arbitrary offset) is shown for the same data.

In this beam separation measurement, the Wien filter was operated at an electric field of 24 kV/cm ($\pm$95 kV), and a corresponding magnetic field of 0.08 T. The separation

between the ^{40}Ar^{15+} and the ^{39}Ar^{15+} beams was 12 mm at F3, and we adjusted movable slits which lie just upstream side of F3 to shut the ^{40}Ar^{15+} beam away. Consequently, the major part of the ^{40}Ar^{15+} beam was screened out, and finally we obtained a purity of 20%, which is one order of magnitude better than the secondary beam at F2.

The result is shown in Figure 3. In Figure 3 (a), the number of the detected particles is plotted against the horizontal position of the beam, measured by a PPAC at F3. The dotted line indicates the original profile of the dominant ^{40}Ar^{15+} beam, when the screening slits were fully open. This part was successfully separated out by the Wien filter. The remaining part is the observed beam, including the ^{39}Ar^{15+} component, which is explicitly indicated in the figure. The particle identification between ^{40}Ar^{15+} and ^{39}Ar^{15+} was performed by the time-of-flight method. The ordinate of Figure 3 (b) shows the time of flight between the PPAC and the production target. Here we had a clear separation between ^{40}Ar^{15+} and ^{39}Ar^{15+}. The remaining particles shown above in the figure were not identified, but they are possibly ^{41}K^{15+} or ^{38}Cl^{14+}.

The velocity dispersion in this measurement was 0.43 cm/%. If we will be able to apply the maximum electric field (50 kV/cm), we have a twice larger separation, which enables us to observe the ^{39}Ar^{15+} as a distinct peak. For this kind of experiments, a stable operation of the Wien filter at higher voltages is awaited. To have a good stability at high voltages, we have been performing "aging" of the electrodes toward the maximum voltage, $\pm$200 kV.

4. Summary

A Wien filter was newly developed for the CRIB system. The focusing and beam separation functions were tested using heavy-ion beams. By changing the focusing condition, the focal plane was successfully moved to 0.72 m downstream from the original position, keeping the beam width fairly small. The separation function was tested for a secondary RI beam of ^{39}Ar from the primary beam ^{40}Ar. A beam purity of 20%, which was one order of magnitude better compared to the beam upstream of the Wien filter, was attained. The Wien filter was stably operated at high electric fields of 24 kV/cm during the measurement, giving a velocity dispersion of 0.43 cm/%.

References

[1] S. Kubono *et al.*, Eur. Phys. J. A **13** (2002) 217.
[2] Y. Yanagisawa *et al.*, Nucl. Instrum. Methods Phys. Res., Sect. A **539** (2005) 74.
[3] T. Teranishi *et al.*, Phys. Lett. B **556** (2003) 27.
[4] M. Notani *et al.*, Nucl. Phys. A **738** (2004) 411.
[5] T. Teranishi *et al.*, CNS Annual Report 2003 (2004) 81.
[6] R. Reedy *et al.*, Science **219** (1983) 127.

---

[1] The reaction ^{3}He(^{40}Ar, ^{39}Cl)^{4}Li is energetically prohibited.

Status of Gamma-Ray Detector Array with Position and Energy sensitivity (CNS GRAPE)

E. Ideguchi, S. Shimoura, T. Fukuchi[a], M. Kurokawa[b], H. Baba[b], S. Ota[c], S. Michimasa[b], M. Tamaki, M. Niikura and H. Sakai

Center for Nuclear Study, Graduate School of Science, University of Tokyo
[a]Department of Physics, Rikkyo University
[b]RIKEN (The Institute of Physical and Chemical Research)
[c]Department of Physics, Kyoto University

Since year 2000, we have been developing a position sensitive germanium (Ge) detector array, CNS GRAPE (**G**amma-**R**ay detector **A**rray with **P**osition and **E**nergy sensitivity) for high-resolution in-beam gamma-ray spectroscopy using RI beams. In order to correct for the Doppler broadening effect from the moving gamma-ray emitters, the array was designed to have position sensitivities in the Ge crystal. The total array consists of 18 detectors and each of which contains two Ge planar crystals with effective radius of 3 cm and thickness of 2 cm. The outer side of each crystal has 3×3 segmented electrodes [1]. The planar structure and the segmented electrodes enable us to extract the position information based on a pulse-shape analysis. The resolution of less than 1% for v/c = 0.3 can be achieved after Doppler shift correction. Total efficiency of 5 % for 1 MeV gamma ray is expected.

In this year we have performed following physics experiment and developments.

- Experiment on studies of single-particle structures of the neutron-rich nuclei in the island-of-inversion (N~20 and Z~12). By using ^{32}Mg as a secondary beam and nucleon transfer reactions, (α,t) and $(\alpha,^3\mathrm{He})$ in inverse kinematics, excited states of ^{33}Al and ^{33}Mg were investigated [2]. In the experiment a liquid helium target [3] as well as a TOF spectrometer [4] was used combining with the GRAPE (see Fig. 1).

- As a second-phase data acquisition, pulse-shape data was acquired by using flash ADC in the above experiment.

- R&D of pulse shape analysis based on an artificial neural network algorithm was performed [5].

- Design of BGO Compton suppressor for GRAPE was made. It covers top and button as well as side of the detector surface with mean thickness of ~2 cm BGO crystal as shown in Fig. 2. A prototype BGO shield for one segmented Ge detector was constructed. Its energy resolution for the 662 keV gamma-ray of ^{137}Cs is ~14%.

In 2005, we plan to perform following physics experiment and detector developments.

- Study of high-spin states in the N~28 and Z~ 20 region by in-beam γ-ray spectroscopy of excited
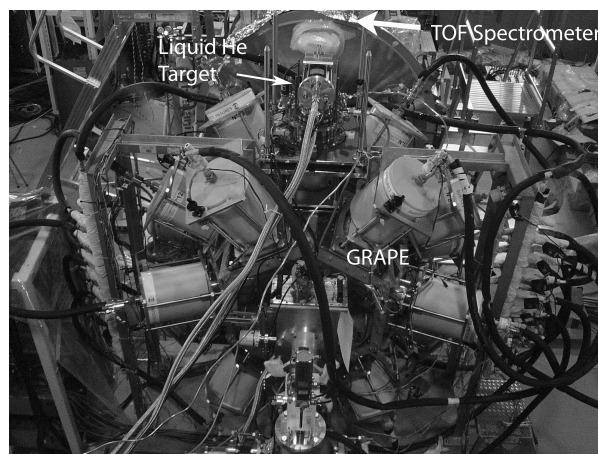
Figure 1. GRAPE with liquid helium target and TOF spectrometer.
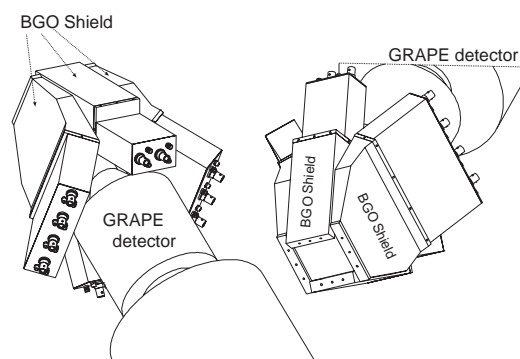
Figure 2. A prototype BGO shield for GRAPE.

states produced by fusion reactions with low-energy neutron-rich RI beams.

- Construction of test bench for BGO shield and performance evaluation of the prototype BGO shield.

- R&D of the digital signal processing and analysis system for the three-dimensional position determination.

References

[1] S. Shimoura *et al.*, CNS Annual Report 2001 (2002) 5.
[2] S. Ota *et al.*, CNS Annual Report 2004 (2005) 24.

[3] H. Akiyoshi *et al.*, CNS Annual Report 2000 (2001) 73.
    H. Akiyoshi *et al.*, RIKEN Accel. Prog. Rep. **34** (2001) 193.
[4] N. Aoi *et al.*, RIKEN Accel. Prog. Rep. **38** (2005) 176.
[5] T. Fukuchi *et al.*, CNS Annual Report 2003 (2004) 90.

Development of 3-Dimensional Position Sensitive Germanium Detector

T. Fukuchi, S. Shimoura[a], E. Ideguchi[a], M. Kurokawa[b], H. Baba[b], S. Ota[c], M. Tamaki[a] and M. Niikura[a]

Department of Physics, Rikkyo University
[a]Center for Nuclear Study, Graduate School of Science, University of Tokyo
[b]RIKEN (The Institute of Physical and Chemical Research)
[c]Department of Physics, Kyoto University

1. Introduction

We have been developing Gamma-Ray detector Array with Position and Energy sensitivity (GRAPE) which is optimized for detecting γ ray from fast moving nuclei. GRAPE consists of 18 high-purity Germanium (Ge) detectors, each of which consists of a pair of stacked planar-type Ge crystals (60 mm in diameter and 20 mm thickness). The electrode of a Ge crystal is segmented in 3×3. These Ge detectors were manufactured by Eurisys Measures. Figure 1 shows a schematic view of the Ge detector used in GRAPE. Presently, γ-ray interaction position of the depth direction in respect to the electrode is extracted from time difference between the anode and the cathode of signal rise-time using analogue modules [1].

For more precise correction with the so-called γ-ray tracking, the Ge detector system with three-dimensional position sensitivity is under development. For the extraction of three-dimensional interaction positions, transient signals which are induced at neighbor segments of γ-ray hit segment are also used with intrinsic signal. Artificial Neural Network (ANN) algorithm is employed to deduce the γ-ray interaction positions from these signals. In addition, a pulse shape sampling method for training of the ANN is being developed.
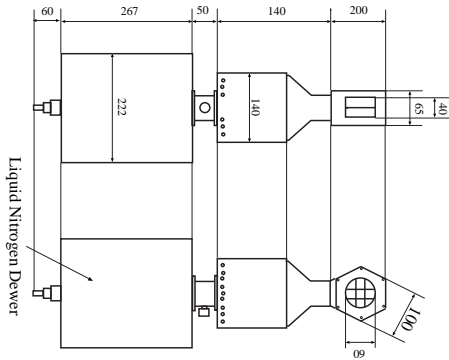
Figure 1. Schematic view of the Ge detector using in the GRAPE.

2. Pulse shape sampling

In order to train ANN, a pulse shape sample at each position in the detector is needed as a supervisor. One method of three-dimensional pulse shape sampling is to measure a position in the detector using a collimator together with another detector with a slit. In this method, for the γ ray which is incident in the collimated direction, the position measurement can be made from the Compton scattered angle selected by the slit of the other detector. However, a scanning of the whole region of the detector requires a long time. In order to reduce period which needs for pulse shape sampling, we have performed a sampling by injecting two independent γ rays from mutually perpendicular directions. This method based on a principle that signal variation of positions in perpendicular with electrodes have unique definition. In particular, (1)gamma ray is injected into the detector in parallel to electrodes, (2)gamma ray is injected in perpendicular to electrodes, and (3)the sampling data of a particular point are chosen from the data set (1) by gating on the data set (2). This measurement was automated. Summed as well as of each of 9 segment signals were taken. The signals from the crystal are amplified by charge-sensitive pre-amplifiers, after which operational amplifiers were used for matching the pre-amplified signals to the dynamic range of flash-ADCs. The pulse shape covering the rising time range of 1 μs are acquired. A data set of 59 different positions produced 145 sampled data positions. Figure 2 shows the sampled data positions and the example of the pulse shape at the center position of 10 mm depth.
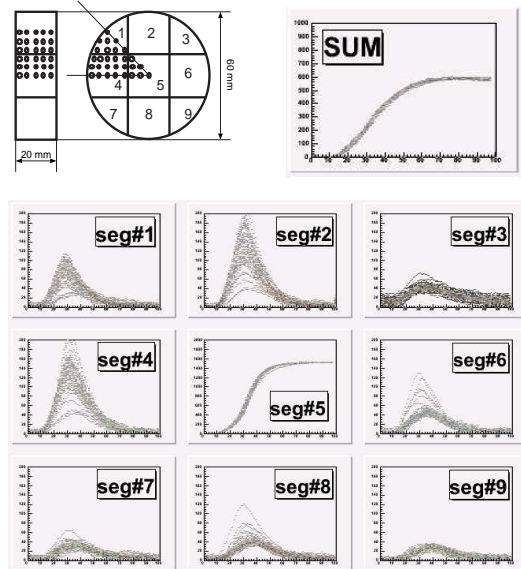
Figure 2. The sampling data positions and the example of the pulse shape at center position in 10 mm depth.

3. Determination algorithm of the γ-ray-interaction position

Then we have applied the ANN algorithm, which is based on the Kohonen's method [2], to determine the γ-ray interaction positions. In this algorithm, firstly, a variance be-

tween input and output v_j is calculated as

$$v_j = \sum (x_i(t) - w_{ij}(t))^2 \qquad (1)$$

where i and j are the ith sampling point of the flash-ADCs and the jth position in the detector, respectively. Parameter t is an number of event. Parameter x_i and w_{ij} are an input value and a pulse shape corresponding to the each position in the detector, respectively. Secondly, searching for a minimum d_j value is executed and the interaction position is deduced. The parameter w_{ij} is then modified according to the deduced position and the sampling position as

$$w_{ij}(t+1) = w_{ij} + g(t)(x_i(t) - w_{ij}(t)), \qquad (2)$$

where g is a gain parameter. In this modification, the parameters of the circumference are also modified. Figure 3 shows an example of the ANN results. For the input, sampling data were arranged in a random order of each detector positions.

The result of center position is shown in Fig.3(a). The vertical axis is a difference between the interaction positions, which are derived form the ANN algorithm, and the sampling position. The horizontal axis is the number of event. The solid line indicates results using ANN algorithm. The dashed line indicates an averaged pulse shape method. In this method, pulse shape is compared with average pulse shape of each position using the equation (1). The parameter of averaged pulse shape is a constant. The ANN result in 3(a) is from a random parameter at the start, while those shown in Fig. 3(b) and (c) are started with the averaged pulse shape. The case of starting from the random parameter and averaged parameter needs about 8000 events and 3000 events to converge, respectively. The ANN method produces a good result for some positions.

4. Future developments

In the future developments, we plan a more effective sampling method using the Compton scattering, in which the energy of the scattering angle θ is related to the energy of the incident photon E_0 and the energy of the scattered photon E_1 via

$$E_0 = E_1 + E_2, \;\; cos\theta = 1 + m_e c^2 (\frac{1}{E_0} - \frac{1}{E_2}). \qquad (3)$$

In this method, the event which is scattered in one crystal and deposited full energy in another crystal is stored. This sampling is performed by a minimum search of variance v_j in Eq.(1) through all possible combinations of the interaction positions based on the scattering angle. Here we plan a two-step sampling with (1) about 5 mm interval using a collimated γ ray on a test-bench and (2) the sampling with 1-2 mm resolution by the Compton scattering (starting from the parameter made by the sampling(1)). Complete all process of the pulse shape sampling by just placing a standard γ-ray source on the target position would be an ultimate objective of the present development.
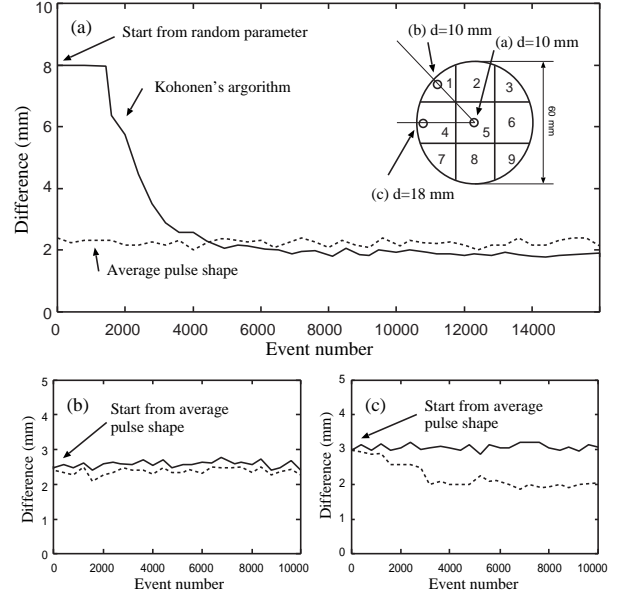
Figure 3. The example of the ANN results. The ANN training is started form random parameter for (a), and average pulse shape parameter for (b) and (c), respectively. Tested positions are also shown by circles.

References

[1] M. Kurokawa *et al.*, IEEE **50** (2003) 1309.
[2] T. Kohonen *et al.*, Self Organization and Associative Memory, third edition, (Spinger-Verlag 1990).

Development of Thick CdTe Detectors

M. Tamaki, M. Niikura, S. Ota[a], H. Baba, T. Fukuchi, E. Ideguchi and S. Shimoura

Center for Nuclear Study, Graduate School of Science, University of Tokyo
[a] Department of Physics, Kyoto University

We started a development of Cadmium telluride (CdTe) detector for one of the candidates of the next generation γ detectors with high efficiency and high energy resolution. Among several semiconductors available for γ-ray detection CdTe is one of the promising because of its high density and the large atomic numbers of its components (Z_{Cd}=48, Z_{Te}=52), as well as a large band-gap (1.5 eV). The former properties gives a high efficiency per unit volume and the latter enables its operation in room temperature. Recent progress in the technology of producing a high-quality single crystal of CdTe provided a possibility of high-resolution room temperature detectors for γ-rays. However, since small mobility of charge carriers especially for the holes and trapping effects due to the defects in a crystal yield incomplete charge collection, a thick detector with a good energy resolution was thought to be less feasible. In order to gain efficiencies with keeping good resolutions, a stack of a large number of thin CdTe detectors were developed for γ-ray astronomy [1].

Another possibility to improve the energy resolution of a thick detector is a correction depending on the interaction point derived from the pulse shape. In order to use possible techniques to extract position information, such as usage of small pixel effect [2], analog timing pickoff [3,4], and digital pulse-shape analysis, we have chosen planar-type CdTe detectors having double-sided strips (Pt) with guard rings, active sizes of which are $10 \times 10 \times 5$ (10) mm^3 (see Fig. 1). The crystals (p-type) were produced by Acrorad Co., Ltd. and were mounted by Clear Pulse Co. Ltd. In this report, basic properties of the CdTe detector, typical pulse shapes, and a possible pulse-height correction using a fast-slow shaping method are presented.

Some physical properties of the CdTe semiconductor are shown in Table. 1. It is noted that the resistivity of the CdTe is 100 times larger than that of Si, whereas the hole mobility is 7 times smaller than that of Si. We measured leakage

	CdTe	Si	Ge
Atomic number Z	48, 52	14	32
Density [g/cm^3]	6.02	2.33	5.32
Dielectric constant (relative)†	11	12	16
Intrinsic resistivity (300K) [Ωcm]	$> 2 \times 10^9$	2.3×10^5	47
Energy gap (300K) [eV]	1.5	1.1	0.7
Average energy per electron-hole pair [eV]	4.43	3.61	2.98
Electron mobility (300 K) [cm^2/Vs]	1000	1350	3900
Hole mobility (300K) [cm^2/Vs]	70	480	1900

Table 1. Some physical properties of CdTe, Si, and Ge. †Taken from ref. [5]

currents of the detectors as a function of the bias voltage. The total leakage current including that of the guard rings for the 10-mm thickness detector was about 400 nA at 1000 V, which corresponded to the resistivity of 5 GΩ cm. The ratio of the leakage currents of the strips and guard rings were found to coincides their areas. This indicates the leakage currents via the surface is much smaller than those via bulk. The large resistivity of 5 GΩcm corresponds to small impurity density of 2×10^7/cm^3, which is 100 times smaller than that of Ge detector.

The small impurity density in the CdTe detector results almost uniform electric field in the detector and almost constant drift velocities of the electrons v_e and holes v_h. Since the mobilities of the electrons and the holes are different, the charge pulse from the CdTe detector is characterized

Figure 1. Top and bottom views of the CdTe detectors. Size of each strip is 2.45×10 mm. The structure of the electrodes are identical for two types of detectors with 5mm and 10mm thicknesses.
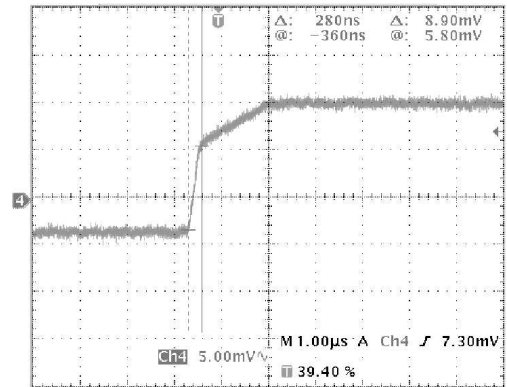
Figure 2. Typical pulse shape from the CdTe detector (5mm). The bias voltage was 800 V.
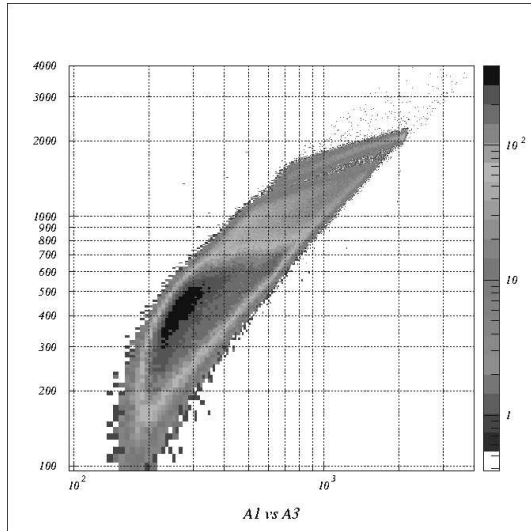
Figure 3. Two dimensional histogram for a ^{137}Cs source as a function of pulse heights of the fast- (0.5 μs; abscissa) and the slow- (3 μs; ordinate) shaping. The bias voltage was 800 V.

References

[1] T. Takahashi *et al.*, Nucl. Instrum. Methods. A **541** (2005) 332 and references therein.
[2] F. Zhang *et al.*, IEEE Trans. Nucl. Sci. **51** (2004) 2427.
[3] M. Kurokawa *et al.*, IEEE Trans. Nucl. Sci. **50** (2003) 1309.
[4] S. Shimoura, Nucl. Instrum. Methods. A **525** (2004) 188.
[5] I. Strzalkowski, S. Joshi, and C.R. Crowell, Appl. Phys. Lett. **28** (1976) 350.
[6] K. Hecht, Z. Phys. **77** (1932) 235.

by a sum of the fast and the slow components with almost constant slopes as seen in Fig. 2, where an output from the charge-sensitive preamplifier (CP-528A) is shown. Here, all the electrodes including guard rings on each surface were connected together. The timings of the vertex points in the pulse shape correspond to the arrival times of electrons and holes to the electrodes, which depend on their path lengths. The pulse height is affected by the trapping effect resulting incomplete charge collection. The incompleteness may be characterized by the ratio of the path lengths to mean free paths which are denoted by $v_e\tau_e$ or $v_h\tau_h$, respectively [6]. Since it is known that the lifetimes τ_e and τ_h are the same order, the incompleteness is larger for the holes than for electrons.

In order to study the above-mentioned characteristics of the CdTe detector in a conventional analog pulse shaping technique, pulse heights after a fast (0.5 μs: A1) and slow (3 μs: A3) shaping (ORTEC 571) of the output of the preamplifier were measured via ADC (Hoshin C008). The fast shaping corresponds to the integration of the fast rise time component which mainly comes from electrons. The total charge including hole component was to be measured by slow shaping. Figure 3 shows a two dimensional histogram for a ^{137}Cs source. The locus in the figure corresponds to the full-energy peak (662 keV). It is seen that the total charge decreases as the fast component coming from electrons decreases. The ratio of A1 to A3 (A1/A3) is almost unity for the position near the cathode and decreases as the position becomes away from the cathode. The amount of the incomplete charge collection is obtained as a function of A1/A3, where the pulse height becomes about 70% near the anode comparing to that near the cathode. Quantitative analysis of the position and the original charge and their resolution by using A1 and A3 is now in progress.

Relaxation of Proton Polarization in Polarized Solid Target

T. Wakui[a], H. Sakai[a,b], T. Uesaka[a] and S. Sakaguchi[a]

[a]*Center for Nuclear Study, Graduate School of Science, University of Tokyo*
[b]*Department of Physics, University of Tokyo*

1. Introduction

A polarized solid proton target for $\vec{p}$-RI scattering experiments has been developed using a crystal of naphthalene doped with pentacene as a target material [1]. The polarized proton target was used for an experiment with a ^{6}He beam at the RIKEN projectile fragment separator (RIPS) in July 2003 [2,3] and also for an experiment with a ^{4}He beam at E3 in September 2004 [4]. The polarization procedure is described in Ref. [5] and the target system is described in Ref. [2].

An attainable proton polarization, P, can be written as

$$P = \frac{A}{A + \Gamma_p} \overline{P_e}, \qquad (1)$$

where $\overline{P_e}$ is the average population difference between two sublevels in the photo-excited triplet state of pentacene, Γ_p the total relaxation rate of proton spins, and A the polarization buildup rate, which is proportional to the laser power. The proton polarization is a result of the competition between A and Γ_p. The relaxation rate, Γ_p, is thus an important factor to assess the target performance.

In the previous report, we described the relaxation caused during the polarization buildup process [6]. The contributions to the relaxation rate are the intrinsic relaxation due to the fluctuating field produced by paramagnetic impurities, the relaxation caused by the interaction between proton and triplet spins, and the relaxation due to the cumulative effect of laser irradiation. In addition to the relaxation process due to these sources, we found the relaxation caused by ion-beam irradiation. The relaxation rate measured without laser irradiation increased after the experiment with the ^{6}He beam. This effect may cause destruction of the proton polarization during a scattering experiment. In this report, we describe the relaxation due to ion-beam irradiation and a comparison of the contribution of each source to the relaxation rate.

2. Relaxation due to ion-beam irradiation

An increase in the relaxation rate measured without laser irradiation was found after the $\vec{p}$–^{6}He scattering experiment. The measured relaxation rate increased from 0.06 to 0.13 h^{-1}. From the measured relaxation rate, the relaxation rate due to ion-beam irradiation was obtained as 0.065 ± 0.11 h^{-1} by subtracting the intrinsic relaxation rate and the relaxation due to the cumulative effect of laser irradiation. In the experiment, the target material was irradiated by a ^{6}He beam of 71 MeV/u with a total dose of 1.5×10^8 mm^{-2}.

A similar phenomenon was observed in the $\vec{p}$–^{4}He scattering experiment. The relaxation rate due to ^{4}He beam irradiation was obtained as 0.284 ± 0.015 h^{-1} in the same manner. In the experiment, the target material was irradiated by a ^{4}He beam of 80 MeV/u with a total dose of 7×10^8 mm^{-2}.
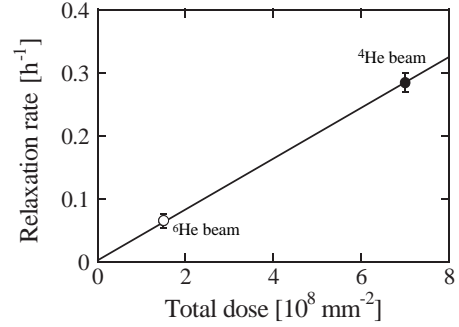
Figure 1. Relaxation rate due to ion-beam irradiation.

Although the experimental conditions such as the beam-spot size on the target material and the beam energy are different in each experiment, we tried to plot the relaxation rate due to the ion-beam irradiation against the total dose. Figure 1 shows the relaxation rate as a function of total dose. The relaxation rate seems to increase almost linearly with the total dose in the range of the experiments. The proportionality constant was $(4.07 \pm 0.04) \times 10^{-2}$ h^{-1}/10^8 mm^{-2}.

3. Comparison of relaxation sources

To evaluate the effect of the ion-beam irradiation on the polarization destruction during a scattering experiment, we estimated the dependence of the relaxation rate on time. Figure 2 shows the result of the estimation. In this estimation, we assumed that the intrinsic relaxation rate is 0.05 h^{-1}, the laser power is 200 mW, the beam intensity is 2×10^5, and the beam-spot size on the target material is 10 mmϕ. The proportionality constants used for the estimation were 0.26 ± 0.06 W^{-1}h^{-1} for the relaxation rate caused by the interaction between proton and triplet spins and $(1.1 \pm 0.5) \times 10^{-3}$ W^{-1}h^{-2} for the relaxation due to the cumulative effect. From this figure, we can see that the relaxation rate due to ion-beam irradiation increases with time and becomes as large as the sum of the relaxation rate due to other sources at the irradiation time of 5 days.

4. Annealing effect

The relaxation rate due to ion-beam irradiation will increase more rapidly for a higher beam intensity. Since the proton polarization decreases with increasing the relaxation rate during a scattering experiment, the relaxation rate due to ion-beam irradiation should periodically be reduced by changing or by annealing the target material. The annealing effect was then investigated after the $\vec{p}$–^{4}He scattering
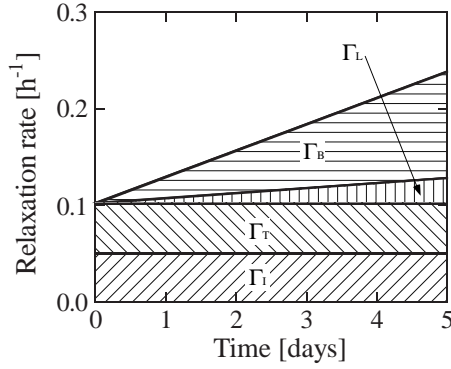
Figure 2. Time dependence of the relaxation rate due to each source.

experiment. The investigation was conducted by measuring the relaxation rate without laser irradiation after annealing at different temperatures. Figure 3 shows the relaxation rate plotted against time. The relaxation rate was obtained by subtracting the intrinsic relaxation rate from the measured relaxation rate. The relaxation rate due to the cumulative effect of laser irradiation was smaller than the error bars. The target material irradiated by ^{4}He beam was maintained at 100 K for the first 63 hours. The relaxation rate remained constant at around 0.3 h^{-1} during the first period. The annealing effect could not be seen at 100 K. The temperature of the target material was then increased and maintained at 150 K for the next 6 hours. The relaxation rate seemed to decrease slightly at 150 K. For the last 16 hours, the temperature of the target material was increased and maintained at 200 K. The relaxation rate clearly decreased at this temperature. From the result, the temperature of the target material should be increased to higher than 200 K to obtain the annealing effect.
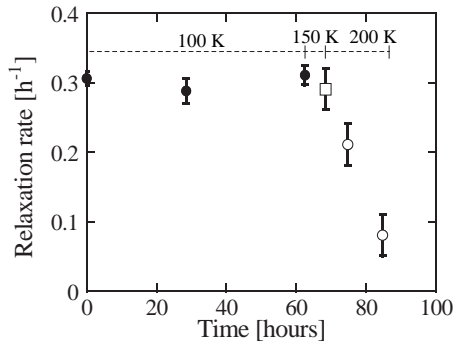
Figure 3. History of relaxation rate due to ion-beam irradiation during annealing.

5. Summary

We found the relaxation of proton polarization due to ion-beam irradiation. The relaxation rate seemed to increase almost linearly with the total dose. The proportionality constant was $(4.07\pm0.04)\times10^{-2}$ h^{-1}/10^8 mm^{-2}. We also estimated the dependence of the relaxation rate on time. The result of the estimation suggested that the relaxation rate due to ion-beam irradiation should be removed by changing

or by annealing the target material. The annealing effect was clearly seen at 200 K.

References

[1] T. Wakui *et al.*, RIKEN Accel. Prog. Rep. **34** (2001) 149.
[2] T. Uesaka *et al.*, Nucl. Instrum. Methods. A **526** (2004) 186.
[3] M. Hatano *et al.*, RIKEN Accel. Prog. Rep. **37** (2004) 44.
[4] S. Sakaguchi *et al.*, CNS Annual Report 2004 (2005) 36.
[5] M. Hatano *et al.*, RIKEN Accel. Prog. Rep. **33** (2000) 182.
[6] T. Wakui *et al.*, CNS Annual Report 2003 (2004) 84.

Polarization Calibration of Polarized ^{3}He Target via $^3\vec{\mathrm{He}}(\vec{p}, \pi^+)^4$He Reaction.

K. Itoh, Y. Shimizu[a], T. Uesaka[b], T. Wakui[b], T. Kawabata[b], Y. Tameshige[a], Y. Sakemi[a], A. Tamii[a],
K. Fujita[a], T. Wakasa[c], H. P. Yoshida[c], T. Kudoh[c], H. Ohira[c] and K. Hatanaka[a]

Department of Physics, Saitama University
[a]Research Center for Nuclear Physics, Osaka University
[b] Center for Nuclear Study, Graduate School of Science, University of Tokyo
[c]Department of Physics, Kyushu University

Spin-exchange-type polarized ^{3}He target apparatuses were developed at CNS/Riken and RCNP [1, 2]. In these target apparatuses, the cell containing ^{3}He gas has the so-called "double-cell" structure. This structure consists of a target cell and an optically pumping cell, connected to each other through a pipe with an inner diameter of 10 mm. ^{3}He nuclei in the pumping cell are polarized via spin exchange with polarized Rb atoms. The polarized ^{3}He nuclei diffuses into the target cell.

The polarization of ^{3}He nuclei in the target cell is monitored by the adiabatic-fast-passage(AFP)-NMR method, which provides a relative polarization value. On the other hand, the polarization of ^{3}He nuclei in the pumping cell is obtained by measuring the frequency shift of the Rb electron spin resonance (ESR) [3]. The ESR method provides the absolute polarization value. If the difference in ^{3}He polarization between the pumping cell and the target cell is sufficiently small, the AFP-NMR signal can be calibrated by measuring the ESR frequency shift. To compare the polarization in the target cell with that in the pumping cell, the absolute polarization of ^{3}He in the target cell was measured via the $^3\vec{\mathrm{He}}(\vec{p}, \pi^+)^4$He reaction, simultaneously with the ESR measurement.

The $^3\vec{\mathrm{He}}(\vec{p}, \pi^+)^4$He reaction measurement has recently been performed to calibrate the AFP-NMR signal. For the case of $\frac{1}{2}^+ + \frac{1}{2}^+ \to 0^- + 0^+$, one can show from the parity conservation that the polarization correlation coefficient takes $C_{y,y}=+1$ [4]. In this case, the target polarization P_y^T is written as

$$P_y^T = \frac{1}{P_y^B} \frac{\sigma_{\uparrow\uparrow} + \sigma_{\downarrow\downarrow} - \sigma_{\uparrow\downarrow} - \sigma_{\downarrow\uparrow}}{\sigma_{\uparrow\uparrow} + \sigma_{\downarrow\downarrow} + \sigma_{\uparrow\downarrow} + \sigma_{\downarrow\uparrow}}, \tag{1}$$

where P_y^B is the beam polarization and σ is the cross section for respective combinations of the spin direction. The first and second subscripts indicate the spin directions of the beam and the target, respectively. Thus, the absolute ^{3}He polarization in the target cell can be directly deduced if the beam polarization is known.

The experiment was performed at the Research Center for Nuclear Physics (RCNP), Osaka University, using a polarized proton beam. The beam energy was 392 MeV, the beam intensity was 20 nA, and the beam polarization was (70±2)%. The beam polarization was monitored using beam-line polarimeters. The pions were momentum analyzed using the high-resolution magnetic spectrometer Grand Raiden, and detected using two plastic scintillation counters and two vertical drift chambers (VDCs).

The excitation energy spectrum is shown in Fig. 1. The
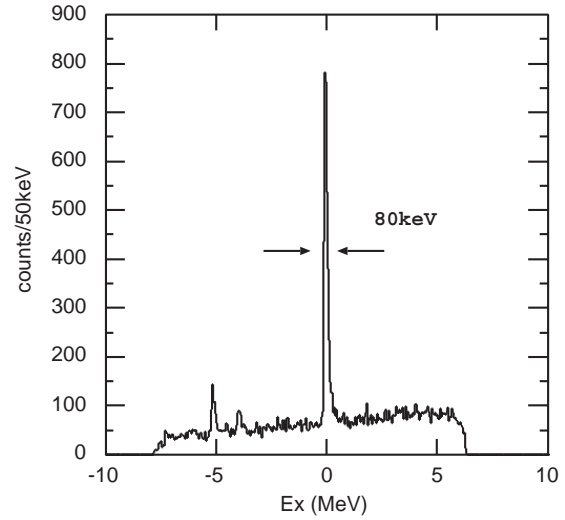
Figure 1. Excitation energy spectrum at a beam energy of 392 MeV. The sharp peak around $E_x = 0$ is due to the $^3\vec{\mathrm{He}}(\vec{p}, \pi^+)^4$He reaction.

peak around E_x=0 was due to the $^3\vec{\mathrm{He}}(\vec{p}, \pi^+)^4$He reaction. Small peaks at negative excitation energies and continuum were background events mainly due to the cell materials. Spin-dependent cross sections were deduced after subtracting background. The absolute target polarization was obtained from the spin-dependent cross sections using Eq. (1). The direction of the beam polarization was reversed every second, and the direction of the target polarization was reversed every 2 hours. The polarization of the ^{3}He target was measured by the AFP-NMR method once per hour. The mean ratio of the polarization to the amplitude of the AFP-NMR signal was deduced to be (6.68±0.58)×10^{-4} mV^{-1}. The result of $^3\vec{\mathrm{He}}(\vec{p}, \pi^+)^4$He measurements is shown in Fig. 2 by the opened triangle.

The calibrations of the polarization obtained from the ESR frequency shift have been performed before and after the $^3\vec{\mathrm{He}}(\vec{p}, \pi^+)^4$He reaction. The mean coefficient of proportionality was deduced to be (4.85 ± 0.03)×10^{-4} mV^{-1}. The polarization deduced by the ESR measurement is shown as a function of the AFP-NMR amplitude in Fig. 2 using the opened and closed circle. Detail of the ESR measurement is shown in Ref [1].
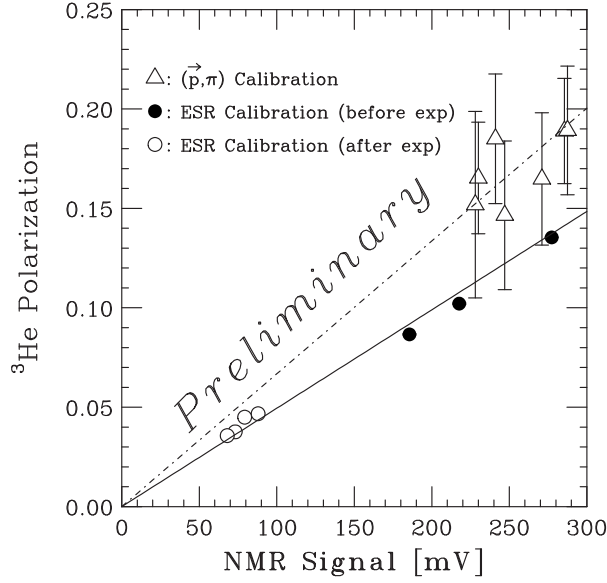
Figure 2. Correlation of the AFP-NMR amplitude and the absolute value of ^{3}He polarization. Solid and dashed lines show the fitting results for the ESR and $^3\vec{\text{He}}(\vec{p}, \pi^+)^4$He measurements, respectively.

The results of the two different calibration measurements do not agree with each other, and the polarization in the target cell is higher than the polarization in the pumping cell. Re-examination of the systematic error in the ESR frequency measurements which is caused by so-called "hot relaxation", and the background estimation of the $^3\vec{\text{He}}(\vec{p}, \pi^+)^4$He measurement are in progress.

References

[1] K. Itoh *et al.* CNS Annual Report 2003 (2004) 82.
[2] Y. Shimizu *et al.* RCNP Annual Report 2002 (2003) 39.
[3] M. V. Romalis and G.D. Cates, Phys. Rev. A **58** (1998) 3004 .
[4] G. G. Ohlsen Rep. Prog. Phys. **35** (1972) 717.

Construction of Deuteron Polarimeter at Internal Target Station of Nuclotron

T. Uesaka, K. Suda, V. P. Ladygin[a], T. A. Vasiliev[a], A. I. Malakhov[a], Yu. V. Gurchin[a],
J. -T. Karachuk[a], A. S. Kiselev[a], A. N. Khrenov[a], A. Yu. Isupov[a], V. A. Krasnov[a], A. N. Livanov[a]
and S. Reznikov[a]

Center for Nuclear Study, Graduate School of Science, University of Tokyo
[a]*Veksler-Baldin Laboratory of High Energies, Joint Institute for Nuclear Research, Russia*

1. Introduction

Spin physics programs with GeV-energy polarized deuteron beams are proposed at JINR in Russia and RIBF in Japan. In the investigations, an established measurement of deuteron polarization is required to deduce values of polarization observables reliably.

Among possible candidates of deuteron polarimetries, the d-p elastic scattering at forward angles [1], the d-p quasi-elastic scattering [2] and the deuteron inclusive breakup [3] have been used as polarimetries in the GeV energy region.

The latter two polarimetries do not suffice the requirement of vector-tensor mixed polarimetry, because the d-p quasi-elastic scattering has no tensor analyzing power while the deuteron inclusive breakup at zero degree has no vector analyzing power. On the other hand, the d-p elastic scattering at forward angles requires a two-arm spectrometer to identify the scattered deuteron from those from other reaction channels or other particles [1].

The proposed polarimetery, the d-p elastic scattering at backward angles ($\theta_{\rm cm} > 70°$) at energies 0.88–2.0 GeV, has several advantages as a beam-line polarimetry over the others. Firstly, both vector and tensor analyzing powers for the reaction can have large values [4, 5, 6, 7]. Secondly, a kinematical coincidence measurement of deuteron and proton with simple plastic scintillation counters suffices for event identification. This is mainly due to a small background event rate, compared with the forward angles. The use of this reaction as a deuteron polarimetry at 140–270 MeV at large angles is established at RIKEN [8, 9, 10].

Overview of the polarimeter setup and results of a test experiment with an unpolarized deuteron beam are described.

2. Experimental Setup

The polarimeter was installed at the Internal Target Station (ITS) of Nuclotron, a superconducting synchrotron constructed at Veksler-Baldin Laboratory of High Energies of JINR. This target station is composed of a spherical hull, a beam duct and the target stage where the target holder carrying up to 6 different targets is located.

For the polarimeter use, a polyethylene sheet of 10μm thickness is used. Details of the ITS can be found in Ref. [11].

A test measurement was carried out in February-March 2005 with unpolarized deuteron beams. Here, one pair of proton and deuteron detectors were used to measure singles rates of the detectors, accidental coincidence rate, and contribution from carbon in polyethylene tar-get. The proton and deuteron detectors were plastic scintillation detectors of 14 mm$^{\rm w}\times$20 mm$^{\rm h}\times$20 mm$^{\rm t}$ and 20 mm$^{\rm w}\times$20 mm$^{\rm h}\times$20 mm$^{\rm t}$, respectively. The detectors were placed 60 cm from the target. The beam intensity was about 1–3×10^9 particles/spill.

3. Results of Test Measurement

In Fig. 1, a spectrum of time difference between proton and deuteron detectors at 800 MeV is shown. An eminent peak corresponding to the d-p elastic scattering was observed.

Figure 2 presents energy loss correlation between proton and deuteron detectors, gated by the time difference, indicated in Fig. 1. A clear locus due to the d-p elastic scattering is observed at $\Delta E_{\rm proton} \sim 700$ channel and $\Delta E_{\rm deuteron} \sim 750$ channel. It has been proved that contributions from accidental coincidences and carbons are small enough at the energy.

The contributions from accidental coincidences and from carbon in polyethylene increase with the deuteron energy. Figures 3 and 4 present results of measurement at $T_d = 1.6$ GeV. In the time difference spectra between the proton and deuteron detectors (Fig. 3), a distinct peak due to true coincidence is observed at 0 ns. Ratio of the true coincidence rate to the accidental one is around 2.5 for a beam intensity of 1.0×10^9 /spill.

Figure 4 shows ADC spectra of the proton detector. A peak corresponds to d-p elastic scattering appears at $\sim$ 600 channel on a broad bump. A part of the bump is due to the accidental coincidence and can be subtracted by use of TDC information in Fig.3, as shown in top panel of Fig. 4 Remaining background originates from carbon in polyethylene target and can be subtracted by use of spectra for carbon target (middle panel of Fig. 4). The resulting spectrum is shown in the bottom panel. It is experimentally confirmed that the d-p elastic scattering events by polyethylene target can be clearly extracted by subtracting accidental coincidence events and carbon events. It should be noted that, at the higher energies, carbon contribution, mainly from quasifree d-p scattering, may have a large analyzing power as free d-p elastic scattering and may be used for the purpose of polarization analysis. Experiment to measure the analyzing powers for the carbon target to clarify the usefulness of the quasifree d-p scattering as polarimetry will be made in the calibration run planned in June 2005.

The experiment demonstrates that event-identification of the d-p elastic scattering at ITS is feasible. Measurement of analyzing powers for the d-p elastic scattering at the ITS po-
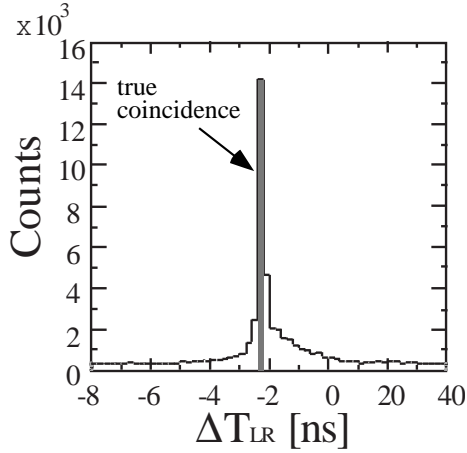
Figure 1. Time difference between proton and deuteron detectors. d-p elastic scattering corresponds to the peak indicated by shade.
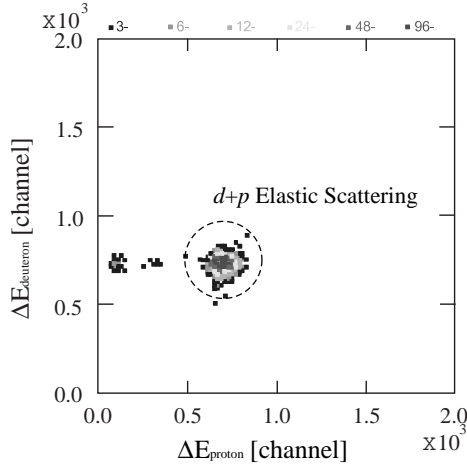
Figure 2. Energy loss correlation of proton and deuteron detectors gated by the time difference. A locus corresponding to d-p elastic scattering can be seen clearly.
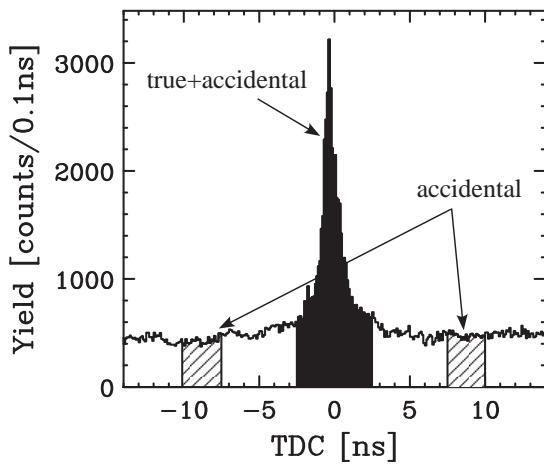
Figure 3. Time difference between proton and deuteron detectors. Filled region around 0 ns includes both true and accidental coincidences, while shaded regions correspond to accidental coincidences.
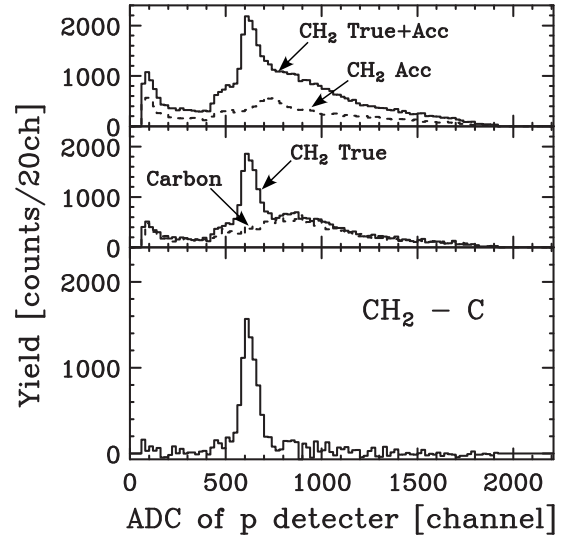
Figure 4. ADC spectra of the proton detector. TOP: spectra for polyethylene target for true+accidental and accidental coincidences. MIDDLE: polyethylene and carbon spectra. BOTTOM: d-p spectra after subtractions of contributions from accidental coincidences and carbon.

larimeter will be performed with polarized deuteron beams in June 2005. The expected results here will be essential both for future operation of new polarized ion source CIPIOS and for the spin physics programs with polarized deuteron beams at Nuclotron.

4. Summary

For the purpose to establish a beam-line polarimeter for GeV-energy deuterons, we are constructing a polarimeter at the internal target station of Nuclotron. In the test measurement, it has been clearly demonstrated that it is feasible to identify the d-p elastic scattering events with pulse height and timing information from plastic scintillation detectors. Calibration measurement with polarized deuteron beams of 300 MeV–2.0 GeV will be performed in June, 2005.

References

[1] V.G. Ableev *et al.*, Nucl. Instrum. Methods. A **306** (1991) 73.
[2] L.S. Azhgirey *et al.*, PTE **1** (1997) 51 [transl. Instr. and Exp.Tech. **40** (1997) 43]; Nucl. Instrum. Methods in Phys. Res. A **497** (2003) 340.
[3] L.S. Zolin *et al.*, JINR Rapid Comm.**2 [88]-98** (1998) 27; Yu.K. Pilipenko *et al.*, AIP Conf. Proc. **570** (2001), 801.
[4] M. Bleszynski *et al.*, Phys. Lett. B **87** (1979) 178.
[5] M. Bleszynski *et al.*, Phys. Lett. B **106** (1981) 42.
[6] M. Haji-Saied *et al.*, Phys. Rev. C **36** (1987) 2010.
[7] V. Ghazikhanian *et al.*, Phys. Rev. C **43** (1991) 1532.
[8] N. Sakamoto *et al.*, Phys. Lett. B **367** (1996) 60.
[9] K. Suda *et al.*, AIP Conf. Proc. **570** (2001) 806.
[10]K. Sekiguchi *et al.*, Phys. Rev. C **65** (2002) 034003.
[11]A.I. Malakhov *et al.*, Nucl. Instrum. Methods. A **440** (2000) 320.

Isochronous Ring for Precision Mass Measurement

Y. Yamaguchi, A. Ozawa[a], I. Arai[a], N. Fukunishi[d], A. Goto[d], T. Kikuchi[e], T. Komatsubara[a],
T. Ohnishi[d], T. Ohtsubo[c], H. Okuno[d], K. Sasa[a], T. Suzuki[b], Y. Tagishi[a], H. Takeda[d],
M. Wakasugi[d], M. Yamaguchi[a], T. Yamaguchi[b] and Y. Yano[d]

Center for Nuclear Study, Graduate School of Science, University of Tokyo
[a]Institute of Physics, University of Tsukuba
[b]Department of Physics, Saitama University
[c]Department of Physics, Niigata University
[d]RIKEN (The Institute of Physical and Chemical Research)
[e]Department of Electric and Electronic Engineering, Utsunomiya University

1. Introduction

Precision mass measurements of neutron-rich nuclei far from the stability-line are indispensable for understanding the rapid neutron capture process (r-process). The r-process is a nucleosynthesis process where elements from heavier than iron to uranium is instantaneously generated under explosive astrophysical conditions. From the nuclear physics point of view, the r-process is only discussed based on theoretical model, such as nuclear mass formula [1], because it passes over unknown neutron-rich nuclei region. In other words there are no experimental precise data exists for such region, up to now. Therefore, it is important to measure the mass of such unknown nuclei in order to study the nucleosynthesis process.

In the near future, a lot of new nuclide, including the r-process region, will be generated with the RI Beam Factory (RIBF) in RIKEN by using projectile fragmentation process and/or uranium fission. Thus, we plan to construct an isochronous ring, which specializes in the mass measurement, in RIBF.

2. Principle

In general, the cyclotron frequency (f_c) can be expressed as

$$f_c = \frac{1}{2\pi}\frac{qB}{m}, \qquad (1)$$

where m/q is mass-to-charge ratio of particle and B is magnetic field. The circulation time (T) in the ring is the inverse of f_c:

$$T = 2\pi\frac{m}{q}\frac{1}{B} = 2\pi\frac{m_0}{q}\frac{1}{B}\gamma, \qquad (2)$$

where $\gamma = 1/\sqrt{1-\beta^2}$, $\beta = v/c$ and c is the light velocity. In the isochronous ring, $B_0\gamma$ takes the place of B at certain m_0/q. Therefore, the circulation time (T_0) for certain m_0/q is expressed by

$$T_0 = 2\pi\frac{m_0}{q}\frac{1}{B_0}. \qquad (3)$$

In this case, if we measure T_0 and B_0 accurately, we can determine the mass (m_0/q) accurately. It is noted that T_0 is common even for different velocity (momentum). Since the relative differential of m_0/q is expressed as

$$\frac{\delta(m_0/q)}{m_0/q} = \frac{\delta T_0}{T_0} + \frac{\delta B_0}{B_0}, \qquad (4)$$

we can determine the mass with the order of 10^{-6} accuracy, if we measure T_0 and B_0 with the order of 10^{-6} accuracy.

For RI beams with different mass-to-charge ratios ((m_1/q)=m_0/q+$\Delta(m_0/q)$), isochronism is not fulfilled. In this case, mass-to-charge ratio can be expressed as

$$\frac{m_1}{q} = \frac{m_0}{q}\frac{T_1}{T_0}\frac{\gamma_0}{\gamma_1} = \frac{m_0}{q}\frac{T_1}{T_0}\sqrt{\frac{1-\beta_1^2}{1-(\frac{T_1}{T_0}\beta_1)^2}}, \qquad (5)$$

where T_1 is circulation time for nuclei with m_1/q and $\gamma_1 = 1/\sqrt{1-\beta_1^2}$. In order to evaluate the mass of nuclei with non-isochronism, correction of velocity is required. The relative differential of m_1/q is expressed as

$$\frac{\delta(m_1/q)}{m_1/q} = \frac{\delta(m_0/q)}{m_0/q} + \frac{\delta(T_1/T_0)}{T_1/T_0} + k\frac{\delta\beta_1}{\beta_1}, \qquad (6)$$

$$k = \frac{\beta_1^2}{1-\beta_1^2} - (\frac{T_1}{T_0})^2\frac{\beta_1^2}{1-(T_1/T_0)^2\beta_1^2}. \qquad (7)$$

Accuracy of the mass depends on the accuracy of the velocity. If we require the order of 10^{-6} mass accuracy, the third term in Eq. (6) should be less than 10^{-6}. Since 10^{-2} difference of the mass (i.e., $\Delta(m_0/q)/(m_0/q) \sim 10^{-2}$) corresponds to $\sim 10^{-2}$ difference of circulation time and $k \sim 10^{-2}$, if we determine velocity with 10^{-4} accuracy, the third term in Eq. (6) amounts to around 10^{-6}.

3. Experimental devices

3.1. Overview

A schematic drawing of the mass measurements system is shown in Fig. 1. The Rare RI, which related to r-process,
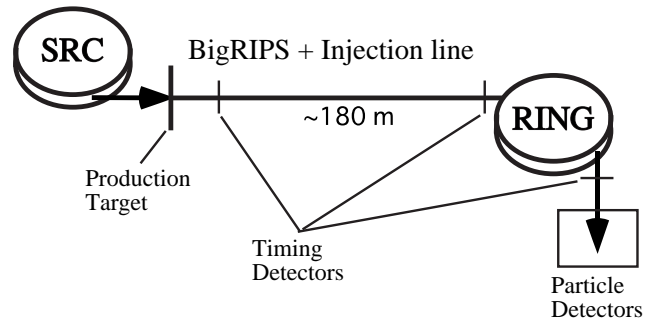
Figure 1. Schematic drawing of the mass measurements system.

is produced as secondary beam by using Ring-Cyclotron and Production-Target in RIBF. As a typical example, it is assumed that it was accelerated to about $200A$ MeV. In order to measure the velocity with 10^{-4} accuracy, as described in Sec. 2, we need a long injection line (~ 180 m), which corresponds to a long flight time ($\sim 1\ \mu$s). We intend to recycle the TARNII [2] as the injection line.

According to Eq. (4), accuracy of the circulation time in the ring directly affects accuracy of the mass. Thus, the circulation time should be more than 100 μs to achieve the 10^{-6} accuracy of the mass, if we suppose that time-resolution in conventional timing detectors is 100 ps. We propose the ring circumference is around 60 m in order to fulfill the condition of 350 ns/turn for the RI with $200A$ MeV, so more than 300 turns is necessary.

3.2. Isochronous ring

The isochronous ring, which is the main device for precision mass measurements, is designed based on the principle of a separate sector ring cyclotron. The isochronous field are created by the combination of main coils and trim coils mounted on the pole surfaces. We propose a eight or ten separated sector ring. We also locate another sector magnet, which has the same specification as the others, in order to monitor the magnetic field of the ring. Main feature of this ring design, unlike the experimental-storage-ring (ESR) at GSI [3], is not using any quadrupole magnets. Since it is not necessary to care about chromatic abberation at quadrupole magnets, our isochronous ring becomes possible to acquire larger momentum acceptance than that of ESR. From the mass measurement of Rare RI point of view, this is an advantage of the proposed system.

Accuracy of the mass depends on not only accuracy of the circulation time, but also accuracy of the magnetic field mentioned in Eq. (4). Therefore, high precision, which does not yet exist once, is required of the magnetic field of the ring, and is should be become the order of 10^{-6} accuracy. This is a substantial technical object for the detailed design of the isochronous ring.

3.3. Kicker magnet

A kicker magnet is one of the most important devices, because it is used for beam injection to and extraction from the isochronous ring. It must be generated high magnetic field with rapid rise and hall time, and make a uniform flat-top in order to efficiently inject and extract.

Concerning our system, an ideal waveform of magnetic field for injection kicker magnet is shown in Fig. 2. The rise and fall time of waveform would be achieved at less than 100 ns. The flat-top time should be 200 ns at the most, because a incidence RI passes the same place after 300ns, as described in Sec. 3.1, it is necessary to adjust the magnetic field to 0 T completely at that time. Furthermore, the response time of start-up device for kicker magnet is crucial point for our system. The response time of less than 300 ns is needed in our system.

It is said that these values can fundamentally be achieved, but we should empirically confirm it by using model kicker magnet [4].
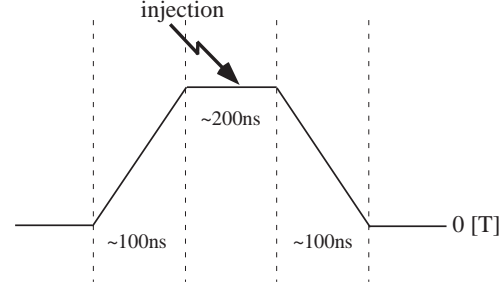
Figure 2. Ideal waveform of magnetic field for injection kicker magnet.

References

[1] H. Koura, *et al.*, Proc. of the Symposium on Nuclear Data, JAERI, Japan (2002) and private communication.
[2] A. Noda, *et al.*, Proc. of the 11th. Int. Conf. on Cyclotrons and their Applications, Tokyo, Japan (1987).
[3] B. Franzke, Nucl. Instrum. Methods. B **24/25** (1987) 18.
[4] T. Ohkawa, *et al.*, Proc. of EPAC, Paris, France (2002).

Performance of SAMURAI spectrometer in the QQQ-D mode

Y. Sasamoto, T. Uesaka, T. Kawabata, T. Kobayashi[a] and T. Nakamura[b]

Center for Nuclear Study, Graduate School of Science, University of Tokyo
[a]Department of Physics, Tohoku University
[b]Department of Physics, Tokyo Institute of Technology

A large acceptance spectrometer SAMURAI [1] is planned to be installed at RIBF. It is a superconducting dipole magnet with a circular pole of 1-m radius. The pole gap is 80 cm and the maximum magnetic field is 3 T. The spectrometer will be mainly used for spectroscopic studies of unstable nuclei with radio active beams. Several experiments concerning few body physics using a 880-MeV primary deuteron beam are also proposed. Such experiments require high momentum resolution of $\Delta p/p \simeq 3\times10^{-4}$, angular resolution of $\Delta\theta \simeq 3$ mr, and solid angle of $\Delta\Omega \simeq 6$ msr for 880-MeV deuterons, whose magnetic rigidity Bρ is 6.7 Tm.

In the original operation mode of SAMURAI, only the dipole magnet is used to analyze charged particles emitted from the reaction target. It is, however, difficult in this mode to achieve the high resolution required in the few-body experiments because the horizontal focus can not be achieved at the detector position for particles with Bρ = 6.7 Tm. To improve the momentum resolution, a new operation mode of the SAMURAI spectrometer is studied. In the new operation mode, a triplet quadrupole magnet [2] in the beam line is used in combination with the dipole magnet to analyze charged particles emitted from the target. The quadrupole triplet consists of superconducting magnets with the warm bore radius is 12 cm.
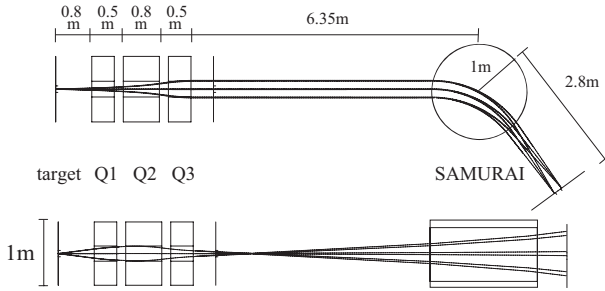
Figure 1. Schematic layout of the SAMURAI spectrometer in the QQQ-D mode. Q1, Q2 and Q3 are quadrupole magnets, while SAMURAI is a dipole magnet. The particle trajectories with $x = \pm1$ mm, $y = \pm1$mm, $\theta = \pm20$ and 0 mr, $\phi = \pm90$ and 0 mr, and $\delta = \pm3\%$ are drawn. The top figure shows trajectories on the horizontal plane, while the bottom figure shows those on the vertical plane.

In the present study, the exit of the third quadrupole magnet (Q3) is located at 6.35 m upstream from the center of the dipole magnet. The target position should be close to the entrance of the first quadrupole magnet (Q1) as much as possible to obtain large acceptance. The target position is, therefore, fixed at 0.8 m upstream from the entrance of the

bending angle	53.7 °
$(x\|x)$	-0.47
$(x\|\delta)$	2.25 m
$(y\|y)$	-19.2
$(y\|b)$	-4.26 m/rad
Resolving Power *	4.79 m
Angular acceptance (horizontal)	±20 mr
Angular acceptance (vertical)	±90 mr
Solid angle (ellipse)	5.7 msr

* Resolving Power $= \frac{(x\|\delta)}{\|(x\|x)\|}$

Table 1. Ion optical properties of the SAMURAI spectrometer in the QQQ-D mode obtained from the first order calculation.

Q1	-0.083 T/cm
Q2	-0.0912 T/cm
Q3	0.108 T/cm
SAMURAI	3.0 T

Table 2. Magnetic field strengths of the SAMURAI spectrometer in the QQQ-D mode.

Q1. The focal plane is 2.8 m downstream from the center of the dipole magnet.

The computer code GIOS [3] is used to calculate the particle trajectories in the magnet system in the first order. Figure 1 shows the layout of the spectrograph in the QQQ-D operation mode. The particle trajectories obtained from the first order calculation are also shown there.

Many combinations of three quadrupole fields are examined to achieve both good resolution and large acceptance simultaneously. One of the realistic solutions is shown in Fig. 1. The ion optical properties obtained from the first order calculation are summarized in Table 1, while the magnetic field strengths are shown in Table 2. The angular acceptance is limited by the aperture of the quadrupole magnets. In Table 1, the acceptance is estimated by an elliptical shape not a rectangle shape. From the present calculation, it is found that the momentum resolution of $\Delta p/p \simeq 2\times10^{-4}$, the angular resolution of $\Delta\theta \simeq 5$ mr, and the solid angle of $\Delta\Omega \simeq 6$ msr are expected if the beam spot size is assumed to be 1 mm.

In the first order matrix calculation described above, the effect of the fringing field is neglected since a sharp cut-off magnetic field is assumed. In order to obtain precise properties of the spectrometer, the more realistic calculation is indispensable.

Therefore, a ray-tracing calculation using the OPTRACE [4] code is performed with a realistically calculated mag-

a_0	a_1	a_2	a_3	a_4	a_5
-0.1532	3.7393	-0.2131	-1.8414	1.6537	4.7966

Table 3.   Coefficients used in the ray-tracing calculation (see text).
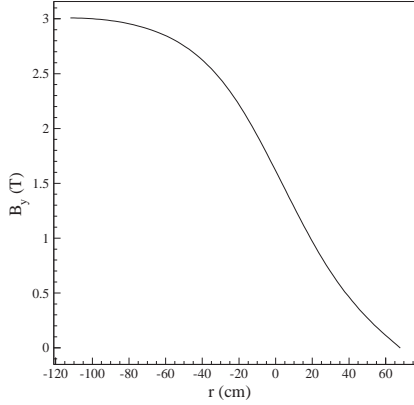
Figure 2. Vertical component of the calculated magnetic field of the dipole magnet on the median plane. The center of the dipole magnet is located at $r = -112$ cm.

netic field of the dipole magnet. The vertical component of the calculated magnetic field on the median plane is shown as a function of r in Fig. 2. The r axis is defined along the radial axis of the dipole magnet. The effective field boundary and the center of the dipole magnet are located at $r = 0$ and -112 cm, respectively. For convenience in the ray-tracing calculation, the magnetic field shown in Fig. 2 is parametrized using the following function

$$B_y = \frac{B_0}{1 + e^s}, \qquad (1)$$

where $s = a_0 + a_1(r/D) + a_2(r/D)^2 + a_3(r/D)^3 + a_4(r/D)^4 + a_5(r/D)^5$, D is the pole gap of the dipole magnet and B_0 is the magnetic field at the center of the dipole magnet. The coefficients a_i ($i = 0 \sim 5$) in Eq. (1) are tabulated in Table 3.3. For the quadrupole magnets, the same field gradients with the previous calculation are used and the fringing field is neglected.

The particle trajectories obtained in the ray-tracing calculation are shown in Fig. 3. The focal plane is located at 2.8 m from the center of the dipole magnet. It is found that the ray-tracing calculation gives almost same position of the focal plane with the previous calculation even if the fringing field of the dipole magnet is taken into account. The ion optical properties obtained from the ray-tracing calculation are summarized in Table 4.

In order to improve the calculation, it is necessary to take the fringing field of the quadrupole magnets not only the dipole magnet into account. Such a calculations is in progress.
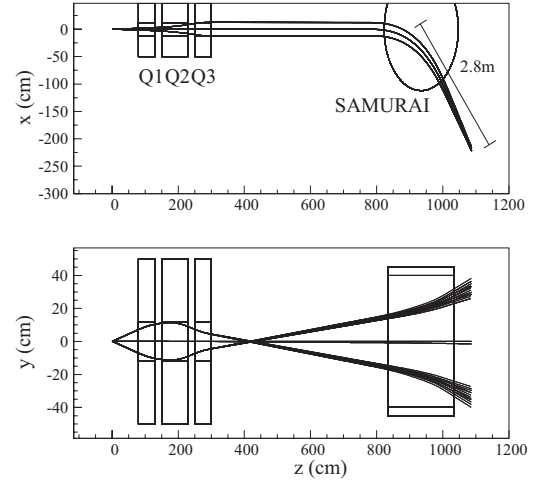
Figure 3. Particle trajectories in the SAMURAI spectrometer in the QQQ-D mode obtained from the ray-tracing calculation by the computer code OPTRACE. The trajectories with $x = \pm 1$ mm, $y = \pm 1$ mm, $\theta = \pm 20$ and 0 mr, $\phi = \pm 90$ and 0 mr, and $\delta = \pm 1\%$ are drawn. The top figure shows trajectories on the horizontal plane, while the bottom figure shows those on the vertical plane.

bending angle	$53.6\,^\circ$
$(x\|x)$	-0.48
$(x\|\delta)$	2.25 m
$(y\|y)$	-15.7
$(y\|b)$	-3.77 m/rad
Resolving Power	4.69 m
Angular acceptance (horizontal)	± 20 mr
Angular acceptance (vertical)	± 90 mr
Solid angle (ellipse)	5.7 msr

Table 4. Ion optical properties of SAMURAI spectrometer in QQQ-D mode obtained from the ray-tracing calculation.

References

[1] T. Kobayashi *et al.*, Proposal to RIBF International Advisory committee 2004.
[2] T. Kubo, Nucl. Instrum. Methods. B **204** 97 (2003).
[3] H. Wollnik *et al.*, Proc. 7th Int. Conf. on Atomic Masses and Fundamental Constants (AMCO-7), Darmstadt-Seeheim, Germany, 1984-9, edited by O. Klepper (Lehrdruckerei, Darmstadt, 1984) pp. 705; GSI Report, THD-26, 679 (1984).
[4] S. Morinobu, private communication.

Study of Digital Pulse Shape Analysis for NaI(Tl) Scintillator

H. Baba, T. Fukuchi, M. Kurokawa[a] and S. Shimoura

Center for Nuclear Study, University of Tokyo
[a] RIKEN (The Institute of Physical and Chemical Research)

1. Introduction

Recently, digital pulse shape analysis is going to be used to obtain energy and timing information, to identify charged particle, and to discriminate neutron and gamma ray [1,2,3] in place of the classical analog circuits such as shaping amplifiers, constant fraction discriminators (CFD) and peak sensitive analog-to-digital converters (ADC). By converting analog pulse to digital pulse using flash ADC (FADC), we can apply rapidly evolving industrial technologies of digital signal processing using the digital signal processor (DSP) and the field programmable gate array (FPGA). Conversion of detector signal to physical values, such as energy, timing, and position within a microsecond, can be realized. Algorithm of extracting the interacting position of gamma rays using the digital pulse shape analysis [4] has studied, and has started development of implementing this algorithm on the FPGA. For the next generation of nuclear physics experiments such as experiments at RIKEN RIBF, we propose a new dead-time free data acquisition system. In order to archive almost dead-time free system, digital pulse shape analysis using FADC and DSP/FPGA will be applied to obtain physical values. As a first step of studies of the digital pulse shape analysis to obtain physical values, performance of FADC required to obtain enough energy resolution of a NaI(Tl) scintillator from the digital pulse shape analysis is reported in this article.

2. Measurement

As a reference for the digital pulse shape analysis, resolution of the NaI(Tl) scintillator was measured using a CAEN V792 charge sensitive analog-to-digital converter (QDC) and gamma-ray source of a ^{22}Na. The gate width for the QDC was 1 μs. From this measurement, resolution was obtained to be 5.9 % at 1275 keV.

In order to obtain pulse shape of the NaI(Tl) scintillator, a SIS 3301 FADC and a Technoland N-TM231 photomultiplier amplifier (PMAMP) were used. The SIS 3301 is eight channel ADC/digitizer with 100 MHz sampling rate and 14 bit resolution in an input range of ±2.5 V. Since pulse height of the NaI(Tl) scintillator was too small for input range of FADC, PMAMP to amplify the pulse height ten times. Figure 1 shows the obtained pulse shapes of NaI(Tl) scintillator with a ^{22}Na gamma-ray source. Pulse shapes were accumulated into this 2-dimensional histogram event-by-event. The darkness corresponds to the occurrence rate. Maximum pulse height of 1275 keV gamma ray was about 0.3 V.

3. Analysis and Result

Energy of a gamma ray was calculated from numerical integration of digital pulse height which was obtained by
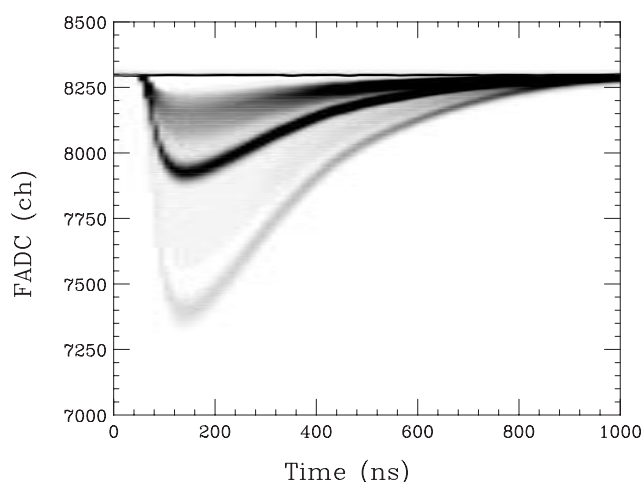
Figure 1. The obtained digital pulse shape of NaI(Tl) scintillator with a ^{22}Na gamma-ray source. The SIS3301 100 MHz / 14 bit FADC was used. The loci of 1275 keV and 511 keV were found.
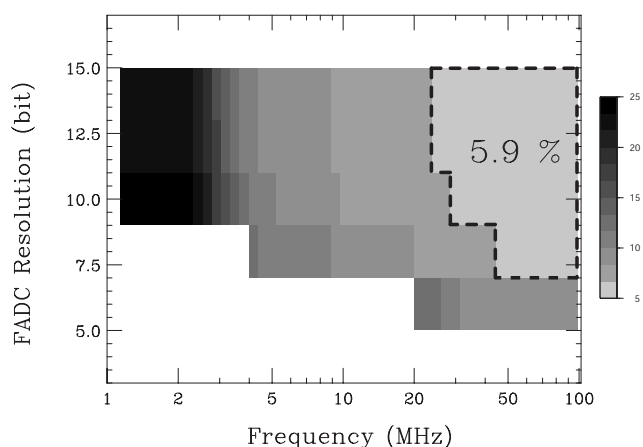
Figure 2. The obtained resolutions of NaI(Tl) scintillator at 1275 keV with several FADC condition. The darkness represents deduced resolutions. The area enclosed by dashed-line indicates enough performance of FADC to obtain resolution equal to analog circuits.

FADC from 0 to 1 μs. With 100 MHz / 14 bit FADC condition, resolution was obtained to be 5.9 % at 1275 keV, and this value is equal to the resolution obtained by analog circuits. In order to discuss required performance of FADC to obtain enough resolution, we measured energy resolutions with several FADC conditions of 100, 50, 33.33..., 25, 16.66... 10, 5, and 2 MHz frequencies and 14, 12, 10, 8, and 6 bit resolutions with $\pm$2.5 V input range. These results are shown in Fig 2. The darkness represents deduced resolutions. For $\leq$20 MHz / 6 bit and 2 MHz / 8 bit conditions, the 1275 keV peak was not able to be identified. From the results, required performance of FADC to obtain enough resolution is obtained to be about $\geq$50 MHz / 8 bit or $\geq$25 MHz / $\geq$10 bit. And these area is enclosed by dashed-line in Fig 2.

4. Summary

We have studied performance of FADC required to obtain enough energy resolution of the NaI(Tl) scintillator from the digital pulse shape analysis. Even the simple numerical integration for obtaining energy spectrum, the required performance of FADC was deduced to be about $\geq$50 MHz / 8 bit or $\geq$25 MHz / $\geq$10 bit with $\pm$2.5 V input range. For the next step, we will study the methodology of obtaining timing information for the NaI(Tl) scintillator from the pulse shape analysis.

References

[1] W. Skulski and M. Momayezi, Nucl. Instrum. Methods. A **458** (2001) 759

[2] N.V. Kornilov *et al.*, Nucl. Instrum. Methods. A **497** (2003) 467.

[3] L. Bardelli *et al.*, Nucl. Instrum. Methods. A **521** (2004) 480.

[4] T. Fukuchi *et al.*, CNS Annual Report 2003 (2004) 88.

Development of a Time Projection Chamber Using Gas Electron Multipliers (GEM-TPC)

S. X. Oda, H. Hamagaki, K. Ozawa, M. Inuzuka, T. Sakaguchi, T. Isobe, T. Gunji, S. Saito, Y. Morino, Y. L. Yamaguchi[a], S. Sawada[b] and S. Yokkaichi[c]

Center for Nuclear Study, Graduate School of Science, University of Tokyo
[a]*Waseda University*
[b]*KEK, High Energy Accelerator Research Organization*
[c]*RIKEN (The Institute of Physical and Chemical Research)*

1. Introduction

Relativistic heavy ion collision experiments are performed to study hadronic matter under high temperature and high density condition. The central tracking detectors of the relativistic heavy ion collision experiments have special difficulty due to high event rates and high particle multiplicity. In $\sqrt{s_{NN}} = 200$ GeV Au+Au collisions at the Relativistic Heavy Ion Collider (RHIC) at Brookhaven National Laboratory, the average charged particle multiplicity is $\langle dN_{ch}/d\eta|_{\eta=0} \rangle = 170$, the average charged particle density is 0.03 cm^{-2} and the charged particle rate is $\sim$300 cps/cm^2 at a point 30 cm away from the vertex [1].

Since a relatively low transverse momentum range ($p_T \sim$ 0.2–20 GeV/c) to be covered for the study of relativistic heavy ion collision, the magnetic field should be kept low ($\sim$1 T). However high momentum resolution of $\delta p_T/p_T^2 \sim 10^{-3}$ (GeV/c)$^{-1}$ is desired in future experiments, e.g. to resolve the Υ states at RHIC-II [2]. To achieve this resolution with a magnetic field of 1 T and, for example, a 1-m radius solenoidal tracker, spatial resolution of 200 μm is needed. High double track resolution of $\sim$1 cm is also required.

Under this high multiplicity and high rate condition, the double track resolution of the existing wire chambers is limited by the space of wires. A TPC using micro-pattern gas detectors (MPGDs), such as gas electron multipliers (GEMs) [3], for signal amplification is a strong candidate for the central tracking detector because the novel structure of MPGD may achieve both excellent spatial resolution and high rate capability with a low material budget.

2. GEM-TPC Prototype

A GEM-TPC prototype, which consists of an end cap chamber, a field cage and a gas vessel, was developed [4, 5, 6]. The field cage is a rectangular parallelepiped (cuboid) with dimensions of $36 \times 17 \times 17$ cm^3. Either a triple GEM (the effective area is 10×10 cm^2) or an MWPC is used for the end cap chamber on readout pads. Two kinds of readout pads with different shapes, rectangle and chevron (zigzag), were made, in order to study the dependence of the spatial resolution on shapes. Since chevron pads may increase the number of hit pads by charge sharing, chevron pad is expected to have better spatial resolution than rectangular one. The rectangular pad and chevron one, which are made of gold-plated copper, have the same area of 1.09×12.0 mm^2. Narrow strip pads are required for charge sharing with small

diffusion gas, such as CF$_4$. The field cage consists of 115 gold-plated copper strips connected with 1-MΩ resistors in series on FR4 boards. At the end of the resistor chain, resistors are added to adjust the voltage of the field cage end to that of the surface of the top GEM. The signals, amplified using charge sensitive preamplifiers, are transmitted to 8-bit and 100-MHz FADCs through 8-m shielded twisted cables.

3. Performance Test

In order to evaluate the fundamental performance of the GEM-TPC, a beam test was performed at π2 test beam line of the 12-GeV Proton Synchrotron at KEK (KEK-PS). Evaluation items of the GEM-TPC were detection efficiency, spatial resolution in the pad-row direction and the drift direction, particle identification capability using dE/dx and double track resolution. Their dependence on gas (Ar(90%)-CH$_4$(10%), Ar(70%)-C$_2$H$_6$(30%) and CF$_4$(100%)), drift length (20–290 mm), readout pad shape (rectangle and chevron), beam momentum (0.5–3.0 GeV/c) and gain of GEM (7×10^2–2×10^4) is also evaluated. The triple GEM made by CERN was used for the measurement.

4. Results

4.1. Detection Efficiency

Detection efficiency was measured as a function of gain of GEM with 3 kinds of gases. Figure 1 shows the efficiency curves, which have the plateaus of $> 99.3\%$, with two kinds of gases.
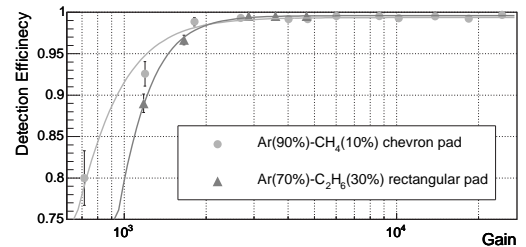
Figure 1. Detection efficiency of the GEM-TPC.

4.2. Spatial Resolution

Spatial resolution in the pad-row direction and the drift direction was evaluated for the drift length of 20–290 mm is shown in Fig. 2. The best resolution is 79 μm in the pad-row direction and 313 μm in the drift direction with Ar-C$_2$H$_6$ gas and rectangular pads for 20-mm drift. Spatial resolution is similar between the two kinds of pads.
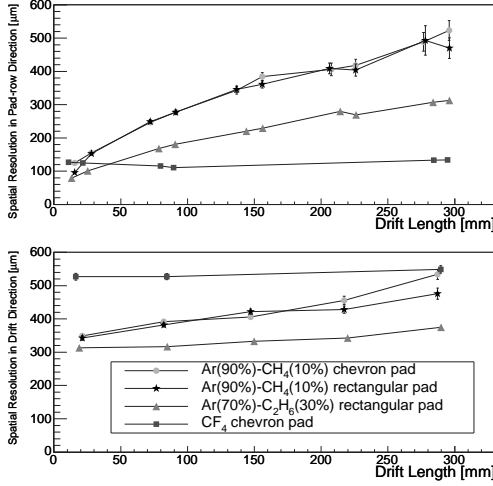
Figure 2. Spatial resolution in the pad-row direction (top) and the drift direction (bottom).

4.3. Particle Identification Capability

Particle identification capability was studied with electrons, muons, pions, protons and deuterons. The beam momentum range is 0.5–3.0 GeV/c. Figure 3 shows the mean energy loss for 5 kinds of particle species. Energy resolution of pion and the pion rejection factor with 99% proton efficiency are expected to be 9% and 200 for 1-GeV/c particle and 50-cm drift by a truncated mean method.
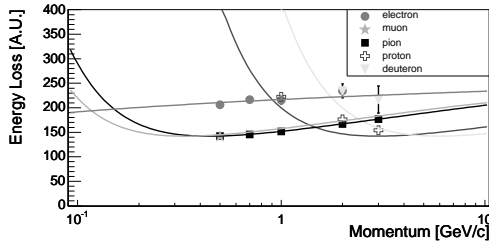
Figure 3. Measured energy loss for 5 kinds of particle species. The curves are Bethe-Bloch formula.

4.4. Double Track Resolution

In order to study double track resolution, the measured distribution of distance of two tracks were compared with the simulated distribution. Double track resolution was evaluated by the distribution of distance between two tracks in the drift direction. The ratio of the measured distribution to the simulated distribution is shown in Fig. 4. Two tracks with distance of 12 mm can almost be distinguished.
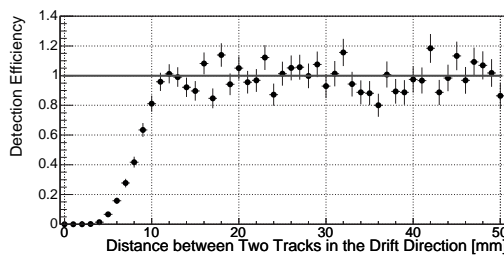
Figure 4. Double track detection efficiency.

4.5. Beam Rate Dependence

One of the advantages of GEM-TPC is ion feedback suppression. The effect of the ion feedback on the GEM-TPC was studied by measuring beam rate dependence of detection efficiency and spatial resolution. (see Fig. 5). Although the detection efficiency and the spatial resolution worsen by factors of 3% and 10% respectively at the maximum beam rate of 4800 cps/cm^2, they still indicate high performance of the GEM-TPC. The beam rate exceeds the rates of RHIC and LHC.
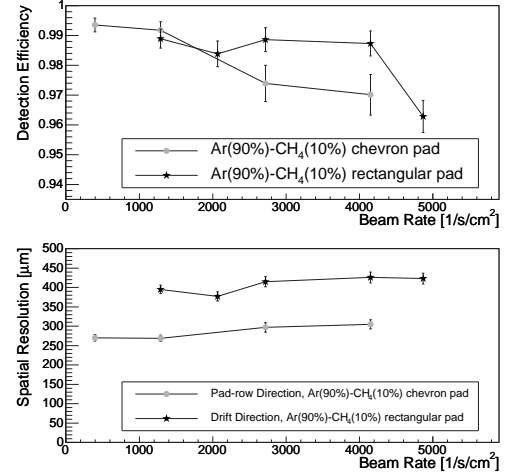
Figure 5. Dependence of the detection efficiency (top) and the spatial resolution on the beam rate.

5. Summary

A GEM-TPC prototype has been constructed toward a tracker which works under high rate and high multiplicity condition.

In order to evaluate the performance of the GEM-TPC, a performance test has been performed at KEK-PS. Detection efficiency, spatial resolution, particle identification capability and double track resolution were studied. The GEM-TPC held high detection efficiency and good spatial resolution with a high particle rate of 4800 cps/cm^2, which exceeds ones of RHIC and LHC.

The results indicate that the GEM-TPC meets the requirements for use as a central tracking detector in the next generation of relativistic heavy ion collision experiments.

References

[1] B.B. Back *et al.*, Phys. Rev. C **65** (2002) 031901.
[2] P. Steinberg *et al.*, nucl-ex/0503002.
[3] F. Sauli, Nucl. Instrum. Methods. A **386** (1997) 531.
[4] T. Isobe *et al.*, CNS Annual Report 2002 (2003) 39.
[5] T. Isobe *et al.*, CNS Annual Report 2003 (2004) 63.
[6] S. X. Oda *et al.*, CNS Annual Report 2003 (2004) 69.

Electron Identification Capability of Real Size, Six Layer Transition Radiation Detector for ALICE

Y. Morino, S. Saito, T. Gunji, H. Hamagaki and K. Ozawa,
for the ALICE TRD Collaboration

Center for Nuclear Study, Graduate School of Science, University of Tokyo

1. Introduction

It is predicted from lattice Quantum Chromo Dynamics (QCD) calculation that a phase transition from hadronic matter to a plasma of deconfined quarks and gluons, called quark-gluon plasma (QGP) may occur at high energy density. ALICE experiment is one of the experiments at Large Hadron Collider (LHC) at CERN ,planned to start operation in 2007. The physics goal of the ALICE experiment is to study such a QCD phase transition in heavy ion collisions at center of mass energy of $\sqrt{s_{NN}} = 5.5$ TeV [1].

The Transition Radiation Detector (TRD) of the ALICE is designed to provide electron identification and tracking capability of charged particles. For electron identification, it is necessary to minimize misidentification of pions as electrons. For measuring quarkonia, which is one of the most crucial observables for QGP studies, it is required for the ALICE TRD to achieve the pion misidentification probability of less than 1% at 90% electron efficiency, which corresponds to pion rejection factor of more than 100, at momenta in excess of 2 GeV/c [2].

2. Real size TRD and test experiment

Transition radiation (TR) is emitted when a charged particle crosses the boundary between two media with different dielectric constants [3]. More than one TR photons, typically soft X-rays, are produced if Lorentz factor γ of the charged particle is larger than about 1000. This Lorentz factor corresponds to electron momentum of about 0.5 GeV/c and pion momentum of about 140 GeV/c. So detecting transition radiation can be utilized to identify electrons effectively in the momentum region from 0.5 GeV/c to 140 GeV/c.

The ALICE TRD consists of six detector layers, where each layer is composed of a radiator and a drift chamber. The radiator consists of polypropylene fiber mats (fiber diameter 15μm), sandwiched between two Rohacell HF71 sheets. A total thickness of the radiator is 4.8 cm. The drift chamber has a drift region of 30 mm and an amplification region of 7mm, and is operated with Xe-CO$_2$ (85%-15%) gas mixture.

After several test experiments with small prototypes and prototype readout electronics [4],the design of TRD and readout electronics were fixed and the real size TRDs and prototype readout electronics were developed and constructed. A first beam test of six layered TRDs with production size ($939\times1070\times105$ and $981\times1070\times105$ mm^3) was performed at the CERN PS accelerator in October 2004. One readout board (ROB), which was mounted on the backend of the TRD, was used for each detector layer to read out the signals from 288 detector pads. ROB consists of 16 Multi Chip Modules (MCMs). A Preamplifier/Shaper
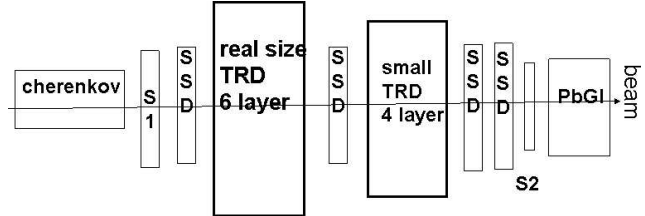
Figure 1. A schematic view of the beam test setup. TRD, two scintillators (S1,S2), Cherenkov detector, Pb-glass calorimeter (PbGl) and four Si-strip detectors (SSD).

(PASA) is mounted on each MCM, and signal digitization (10-bit,10 MHz sample frequency) is also performed on the board [2].

Measurements were carried out with electron-pion mixed beam with momentum of 1 to10 GeV/c. Figure 1 shows a schematic view of the test experimental setup. Scintillators provided beam trigger. The Cherenkov detector and the Pb-glass calorimeter were used for separating electron events and pion events. Four Si-strip detectors were used for precise beam position measurements.
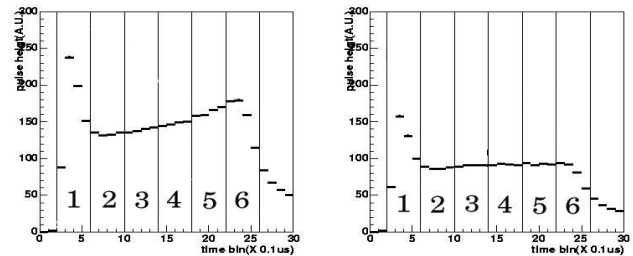
Figure 2. Average pulse height in one detector layer as a function of drift time at the beam momentum of 4 GeV/c.Left panel shows electron events and right one shows pion events.

3. Analysis

Figure 2 shows the average measured pulse height for pions and electrons as a function of drift time in one layer at the beam momentum of 4 GeV/c. The peak at the small drift time, marked as "1" in Fig.2, originates from the amplification region, and the plateau after the peak is from the drift region. In the case of electron events, TR photons are absorbed at the entrance of the drift chamber, and these contributions are clearly seen around the end of drift time clearly. TR contribution can be used for electron identification. For exploiting TR contribution for electron identification, the drift region was split into six sections, as indicated in Fig.2. The distribution of measured energy deposit at each section
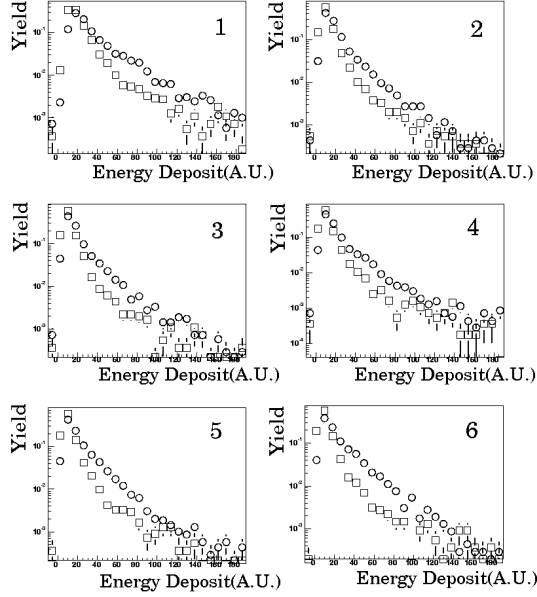
Figure 3. Energy deposit distribution of electron (open circle) and pion (open square) in one layer at each section at 4 GeV/c. The number of each panel corresponds to the number of Fig.2

is shown in figure 3 for electron and pion in one layer. It is clearly seen that TR contribution becomes large at large drift time section in Fig.3.

A bi-dimensional likelihood analysis method was used for evaluating electron identification capability [5]. The likelihood ratio is defined for each event as the ratio of electron probability to pion probability. These probability is determined from energy deposit distribution at each section in each layer as shown in Fig.3. Figure 4 shows the distribution of calculated likelihood ratio for electron events and pion events. In the figure, the vertical line correspond to 90% electron efficiency. Since events in a right region
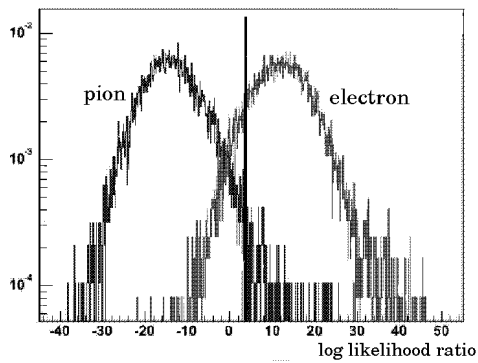
Figure 4. Log likelihood ratio distribution of electron events and pion events at 4 GeV/c. A line in this figure corresponds to 90% electron efficiency
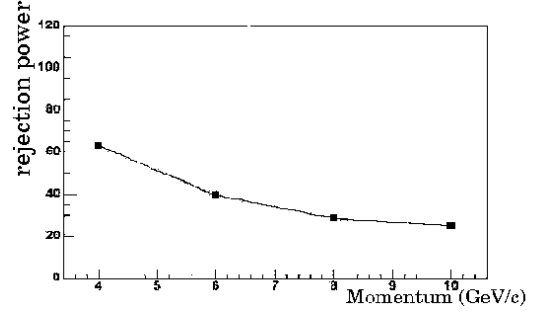
Figure 5. The inverse of pion misidentification probability (pion rejection power) as a function of beam momentum

of the line are identified as electron events, pion events in this region are misidentified pion events. The ratio of these misidentified pion events to pion events sample is defined as pion misidentification probability.

Figure 5 shows the inverse of evaluated pion misidentification probability (pion rejection power) as a function of beam momentum. Compared to earlier results from small prototype TRDs [4], this result gives slightly worse pion rejection. It may come from the poorer signal-to-noise ratio for readout electronics in these measurements and increasing δ-ray due to larger material budget (ROB and radiator's crossbar) behind the detectors, compared to the earlier measurement. By requiring the track matching for δ-ray rejection, an improvement of pion rejection by a factor of 1.5 is achieved. It is important for pion rejection to exploit the drift time dependence of pulse height from TR contribution, as described before. This work is not straightforward because there is a strong correlation between drift time and pulse height. Improvements in cancellation out this correlation and rejection of remaining effect of δ-ray are under study.

4. Summary

The ALICE TRD project is now in detector production stage, and a first beam test of real size TRDs was performed successfully. Electron identification capability has been studied using a likelihood method. Pion rejection power 60 is achieved at the beam momenta of 4 GeV/c. Improvements are under study for further improvement of electron identification capability.

References

[1] ALICE Collaboration Technical Proposal, CERN/LHCC, 95–71.
[2] ALICE TRD Technical Design Report, CERN/LHCC, 2001-021;
http://www-alice.gsi.de/trd.
[3] M. L. Cherry *et al.*, Phys. Rev. D **10** (1974) 3594.
[4] T. Gunji *et al.*, CNS Annual Report 2003 (2004) 65.
[5] A. Andronic *et al.*, Nucl. Instrum. Methods. A **522** (2004) 40.

Measurements of Stability of Gas Electron Multiplier (GEM)

Y. L. Yamaguchi, H. Hamagaki, K. Ozawa, S. X. Oda and M. Inuzuka[a]

Center for Nuclear Study, Graduate School of Science, University of Tokyo
[a] National Research Institute for Cultural Properties, Tokyo

1. Introduction

The Gas Electron Multiplier (GEM), which was originally invented by F. Sauli at CERN, consists of a metalized polymer foil with holes [1]. Mechanism of signal amplification in a GEM is as follows. The metal layers play a role of electrodes and a few hundred volts are applied between them. When a drift electron passes through the hole on the GEM, strong electric field inside the hole induces the cascade of electrons. The GEM is expected to be capable of high rate operation while maintaining good spatial resolution. In fact, the GEM is used in some rate-critical high-energy experiments [2].

The GEM made at CERN (CERN-GEM) is fabricated by the chemical etching method and has holes with a double-conical shape. However, the CERN-GEM has room of improvement because it has been reported that the CERN-GEM could not maintain its gain stable [3]. With better gain stability attained, the GEM will be used in more varieties of applications.

We succeeded in fabricating a new type of the GEM (CNS-GEM) by the plasma etching method [4]. The CNS-GEM has holes with a cylindrical shape.

In this report, the result of measurements for gain stability of the CNS-GEM compared with that of the CERN-GEM is described.

2. Fabrication of GEM

2.1. Fabrication by the plasma etching method

The essential point in the fabrication process of the GEM is the choice of technology for piercing metalized polymer foils.

The standard GEM consists of a 50 μm-thick Kapton coated with 5 μm-thick copper, and the pitch and diameter of the holes are 140 μm and 70 μm, respectively [3]. In
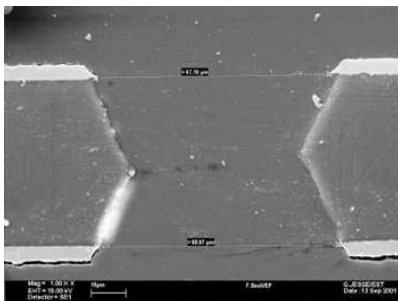
Figure 1. The cross section of a hole of the CERN-GEM

the case of the CERN-GEM, after making the holes on copper layers by conventional photo-lithography, the foil is immersed in a specific solvent, which dissolves Kapton. The CERN-GEM has holes with a double-conical shape which

is characteristic of the chemical etching of the polymer (Fig. 1).

On the other hand, the CNS-GEM is fabricated by the plasma etching method at Fuchigami Micro CO., Ltd. The CNS-GEM has holes with a cylindrical shape (Fig. 2).
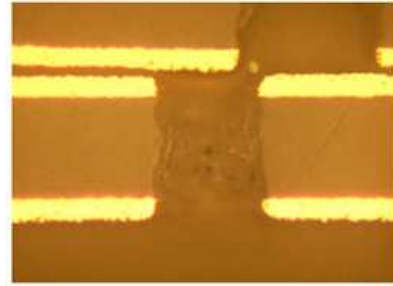
Figure 2. The cross section of a hole of the CNS-GEM

2.2. Charging-up

It has been reported that the gas gain of the CERN-GEM increases (or decreases) as a function of illumination time. One possible reason for this is charge up of the Kapton insulator surface inside the holes. The charging-up is thought to be due to double-conical shapes of holes of the CERN-GEM.

The CNS-GEM which has holes with a cylindrical shape is expected to have better gain stability than the CERN-GEM since the CNS-GEM in whose holes there are no bulge has a better electron transmission and less probability of charging-up.

3. Measurements of time dependence of GEM

3.1. GEM setup

Figure 3 shows the schematic view of the GEM setup. Measurements were carried out with three GEM foils
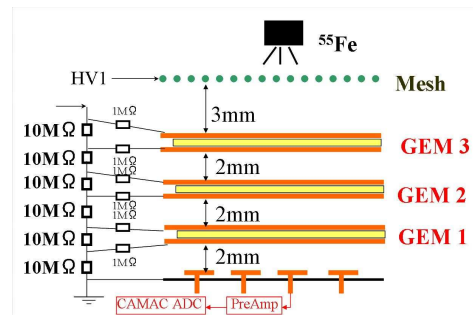
Figure 3. A schematic view of the GEM test setup

mounted in a chamber [5]. The distance between neighboring GEM's is 2 mm. The high voltages to the GEM electrodes are supplied from a single HV source applied to 'HV2' in Fig. 3. The HV2 is equally divided using the chain

of 10 MΩ resistors and sub-divided voltages are provided to individual electrodes. A drift plane, which is a metallic mesh, is mounted 3 mm above the uppermost GEM. The high voltage 'HV1' is given to the drift plane. HV1 is 200 V higher than HV2 during our measurements. The electrons created inside the drift region between the drift plane and the uppermost GEM are transferred to the GEM layers. When cascade electrons produced in the GEM holes approach by copper readout pads, positive charges are induced on the readout pads and negative charges flow into a charge-sensitive pre-amplifier,consisting of a 325 MHz amplifier with the feedback of 1 pF capacitor, and are recorded using a VME ADC module.

3.2. Measurements

In our measurements, ^{55}Fe (X-ray, 5.9 keV) standard source with intensity of 370 kBq is used. The chamber is filled with Ar(70%)–CO_2(30%). The flow rate of the gas is adjusted to about 200 cc/min at an atmospheric pressure. During each measurement, the voltage applied to each GEM is kept 365 V. Each measurement is carried out for about 10 hours.

4. Results

Figure 4 shows a typical spectrum obtained for three layers of GEM's. In Fig. 4, a higher peak corresponds to the peak of 5.9 keV and a lower peak corresponds to the peak of the escape peak of Ar. The 5.9 keV peak is fitted with a Gaussian. ¿From the mean value (S_{mean}), the gain (G)
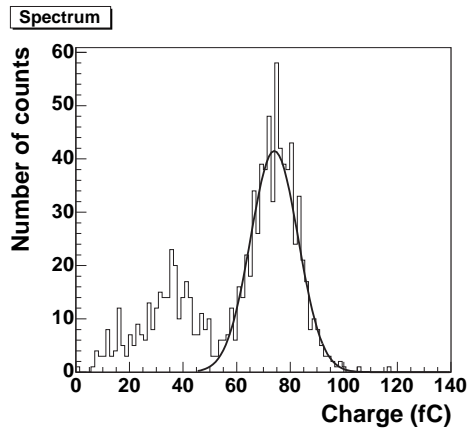
Figure 4. An ^{55}Fe X-ray charge spectrum with Ar(70%)–CO_2(30%) at the voltage applied to each GEM, $V_{GEM} = 365$ V.

is calculated as $G = (S_{mean}/C) \cdot (1/q_e n_e)$, where q_e is the electron charge, and n_e is the number of electron-ion pairs created by the absorption of 5.9 keV X-ray: $n_e = 212$ for Ar(70%)–CO_2(30%) [6]. The coefficient, C, was determined to be 16.53 fC^{-1} from the calibration of the pre-amplifier and the ADC.

Figure 5 shows the measured gain as a function of the illumination time, where the illumination time means a time while the voltage is applied to the GEM's. The open and the closed symbols show the results for the CERN-GEM and the CNS-GEM, respectively. Gain of both GEM's increases in the first few hours, which will be interpreted as an aging
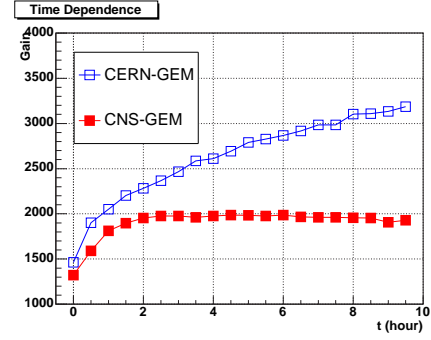
Figure 5. The illumination-time dependence of the gain. The open and the closed symbols show the result of CERN-GEM and CNS-GEM, respectively.

effect. As clearly seen from the figure, the gain of the CNS-GEM is more stable than that of the CERN-GEM. It has been considered that the shape of holes in a GEM could affect significantly to a gain stability.

5. Summary and Outlook

Measurements for illumination-time dependence of gain of the CERN-GEM and the CNS-GEM are carried out. Gain of the CNS-GEM is found to be more stable than that of the CERN-GEM.

The absolute value of the gain is very sensitive to the gas density. The variation of the gas pressure and/or temperature affect the gain [7]. It is necessary to take data of the gas pressure and temperature during measurements for a gas gain in order to study for the gas density dependence of gain. An environment for measurements is being prepared.

References

[1] F. Sauli, Nucl. Instrum. Methods. A **386** (1997) 531.
[2] B. Ketzer, IEEE Trans. Nucl. Sci. NS **49** (2002) 2403.
[3] S. Bachmann *et al.*, Nucl. Instrum. Methods. A **438** (1999) 376.
[4] M. Inuzuka *et al.*, CNS Annual Report (2003) 67.
[5] M. Inuzuka *et al.*, Nucl. Instrum. Methods. A **525** (2004) 529.
[6] F. Sauli, CERN Yellow Report 77-09 (1997).
[7] A. Kozlov *et al.*, Nucl. Instrum. Methods. A **523** (2004) 345.

Theoretical Nuclear Physics

Large Scale Nuclear Structure Calculations in CNS

N. Shimizu[a], T. Otsuka[a,b,c], N. Itagaki[a], T. Mizusaki[d], M. Honma[e] and Y. Utsuno[f]

[a]Department of Physics, University of Tokyo
[b]Center for Nuclear Study, Graduate School of Science, University of Tokyo
[c]RIKEN (The Institute of Physics and Chemical Research)
[d]Institute of Natural Sciences, Senshu University
[e]Center for Mathematical Sciences, University of Aizu
[f]Japan Atomic Energy Research Institute

1. Introduction

The CNS has started theoretical studies since the year 2001. One of its major activities is the project of large-scale nuclear structure calculation. This project has been carried out based on a collaboration agreement between CNS and RIKEN Accelerator Research Facility (RARF) [1, 2]. Because we require a large amount of numerical computation to study the nuclear structure theoretically as a quantum many-body problem, massive parallel computers had been installed [2]. The introduction of the computers had been almost finished until 2003, and various achievements were produced under this project in the fiscal year 2004. We briefly show the overview of the achievements in this report.

2. Physical Achievement

We describe various physical achievements respectively, classified mainly according to the mass regions of nuclei.

First, we studied cluster structure of light neutron-rich nuclei. For example, an equilateral-triangular shape of 3α surrounded by excess neutrons has been suggested for ^{14}C, based on the molecular-orbit model [3]. It is found that the attractive interaction between an excess neutron and an α-particle stabilizes the $K^{\pi} = 0^+$ and 3^- rotational bands, which demonstrates an equilateral-triangular symmetry. This $K^{\pi} = 3^-$ band at 3 MeV below the ^{10}Be+α threshold energy corresponds to the experimentally observed band built on top of the second 3^- state. A positive-parity rotational band (0^+, 2^+, 4^+) arises similarly. These two bands suggest a molecular structure of 3α's stabilized by the excess neutrons and can be viewed as a realization of the α crystallization in the dilute nuclear medium.

We have demonstrated whether the cluster structure dissolves or remains, when the shell-model-like model space is introduced in addition to the cluster model space, in light nuclei [4]. Although the binding energies of ^{8}Be, ^{10}Be, and ^{10}B become larger by about 1-2 MeV by adding shell-model-like basis states to the $\alpha+\alpha+N+N+\cdots$ basis states, essentially α-α structure is a dominant configuration of the ground states. However, α-breaking wave functions strongly mixes in ^{12}C, and the decrease of the energy from the 3α configuration by about 6 MeV is a clue to resolve a long-standing problem of the binding energies of ^{12}C and ^{16}O. The improved version of Antisymmetrized Molecular Dynamics (AMD), AMD Superposition of Selected Snap-shots (AMD triple-S) is used to show the cluster-shell competition of these nuclei.

Furthermore, we have proposed a simple model to describe the cluster-shell competition [5]. By introducing only one parameter (Λ) to the wave function, describing an asymptotic transition of two valence neutrons in ^{10}Be ($\alpha+\alpha+n+n$) from a di-neutron to independent particles is possible when the contribution of the spin-orbit interaction is taken into account. Similarly in ^{12}C, a transition from a 3α configuration to a $2\alpha+4N$ configuration is represented, and we show a strong contribution of the spin-orbit interaction in the ground state. We investigate further this transition from the cluster state ($\alpha+^{16}$O) to the shell-model state (^{16}O+four nucleons) in ^{20}Ne. In these examples, the wave functions for cluster-breaking states are prepared in the same general way.

Secondly, we have studied the structure of unstable nuclei in the sd-shell on the basis of large-scale shell-model calculation, whose model space consists of both sd-shell and pf-shell. The disappearance of the magic structure of neutron-rich $N = 20$ nuclei is investigated [6], and the structures of ^{34}S and ^{31}Mg are also discussed [7, 8]. In addition, anomalous magnetic moment of ^{9}C is discussed in terms of the nuclear shell model [9].

Thirdly, we have studied the structure of unstable nuclei in the pf-shell on the basis of the large-scale shell-model calculations with our effective interaction GXPF1 [10]. On the proton-rich side, new experimental data of $B(E2; 0^+ \rightarrow 2^+)$ values for Fe and Ni isotopes were found to be basically in good agreement with the shell-model results [11, 12, 13], demonstrating the predictive power of the effective interaction in this mass region. On the neutron-rich side, the new data of ^{59}Cr show deviations from the shell-model predictions, indicating the insufficiency of the full pf-shell model space [14]. Also, it has been shown that the $N = 32$ shell-closure develops in Ti and Cr isotopes, while definite evidence of the predicted $N = 34$ shell gap has not been observed experimentally in these isotopes [15, 16].

Fourthly, the ground and low-lying collective excited states of neutron-rich Te isotopes are studied using the nuclear shell model and the MCSM [17]. The observed anomalously small $B(E2; 0_1^+ \rightarrow 2_1^+)$ value of ^{136}Te is described using the nuclear shell model as a simple microscopic framework. The 2_1^+ state is mainly contributed by the proton excitation. The nuclear structures of the 2_2^+ state

of ^{136}Te and other isotopes are also discussed.

Fifthly, the mechanism of the dominance (preponderance) of the 0^+ ground state for random interactions is proposed to be the chaotic realization of the highest rotational symmetry [18]. This is a consequence of a general principle on the chaos and symmetry that the highest symmetry is given to the ground state if sufficient mixing occurs in a chaotic way by a random interaction. Under this symmetry-realization mechanism, the ground-state parity and isospin can be predicted so that the positive parity is favored over the negative parity and the isospin $T = 0$ state is favored over higher isospin. It is further suggested how one can enhance the realization of highest symmetries within random interactions. Thus, chaos and symmetry are shown to be linked deeply.

Lastly, we newly developed an extrapolation method to solve large-scale shell model calculations with deformed basis [19]. The extrapolation is based on a scaling property of energy and energy variance for a series of systematically approximated wave functions to the true one. For such systematically approximated wave functions, we use variation-after-projection method concerning the full angular momentum projection. For a numerical test, we performed a shell model calculation whose dimension is about 1 billion and found this new extrapolation method can solve it with enough accuracy.

3. Summary

Various works are published and some are prepared under the project of the large-scale nuclear structure calculation. In the fiscal year 2004, we performed not only investigation of nuclear structure of various nuclei [3, 4, 5, 6, 7, 8, 9, 11, 12, 13, 14, 15, 16, 17], but also the accompanying works about quantum chaos [18] and the new numerical method for quantum many-body problem [19].

References

[1] Grant-in-Aid for Specially Promoted Research (13002001) from the Ministry of Education, Science, Sport, Culture and Technology.

[2] T. Otsuka, N. Shimizu, and S. Shimoura, CNS Annual Report 2002 (2003) 81: N. Shimizu, T. Otsuka, N. Itagaki, T. Mizusaki, M. Honma, and Y. Utsuno, CNS Annual Report 2003 (2004) 93.

[3] N. Itagaki, T. Otsuka, K. Ikeda, and S. Okabe, Phys. Rev. Lett. **92** (2004) 142501.

[4] N. Itagaki, S. Aoyama, K. Ikeda, and S. Okabe, Phys. Rev. C **70** (2004) 054307.

[5] N. Itagaki, H. Masui, M. Ito, and S. Aoyama, Phys. Rev. C **71** (2005) 064307.

[6] Y. Utsuno, T. Otsuka, T. Glasmacher, T. Mizusaki, and M. Honma, Phys. Rev. C **70** (2004) 044307.

[7] P. Mason, *et al.*, Phys. Rev. C **71** (2005) 014316.

[8] G. Neyens, *et al.*, Phys. Rev. Lett. **94** (2005) 022501.

[9] Y. Utsuno, Phys. Rev. C **70** 011303 (2004).

[10] M. Honma, T. Otsuka, B. A. Brown, and T. Mizusaki, Phys. Rev. C **69** (2004) 034335.

[11] K. L. Yurkewicz *et al.*, Phys. Rev. C **70** (2004) 034301.

[12] K. L. Yurkewicz *et al.*, Phys. Rev. C **70** (2004) 054319.

[13] K. L. Yurkewicz *et al.*, Phys. Rev. C **70** (2004) 064321.

[14] S. J. Freeman *et al.*, Phys. Rev. C **69** (2004) 064301.

[15] S. N. Liddick *et al.*, Phys. Rev. C **70** (2004) 064303.

[16] B. Fornal *et al.*, Phys. Rev. C **70** (2004) 064304.

[17] N. Shimizu, T. Otsuka, T. Mizusaki and M. Honma, Phys. Rev. C **70** (2004) 054313.

[18] T. Otsuka and N. Shimizu, AIP Conf. Proc. **726** (2004) 43.

[19] T. Mizusaki, Phys. Rev. C **70** (2004) 044316.

Other Activities

The Third CNS International Summer School (CISS04)

S. Shimoura, T. Otsuka[a], Y. Koike[b] and H. Sakai[a]

Center for Nuclear Study, Graduate School of Science, University of Tokyo
[a] Department of Physics, Graduate School of Science, University of Tokyo
[c] Department of Physics, Hosei University

The 3rd CNS International Summer School (CISS04) was held at the Wako campus of the Center for Nuclear Study (CNS), the University of Tokyo, in the period of August 17–20, 2004.

This summer school is the third one in the series which aimed at providing graduate students and postdocs with basic knowledge and perspectives of nuclear physics. Topics of this year were "*ab initio* calculation", "mean field calculation", and "spin-isospin excitation" of nuclei. Short lectures on recent progress in unstable nuclear physics were also presented. Addigionally, special lectures on experimental and theoretical studies of penta-quark were given.

The list of lecturers and the titles of lectures are shown below.

D. Frekeres (Münster, Germany)	"The Facets of Nuclear Charge-Exchange Reactions"
P. Navratil (LLNL, USA)	"Nuclear Structure from First Principles"
W. Nazarewicz (Tennessee/ORNL)	"Towards the Universal Nuclear Energy Density Functional"
Y. Fujita (Osaka)	"High-Resolution Study of Gamow-Teller Transitions"
K. Hagino (Tohoku)	"Heavy-Ion Fusion Reactions around the Coulomb Barrier"
T. Otsuka (Tokyo)	"Evolution of Shell Structure and Spin-Isospin Interaction"
H. Sakurai (Tokyo)	"In-Beam Gamma Spectroscopy on Unstable Nuclei with Fast Radioactive Ion Beams"
T. Nakano (RCNP, Osaka)	"Experimental Study of the Pentaquarks"
M. Oka (Titech)	"Theoretical Overview of the Pentaquarks"

This year, 107 attendances were gathered together from 6 countries: Among them, 10 attendances were from Asian countries, China, Vietnam, Myanmer, Indonesia. Domestic attendances were from 15 universities and 2 institutes over the country.

The lectures were given from 10:00 in the morning to 17:20 in the evening. After dinner on Wednesday and Thursday, student sessions were held in a relaxed atmosphere. Ten talks were given by graduate students and active discussions about the topics followed.

All the information concerning the summer school, including lecture notes, is open for access at the following URL:

http://www.cns.s.u-tokyo.ac.jp/summerschool/

Nuclear Scattering Experiments for Education of Undergraduate Students

K. Yako, T. Kawabata[a], S. Sakaguchi[a], H. Sakai and S. Shimoura[a]

Department of Physics, University of Tokyo, Tokyo
[a]*Center for Nuclear Study, Graduate School of Science, University of Tokyo*

Nuclear scattering experiments were performed for education of undergraduate students of the University of Tokyo as a part of the curriculum of experimental physics. This program was aiming at providing undergraduate students with an opportunity to learn how to study the world of $< 10^{-14}$ m by using an ion beam from an accelerator and basic experimental equipment.

In this year 32 students participated in four beam times. They used an α beam at $E_\alpha = 6.5$ MeV/A accelerated by the AVF cyclotron and the CRIB beam line in the E7 experimental hall at RIKEN. In each experiment, students were divided into two groups and took one of the following two subjects;

1. Measurement of elastic scattering of α particles from ^{197}Au nucleus.

2. Measurement of gamma-rays emitted in the cascade decay of the rotational bands in ^{154}Gd and ^{184}Os nuclei.

Before the experiment, they learned the operation of the semiconductor detectors at the Hongo campus and took a radiation safety course at RIKEN.

In the $\alpha + {}^{197}$Au measurement, the α particles scattered from a 1.42 mg/cm^2 thick Au foil were detected by a silicon PIN-diode with a thickness of 50 μm located 11 cm away from the target. A plastic collimator with a diameter of 6 mm were attached on the silicon detector. The energy spectrum of the scattered α particles was recorded by a multi-channel analyzer (MCA) system. The beam was stopped by a Faraday cup in the scattering chamber and the charge was measured by a current integrator. The cross section of the reaction was measured typically in the angular region of $\theta_{\rm lab} = 25$–$150°$. The obtained data were compared with the Rutherford scattering cross sections. The size of gold nucleus was discussed by taking account of the nuclear potential. Some students obtained radius of $\sim$10 fm by using a classical model where the trajectory of the α particle in the nuclear potential is obtained by the Runge-Kutta method. Others tried to understand the scattering process by calculating the angular distribution by the distorted wave Born approximation with a Coulomb wave function and a realistic nuclear potential (see Fig. 1).

In the measurement of the rotational bands, excited states in ^{154}Gd and ^{184}Os nuclei were populated by the ^{152}Sm$(\alpha, 2n)$ and ^{182}W$(\alpha, 2n)$ reactions, respectively. The gamma-rays from the cascade decay of the rotational bands were measured by a high purity germanium (HPGe) detector located 50 cm away from the target (see Fig. 2). The gain and the efficiency of the detector system had been calibrated with standard gamma-ray sources of ^{22}Na, ^{60}Co,

^{133}Ba, and ^{137}Cs. The moment of inertia and the deformation parameters of the excited states were discussed by using a classical rigid rotor model and a irrotational fluid model. It was found that the reality lies between the two extreme models. The initial population among the levels of the rotational band was also discussed by taking account of the effect of internal conversion.

We believe that this program helped the students to grasp vivid pictures of nuclei and basic concepts on physics related to accelerators.
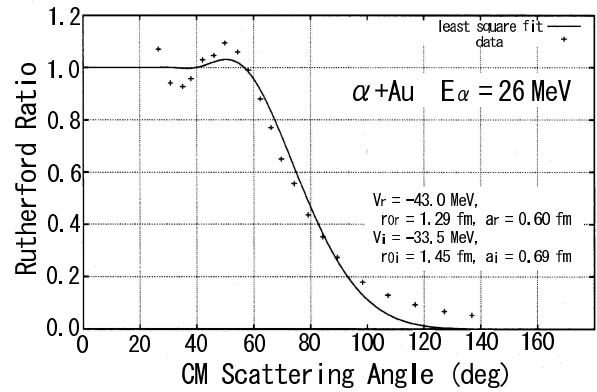
Figure 1. Data and analysis of $\alpha + {}^{197}$Au scattering by a student.
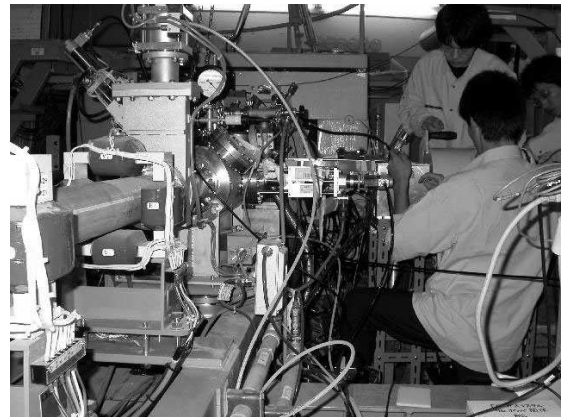
Figure 2. A snapshot during preparation of Ge detector.

Appendices

Symposium, Workshop, Seminar, PAC and External Review
CNS Reports
Publication List
Talks and Presentations
Personnel

Symposium, Workshop, Seminar, PAC and External Review

A. Symposium

The International Symposium on "Correlation Dynamics in Nuclei" was held at the Sanjo Kaikan, the University of Tokyo, from the 31st of January till the 4th of February, 2005. This symposium was organized on the occasion of the 50th anniversary of the Configuration Mixing theory of Arima and Horie. It was hosted by the University of Tokyo, and supported by the Inoue Foundation for Science, the Japan Atomic Energy Research Institute and the Ministry of Education, Cultute, Sports, Science and Technology.

The purpose of the symposium was to discuss on theoretical and experimental developements and future prospects in physics of correlation dynamics in nuclei, including topics such as effective interactions, shell model studies of configuration mixing and spin-isospin modes in nuclei. It was shown in many ways and angles that the Arima-Horie theory has been the starting point of a variety of developments of the studies in these fields over many decades. This was accompanied by the expansion of the computational abilities and the recent progress in accelerators, detectors and radioactive beam facilities.

We enjoyed excellent and lively 28 invited talks and 30 oral presentations in the symposium with about 90 participants.

The proceedings will be published by the Institute of Physics.

The organizing committee was comprised of Takaharu Otsuka (chair), Toshio Suzuki (Nihon Univ., chief editor of the proceedings), Munetake Ichimura, Naoyuki Itagaki, Tohru Motobayashi, Kengo Ogawa, Hideyuki Sakai, and Toshio Suzuki (Fukui Univ.).

B. Workshop

CNS Workshop on "Interdisciplinary Developments of Shell Model Study – Astrophysics and Condensed Matter Physics –"
March 3-5, 2005, CNS Wako Campus, Saitama, Japan.

The purpose of this workshop was to show recent developments of the shell model and some of the methods for studying nuclear physics and to discuss possibilities of applying those methods to other research fields such as condensed matter physics. The number of participants was about 50 including 4 speakers from abroad.

Organizers: T. Kajino (NAOJ), T. Mizusaki (Senshu), T. Otsuka (Tokyo), S. Shimoura (CNS), S. Fujii (Tokyo)

C. CNS Seminar

1. "The nuclear physics reason that your laptop crashes when you are flying",
   Jan Blomgren (Dept. of Neutron Research, Uppsala Univ.), Oct. 5, 2004.

2. "Progress of Nuclear Astrophysics Experiments in CIAE",
   Zhaihong Li (China Institute of Atomic Energy), Oct. 15, 2004.

3. "Electron Screening Effects in Fusion Reactions at Low Energies",
   Gang Lian (China Institute of Atomic Energy), Oct. 15, 2004.

D. CNS Program Advisory Committee

The 5th CNS PAC meeting
Dec. 6, 2004.

The CNS Program Advisory Committee considered 4 proposals for 27 days of beam time. The PAC recommended allocation of 18 days for the 4 experiments.

1. A. Chen: Measurement of ^{25}Al $+ p$ resonances through elastic scattering with CRIB
   (3 days)

2. Zs. Fülöp: Measurement of the half-life of ^{39}Ar (2 days)

3. H. Yamaguchi: Proton resonance scattering of ^{7}Be (6 days)

4. C. S. Lee: Study of astrophysically important resonance states in ^{26}Si using a high-resolution spectrograph at CNS
   (7 days)

E. The External Review

The first external review meeting
Feb. 7–8, 2004.

The CNS external review was held at the request of the dean of the Graduate School of Science, in order to review the scienetific achievements, management and operation, and future plans. The review went quite well, and the CNS activities were rated quite high by the committee. The committee report was delivered to the dean in May 2005, and was publicized by CNS in June 2005.

The Committee Members

M. Inoue	*Ritsumeikan University, Kyoto, Japan*
H. Orihara	*Tohoku Institute of Technology, Miyagi, Japan*
R. H. Siemssen (chair)	*Groningen University, Netherlands*
T. J. Symons	*Lawrence Berkeley National Laboratory, California, USA*
B. M. Sherrill	*Michigan State University, Michigan, USA*
H. Toki	*Research Center for Nuclear Physics, Osaka University, Osaka, Japan*

CNS Reports

#61 "CNS Annual Report 2003",
   edited by T. Kawabata and N. Suzuki, Aug. 2004.

#62 "Low-Energy Radioisotope Beam Separator CRIB",
   Y. Yanagisawa, S. Kubono, T. Teranishi, K. Ue, S. Michimasa, N. Notani, J. J. He,
   Y. Ohshiro, S. Shimoura, S. Watanabe, N. Yamazaki, H. Iwasaki, S. Kato , T. Kishida,
   T. Morikawa and Y. Mizoi, Aug. 2004.

#63 "Study of Stellar Reactions in Expolosive Hydrogen Burning with CRIB",
   S. Kubono, T. Teranishi, M. Notani, H. Yamaguchi, A. Saito, J.J. He, M. Wakabayashi,
   H. Fujikawa, Y. Amadio, H. Baba, T. Fukuchi, S. Shimoura, S. Michimasa, S. Nishimura
   M. Nishimura, Y. Gono, A. Odahara, S. Kato, J. Y. Moon, J. H. Lee, C. S. Lee, J. C. Kim,
   K. L. Hahn, T. Ishikawa, T. Hashimoto, H. Ishiyama, Y.X. Watanabe, M. H. Tanaka,
   H. Miyatake, Zs. Fülöp, V. Guimarães and R. Lichtenthaler, Aug. 2004.

#64 "CNS/RIKEN Joint Symposium on Frontier of gamma-ray spectroscopy and its applica-
   tion (Gamma04)",
   March 18–19, 2004, RIKEN Campus, Wako, Japan, Nov. 2004.

#65 "Proton Polarizing system with Ar-ion laser for $\vec{p}$-RI scattering experiments",
   T. Wakui, M. Hatano, H. Sakai, T. Uesaka and T. Tamii, Dec. 2004.

Publication List

A. Original Papers

1. S. S. Adler et al. (PHENIX Collaboration): "Measurement of Non-Random Event-by-Event Fluctuations of Average Transverse Momentum in $\sqrt{s_{NN}} = 200$ GeV $\mathrm{Au} + \mathrm{Au}$ and $p + p$

   Collisions", Phys. Rev. Lett. **93** (2004) 092301 (6 pages).

2. S. S. Adler et al. (PHENIX Collaboration): "Bose-Einstein Correlations of Charged Pion Pairs in Au+Au Collisions at $\sqrt{s_{NN}} = 200$ GeV", Phys. Rev. Lett. **93** (2004) 152302 (6 pages).

3. S. S. Adler et al. (PHENIX Collaboration): "Double Helicity Asymmetry in Inclusive Mid-Rapidity π^0 Production for Polarized $p + p$ Collisions at $\sqrt{s_{NN}} = 200$ GeV", Phys. Rev. Lett. **93** (2004) 202002 (6 pages).

4. S. S. Adler et al. (PHENIX Collaboration): "Centrality Dependence of Charm Production from a Measurement of Single Electrons in Au+Au Collisions at $\sqrt{s_{NN}} = 200$ GeV", Phys. Rev. Lett. **94** (2005) 082301 (6 pages).

5. A. Andronic, H. Appelshäuser, C. Blume, P. Braun-Munzinger, D. Bucher, O. Busch, V. Cătănescu, M. Ciobanu, H. Daues, D. Emschermann, O. Fateev, Y. Foka, C. Garabatos, T. Gunji, N. Herrmann, M. Inuzuka, E. Kislov, V. Lindenstruth, W. Ludolphs, T. Mahmoud, V. Petracek, M. Petrovici, I. Rusanov, A. Sandoval, R. Santo, R. Schicker, R. S. Simon, L. Smykov, H. K. Soltveit, J. Stachel, H. Stelzer, G. Tsiledakis, B. Vulpescu, J. P. Wessels, B. Windelband, C. Xu, O. Zaudtke, Yu. Zanevsky and V. Yurevich: " Energy loss of pions and electrons of 1 to 6 GeV/c in drift chambers operated with Xe, CO_2 (15%)", Nucl. Instrum. Methods. A **519** (2004) 508–517.

6. A. Andronic, H. Appelshäuser, C. Blume, P. Braun-Munzinger, D. Bucher, O. Busch, V. Cătănescu, M. Ciobanu, H. Daues, D. Emschermann, O. Fateev, Y. Foka, C. Garabatos, T. Gunji, N. Herrmann, M. Inuzuka, E. Kislov, V. Lindenstruth, W. Ludolphs, T. Mahmoud, V. Petracek, M. Petrovici, I. Rusanov, A. Sandoval, R. Santo, R. Schicker, R. S. Simon, L. Smykov, H. K. Soltveit, J. Stachel, H. Stelzer, G. Tsiledakis, B. Vulpescu, J. P. Wessels, B. Windelband, C. Xu, O. Zaudtke, Yu. Zanevsky and V. Yurevich: "Space charge in drift chambers operated with the Xe, CO_2 (15%) mixture", Nucl. Instrum. Methods. A **525** (2004) 447–457.

7. J. Ekman, D. Rudolph, C. Andreoiu, C. Fahlander, M. N. Mineva, M. A. Bentley, S. J. Williams, R. Charity, E. Ideguchi, W. Reviol, D. G. Sarantites, V. Tomov, R. M. Clark, M. Cromaz, P. Fallon, A. O. Macchiavelli, M. P. Carpenter and D. Seweryniak: "γ-ray spectroscopy of core-excited states in ^{51}Mn", Phys. Rev. C **70** (2004) 014306 (14 pages).

8. J. Ekman, D. Rudolph, C. Andreoiu, C. Fahlander, M. N. Mineva, M. A. Bentley, S. J. Williams, R. Charity, E. Ideguchi, W. Reviol, D. G. Sarantites, V. Tomov, R. M. Clark, M. Cromaz, P. Fallon, A. O. Macchiavelli, M. P. Carpenter and D. Seweryniak: "Core excited states in the $A = 51$ mirror nuclei", Phys. Rev. C **70** (2004) 057305 (4 pages).

9. Z. Elekes, Zs. Dombrádi, A. Krasznahorkay, H. Baba, M. Csatlós, L. Csige, N. Fukuda, Zs. Fülöp, Z. Gácsi, J. Gulyás, N. Iwasa, H. Kinugawa, S. Kubono, M. Kurokawa, X. Liu, S. Michimasa, T. Minemura, T. Motobayashi, A. Ozawa, A. Saito, S. Shimoura, S. Takeuchi, I. Tanihata, P. Thirolf, Y. Yanagisawa and K. Yoshida: "Decoupling of Valence Neutrons from the Core in ^{16}C", Phys. Lett. B **586** (2004) 34–40.

10. Z. Elekes, Zs. Dombrádi, A. Saito, N. Aoi, H. Baba, K. Demichi, Zs. Fülöp, J. Gibelin, T. Gomi, H. Hasegawa, N. Imai, M. Ishihara, H. Iwasaki, S. Kanno, S. Kawai, T. Kishida, T. Kubo, K. Kurita, Y. Matsuyama, S. Michimasa, T. Minemura, T. Motobayashi, M. Notani, T. Ohnishi, H. J. Ong, S. Ota, A. Ozawa, H. K. Sakai, H. Sakurai, S. Shimoura, E. Takeshita, S. Takeuchi, M. Tamaki, Y. Togano, K. Yamada, Y. Yanagisawa and K. Yoneda: "Bound excited states in ^{27}F", Phys. Lett. B **599** (2004) 17–22.

11. B. Fornal, S. Zhu, R. V. F. Janssens, M. Honma, R. Broda, P. F. Mantica, B. A. Brown, M. P. Carpenter, P. J. Daly, S. J. Freeman, Z. W. Grabowski, N. J. Hammond, F. G. Kondev, W. Krolas, T. Lauritsen, S. N. Liddick, C. J. Lister, E. F. Moore, T. Otsuka, T. Pawlat, D. Seweryniak, B. E. Tomlin, and J. Wrzesinski: "Development of shell closures at $N = 32, 34$. II. Lowest yrast excitations in even-even Ti isotopes from deep-inelastic heavy-ion collisions", Phys. Rev. C **70** (2004) 064304 (6 pages).

12. H. Fujimura, H. Akimune, I. Daito, M. Fujiwara, K. Hara, K. Y. Hara, M. N. Harakeh, F. Ihara, T. Inomata, K. Ishibashi, T. Ishikawa, T. Kawabata, A. Tamii, M. Tanaka, H. Toyokawa, T. Yamanaka and M. Yosoi: "Nuclear structure of the spin-isospin excited states in ^{13}N studied via the (^{3}He,t) and (^{3}He,tp) reactions at 450 MeV", Phys. Rev. C **69** (2004) 064327 (11 pages).

13. N. Fukuda, T. Nakamura, N. Aoi, N. Imai, M. Ishihara, T. Kobayashi, H. Iwasaki, T. Kubo, A. Mengoni, M. Notani, H. Otsu, H. Sakurai, S. Shimoura, T. Teranishi, Y. X. Watanabe and K. Yoneda: "Coulomb and nuclear breakup of a halo nucleus ^{11}Be", Phys. Rev. C **70** (2004) 54606 (12 pages).

14. M. Hori, J. Eades, R. S. Hayano, W. Pirkl, E. Widmann, H. Yamaguchi, H. A. Torii, B. Juhász, D. Horváth, K. Suzuki and T. Yamazaki: "Observation of Cold, Long-Lived Antiprotonic Helium Ions", Phys. Rev. Lett. **94** (2005) 063401 (4 pages).

15. M. Imanaka, T. Katayama, Y. Ohshiro, S. Watanabe, H. Arai and T. Nakagawa: "Nanocluster ion source by plasma-gas aggregation", Rev. Sci. Instrum. **75** (2004) 1907–1909.

16. R. Kanungo, Z. Elekes, H. Baba, Z. Dombradi, Z. Fülöp, J. Gibelin, A. Horvath, Y. Ichikawa, E. Ideguchi, N. Iwasa, H. Iwasaki, S. Kawai, Y. Kondo, T. Motobayashi, M. Notani, T. Ohnishi, A. Ozawa, H. Sakurai, S. Shimoura, E. Takeshita, S. Takeuchi, I. Tanihata, Y. Togano, C. Wu, Y. Yamaguchi, Y. Yanagisawa, A. Yoshida and K. Yoshida: "Excited states in neutron rich boron isotopes", Phys. Lett. B **608** (2004) 206–214.

17. T. Kawabata, H. Akimune, H. Fujimura, H. Fujita, Y. Fujita, M. Fujiwara, K. Hara, K. Y. Hara, K. Hatanaka, T. Ishikawa, M. Itoh, J. Kamiya, S. Kishi, M. Nakmura, K. Nakanishi, T. Noro, H. Sakaguchi, Y. Shimbara, H. Takeda, A. Tamii, S. Terashima, H. Toyokawa, M. Uchida, H. Ueno, T. Wakasa, Y. Yasuda, H. P. Yoshida, and M. Yosoi: "Isovector and isoscalar spin-flip $M1$ strengths in ^{11}B", Phys. Rev. C **70** (2004) 034318 (10 pages).

18. V. P. Ladygin, T. Uesaka, T. Saito, M. Hatano, A. Yu. Isupov, H. Kato, N. B. Ladygina, Y. Maeda, A. I. Malakhov, J. Nishikawa, T. Ohnishi, H. Okamura, S. G. Reznikov, H. Sakai, N. Sakamoto, S. Sakoda, Y. Satou, K. Sekiguchi, K. Suda, A. Tamii, N. Uchigashima and K. Yako: "Measurement of the tensor analyzing power T_{20} in the $dd \rightarrow ^3$Hen and $dd \rightarrow ^3$Hp at intermediate energies and at zero degree", Phys. Lett. B **598** (2004) 47–54.

19. S. N. Liddick, P. F. Mantica, R. Broda, B. A. Brown, M. P. Carpenter, A. D. Davies, B. Fornal, T. Glasmacher, D. E. Groh, M. Honma, M. Horoi, R. V. F. Janssens, T. Mizusaki, D. J. Morrissey, A. C. Morton, W. F. Mueller, T. Otsuka, J. Pavan, H. Schatz, A. Stolz, S. L. Tabor, B. E. Tomlin and M. Wiedeking: "Development of shell closures at $N = 32, 34$. I. β decay of neutron-rich Sc isotopes", Phys. Rev. C **70** (2004) 064303 (9 pages).

20. P. Mermod, J. Blomgren, B. Bergenwall, A. Hildebrand, C. Johansson, J. Klug, L. Nilsson, N. Olsson, M. Österlund, S. Pomp, U. Tippawan, O. Jonsson, A. Prokofiev, P. U. Renberg, P. Nadel-Turonski, Y. Maeda, H. Sakai and A. Tamii: "Search for three-body force effects in neutron-deuteron scattering at 95 MeV", Phys. Lett. B **597** (2004) 243–248.

21. K. Morita, K. Morimoto, D. Kaji, H. Haba, E. Ideguchi, J. C. Peter, R. Kanungo, K. Katori, H. Koura, H. Kudo, T. Ohnishi, A. Ozawa, T. Suda, K. Sueki, I. Tanihata, H. Xu, A. V. Yeremin, A. Yoneda, A. Yoshida, Y. L. Zhao, T. Zheng, S. Goto and F. Tokanai: "Production and Decay Properties of ^{272}Rg and its Daughter Nuclei", J. Phys. Soc. Jpn. **73** (2004) 1738–1744.

22. K. Morita, K. Morimoto, D. Kaji, H. Haba, E. Ideguchi, R. Kanungo, K. Katori, H. Koura, H. Kudo, T. Ohnishi, A. Ozawa, T. Suda, K. Sueki, I. Tanihata, H. Xu, A.V. Yeremin, A. Yoneda, A. Yoshida, Y. L. Zhao and T. Zheng: "Production and decay of the isotope ^{271}Ds (Z=110)", Eur. Phys. A **21** (2004) 257–263.

23. K. Morita, K. Morimoto, D. Kaji, T. Akiyama, S. Goto, H. Haba, E. Ideguchi, R. Kanungo, K. Katori, H. Koura, H. Kudo, T. Ohnishi, A. Ozawa, T. Suda, K. Sueki, H. Xu, T. Yamaguchi, A. Yoneda, A. Yoshida and Y. Zhao: "Experiment on the Synthesis of Element 113 in the Reaction ^{209}Bi(^{70}Zn,n)^{278}113", J. Phys. Soc. Jpn. **73** (2004) 2593–2596.

24. G. Neyens, M. Kowalska, D. Yordanov, K. Blaum, P. Himpe, P. Lievens, S. Mallion, R. Neugart, N. Vermeulen, Y. Utsuno and T. Otsuka: "Measurement of the Spin and Magnetic Moment of ^{31}Mg: Evidence for a Strongly Deformed Intruder Ground State", Phys. Rev. Lett. **94** (2005) 022501 (4 pages).

25. J. Sakaguchi, H. Gilg, R.S. Hayano, T. Ishikawa, K. Suzuki, E. Widmann, H. Yamaguchi, F. Caspers, J. Eades, M. Hori, D. Barna, D. Horváth, B. Juhász, H.A. Torii and T. Yamazaki: "Cryogenic tunable microwave cavity at 13 GHz for hyperfine spectroscopy of antiprotonic helium", Nucl. Instrum. Methods. A **533** (2004) 598–611.

26. K. Sekiguchi, H. Sakai, H. Witała, K. Ermisch, W. Glöckle, J. Golak, M. Hatano, H. Kamada, N. Kalantar-Nayestanaki, H. Kato, Y. Maeda, J. Nishikawa, A. Nogga, T. Ohnishi, H. Okamura, T. Saito, N. Sakamoto, S. Sakoda, Y. Sato, K. Suda, A. Tamii, T. Uchigashima, T. Uesaka, T. Wakasa and K. Yako: "Polarization transfer measurement for ^{1}H$(\vec{d},\vec{p})^2$H elastic scattering at 135 MeV/nucleon and three-nucleon force effects", Phys. Rev. C **70** (2004) 014001 (17 pages).

27. N. Shimizu, T. Otsuka, T. Mizusaki and M. Honma: "Anomalous properties of quadrupole collective states in ^{136}Te and beyond", Phys. Rev. C **70** (2004) 054313 (8 pages).

28. M. Uchida, H. Sakaguchi, M. Itoh, M. Yosoi, T. Kawabata, Y. Yasuda, H. Takeda, T. Murakami, S. Terashima, S. Kishi, U. Garg, P. Boutachkov, M. Hedden, B. Kharraja, M. Koss, B. K. Nayak, S. Zhu, M. Fujiwara, H. Fujimura, H. P. Yoshida, K. Hara, H. Akimune and M. N. Harakeh: "Systematics of the bimodal isoscalar giant dipole resonance", Phys. Rev. C **69** (2004) 051301 (5 pages).

29. Y. Utsuno, T. Otsuka, T. Glasmacher, T. Mizusaki and M. Honma: "Onset of intruder ground state in exotic Na isotopes and evolution of the $N = 20$ shell gap", Phys. Rev. C **70** (2004) 044307 (8 pages).

30. T. Wakasa, H. Sakai,, M. Ichimura, K. Hatanaka, M. B. Greenfield, M. Hatano, J. Kamiya, H. Kato, Y. Maeda, H. Okamura, T. Ohnishi, H. Otsu, K. Sekiguchi, K. Suda, A. Tamii, T. Uesaka, T. Yagita and K. Yako: "Polarization transfer and spin response functions of the ^{2}H$(\vec{p},\vec{n})$ reaction at 345 MeV", Phys. Rev. C **69** (2004) 044602 (17 pages).

31. T. Wakasa, H. Sakai, M. Ichimura, K. Hatanaka, M. B. Greenfield, M. Hatano, J. Kamiya, H. Kato, K. Kawahigashi, Y. Maeda, Y. Nakaoka, H. Okamura, T. Ohnishi, H. Otsu, K. Sekiguchi, K. Suda, A. Tamii, T. Uesaka, T. Yagita and K. Yako: "Pionic enhancement in quasielastic $(\vec{p},\vec{n})$ reactions at 345 MeV", Phys. Rev. C **69** (2004) 054609 (5 pages).

32. M. Watanabe, Y. Chiba, T. Katayama, T. Koseki, K. Ohtomo and H. Tsutsui: "Measurement of RF characteristics of magnetic alloys for an RF cavity of the accumulator cooler ring", Nucl. Instrum. Methods A **532** (2004) 503–507 .

33. H. Yamaguchi, R. S. Hayano, T. Ishikawa, J. Sakaguchi, E. Widmann, J. Eades, M. Hori, H. A. Torii, B. Juhász, D. Horváth and T. Yamazaki: "Systematic study of the decay rates of antiprotonic helium states", Phys. Rev. A **70** (2004) 012501 (5 pages).

34. Y. Yamaguchi, C. Wu, T. Suzuki, A. Ozawa, D. Q. Fang, M. Fukuda, N. Iwasa, T. Izumikawa, H. Jeppesen, R. Kanungo, R. Koyama, T. Ohnishi, T. Ohtsubo, W. Shinozaki, T. Suda, M. Takahashi and I. Tanihata: "Density distribution of ^{17}B from a reaction cross-section measurement", Phys. Rev. C **70** (2004) 054320 (6 pages).

35. Y. Yanagisawa, S. Kubono, T. Teranishi, K. Ue, S. Michimasa, M. Notani, J. J. He, Y. Ohshiro, S. Shimoura, S. Watanabe, N. Yamazaki, H. Iwasaki, S. Kato, T. Kishida, T. Morikawa and Y. Mizoi: "Low-energy radioisotope beam separator CRIB", Nucl. Instrum. Methods A **539** (2005) 74–83.

36. K. L. Yurkewicz, D. Bazin, B. A. Brown, C. M. Campbell, J. A. Church, D. C. Dinca, A. Gade, T. Glasmacher, M. Honma, T. Mizusaki, W. F. Mueller, H. Olliver, T. Otsuka, L. A. Riley and J R. Terry: "Intermediate-energy Coulomb excitation of ^{52}Fe", Phys. Rev. C **70** (2004) 034301 (5 pages).

37. K. L. Yurkewicz, D. Bazin, B. A. Brown, C. M. Campbell, J. A. Church, D. C. Dinca, A. Gade, T. Glasmacher, M. Honma, T. Mizusaki, W. F. Mueller, H. Olliver, T. Otsuka, L. A. Riley and J. R. Terry: "Nuclear structure in the vicinity of $N = Z = 28$ ^{56}Ni", Phys. Rev. C **70** (2004) 054319 (7 pages).

38. K. L. Yurkewicz, D. Bazin, B. A. Brown, C. M. Campbell, J. A. Church, D. C. Dinca, A. Gade, T. Glasmacher, M. Honma, T. Mizusaki, W. F. Mueller, H. Olliver, T. Otsuka, L. A. Riley and J. R. Terry: "E2 excitation strength in ^{55}Ni: Coupling of the ^{56}Ni 2_1^+ collective core vibration to the f$_{7/2}$ odd neutron hole", Phys. Rev. C **70** (2004) 064321 (4 pages).

B. Proceedings

1. O. Busch for the ALICE TRD Collaboration: "Transition radiation spectroscopy with prototypes of the ALICE TRD.", Proc. of 2nd Workshop on Advanced Transition Radiation Detectors for Accelerator and Space Applications, Sep. 4–7, 2003, Bari, Italy, Nucl. Instrum. Methods. A **522** (2004) 45–49.

2. S. Shimoura: "Position sensitivity of Ge detectors and its applications to in-beam nuclear spectroscopy", Proceedings of the International Conference on Imaging Techniques in Subatomic Physics, Astrophysics, Medicine, Biology and Industry, June 24–27, 2003, Stockholm, Sweden, ed. by P. Carlson, B. Cederwall and V. Peskov, Nucl. Instrum. Methods. A **525** (20) 188–192.

3. T. Wakui, M. Hatano, H. Sakai, T. Uesaka and A. Tamii: "Optimization of laser parameters for polarizing protons in naphthalene crystals", Proc. of 9th International Workshop on Polarized Solid Targets and Techniques, Oct. 27–29, 2003, Bad Honnef, Germany, ed. by St. Goertz, W. Meyer and G. Reicherz, Nucl. Instrum. Methods. A **526** (2004) 182–185.

4. A. D. Frawley for the PHENIX Collaboration: "PHENIX highlights", Proc. of 17th International Conference on Ultra Relativistic Nucleus-Nucleus Collisions (Quark Matter 2004), Oakland, California, Jan. 11–17, 2004, J. Phys. G **30** (2004) S675–S682.

5. C. Klein-Boesing for the PHENIX Collaboration: "PHENIX measurement of high p_T particles in $Au + Au$ and $d + Au$ collisions at $\sqrt{s_{NN}} = 200$ GeV", Proc. of 17th International Conference on Ultra Relativistic Nucleus-Nucleus Collisions (Quark Matter 2004), Oakland, California, Jan. 11–17, 2004, J. Phys. G **30** (2004) S975–S978.

6. J. Frantz for the PHENIX Collaboration: "PHENIX direct photons in 200 GeV $p+p$ and $Au+Au$ collisions", Proc. of 17th International Conference on Ultra Relativistic Nucleus-Nucleus Collisions (Quark Matter 2004), Oakland, California, Jan. 11–17, 2004, J. Phys. G **30** (2004) S1003–S1006.

7. R. Seto for the PHENIX Collaboration: "Light vector mesons from d-Au in PHENIX", Proc. of 17th International Conference on Ultra Relativistic Nucleus-Nucleus Collisions (Quark Matter 2004), Oakland, California, Jan. 11–17, 2004, J. Phys. G **30** (2004) S1017–S1022.

8. M. Heffner for the PHENIX Collaboration: "Two-particle interferometry of 200 GeV $Au + Au$ collisions at PHENIX", Proc. of 17th International Conference on Ultra Relativistic Nucleus-Nucleus Collisions (Quark Matter 2004), Oakland, California, Jan. 11–17, 2004, J. Phys. G **30** (2004) S1043–S1047.

9. F. Matathias for the PHENIX Collaboration: "π / K / p production and Cronin effect from $p + p$, $d + Au$ and $Au + Au$ collisions at $\sqrt{s_{NN}} = 200$ GeV from the PHENIX experiment" Proc. of 17th International Conference on Ultra Relativistic Nucleus-Nucleus Collisions (Quark Matter 2004), Oakland, California, Jan. 11–17, 2004, J. Phys. G **30** (2004) S1113–S1116.

10. S. Kelly for the PHENIX Collaboration : "The PHENIX measurement of heavy flavor via single electrons in pp, d-Au, and Au-Au collisions at $\sqrt{s_{NN}} = 200$ GeV", Proc. of 17th International Conference on Ultra Relativistic Nucleus-Nucleus Collisions (Quark Matter 2004), Oakland, California, Jan. 11–17 2004, J. Phys. G **30** (2004) S1189–S1192.

11. M. X. Liu for the PHENIX Collaboration: "Hadron production in the forward and backward rapidities in d-Au collisions at RHIC", Proc. of 17th International Conference on Ultra Relativistic Nucleus-Nucleus Collisions (Quark Matter 2004) Oakland, California, Jan. 11–17, 2004, J. Phys. G **30** (2004) S1193–S1196.

12. C. Pinkenburg for the PHENIX Collaboration: "Search for the $\bar{\Theta}$- $\rightarrow K^- \bar{n}$ with PHENIX", Proc. of 17th International Conference on Ultra Relativistic Nucleus-Nucleus Collisions (Quark Matter 2004), Oakland, California, Jan. 11–17, 2004, J. Phys. G **30** (2004) S1201–S1206.

13. M. Kaneta for the PHENIX Collaboration : "Event anisotropy of identified π^0, photon and electron compared to charged π, K, p and deuteron in $\sqrt{s_{NN}} = 200$ GeV $Au + Au$ at PHENIX", Proc. of 17th International Conference on Ultra Relativistic Nucleus-Nucleus Collisions (Quark Matter 2004), Oakland, California, Jan. 11–17, 2004, J. Phys. G **30** (2004) S1217–S1220.

14. A. Sickles for the PHENIX Collaboration: "Jet correlations of identified particles in PHENIX", Proc. of 17th International Conference on Ultra Relativistic Nucleus-Nucleus Collisions (Quark Matter 2004), Oakland, California, Jan. 11–17, 2004, J. Phys. G **30** (2004) S1291–S1294.

15. J. Rak for the PHENIX Collaboration: "PHENIX measurement of jet properties and their modification in heavy-ion collisions", Proc. of 17th International Conference on Ultra Relativistic Nucleus-Nucleus Collisions (Quark Matter 2004), Oakland, California, Jan. 11–17, 2004, J. Phys. G **30** (2004) S1309–S1312.

16. D. Kotchetkov for the PHENIX Collaboration: "Study of Cronin effect and nuclear modification of strange particles in d-Au and Au-Au collisions at 200 GeV in PHENIX", Proc. of 17th International Conference on Ultra Relativistic Nucleus-Nucleus Collisions (Quark Matter 2004) Oakland, California, Jan. 11–17, 2004, J. Phys. G **30** (2004) S1317–S1320.

17. R. G. de Cassagnac for the PHENIX Collaboration: "J/ψ production and nuclear effects for $d + \text{Au}$ and $p + p$ collisions in PHENIX", Proc. of 17th International Conference on Ultra Relativistic Nucleus-Nucleus Collisions (Quark Matter 2004), Oakland, California, Jan. 11–17, 2004, J. Phys. G **30** (2004) S1341–S1346.

18. M. J. Tannenbaum for the PHENIX Collaboration: "Event-by-event average p_T fluctuations in $\sqrt{s_{NN}} = 200$ GeV Au $+$ Au and $p + p$ collisions in PHENIX: Measurements and jet contribution simulations", Proc. of 17th International Conference on Ultra Relativistic Nucleus-Nucleus Collisions (Quark Matter 2004), Oakland, California, Jan. 11–17, 2004, J. Phys. G **30** (2004) S1367–S1370.

19. A. Odahara, Y. Gono, Y. Wakabayashi, N. Hokoiwa, M. Kibe, T. Fukuchi, T. Teranishi, S. Kubono, M. Notani, S. Michimasa, J. J. He, S. Shimoura, E. Ideguchi, Y. Yanagisawa, H. Watanabe, T. Kishida, S. Nishimura, M. Nishimura, H. Baba, H. Iwasaki, J. Y. Moon, S. Kato and H. Sagawa: "Development of Unstable Nuclear Beam ^{17}N to Search for High–Spin Isomers in $N = 51$ Isotones", Proc. of the International Symposium on A New Era of Nuclear Structure Physics (NENS03), Kurokawa Village, Nigata, Japan, Nov. 19–22, 2003, ed. by Y. Suzuki, S. Ohya, M. Matsuo and T. Ohtsubo, World Scientific (2004) pp. 87–91.

20. H. Watanabe, K. Asahi, T. Kishida, H. Ueno, W. Sato, A. Yoshimi, Y. Kobayashi, M. Ishihara, D. Kameda, H. Miyoshi, Y. Gono, T. Fukuchi, Y. Wakabayashi, M. Kibe, N. Hokoiwa, A. Odahara, B. Cederwall, K. Lagergren and Zs. Podolyák: "Application of the high-spin isomer beams to secondary fusion reaction and measurement of g-factor", Proc. of International Symposium on A New Era of Nuclear Structure Physics (NENS03), Kurokawa Village, Nigata, Japan, Nov. 19–22, 2003, ed. by Y. Suzuki, S. Ohya, M. Matsuo and T. Ohtsubo, World Scientific (2004) pp. 99–103.

21. T. Otsuka: "Perspectives of the Shell Model", Proc. of International Symposium on A New Era of Nuclear Structure Physics (NENS03), Kurokawa Village, Nigata, Japan, Nov. 19–22, 2003, ed. by Y. Suzuki, S. Ohya, M. Matsuo and T. Ohtsubo, World Scientific (2004) pp. 201–206.

22. S. Ota, T. Murakami, S. Shimoura, S. Michimasa, S. Kubono, T. Teranishi, M. Notani, M. Tamaki, E. Ideguchi, T. Fukuchi, H. Iwasaki, H. Sakurai, M. Kurokawa, T. Motobayashi, Y. Yanagisawa, T. Minemura, S. Takeuchi, N. Aoi, Z. Elekes, M. Ishihara, N. Iwasa, T. Gomi, K. Yamada, A. Saito, H. Baba, Y. U. Matsuyama, S. Kanno, E. Takeshita, K. Demichi, K. Hasegawa, K. Kurita, A. Odahara and K. Miller: "Spectroscopy of ^{13}B via ^{4}He(^{12}Be,^{13}Bγ) reaction", Proc. of International Symposium on A New Era of Nuclear Structure (NENS03), Kurokawa Village, Nigata, Japan, Nov. 19–22, 2003, ed. by Y. Suzuki, S. Ohya, M. Matsuo and T. Ohtsubo, World Scientific (2004) pp. 207–211.

23. T. Fukuchi, Y. Gono, A. Odahara, H. Watanabe, S. Tanaka, M. Inoue, Y. Wakabayashi, T. Sasaki, M. Kibe, N. Hokoiwa, T. Shinozuka, M. Fujita, A. Yamazaki, T. Sonoda, C. S. Lee, Y. K. Kwon and J. H. Lee: "High-Spin Isomer in ^{93}Mo", Proc. of International Sympo. on A New Era of Nuclear Structure (NENS03), Kurokawa Village, Nigata, Japan, Nov. 19–22, 2004, ed. by Y. Suzuki, S. Ohya, M. Matsuo and T. Ohtsubo, World Scientific (2004) pp. 332–333.

24. T. Sakaguchi for the PHENIX Collaboration: "Measurement of High-p_T and Leptonic Observables with the PHENIX Experiment at RHIC", Particles and the Universe, Proc. of 18th Lake Louise Winter Institute, World Scientific (2004) pp. 338–343.

25. T. Gomi, T. Motobayashi, Y. Ando, N. Aoi, H. Baba, K. Demichi, Z. Elekes, N. Fukuda, Zs. Fülöp, U. Futakami, H. Hasegawa, Y. Higurashi, K. Ieki, N. Imai, M. Ishihara, K. Ishikawa, N. Iwasa, H. Iwasaki, S. Kanno, Y. Kondo, T. Kubo, S. Kubono, M. Kunibu, K. Kurita, Y. U. Matsuyama, S. Michimasa, T. Minemura, M. Miura, H. Murakami, T. Nakamura, M. Notani, S. Ota, A. Saito, H. Sakurai, M. Serata, S. Shimoura, T. Sugimoto, E. Takeshita, S. Takeuchi, Y. Togano, K. Ue, K. Yamada, Y. Yanagisawa, K. Yoneda and A. Yoshida: "Study of the Stellar ^{22}Mg(p,γ)^{23}Al Reaction using the Coulomb-Dissociation Method", Proc. of 8th International Conference on Nucleus-Nucleus Collisions (NN2003), June 17–21, 2003, Dubna, Russia, Nucl. Phys. A **734** (2004) E77–E79.

26. K. Morita, K. Morimoto, D. Kaji, S. Goto, H. Haba, E. Ideguchi, R. Kanungo, K. Katori, H. Koura, H. Kudo, T. Ohnishi, A. Ozawa, J. C. Peter, T. Suda, K. Sueki, I. Tanihata, F. Tokanai, H. Xu, A. V. Yeremin, A. Yoneda,

A. Yoshida, Y. L. Zhao and T. Zheng: "Status of heavy element research using GARIS at RIKEN", Proc. of 8th International Conference on Nucleus-Nucleus Collisions (NN2003), June 17–21, 2003, Dubna, Russia, Nucl. Phys. A **734** (2004) 101–108.

27. Y. Yanagisawa, M. Notani, H. Sakurai, M. Kunibu, H. Akiyoshi, N. Aoi, H. Baba, K. Demichi, N. Fukuda, H. Hasegawa, Y. Higurashi, M. Ishihara, N. Iwasa, H. Iwasaki, T. Gomi, S. Kanno, M. Kurokawa, Y. U.Matsuyama, S. Michimasa, T. Minemura, T. Mizoi, T. Nakamura, A. Saito, M. Serata, S. Shimoura, T. Sugimoto, E. Takeshita, S. Takeuchi, K. Ue, K. Yamada, K. Yoneda and T. Motobayashi: "The First Excited State of ^{30}Ne Studied by Proton Inelastic Scattering in Reversed Kinematics", Proc. of 8th International Conference on Nucleus-Nucleus Collisions (NN2003), June 17–21, 2003, Dubna, Russia, Nucl. Phys. A **734** (2004) 374–377.

28. K. Morimoto, K. Morita, D. Kaji, S. Goto, H. Haba, E. Ideguchi, R. Kanungo, K. Katori, H. Koura, H. Kudo, T. Ohnishi, A. Ozawa, J. C. Peter, T. Suda, K. Sueki, I. Tanihata, F. Tokanai, H. Xu, A. V. Yeremin, A. Yoneda, A. Yoshida, T. L. Zhao and T. Zheng: "Status of super heavy element research using GARIS at RIKEN", Proc. of 8th International Conference on Clustering Aspects of Nuclear Structure and Dynamics (CLUSTER03), Nov. 24–29, 2003, Nara, Japan, Nucl. Phys. A **738** (2004) 129–135.

29. S. Shimoura: "Excited states in exotic nuclei populated by direct reactions of RI beams", Proc. of 8th International Conference on Clustering Aspects of Nuclear Structure and Dynamics (CLUSTER03), Nov. 24–29, 2003, Nara, Japan, Nucl. Phys. A **738** (2004) 162–167.

30. M. Itoh, H. Akimune, M. Fujiwara, U. Garg, H. Hashimooto, T. Kawabata, K. Kawase, S. Kishi, T. Murakami, K. Nakanishi, Y. Nakatsugawa, B. K. Nayak, S. Okumura, H. Sakaguchi, H. Takeda, S. Terashima, M. Uchida, Y. Yasuda, M. Yosoi and J. Zenihiro: "Study of the cluster state at $E_x = 10.3$ MeV in ^{12}C", Proc. of 8th International Conference on Clustering Aspects of Nuclear Structure and Dynamics (CLUSTER03), Nov. 24–29, 2003, Nara, Japan, Nucl. Phys. A **738** (2004) 268–272.

31. A. Saito, S. Shimoura, S. Takeuchi, T. Motobayashi, T. Minemura, Y. U. Matsuyama, H. Baba, H. Akiyoshi, Y. Ando, N. Aoi, Zs. Fülöp, T. Gomi, Y. Higurashi, M. Hirai, K. Ieki, N. Imai, N. Iwasa, H. Iwasaki, Y. Iwata, S. Kanno, H. Kobayashi, S. Kubono, M. Kunibu, M. Kurokawa, Z. Liu, S. Michimasa, T. Nakamura, S. Ozawa, H. Sakurai, M. Serata, E. Takeshita, T. Teranishi, K. Ue, K. Yamada, Y. Yanagisawa and M. Ishihara: "Molecular states in neutron-rich beryllium isotopes", Proc. of 8th International Conference on Clustering Aspects of Nuclear Structure and Dynamics (CLUSTER03), Nov. 24–29, 2003, Nara, Japan, Nucl. Phys. A **738** (2004) 337–341.

32. M. Notani, S. Kubono, T. Teranishi, Y. Yanagisawa, S. Michimasa, K. Ue, J. J. He, H. Iwasaki, H. Baba, M. Tamaki, T. Minemura, S. Shimoura, N. Hokoiwa, Y. Wakabayashi, T. Sasaki, T. Fukuchi, A. Odahara, Y. Gono, Zs. Fülöp, E. K. Lee, K. I. Hahn, J. Y. Moon, C. C. Yun, J. H. Lee, C. S. Lee and S. Kato: "Direct measurement of the astrophysical reaction ^{14}O$(\alpha,p)^{17}$F", Proc. of 8th International Conference on Clustering Aspects of Nuclear Structure and Dynamics (CLUSTER03), Nov. 24–29, 2003, Nara, Japan, Nucl. Phys. A **738** (2004) 411–415.

33. M. Yosoi, H. Akimune, I. Daito, H. Ejiri, H. Fujimura, M. Fujiwara, K. Fushimi, K. Hara, K. Y. Hara, H. Hashimoto, T. Ishikawa, M. Itoh, Y. Itow, S. Kishi, T. Kawabata, K. Kawase, M. Kinoshita, K. Kobayashi, M. Nakamura, K. Nakanishi, Y. Nakatsugawa, S. Nakayama, T. Noro, E. Obayashi, S. Okumura, H. Sakaguchi, Y. Sakemi, M. Shiozawa, H. Takeda, T. Taki, A. Tamii, M. Tanaka, S. Terashima, H. Toyokama, N. Tsukahara, M. Uchida, T. Yamada, T. Yamagata, Y. Yasuda, H. P. Yoshida, R. G. T. Zegers and J. Zenihiro: "Cluster fragmentations of deep(1s)-hole states in light nuclei", Proc. of 8th International Conference on Clustering Aspects of Nuclear Structure and Dynamics (CLUSTER03), Nov. 24–29, 2003, Nara, Japan, Nucl. Phys. A **738** (2004) 451–454.

34. M. Notani, S. Kubono, T. Teranishi, Y. Yanagisawa, S. Michimasa, K. Ue, J. J. He, H. Iwasaki, H. Baba, M. Tamaki, T. Minemura, S. Shimoura, N. Hokoiwa, Y. Wakabayashi, T. Sasaki, T. Fukuchi, A. Odahara, Y. Gono, Z. Fülöp, E. K. Lee, K. I. Hahn, J. Y. Moon, C. C. Yun, J. H. Lee, C. S. Lee and S. Kato: "Direct measurement of the astrophysical reaction ^{14}O$(\alpha,p)^{17}$F", Proc. of 6th International Conference on Radioactive Nuclear Beams (RNB6), Sep. 22–26, 2003, Argonne, Illinois, USA, Nucl. Phys. A **746** (2004) 113c–117c.

35. T. Kawabata, H. Akimune, H. Fujimura, H. Fujita, M. Fujiwara, K. Hara, K. Y. Hara, K. Hatanaka, T. Ishikawa, M. Itoh, J. Kamiya, M. Nakamura, H. Sakaguchi, Y. Shimbara, H. Takeda, A. Tamii, T. Noro, H. Toyokawa, M. Uchida, T. Wakasa, Y. Yasuda, H. P. Yoshida and M. Yosoi: "Weak isoscalar response of ^{11}B", Proc. of International Conference on Nuclear Structure and Related Topics (NSRT03), Sep. 2–6, 2003, Dubna, Russia, Phys. Atom. Nuclei **67** (2004) 1794–1798.

36. M. Yosoi, H. Akimune, I. Daito, H. Ejiri, H. Fujimura, M. Fujiwara, K. Hara, K. Y. Hara, T. Ishikawa, M. Itoh, Y. Itow, T. Kawabata, K. Kobayashi, M. Nakamura, T. Noro, E. Obayashi, H. Sakaguchi, Y. Sakemi, M. Shiozawa, H. Takeda, T. Taki, A. Tamii, H. Toyokama, N. Tsukahara, M. Uchida, T. Yamada, Y. Yasuda, H. P. Yoshida and R. G. T. Zegers: "Structures and decay of deep-hole states in light nuclei populated by the (p,2p) reactions", Proc. of International Conference on Nuclear Structure and Related Topics (NSRT03), Sep. 2–6, 2003, Dubna, Russia, Phys. Atom. Nuclei **67** (2004) 1810–1817.

37. K. Kobayashi, Y. Itow, M. Shiozawa, M. Yosoi, H. Toyokawa, H. Akimune, H. Ejiri, H. Fujimura, M. Fujiwara, K. Hara, K. Y. Hara, T. Ishikawa, M. Itoh, T. Kawabata, M. Nakamura, H. Sakaguchi, Y. Sakemi, H. Takeda, M. Uchida, T. Yamada, Y. Yasuda, H. P. Yoshida and R. G. T. Zegers: "Detection of nuclear de-excitation gamma-rays in water Cherenkov detector", Proc. of 3rd International Workshop on Neutrino-Nucleus Interactions in the Few-GeV Region (NuInt04), March 17–21, 2004, Assergi, Italy, Nucl. Phys. B (Proc. Suppl.) (2005) 72–76.

38. S. Michimasa, S. Shimoura, H. Iwasaki, M. Tamaki, N. Aoi, H. Baba, N. Iwasa, S. Kanno, S. Kubono, K. Kurita, M. Kurokawa, T. Minemura, T. Motobayashi, M. Notani, H.J. Ong, S. Ota, A. Saito, H. Sakurai, E. Takeshita, S. Takeuchi, Y. Yanagisawa and A. Yoshida: "Gamma-ray spectroscopy of ^{23}F with proton transfer reaction", Proc. of 5th Japan-China Joint Nuclear Physics Symposium, March 7–10, 2004, Fukuoka, Japan, ed. by Y. Gono, N. Ikeda and K. Ogata, Kyushu University (2004) 251–256.

39. A. Odahara, Y. Gono, E. Ideguchi, H. Watanabe, T. Fukuchi and H. Sagawa: "High spin shape isomers in $N = 83$ isotone", Proc. of 5th Japan-China Joint Nuclear Physics Symposium, March 7–10, 2004 Fukuoka, Japan, ed. by Y. Gono, N. Ikeda and K. Ogata, Kyushu University (2004) 306–313.

40. H. Watanabe, K. Asahi, H. Ueno, Y. Kobayashi, A. Yoshimi, T. Haseyama, T. Kishida, D. Kameda, H. Miyoshi, K. Shimada, S. Emori, G. Kato, A. Odahara and Y. Gono: "g-Factor measurements of high-spin isomers and condensed matter studies using spin-aligned isomeric beams" Proc. of 5th Japan-China Joint Nuclear Physics Symposium, March 7–10, 2004 Fukuoka, Japan, ed. by Y. Gono, N. Ikeda and K. Ogata, Kyushu University (2004) 235–243.

41. K. Morita, K. Morimoto, D. Kaji, Yu. L. Zhao, A. Yoshida, T. Suda, A. Yoneda, T. Ohnishi, H. Haba, E. Ideguchi, H. S. Xu, T. Zheng, H. Kudo, K. Sueki, K. Katori and I. Tanihata: "Status of Heavy Element Research Using a Gas-Filled Recoil Separator at RIKEN", Proc. of Symposium on Nuclear Clusters, Aug. 5–9, 2002, Debrecen, Hungary, Acta. Phys. Hung. N. S. **19** (2004) 53–60.

42. T. Otsuka and N. Shimizu: "Chaos and Symmetry", Proc. of International Conference on Microscopic Studies of Collective Phenomena, April 19–22, 2004, Morelos, Mexico, AIP Conf. Proc. **726** (2004) 43–50.

43. E. Ideguchi, M. Niikura, C. Ishida, T. Fukuchi, H. Baba, N. Hokoiwa, H. Iwasaki, T. Koike, T. Komatsubara, T. Kubo, M. Kurokawa, S. Michimasa, K. Miyakawa, K. Morimoto, T. Ohnishi, S. Ota, A. Ozawa, S. Shimoura, T. Suda, M. Tamaki, I. Tanihata, Y. Wakabayashi, K. Yoshida and B. Cederwall: "Study of High-Spin States in ^{48}Ca Region Induced by Secondary Fusion Reactions", Proc. International Conference on Nuclei at the Limits, July 26–30, 2004, Argonne, Illinois, USA, AIP Conf. Proc. **764** (2004) 136–141.

44. S. Watanabe: "   ",   , Dec. 21–22, 2004, KEK, Tsukuba, Japan,   **49** (5) (2005) 33–38.

C. Theses

1. M. Niikura: "Production of High-Spin States in $^{49-52}$Ti using Fusion Reactions of RI Beams", Master's Thesis, University of Tokyo, March 2005.

2. S. X. Oda: "Development of a Time Projection Chamber Using Gas Electron Multipliers (GEM-TPC)", Master's Thesis, University of Tokyo, March 2005.

D. Other Publications

1. Y. Akiba and H. Hamagaki: "The Beginning of High Energy Nucleus-Nucleus Collision Experiment at RHIC", BUTSURI **59** No. 5 (2004) 291–299.

2. T. Hirano and H. Hamagaki: "Analysis of Quark Gluon Plasma in Relativistic Heavy Ion Collisions through Jet Quenching", BUTSURI **59** No. 12 (2004) 862–870.

Talks and Presentations

A. Conferences

1. T. Otsuka (invited): "Chaos and Symmetry", International Conference on Microscopic Studies of Collective Phenomena, April 19–22, 2004, Cocoyoc, Mexico.

2. M. Imanaka, H. Arai, T. Nakagawa, Y. Ohshiro, S. Watanabe and T. Katayama (poster): "Development and Industrial Application of Boron-Nanocluster Ion Source", 2nd Meeting on Society of Nano Science and Technology, May 9–11, 2004, Tokyo, Japan.

3. T. Sakaguchi for the PHENIX Collaboration (invited): "High P_T particle Measurement from the PHENIX experiment", 2004 RHIC & AGS Annual Users' Meeting, May 10–14, 2004, Brookhaven National Laboratory, Upton, New York, USA.

4. T. Otsuka (invited): "Nuclear Forces and Shell evolution in Exotic Nuclei", International Workshop on Blueprints for the Nucleus: From First Principles to Collective Motion, Feza Gursey Inst., May 17–23, 2004, Istanbul, Turkey.

5. T. Otsuka (invited): "Chaos and Symmetry", 8th International Spring Seminar on Nuclear Physics "Key Topics in Nuclear Structure", May 23–27, 2004, Paestum, Italy.

6. Y. Maeda: "Study of three nucleon force effects via the n+d elastic scattering at 250 MeV", The International Nuclear Physics Conference (INPC2004), June 27–July 2, 2004. Göteborg, Sweden.

7. T. Otsuka, T. Suzuki, R. Fujimoto, T. Matsuo, D. Abe, H. Grawe and Y. Akaishi (invited): "Shell structure of exotic nuclei and nuclear force", International Symposium on Exotic Nuclei (EXON 2004), July 5–12, 2004, Peterhof, Russia.

8. S. Shimoura (invited): "In beam spectroscopy of exotic nuclei via direct reactions of RI beams", International Symposium on Exotic Nuclei (EXON 2004), July 5–12, 2004, Peterhof, Russia.

9. S. Kubono: "Study of Stellar Reactions in Explosive Hydrogen Burning with CRIB", 8th International Symposium on Nuclei in the Cosmos, July 19–23, 2004, Vancouver, Canada.

10. T. Otsuka (invited): "Effective Interactions in the Shell Model", Workshop on New perspectives on p-shell nuclei – the nuclear shell model and beyond, July 22–24, 2004, East Lansing, Michigan, USA.

11. E. Ideguchi, M. Niikura, C. Ishida, T. Fukuchi, H. Baba, N. Hokoiwa, H. Iwasaki, T. Koike, T. Komatsubara, T. Kubo, M. Kurokawa, S. Michimasa, K. Miyakawa, K. Morimoto, T. Ohnishi, S. Ota, A. Ozawa, S. Shimoura, T. Suda, M. Tamaki, I. Tanihata, Y. Wakabayashi, K. Yoshida and B. Cederwall: "Study of High-Spin States in ^{48}Ca Region Induced by Secondary Fusion Reactions", International Conference on Nuclei at the Limits, July 26–30, 2004, Argonne, Illinois, USA.

12. T. Otsuka (invited): "Evolution of Single-Particle Structure and Nuclear Force", International Conference on Nuclei at the Limits, July 26–30, 2004, Argonne, Illinois, USA.

13. T. Otsuka (invited): "Evolution of Shell Structure and Spin-Isospin Interaction", International Summer School on Subatomic Physics, Aug. 25–30, 2004, Beijing, China.

14. T. Otsuka, T. Suzuki, R. Fujimoto, T. Matsuo, D. Abe, H. Grawe and Y. Akaishi (invited): "Shell structure of exotic nuclei and nuclear force", International Symposium Atomic nuclei at extreme values of temperature, spin and isospin XXXIX Zakopane School of Physics, Aug. 31–Sep. 5, 2004, Zakopane, Poland.

15. T. Fukuchi, Y. Gono, A. Odahara, E. Ideguchi, H. Watanabe, W. Wakabayashi and H. Sagawa: "Study of High-spin Shape Isomer", RIBF Physics Workshop on Mean Fields and Collective Motions in Unstable Nuclei, Sep. 5–7, 2004, RIKEN, Wako, Japan.

16. M. Imanaka, H. Arai, T. Nakagawa, Y. Ohshiro, S. Watanabe and T. Katayama (poster): "Development of Long Lifetime and High Intensity Nano-Cluster Ion Source by Plasma-Gas-Aggregation", 12th International Symposium on Small Particles and Inorganic Clusters (ISSPIC12), Sep. 6–10, 2004, Nanjing, China.

17. E. Ideguchi, M. Niikura, C. Ishida, T. Fukuchi, H. Baba, N. Hokoiwa, H. Iwasaki, T. Koike, T. Komatsubara, T. Kubo, M. Kurokawa, S. Michimasa, K. Miyakawa, K. Morimoto, T. Ohnishi, S. Ota, A. Ozawa, S. Shimoura, T. Suda, M. Tamaki, I. Tanihata, Y. Wakabayashi, K. Yoshida and B. Cederwall: "Study of high-spin states in the ^{48}Ca region by using secondary fusion reactions", 4th International Conference on Exotic Nuclei and Atomic Masses (ENAM 04), Sep. 12–16, 2004, Pine Mountain, Georgia, USA.

18. S. Michimasa, S. Shimoura, H. Iwasaki, M. Tamaki, S. Ota, N. Aoi, H. Baba, N. Iwasa, S. Kanno, S. Kubono, K. Kurita, M. Kurokawa, T. Minemura, T. Motobayashi, M. Notani, H.J. Ong, A. Saito, H. Sakurai, E. Takeshita, S. Takeuchi, Y. Yanagisawa and A. Yoshida: "Study of single-particle states in ^{23}F using a proton transfer reaction", 4th International Conference on Exotic Nuclei and Atomic Masses (ENAM 04), Sep. 12–16, 2004, Pine Mountain, Georgia, USA.

19. A. Odahara, Y. Wakabayashi, T. Fukuchi, Y. Gono and H. Sagawa (poster): "High-Spin Shape Isomers and the Nuclear Jahn-Teller Effect", 4th International Conference on Exotic Nuclei and Atomic Masses (ENAM 04), Sep. 12–16, 2004, Pine Mountain, Georgia, USA.

20. S. Kubono (invited): "Experimental Study of the r-Process", Sep. 21–23, 2004, TRIAC Workshop, Japan.

21. S. Kubono (invited): "Recent Development in Nuclear Astrophysics", Annual meeting of the High-Energy Astrophysics Societies, Oct. 1–2, 2004, Metropolitan University, Tokyo, Japan.

22. T. Otsuka (invited): "Lessons from shell model to effective interactions", Workshop on Nuclear Forces and the Quantum Many-Body Problem, Oct. 4–8, 2004, Seattle, Washington, USA.

23. T. Kawabata, H. Akimune, H. Fujimura, H. Fujita, Y. Fujita, M. Fujiwara, K. Hara, K .Y. Hara, K. Hatanaka, T. Ishikawa, M. Itoh, J. Kamiya, S. Kishi, M. Nakamura, K. Nakanishi, T. Noro, H. Sakaguchi, Y. Shimbara, H. Takeda, A. Tamii, S. Terashima, H. Toyokawa, M. Uchida, H. Ueno, T. Wakasa, Y. Yasuda, H. P. Yoshida and M. Yosoi: "Isovector and isoscalar spin-flip $M1$ strengths in ^{11}B", 16th International Spin Physics Symposium (SPIN2004), Oct. 10–16, 2004, Trieste, Italy.

24. Y. Maeda, H. Sakai, T. Kawabata, K. Suda, K. Yako, M. Hatano, T. Saito, H. Kuboki, M. Sasano, K. Hatanaka, Y. Sakemi, A. Tamii, J. Kamiya, Y. Shimizu, K. Fujita, H. Okamura, T. Wakasa, T. Kudoh, Y. Hagiwara, Y. Nagasue, K. Sekiguchi, K. Itoh, M. B. Greenfield and H. Kamada: "Measurements of the n+d elastic scattering at 250 MeV and the three-nucleon forces", 16th International Spin Physics Symposium (SPIN2004), Oct. 10–16, 2004, Trieste, Italy.

25. K. Suda, H. Okamura, T. Uesaka, R. Suzuki, H. Kumasaka, T. Ikeda, K. Itoh, H. Sakai, A. Tamii, K. Sekiguchi, K. Yako, Y. Maeda, M. Hatano, T. Saito, H. Kuboki, N. Sakamoto, Y. Sato: "Tensor analyzing power of the ^{16}O(d, ^{2}He) reaction at 0 degrees and structure of the spin-dipole resonances", 16th International Spin Physics Symposium (SPIN2004), Oct. 10–16, 2004, Trieste, Italy.

26. Y. Ohshiro, S. Yamaka, S. Kubono and S. Watanabe: "Development of An ECR Ion Source At CNS", 17th International Conference on Cyclotrons and Their Applications (Cyclotrons 2004), Oct. 17–22, 2004, National Olympics Memorial Youth Center, Yoyogi, Tokyo, Japan.

27. T. Watanabe, S. Watanabe, T. Ikeda, Y. Sakai, T. Kawaguchi and M. Kase: "Development of highly sensitive current-position monitor with an HTS SQUID and HTS magnetic shield", 17th International Conference on Cyclotrons and Their Applications (Cyclotrons 2004), Oct. 17–22, 2004, National Olympics Memorial Youth Center, Yoyogi, Tokyo, Japan.

28. M. Watanabe, Y. Chiba, T. Koseki, T. Katayama, Y. ohshiro and S. Watanabe: "A Broad-band RF Buncher Cavity using FINEMET Cut Cores for Ion Beams", 17th International Conference on Cyclotrons and Their Applications (Cyclotrons 2004), Oct. 17–22, 2004, National Olympics Memorial Youth Center, Yoyogi, Tokyo, Japan

29. S. Kubono (invited): "Experimental Approach to Experimental Nuclear Astrophysics", Korea-Japan Workshop on Nuclear Physics, Oct. 21–22, 2004, Jeju Island, Korea.

30. T. Otsuka and N. Shimizu (invited): "Quantum Chaos and Symmetries", Nuclei and Mesoscopic Physics Workshop, Oct. 23–27, 2004, East Lansing, Michigan, USA.

31. T. Fukuchi, S. Shimoura, E. Ideguchi, M. Kurokawa, H. Baba, S. Ota, M. Tamaki and M. Niikura (invited): "Development of Position Sensitive Ge Detector" 5th Italy-Japan Symposium on Recent Achievements and Perspectives in Nuclear Physics, Nov. 3–7, 2004, Naples, Italy.

32. S. Kubono (invited): "Experimental Study of Explosive Hydrogen Burning with CRIB", 5th Italy-Japan Symposium on Recent Achievement and Perspectives in Nuclear Physics, Nov. 3–7, 2004, Naples, Italy.

33. H. Hamagaki (invited): "Is QGP found at RHIC?", 5th Italy-Japan Symposium on Recent Achievements and Perspectives in Nuclear Physics, Nov. 3–7, 2004, Naples, Italy.

34. S. Shimoura (invited): "In-beam spectroscopy of exotic nuclei using direct reactions", 5th Italy–Japan Symposium on Recent Achievements and Perspectives in Nuclear Physics, Nov. 3–7, 2004, Naples, Italy.

35. H. Hamagaki (invited): "Development of GEM at CNS", Workshop on Micro Pattern Gas Detector, Dec. 9–10, Kyoto University, Kyoto, Japan.

36. S. Kubono (invited): "Experimental Approach to Nuclear Astrophysics", Japanese-German Nuclear Structure and Astrophysics Workshop, Dec. 16–18, 2004, Darmstadt (GSI), Germany.

37. T. Otsuka (invited): "Mean Field Calculation with Spin-Isospin NN Interactions", Japanese-German Nuclear Structure and Astrophysics Workshop, Dec. 16–18, 2004, Darmstadt (GSI), Germany.

38. S. Watanabe (papers): "   ",   , Dec. 21–22, 2004, KEK, Tsukuba, Japan.

39. Y. Maeda: "Study of three nucleon force effects via the n+d elastic scattering", Workshop on Few-Body physics, Dec. 23–25, 2004, RCNP, Osaka, Japan.

40. S. Shimoura (invited): "In-Beam Nuclear Spectroscopy Using RI beams", Workshop on γ-Ray Detectors, Dec. 27, 2004, Saitama University, Saitama, Japan.

41. S. Shimoura (invited): "Single Particle States in Exotic Nuclei via Nucleon Transfer Reactions at 30–60 A MeV", International Conference on the Interface between Nuclear Structure, Astrophysics and Reactions (NUSTAR'05), Jan. 5–8, 2005, Guildford, UK.

42. H. Hamagaki (invited): "J/ψ and open quark production at RHIC", The XXXIII International workshop on gross properties of nuclei and nuclear excitations (Hirschegg 2005), Jan. 16–22, 2005, Hirschegg, Kleinwalsertal, Austria.

43. T. Kawabata, H. Akimune, H. Fujimura, H. Fujita, Y. Fujita, M. Fujiwara, K. Hara, K. Y. Hara, K. Hatanaka, T. Ishikawa, M. Itoh, J. Kamiya, S. Kishi, M. Nakamura, K. Nakanishi, T. Noro, H. Sakaguchi, Y. Shimbara, H. Takeda, A. Tamii, S. Terashima, H. Toyokawa, M. Uchida, H. Ueno, T. Wakasa, Y. Yasuda, H. P. Yoshida and M. Yosoi: "Isovector and isoscalar spin-flip $M1$ strengths in ^{11}B", International Symposium on Correlation Dynamics in Nuclei (CDN05), Jan. 31–Feb. 4, 2005, Tokyo, Japan.

44. T. Sakaguchi for the PHENIX Collaboration: "Direct Photon Measurement at RHIC-PHENIX", 21st Winter Workshop on Nuclear Dynamics, Feb. 5–12, 2005. Breckenridge, Colorado, USA.

45. H. Hamagaki (invited): "Electromagnetic measurements at RHIC", 5th International Conference on Physics and Astrophysics of Quark Gluon Plasma (ICPAQGP 2005), Feb. 8–12, 2005, Salt Lake City, Kolkata, India.

46. T. Otsuka, T. Suzuki, R. Fujimoto, T. Matsuo, D. Abe, H. Grawe, Y. Akaishi, M. Honma, T. Mizusaki and B. A. Brown (invited): "Shell structure of exotic nuclei and NN force", INFN Workshop on Reactions and Structure with Exotic Nuclei. Feb. 24–26, 2005, Pisa, Italy.

47. T. Kawabata, H. Akimune, H. Fujimura, H. Fujita, Y. Fujita, M. Fujiwara, K. Hara, K. Y. Hara, K. Hatanaka, T. Ishikawa, M. Itoh, J. Kamiya, S. Kishi, M. Nakamura, K. Nakanishi, T. Noro, H. Sakaguchi, Y. Shimbara, H. Takeda, A. Tamii, S. Terashima, H. Toyokawa, M. Uchida, H. Ueno, T. Wakasa, Y. Yasuda, H. P. Yoshida and M. Yosoi: "Isovector and isoscalar spin-flip $M1$ strengths in ^{11}B", CNS Workshop on Interdisciplinary Developments of Shell Model Study, March 3–5, 2005, CNS, Wako, Saitama, Japan.

48. S. Michimasa, S. Shimoura, H. Iwasaki, M. Tamaki, S. Ota, N. Aoi, H. Baba, N. Iwasa, S. Kanno, S. Kubono, K. Kurita, M. Kurokawa, T. Minemura, T. Motobayashi, M. Notani, H.J. Ong, A. Saito, H. Sakurai, E. Takeshita, S. Takeuchi, Y. Yanagisawa and A. Yoshida : "Proton single particle states in ^{23}F", CNS Workshop on Interdisciplinary Developments of Shell Model Study, March 3–5, 2005, CNS, Wako, Saitama, Japan.

49. H. Hamagaki (invited): "Quark Gluon Plasma at RHIC", KEK Theory Meeting 2005 "Particle Physics Phenomenology" March 3–5, 2005, KEK, Tsukuba, Japan.

50. T. Otsuka, T. Suzuki, R. Fujimoto, T. Matsuo, D. Abe, H. Grawe, Y. Akaishi, M. Honma, T. Mizusaki and B. A. Brown (invited): "Structure issues of exotic heavy nuclei", International Workshop on Neutron-Rich Radioactive Ion Beams –Physics with MAFF–, March 29–April 1, 2005, Kloster Banz, Germany.

B. JPS Meetings

1. T. Fukuchi, S. Shimoura, E. Ideguchi and M. Kurokawa: "Development of Position Sensitive Germanium Detector", JPS Autumn Meeting, Sep. 27–30, 2004, Kochi University, Kochi, Japan.

2. T. Gunji for the PHENIX Collaboration: "$J/\psi \to e^+e^-$ Measurements in $\mathrm{Au+Au}$ Collisions at RHIC-PHENIX", JPS Autumn Meeting, Sep. 27–30, 2004, Kochi University, Kochi, Japan.

3. T. Isobe for the PHENIX Collaboration: Measurements of the neutral mesons in $\mathrm{Au+Au}$ collisions at RHIC-PHENIX, JPS Autumn Meeting, Sep. 27–30, 2004, Kochi University, Kochi, Japan.

4. F. Kajihara for the PHENIX Collaboration: "Single Electron Measurement in the PHENIX Run3 d-Au Experiment", JPS Autumn Meeting, Sep. 27–30, 2004, Kochi University, Kochi, Japan.

5. N. Kurihara for the PHENIX collaboration: "Measurement of singele particle spectrum with Aerogel Counter at RHIC-PHENIX" JPS Autumn Meeting, Sep. 27–30, 2004, Kochi University, Kochi, Japan.

6. M. Niikura, E. Ideguchi, T. Fukuchi, H. Baba, N. Hokoiwa, C. Ishida, H. Iwasaki, T. Koike, T. Komatsubara, T. Kubo, M. Kurakawa, S. Michimasa, K. Miyagawa, K. Morimoto, T. Ohnishi, S. Ota, A. Ozawa, S. Shimoura, T. Suca, M. Tamaki, I. Tanihata, Y. Wakabayashi and K. Yoshida: "High-Spin States in ^{50}Ti via Fusion Reaction of Secondary Beam", JPS Autumn Meeting, Sep. 27–30, 2004, Kochi University, Kochi, Japan.

7. S. X. Oda, H. Hamagaki, K. Ozawa, M. Inuzuka, T. Sakaguchi, T. Isobe, T. Gunji, S. Saito, Y. Morino, Y.L. Yamaguchi, S. Sawada, S. Yokkaichi: "Reseach and Development of a Time Projection Chamber Using Gas Electron Multipliers (GEM-TPC)", JPS Autumn Meeting, Sep. 27–30, 2004, Kochi University, Kochi, Japan.

8. A. Odahara, Y. Gono, S. Motomura, Y. Isozumi, T. Kikegawa, Y. Mochizuki, T. Fukuchi and Y. Wakabayashi: "Change of decay constant of ^{40}K under ultra high-pressure", JPS Autumn Meeting, Sep. 27–30, 2004, Kochi University, Kochi, Japan.

9. S. Shimoura: "High Resolution Spectrometer and Physics Perspectives", JPS Autumn Meeting, Sep. 27–30, 2004, Kochi University, Kochi, Japan.

10. Y. Wakabayashi, A. Odahara, Y. Gono, T. Fukuchi, S. Kubono, T. Teranishi, S. Ota, H. Yamaguchi, A. Saitoh, E. Ideguchi, S. Nishimura, J. J. He, H. Fujikawa, G. Amadio, M. Notani, Y. Yanagisawa, S. Michimasa, S. Shimoura,H. Watanabe, T. Kishida, H. Baba and M. Nishimura: "Search for high-spin isomers in N=51 isotones", JPS Autumn Meeting, Sep. 27–30, 2004, Kochi University, Kochi, Japan.

11. A. Odahara, Y. Gono, S. Motomura, Y. Isozumi, T. Kikegawa, Y. Mochizuki, T. Fukuchi and Y. Wakabayashi: "Change of decay constant of ^{40}K under ultra high-pressure", JPS Kyushu Branch Meeting, Dec. 4, 2004, Kyushu Institute of Technology, Fukuoka, Japan.

12. T. Isobe for the PHENIX Collaboration: π^0 measurement in Au+Au collisions at RHIC-PHENIX, JPS Spring Meeting, March 24–27, 2005, Tokyo University of Science, Noda, Japan.

13. F. Kajihara for the PHENIX Collaboration: "Single Electron Measurement in the PHENIX Experiment", JPS Spring Meeting, March 24–27, 2005, Tokyo University of Science, Noda, Japan.

14. Y. Morino, S. Shota, T. Gunji and H. Hamagaki for the ALICE Collaboration: "Electron Identification Capability of real size TRD for ALICE", JPS Spring Meeting, March 24–27, 2005, Tokyo University of Science, Noda, Japan.

15. A. Odahara, Y. Gono, T. Fukuchi, Y. Wakabayashi, Y. Gono and H. Sagawa: "Experimental pairing energies at high-spin states", JPS Spring Meeting, March 24–27, 2005, Tokyo University of Science, Noda, Japan.

16. S. Sakaguchi, T. Wakui, T. Uesaka, K. Itoh, T. Kawabata, H. Kuboki, Y. Maeda, H. Sakai, Y. Sasamoto, M. Sasano, K. Sekiguchi, K. Suda, Y. Takahashi and K. Yako: "Performance evaluation of polarized proton solid target by α beam irradiation", JPS Spring Meeting, March 24–27, 2005, Tokyo University of Science, Noda, Japan.

17. T. Sakaguchi (Invited): "Heavy-ion collisions at RHIC", Invited talk at symposium "30 years of QCD current status and prospect", JPS Spring Meeting, March 24–27, 2004, Tokyo University of Science, Noda, Japan.

18. Y. Wakabayashi, A. Odahara, Y. Gono, T. Fukuchi, S. Kubono, T. Teranishi, S. Ota, H. Yamaguchi, A. Saitoh, E. Ideguchi, S. Nishimura, J. J. He, H. Fujikawa, G. Amadio, M. Notani, Y. Yanagisawa, S. Michimasa, S. Shimoura, H. Watanabe, T. Kishida, H. Baba and M. Nishimura: "Search for high-spin isomers using unstable nuclear beam ^{17}N", JPS Spring Meeting, March 24–27, 2005, Tokyo University of Science, Noda, Japan.

C. Lectures

1. S. Shimoura: "Special Lectures on Structure of Unstable Nuclei", May 26–28, 2004, Osaka University, Osaka, Japan.

2. S. Shimoura: "Special Lectures on Structure and Reactions of Nuclei far from the Stable Line", June 10–11, 2004, Osaka City University, Osaka, Japan.

3. S. Shimoura: "Special Lectures on Nanometer-scale Quantum Physics", June 21–23, 2004, Tokyo Institute of Technology, Tokyo, Japan.

4. S. Kubono: "Nuclear Astrophysics", Feb. 14-19, 2005, Canpo de Jordan, Brazil.

D. Seminars

1. H. Hamagaki: "Development of GEM at CNS", March 2, 2005, Seminar at the Kamioka Observatory Group, ICRR, University of Tokyo, Kashiwa, Japan.

2. T. Kawabata: "Isovector and isoscalar spin-flip $M1$ strengths in ^{11}B", March 15, 2005, Nuclear Physics Seminar at Kernfysisch Versneller Instituut (KVI), Groningen, Netherlands.

Personnel

Director

    SAKAI, Hideyuki   *Professor, Department of Physics, Graduate School of Science*

Scientific Staff

1. Accelerator Research

    KATAYAMA, Takeshi (June 2004)   *Professor*

    WATANABE, Shin-ichi   *Research Associate*

2. Heavy-Ion Collisions

    SHIMOURA, Susumu   *Professor*

    UESAKA, Tomohiro   *Lecturer*

    IDEGUCHI, Eiji   *Lecturer*

    IWASAKI, Hironori   *Research Associate*

    KAWABATA, Takahiro   *Research Associate*

    WAKUI, Takashi   *Research Associate*

3. Nuclear Structure in Extreme States

    KUBONO, Shigeru   *Professor*

    HAMAGAKI, Hideki   *Associate Professor*

    YAMAGUCHI, Hidetoshi (April 2004)   *Research Associate*

    OZAWA, Kyoichiro   *Research Associate*

Guest Professors

    KOIKE, Yasuro   *Hosei University*

    FUKUDA, Mitsuhiro   *Japan Atomic Energy Research Institute*

    OTSUKA, Takaharu   *University of Tokyo*

Technical Staff

    OHSHIRO, Yukimitsu   YAMAZAKI, Norio

Technical Assistants

SHIMAZAKI, Takaichi (　Oct. 2004)　　　　SUZUKI, Masaharu

YAMAKA, Shoichi　　　　　　　　　　　MARUNO, Tomohiro (Feb. 2005　)

Post Doctoral Associates

SAKAGUCHI, Takao (　Sep. 2004)　　　　NOTANI, Masahiro (　June 1, 2004)

HE, Jianjun　　　　　　　　　　　　　INUZUKA, Masahide (　May 2004)

IMANAKA, Masashi (　Sep. 2004)　　　　FUKUCHI, Tomonori

KAMETANI, Soichiro　　　　　　　　　SAITO, Akito

MAEDA, Yukie　　　　　　　　　　　　BABA, Hidetada

YAMAGUCHI, Yoshitaka　　　　　　　　SUDA, Kenji

Graduate Students

KAJIHARA, Fukutaro　　　　　　　　　WAKABAYASHI, Yasuo

GUNJI, Taku　　　　　　　　　　　　　ISOBE, Tadaaki

KURIHARA, Narumi　　　　　　　　　　TAMAKI, Mitsuru

NIIKURA, Megumi　　　　　　　　　　　ODA, Susumu

FUJIKAWA, Hisashi　　　　　　　　　　MORINO, Yuhei

SAITO, Shota　　　　　　　　　　　　　SAKAGUCHI, Satoshi

SASAMOTO, Yoshiko　　　　　　　　　AMADIO, Guilherme

Administration Staff

HIRANO, Midori　　　　　　　　　　　TAKEUCHI, Kazuko

YAMAMOTO, Ikuko　　　　　　　　　　ITAGAKI, Toshiko

SUZUKI, Naho　　　　　　　　　　　　ENDO, Takako

AYABE, Hiroko (Oct. 2004　)　　　　　　YAMAGUCHI, Miwa (March 2005　)

Committees

Council

OKAMURA, Sadanori (chair)	*Dean, Graduate School of Science*
WADATI, Miki	*Department of Physics, Graduate School of Science*
YAMAMOTO, Masayuki	*Department of Biophysics and Biochemistry, Graduate School of Science*
EGUCHI, Tohru	*Department of Physics, Graduate School of Science*
SAKAI, Hideyuki	*Department of Physics, Graduate School of Science*
OTSUKA, Takaharu	*Department of Physics, Graduate School of Science*
KUBONO, Shigeru	*Center for Nuclear Study, Graduate School of Science*
SHIMOURA, Susumu	*Center for Nuclear Study, Graduate School of Science*
NAGAMINE, Kanetada	*Institute of Materials Structure Science, High Energy Accelerator Research Organization*

Steering Committee

SAKAI, Hideyuki	*Department of Physics, Graduate School of Science*
SHIMOURA, Susumu	*Center for Nuclear Study, Graduate School of Science*
KUBONO, Shigeru	*Center for Nuclear Study, Graduate School of Science*
HAMAGAKI, Hideki	*Center for Nuclear Study, Graduate School of Science*
AIHARA, Hiroaki	*Department of Physics, Graduate School of Science*
OTSUKA, Takaharu (chair)	*Department of Physics, Graduate School of Science*
HAYANO, Ryugo	*Department of Physics, Graduate School of Science*
SAKURAI, Hiroyoshi	*Department of Physics, Graduate School of Science*
OHTA, Toshiaki	*Department of Chemistry, Graduate School of Science*
KOBAYASHI, Tomio	*International Center for Elementary Particle Physics*
KOMAKI, Ken'ichiro	*Institute of Physics, Graduate School of Arts and Sciences*
NAKAZAWA, Masaharu	*Department of Quantum Engineering and Systems Science, Graduate School of Engineering*

Program Advisory Committee

NAKAMURA, Takashi (chair)	*Tokyo Institute of Technology*
HAMAMOTO, Ikuko	*University of Lund, Sweden*
ISHII, Tetsuo	*Japan Atomic Energy Research Institute*
SHIMODA, Tadashi	*Osaka University*
NORO, Tetsuo	*Kyushu Univeristy*